RISK ASSESSMENT AND MITIGATION FOR AUSTRALIAN CONTEMPORARY HOUSES SUBJECTED TO NON-CYCLONIC WINDSTORMS

Hao Qin

BEng (HIT, China)
MESc (UWO, Canada)

A thesis submitted in fulfilment of the requirements for the degree of Doctor of Philosophy in Civil Engineering
The University of Newcastle

December 2019

This research was supported by an Australian Government Research Training Program (RTP) Scholarship

DECLARATION

STATEMENT OF ORIGINALITY

I hereby certify that the work embodied in the thesis is my own work, conducted under normal supervision. The thesis contains no material which has been accepted, or is being examined, for the award of any other degree or diploma in any university or other tertiary institution and, to the best of my knowledge and belief, contains no material previously published or written by another person, except where due reference has been made. I give consent to the final version of my thesis being made available worldwide when deposited in the University's Digital Repository, subject to the provisions of the Copyright Act 1968 and any approved embargo.

Hao Qin

ABSTRACT

Non-cyclonic windstorm is a major natural peril that causes substantial economic losses to housing in New South Wales, Victoria and southeastern Queensland where the majority of Australia's population live. Housing in non-cyclonic regions of Australia comprises a large portion of metal-clad contemporary houses with complex hip-roof geometries. According to post-damage surveys, wind-induced losses to Australian contemporary houses mainly result from direct wind damage to roof and windows as well as associated rainwater damage to building interior and contents. Construction defects have also been observed as a major contributor to housing damage during windstorms. There is a lack of systematic approaches to assess wind and rainfall losses for metal-clad contemporary houses in non-cyclonic regions of Australia with an explicit modelling of construction defects. Risk mitigation and climate adaptation aim to improve building resilience to wind hazards and reduce economic losses associated with wind damage under a changing climate. Although several mitigation/adaptation measures for Australian housing have been proposed in the literature, quantitative evaluations of their cost-effectiveness are still limited. There is a need for a quantitative decision support model to assist relevant decision-makers and stakeholders in choosing appropriate mitigation/adaptation measures for the protection of houses against wind hazards.

This PhD research develops a probabilistic risk assessment (PRA) and decision support framework for metal-clad contemporary houses subjected to non-cyclonic windstorms. The PRA framework integrates hazard modelling for extreme wind speed and associated rainfall, reliability-based wind damage assessment for roof system and windows, rainwater intrusion evaluation and economic loss estimation. A probabilistic construction defect model including five types of defects in roof connections is also developed, which can be readily integrated into the PRA framework to account for the reduced roof reliability and performance due to defective roof components. A scenario-based approach is adopted to include climate change impact on extreme wind speed and associated rainfall. The developed PRA framework is illustrated on representative metal-clad contemporary houses in two Australian cities − Brisbane and Melbourne (i.e. capital cities in Queensland and Victoria). Risk-based decision models are employed to provide decision support to identify cost-effective measures for risk mitigation and climate adaptation. The magnitude of

uncertainty and decision-makers' risk preferences (i.e. risk aversion, risk-neutrality and risk proneness) are taken into account in the decision-making. The implications for mitigation/adaptation decisions with the consideration of insurance and economic incentives are also discussed.

The PRA and decision analysis results suggest that rainwater damage to building interior and contents is a major contributor to economic risks for Australian contemporary houses subjected to non-cyclonic windstorms. Installing window shutters is a promising mitigation/adaptation measure for homeowners in Brisbane to implement. Climate change has a marginal influence on the cost-effectiveness of mitigation/adaptation measures. The outputs of this PhD research can assist insurance and re-insurance industries in catastrophe risk management, government agencies in disaster planning and management, and homeowners in choosing cost-effective mitigation/adaptation measures to protect their home against windstorms. This research paves the way towards a more resilient residential community under wind hazards.

ACKNOWLEDGEMENT

First and foremost, I would like to thank my supervisor, Professor Mark Stewart, for his continuous guidance and support as well as many opportunities he has provided throughout the completion of this thesis. The considerable insights and timely feedback offered by Mark shape the way I think and guide me towards a problem-driven research methodology. I feel extremely lucky to have a mentor like Mark.

This PhD research has received many helpful inputs and support. I would like to express my appreciation to the following people:

Dr. Satheeskumar Navaratnam (RMIT University) for the helpful discussions and test data for truss connections;

Mr. Aaron Scott (The University of Newcastle) for giving support to the high performance computing;

Dr. Omer Yetemen (The University of Newcastle) for the inspiring discussions regarding rainfall modelling;

Dr. Kazuyoshi Nishijima and Mr. Hironobu Ito (Kyoto University) for providing some experimental evidence regarding internal pressure;

Dr. Phil Clausen (The University of Newcastle) for lending multiple licenses of finite element software;

Acacia Pepler, Felicity Gamble and Louise Garbers (Australian Bureau of Meteorology) for providing wind and rainfall data as well as the access to storm database.

The financial support from Australian Government Research Training Program (RTP) Scholarship is greatly acknowledged. I also thank all my friends and office mates at Newcastle for sharing this PhD journey. I will cherish the memories of these days.

Finally, I am very thankful to my family. My parents Chunling and Yuming have offered unwavering support and love throughout my life. My wife Yujing has given me her understanding, encouragement and true love throughout this journey. They are the driving force for me to complete this degree.

LIST OF PUBLICATIONS

This thesis includes contents from published/accepted papers and unpublished manuscripts that are submitted or under preparation for publishing in peer-reviewed journals. See appendix for the publications.

Chapter 3: **Qin, H.**, & Stewart, M. G. (2019). System fragility analysis of roof cladding and trusses for Australian contemporary housing subjected to wind uplift. *Structural Safety*, 79, 80-93. https://doi.org/10.1016/j.strusafe.2019.03.005.

Chapter 4: **Qin, H.**, & Stewart, M. G. (2019). Construction defects and wind fragility assessment for metal roof failure: a Bayesian approach. *Reliability Engineering & System Safety*, accepted. https://doi.org/10.1016/j.ress.2019.106777.

Chapter 5: **Qin, H.**, & Stewart, M. G. (2019). Wind and rain losses for metal-clad contemporary houses subjected to non-cyclonic windstorms. *Structural Safety*, under review.

Chapter 6: **Qin, H.**, & Stewart, M. G. (2019). Risk-based Cost-benefit Analysis of Climate Adaptation Measures for Australian Contemporary Houses under Extreme Winds. *Journal of Infrastructure Preservation and Resilience*, under review.

Chapter 7: **Qin, H.**, & Stewart, M. G. Risk Preferences and Decision-making for Wind Hazard Mitigation under Uncertainty, under preparation.

TABLE OF CONTENTS

ABBREVIATIONS AND SYMBOLS

α_0	Parameter in Dirichlet distribution
A_g	Factor accounting for geometric uncertainties
A_G	Area of gaps around the window
A_S	Area of a metal roof sheet opening
A_{SV}	Vertical projection area of a metal roof sheet opening
A_w	Area of windward wall openings (i.e. window opening in this thesis)
A_R	Area of roof openings
AFSD	Almost first-degree stochastic dominance
ANOVA	Analysis of variance
ANSYS	Commercial FE software
ASD	Almost stochastic dominance
$\beta(D_{ur})$	Scale parameter of gamma distribution as a function of storm duration
BAU	Business as usual
BMT	Base metal thickness
BoM	Bureau of Meteorology
BTR	Batten-to-rafter/truss
C	Climate
C_A	Annual damage cost/loss
C_D	Damage cost for a given time horizon
C_M	Mitigation cost
C_P	Quasi-steady pressure coefficient
C_{Pe}	External pressure coefficient
C_{Pi}	Internal pressure coefficient
C_{PR}	Average of external pressure coefficients at multiple roof openings

C_{PW}	Average of external pressure coefficients at multiple windward wall openings
CDF	Cumulative distribution function
CFD	Computational fluid dynamics
CO	Co-insurance factor
COV	Coefficient of variation
CPC	Common performance condition
CPT	Cumulative prospect theory
CREAM	Cognitive Reliability and Error Analysis Method
CTB	Cladding-to-batten
CTS	Cyclone Testing Station
D_L	Dead load
δ_u	Displacement at peak load
δ_y	Displacement at yielding
δ_{max}	Displacement at complete failure
ΔB	Co-benefit
ΔR	Risk reduction
D	Wind directionality factor
D_{ur}	Duration of windstorm
DRF	Driving rain factor
DS	Damage state
ε	Ratio of violation area for almost stochastic dominance
η	Insurance loading factor
E	Terrain factor
EI	Flexural rigidity
E(L)	Economic risk expressed by expected monetary losses
E_{annual} (L)	Annual expected loss

EU	Expected utility
EX	Excess fee
F_u	Peak load
f_r	Reduction factor for rainwater runoff
f_v	Velocity ratio
F_y	Yield load
FE	Finite element
FPHLM	Florida Public Hurricane Loss Model
FSD	First-degree stochastic dominance
H	Hazard
h_I	Accumulated water depth
h_R	Accumulated water depth due to rainwater intrusion via roof
h_T	Threshold value of water depth leading to total interior and contents loss
h_W	Accumulated water depth due to rainwater intrusion via windows
HAZUS-MH	Hazards US Multi-Hazard hurricane model
HEP	Human error probability
HRA	Human reliability analysis
I(ML), I(C_A)	Annual indemnity paid by insurer
INP	Annual insurance premium
INV	Sum insured
IW	Increase water-resistance of building interior
κ	Rate parameter of exponential distribution
k_0	Initial secant stiffness
L	Loss or consequence if full damage occurs
L_{INS}	Insurance loss or claim cost
LCC	Life-cycle cost

LCC_{HO}	Life-cycle cost for homeowner with insurance
λ	Factor accounting for wind loading modelling inaccuracies and uncertainties
γ	Shape parameter of gamma distribution
g	Limit state function
g_a	Probability density of gamma distribution
G_a	Cumulative probability of gamma distribution
G_E	Factor related to gust effect and area reduction
G_u	Velocity gust factor
JCU	James Cook University
μ	Location parameter of exponential distribution
M	Factor accounting for wind tunnel modelling inaccuracies
MCS	Monte Carlo simulation
MELC	Minimum expected life-cycle cost
ML	Monetary loss
N1, N2, N3	Design wind classifications defined in Australian standards for housing design
N_{cr}	The critical number of failed fasteners leading to the roof sheet failure
N_{lou}	Loss of use (days)
N_f	Number of failed fasteners on a roof sheet
NPV	Net present value
ω	Roof slope
$\boldsymbol{\pi}$	Decision weights in rank-dependent utility model
P_{no}	Probability of no rain during a windstorm
PDF	Probability density function
PRA	Probabilistic risk assessment
PSF	Performance shaping factor
PT	Prospect theory

q_α	α-quantile
$\bar{q}_\alpha$	α-superquantile
ρ	Air density
r	discount rate
R	Software package for statistical analysis
R_c	Resistance of roof connection
R_{clad}	Proportion of metal roof sheeting loss
R_h	Average rainfall intensity
R_{loss}	Extent of damage to roof system
R_{ult}	Ultimate strength of window
R_{truss}	Damage proportion of critical roof trusses
R_W	Resistance of windows
R_{water}	Water penetration resistance of window
R_{WDR}	Free-field wind-driven rain intensity
RAF_R	Rain admittance factor for roof
RAF_W	Rain admittance factor for window
RCP	Representative concentration pathway
RDEU	Rank-dependent expected utility
RDUT	Rank-dependent utility theory
RF	Strengthen roof
RTW	Rafter/truss-to-wall
σ_g	Scale parameter in Gumbel distribution
SD	Stochastic dominance
SPAR-H	The Standardized Plant Analysis Risk-Human Reliability Analysis
Γ	Gamma function
T	Shielding factor

T_M	Occurrence time of the maximum gust wind speed during a windstorm
T_R	Length of time after the occurrence of maximum gust wind speed during a storm
THERP	The Technique for Human Error-rate Prediction
θ	Defect rate
U	Mean wind speed at roof height
u(x)	Utility function
UT	Utility theory
v	Maximum 0.2 second gust velocity at 10m height in open terrain
v_g	Location parameter in Gumbel distribution
V_t	Terminal velocity of raindrops
VOL	Total volume of rainwater intrusion
VOL_G	Volumetric rate of driving rain intrusion via gaps around a window
VOL_R	Volumetric rate of oblique driving rain intrusion via a roof opening
VOL_{RO}	Volumetric rate of rainwater runoff
VOL_T	Total volumetric rate of rainwater intrusion
VOL_W	Volumetric rate of driving rain intrusion via a window opening
VRC	Vertical reaction coefficient
W	Wind loading
W_0	Weighting factor in loss function for contents
W_c	Wind uplift force in roof connections.
W_{LS}	Window limit state
W_{win}	Wind pressure acting on windward windows
w(p)	Probability weighting function
WDR	Wind-driven rain
WR	Increase window resistance
WS	Install window shutters

LIST OF TABLES

LIST OF FIGURES

CHAPTER 1. INTRODUCTION

1.1 Background and Motivation

Non-cyclonic wind regions contain the majority of Australia's population and urbanization. Figure 1.1 shows the wind regions specified in AS/NZS 1170.2 (2011) with Region A, B and W defined as non-cyclonic regions. New South Wales, Victoria and southeast Queensland have nearly 70% of Australia's population, and are classified as non-cyclonic regions of Australia in AS/NZS 1170.2 (2011). Only about 5% of Australia's population live in cyclonic regions. Non-cyclonic windstorms (e.g. severe thunderstorms and synoptic winds associated with low-pressure systems) account for nearly 25% of annual economic losses caused by natural hazards in Australia (BITRE 2008) with most damage occurring to housing (e.g. Holmes 2015; Leitch et al. 2009). Wind damage prediction and risk assessment for housing in non-cyclonic regions are evidently essential and the key to assessing the cost-effectiveness of relevant wind mitigation measures. An accurate and detailed wind risk assessment can also benefit insurance and re-insurance industries in catastrophe risk management, and government bodies in planning for disaster and emergency management (Holmes 2015). Risk mitigation and climate adaptation aim to improve building resilience to extreme winds and reduce economic losses associated with wind damage under a changing climate. The adoption of a specific wind mitigation or climate adaptation measure for housing is determined not only by its effectiveness in risk reduction but also the cost efficiency, and hence there is a need to quantify the cost-effectiveness of relevant risk mitigation and climate adaptation measures.

Losses and risks to housing during severe windstorms often accrue to damage to the building envelope (Henderson & Ginger 2008; Stewart et al. 2018). Rainfall often concurs with extreme winds. The breaches of roof cladding and windows/doors may subsequently induce significant losses to building interior and contents due to rainwater intrusion (e.g. Henderson & Ginger 2008; Leitch et al. 2009; Ginger et al. 2010). To this end, the main task of the risk assessment for housing under extreme winds is to evaluate the direct losses from wind damage to the building envelope and the economic losses caused by rainwater damage to building interior and contents. A probabilistic risk assessment (PRA) framework is thus needed, which integrates hazard modelling for extreme wind and associated rainfall,

wind damage assessment for the building envelope, rainwater intrusion evaluation and economic loss estimation.

The extreme wind speed is typically modelled by the extreme value distributions (e.g. Simiu & Scanlan 1986; Palutikof et al. 1999). For a specific type of windstorm (e.g. tropical cyclones, thunderstorm downbursts), event-based wind field models may also be used to capture the temporal and spatial variations of wind speed and direction (e.g. Vickery et al. 2000; Holmes & Oliver 2000). To assess the wind and rain losses for housing, the hazard modelling needs to account for the simultaneous occurrence of extreme wind and associated rainfall. Event-based hurricane models capture the wind speed and rainfall intensity during cyclonic windstorms (e.g. Pita et al. 2012; Mudd et al. 2016) and have been applied to the risk assessment for houses in the US (e.g. Pita et al. 2012; Johnson et al. 2018; Pant & Cha 2019). However, there is a lack of hazard models for rainfall associated with non-cyclonic extreme winds.

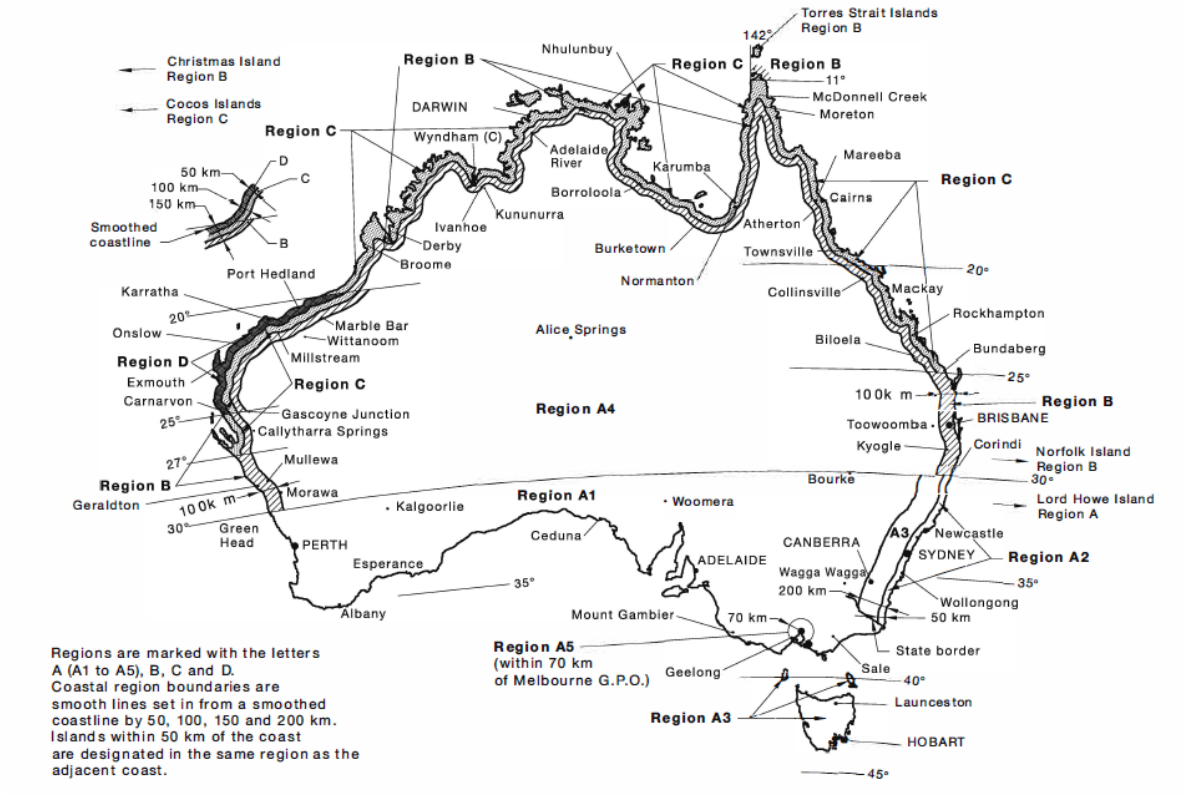

Figure 1.1 Wind regions of Australia (AS/NZS 1170.2 2011).

The wind damage assessment produces fragility/vulnerability curves for housing components that expresses the extent of wind damage as a function of wind speed. The empirical vulnerability curves are conventionally used in insurance industries and the

application may have limitations due to a lack of extensive historical damage data at various geographical locations. Engineering-based fragility/vulnerability models (e.g. Rosowsky & Ellingwood 2002; Lee & Rosowsky 2005) have been increasingly advocated (Walker 2011) as it utilizes the scientific knowledge from many research areas (e.g. wind engineering, structural reliability and mechanics) to achieve more rational and reliable predictions. The engineering-based approach is also capable to provide detailed damage assessment for housing components, which facilitates the decision analysis for wind risk mitigation and climate adaptation.

It has been widely acknowledged that the occurrence of human error during design and construction may significantly reduce the reliability of structures (Ellingwood 1987). Post-damage observations reveal that construction error may largely increase housing vulnerability under wind hazards (Ginger et al. 2010; Yazdani et al. 2010; Smith et al. 2016). Wind damage tend to initiate on defective house components that leads to load redistribution to adjacent components and may trigger a cascading failure of the structural system. Construction defects are common for residential construction, the effects of which have not been accounted for in most reliability/fragility assessments. Figure 1.2 shows an example of construction defects in roof connections (screws for roof cladding fastener and nails for truss-to-wall connections) of Australian contemporary houses.

The subsequent rainwater intrusion after the wind damage incurs losses to building interior and contents. Rainwater penetration through gaps and cracks in the undamaged building envelope has also been commonly reported in post-damage surveys (e.g. Henderson & Ginger 2008; Henderson et al. 2017). Figure 1.3 shows an example of building interior damage due to rainwater intrusion through roof breaches. The semi-empirical wind-driven rain (WDR) model and numerical analysis using computational fluid dynamics (CFD) are two options for the rainwater intrusion evaluation (e.g. Dao & van de Lindt 2010; Pita et al. 2012; Baheru et al. 2015). The CFD approach provides a more detailed assessment of WDR at a price of greatly increased complexity and cost in both modelling and computation. The semi-empirical WDR model provides a convenient and fast evaluation of rainwater intrusion, and its accuracy can be improved with more evidence from numerical analysis, experiments and field monitoring.

Loss estimation typically uses an assembly-based approach (e.g. Porter et al. 2001; HAZUS 2014; Hamid et al. 2010; Stewart et al. 2018). The entire house is divided into components/ subassemblies based on specific building details. The loss of each individual

housing components is obtained based on the damage state of the component. Then the total loss is equal to the sum of repair or replacement costs of every housing components. Empirical loss functions are commonly adopted to relate the damage states of individual housing components with the loss ratios (e.g. HAZUS 2014; Stewart et al. 2018).

(a) Missing screw fasteners on metal roof cladding (photo by Hao Qin).

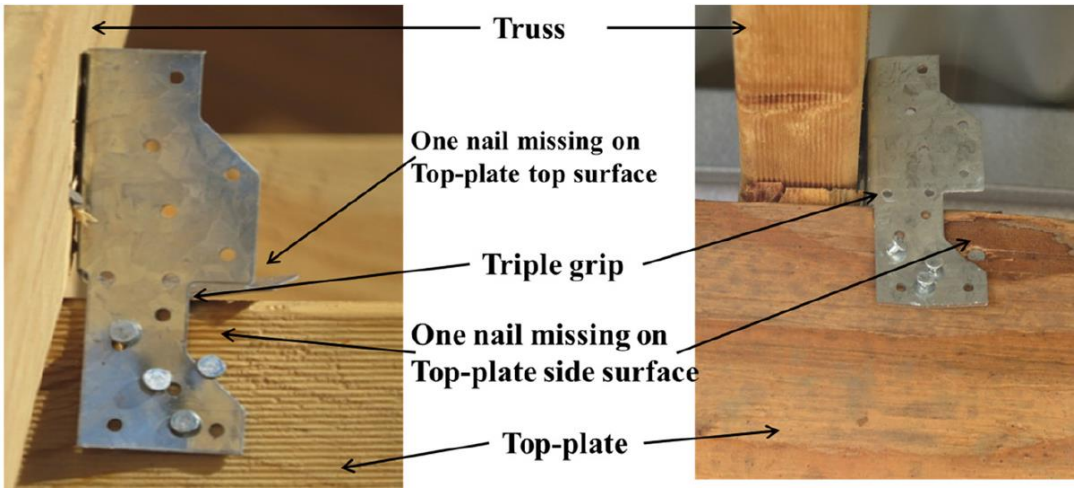

(b) Missing nails in triple grip truss-to-wall connections (photo from Satheeskumar et al. 2016).

Figure 1.2 Construction defects in roof connections of Australian contemporary houses.

Figure 1.3 Ceiling damage caused by rainwater intrusion during the Brisbane windstorm in 2008 (Leitch et al. 2009).

A risk mitigation or climate adaptation measure for housing reduces economic risks associated with extreme winds at a mitigation/adaptation cost. Cost-benefit analysis is often required to assess the potential benefits and costs of a risk mitigation or climate adaptation measure to ensure money is well spent. 'Business as usual' is preferred if costs overwhelm benefits, and the optimal risk mitigation or climate adaptation measure can be determined by comparing the net benefits/returns of different mitigation/adaptation measures. Such risk-based decision approach for the selection of optimal housing mitigation/adaptation measures is equivalent to either maximizing the expected life-cycle return or minimizing the expected life-cycle cost, which is economically efficient and adequate for risk-neutral decision-makers. However, this approach only considers the mean of life-cycle return or cost, and fails to capture the associated uncertainties by ignoring other statistical moments (e.g. variance, skewness, etc.). Distinct risk attitudes of decision-makers (e.g. risk-seeking, risk-averse) are also not taken into account. To this end, more work is needed to incorporate risk preferences, and enable the decision-making under uncertainty for wind hazard mitigation and climate adaptation.

1.2 Objectives and Research Significance

This study aims to develop a probabilistic risk assessment (PRA) method to evaluate economic losses for Australian contemporary housing in Brisbane and Melbourne subjected to non-cyclonic windstorms. Decision analysis is subsequently conducted based on the PRA results to select optimal risk mitigation or climate adaptation measures. The outputs of this

study pave the way towards a more resilient residential community under wind hazards. Specifically, the major components in this thesis include:

1) A probabilistic hazard model for extreme wind and associated rainfall based on meteorological data;
2) A reliability-based fragility method to assess wind damage to metal-roof cladding, timber roof trusses and windward windows;
3) A construction defect model that is incorporated into the reliability-based fragility assessment to examine the effect of construction error on the wind damage to roof;
4) A semi-empirical rainwater intrusion model to evaluate the amount of rainwater entering from breaches and gaps in the building envelope;
5) Assembly-based loss estimation for housing components/subassemblies based on empirical loss functions, cost data and engineering judgement;
6) A PRA for metal-clad contemporary houses using a Monte Carlo simulation, which integrates the hazard model for extreme wind and associated rainfall, wind damage/fragility assessment, rainwater intrusion and loss estimation;
7) A cost-benefit analysis of the proposed wind risk mitigation or climate adaptation measures for metal-clad contemporary houses. The mitigation/adaptation measures include: (i) strengthening roof cladding, (ii) installing window shutters, (iii) increasing window resistances, and (iv) using water-resistant materials for building interior;
8) Application of in-depth decision analysis approach to explicitly capture the magnitude of uncertainty and risk preferences involved in the decision-making for wind risk mitigation and climate adaptation;
9) Implications of the research outputs for homeowners and insurers including the devise of incentives to motivate homeowners to install window shutters.

The primary contributions of this study are i) a PRA method to evaluate economic losses incurred by wind and rainfall damage for housing subjected to non-cyclonic windstorms, and (ii) the application of decision analysis approaches to explicitly account for the magnitude of uncertainty and risk preferences involved in the decision-making for wind risk mitigation and climate adaptation. Specifically, this study has made attempts to fill the following research gaps:

1) Probabilistic modelling and statistical inferences for rainfall associated with non-cyclonic windstorms;
2) Probabilistic characterizations of wind damage to metal roof cladding and timber roof trusses of Australian contemporary houses accounting for the spatially varying wind uplift pressures, internal pressure evolution with increasing damage to the building envelope and progressive failures of roof connections through a Monte Carlo simulation and a finite element approach;
3) Modelling of construction defects for roof cladding and trusses that systematically integrates engineering judgement, human reliability analysis techniques and limited observed defect data through a Bayesian approach;
4) Estimation of economic losses to metal-clad contemporary houses incurred by extreme wind and associated rainfall in non-cyclonic regions of Australia;
5) Identification of appropriate risk mitigation and climate adaptation measures for Australian contemporary houses through a cost-benefit analysis with the consideration of climate change impacts;
6) Explicit inclusion of risk preferences and magnitude of uncertainty in wind mitigation decision-making through a variety of decision models including superquantile, utility theory and almost stochastic dominance.
7) Proposed new application of the descriptive decision models in behaviour economics in devising incentives for homeowners to implement mitigation measures for the protection of their houses, which potentially leads to a significant reduction of insurance losses and an improvement for the resilience of residential community against wind hazards.

1.3 Risk Assessment and Decision Support Framework

1.3.1 Risk formulation

The risk from extreme wind events is expressed as (Stewart 2015)

$$E(L) = \sum \Pr(C)\Pr(H|C)\Pr(DS|H)\Pr(L|DS)\,L \tag{1.1}$$

where $\Pr(C)$ is the annual probability that a specific climate scenario will occur, $\Pr(H|C)$ is the annual probability of a wind hazard conditional on the climate, $\Pr(DS|H)$ is the probability of a damage state conditional on the hazard (also known as fragility), $\Pr(L|DS)$ is the conditional probability of a loss given the occurrence of damage, and L is the loss or

consequence if full damage occurs, Pr($DS|H$) is the probability of a damage state conditional on the hazard (also known as fragility), Pr($L|DS$) is the conditional probability of a loss given occurrence of the damage, and L is the loss or consequence if full damage occurs. The wind hazard is typically represented by the wind speed, which can be further extended to include other environmental hazards (e.g. heavy rainfall, windborne debris, storm surge, etc.) commonly associated with or induced by the extreme wind event. If the loss refers to a monetary loss, then $E(L)$ represents an economic risk. The summation sign in Eq. (1.1) refers to the summation of a number of possible climate scenarios, hazards, damage states and losses. If the probability that a specific climate scenario will occur, Pr(C) is too unreliable, then a scenario-based analysis where climate scenario probability is decoupled from Eq. (1.1) is typically adopted for risk assessment and decision analysis (e.g. Stewart 2015; Stewart et al. 2018).

1.3.2 Risk-based Decision-Support Framework

The risk assessment provides the basis for decision-making of risk mitigation and climate adaptation. A risk-based decision-support framework derived from Stewart & Deng (2015) is illustrated in Fig. 1.4. The methods and models proposed in this study contribute to the development of every components in this framework. The details of the components in this framework are described herein:

1) Climate modelling Pr(C): stochastic models used to predict climate variables in the future. The climate change impacts on wind hazards are projected using climate models. A review of various climate models and their usage is given in CSIRO & BOM (2015). Although there are many models available for the prediction of climate variables in the future, the trend of climate change is still not well understood, and the projections yielded by different models are often contradicted. This makes the modelling of Pr(C) too unreliable and uncertain, and therefore, in this study, the climate change impacts on wind hazards are only simply investigated by a scenario-based approach.
2) Hazard modelling Pr($H|C$): probabilistic modelling of wind hazard and other associated environmental hazard (e.g. rainfall, storm surge) conditional on a given climate. It may require joint probability models for hazard variables such as wind speed, windstorm duration and rainfall intensity (e.g. Mudd et al. 2016).

3) Engineering models: engineering modelling of structural loading, resistances and response for housing elements and systems of interest. It may involve various materials, design and construction methods in engineering models.
4) Damage modelling (fragility) Pr($DS|H$): probabilistic and reliability modelling to predict the extent of damage conditional on a given hazard (e.g. separate or joint occurrence of wind, rainfall, windborne debris) based on the engineering model. Hazards are decoupled in the damage assessment, and the damage states are typically expressed as a function of all likely magnitudes or intensities of the hazard (e.g. wind fragility expresses housing damage state as a function of wind speed).
5) Loss and exposure Pr($L|DS$): likelihood of direct and indirect loss or consequence conditional on the damage state. Loss L is direct and indirect loss or consequence if full damage occurs for existing exposure and future exposure under a changing climate.
6) Existing risks: stochastic methods to assess economic risks for housing by integrating 1) to 5). The risk assessment results will identify the critical attributes that lead to a vulnerable house (e.g. materials, design and construction practice for housing components, locations and exposure for the house).
7) Risk mitigation and climate adaptation measures: use of new materials, design and construction methods to improve the resilience of housing to wind hazards and climate change.
8) Benefits, co-benefits and costs: the major benefits from the risk reduction due to improved wind resistance and decreased housing vulnerability. The co-benefits may include reduced losses to other hazards, increased energy efficiency, etc. The mitigation/ adaptation costs are the expenses directly and indirectly related to the mitigation/adaptation measures.
9) Risk-based decision analysis: decision-making for wind risk mitigation and climate adaptation. The cost-effectiveness of a mitigation/adaptation measure can be evaluated through a cost-benefit analysis. The selection of optimal mitigation measures is typically based on the maximum expected net benefit/return or the minimum expected life-cycle cost criteria. Explicit inclusion of risk preferences and magnitude of uncertainty in decision-making can be achieved by using more advanced decision analysis approaches.

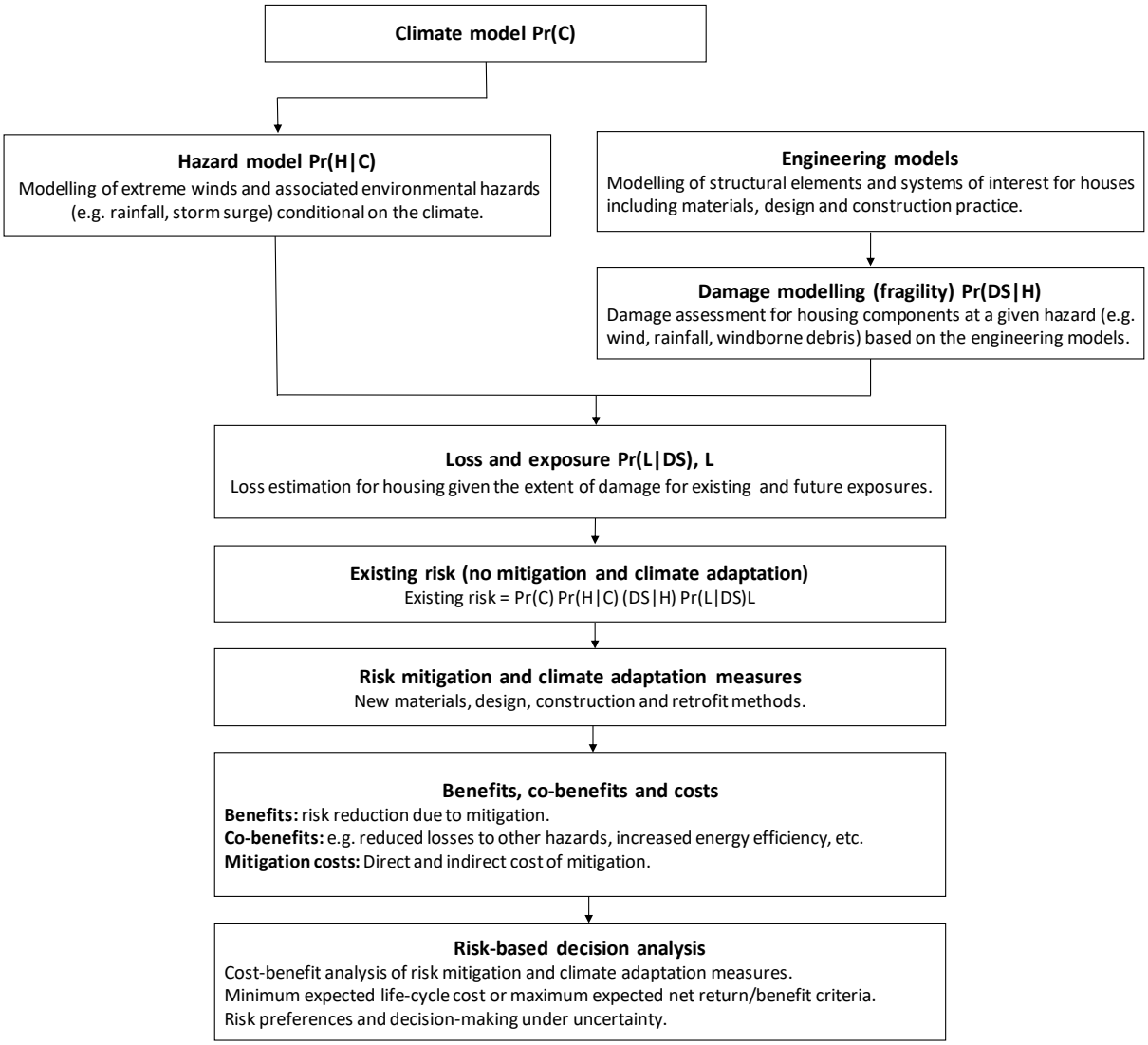

Figure 1.4. Risk-based decision framework of wind risk mitigation and climate adaptation.

1.4 Organization

This thesis consists of eight chapters. The subsequent seven chapters are summarized briefly in the following:

Chapter 2 presents a literature review to describe the state-of-the-art research studies in the risk management of wind hazard for low-rise residential buildings. The literature review includes topics regarding wind hazard modelling, wind damage/fragility assessment, rainwater intrusion, loss estimation, risk assessment and risk-based decision-making for wind hazard mitigation and climate adaptation.

Chapter 3 presents a reliability-based fragility method to assess the wind damage to metal roof cladding, timber roof trusses and windward windows for representative contemporary houses in Brisbane and Melbourne. The fragility is expressed as a function of gust wind

speed. A Monte Carlo Simulation analysis in conjunction with a finite element method is developed to conduct the fragility assessment, which enables the probabilistic characterization of spatially variable wind loads, structural resistances, structural response, load redistribution and failure progression.

Chapter 4 presents a systematic approach to model construction defects in roof connections, which integrates engineering judgment, human reliability analysis technique and limited observed defect data through a Bayesian approach. The effect of construction defects on wind fragility for metal roof cladding and timber roof trusses is then examined.

Chapter 5 presents a probabilistic risk assessment framework to calculate annual expected losses for metal-clad contemporary houses in Brisbane and Melbourne subjected to non-cyclonic windstorms, which includes hazard modelling for extreme wind and associated rainfall, reliability-based wind damage assessment, rainwater intrusion evaluation and economic loss estimation. The effect of construction defects on annual risks is also examined.

Chapter 6 presents a risk-based cost-benefit analysis of wind risk mitigation or climate adaptation measures for contemporary houses in Brisbane and Melbourne. Four mitigation/adaptation measures are proposed, and the cost-effective alternatives are selected based on the mean net present values (NPVs). The climate change impact on the cost-effectiveness of mitigation/adaptation measures is also examined.

Chapter 7 presents several approaches for decision analysis that can be used to explicitly account for risk preferences and the magnitude of uncertainty involved in the risk-based decision-making for wind risk mitigation and climate adaptation for housing under non-cyclonic extreme winds. A potential application of the descriptive decision models in devising incentives for homeowners to install window shutters is described.

Chapter 8 summarizes the methods and models developed in this study as well as the key findings of the results. Recommendations for future research are also presented.

CHAPTER 2. LITERATURE REVIEW

2.1 Wind Hazard Models

Many wind hazard models simulating intensities and tracks for tropical cyclones or hurricanes have been reported in the literature (e.g. Georgiou 1985; Vickery et al. 2000; Huang et al. 2001a; Powell et al. 2005; Vickery et al. 2009; Mudd et al. 2016), which can be applied in the wind damage assessment and loss estimation for residential buildings (e.g. Vickery et al. 2006a; Vickery et al. 2006b; Pinelli et al. 2011; Pita et al. 2012; Johnson et al. 2018; Pant & Cha 2019). Wang & Rosowsky (2017) applied an event-based hurricane model to assess regional losses to residential buildings in the US. Climate change impacts on hurricane size, wind speed and rainfall intensity were included in this study. Pita et al. (2012) modelled the wind speed and rainfall intensity associated with hurricanes to evaluate the wind damage to the building envelope and rainwater damage to building interior and contents. Pant & Cha (2019) used the same method by Pita et al. (2012) to assess hurricane-induced losses for residential buildings with an emphasis on the climate change impacts on hurricane wind and rainfall.

Extreme wind speed in non-cyclonic regions is typically modelled by the extreme value distributions (e.g. Simiu & Scanlan 1986; Palutikof et al. 1999). The generalized extreme value distribution and the method of 'peaks over threshold' using the generalized Pareto distribution (e.g. Palutikof et al. 1999; Holmes & Moriarty 1999; Holmes 2002; Wang et al. 2013) are widely used to model the extreme wind speed corresponding to various return periods. However, there is a lack of hazard models for rainfall simultaneously occurred with non-cyclonic windstorms. The evaluation of rainwater damage to buildings subjected to non-cyclonic extreme winds has received little attention or only been implicitly accounted for in the literature.

2.2 Wind Damage Assessment for Houses

2.2.1 North American houses

North American houses are typically timber framed with asphalt roof covers, timber roof sheathing/decking fastened by nails and wood or unreinforced masonry walls. The timber roof trusses are typically connected to wall top plate via truss-to-wall connections using toe nails or hurricane clips. Hurricanes and tornados are the major causes of housing damage in the US.

Many research studies have been reported in the literature regarding reliability, fragility and vulnerability assessment for housing in North America subjected to hurricanes (e.g. Rosowsky & Cheng 1999; Unanwa et al. 2000; Rosowsky & Ellingwood 2002; Pinelli et al. 2004; Ellingwood et al. 2004; Lee & Rosowsky 2005; Li & Ellingwood 2006; van de Lindt & Dao 2009; Lin et al. 2010; Rocha et al. 2011; Gavanski et al. 2014; Hong & He 2015). Unanwa et al. (2000) was an earlier paper that attempted to comprehensively model the wind damage to individual building components in a probabilistic manner. The correlations between failures of different building components were also taken into account by using fault trees. The confidence intervals of damage level for each building category were characterized as a function of wind speed. The simplifications in this study are that the randomness of wind loads was not considered, and large amount of engineering judgement was used to estimate the failure probabilities of building components as well as their interdependencies. This study provides a significant starting point for the development of reliability and engineering-based wind vulnerability models.

Driven by the goal to achieve performance-based design of structures (Rosowsky & Ellingwood 2002), extensive studies have been reported in the literature focusing on the fragility assessment for timber-framed structures in hurricane-prone areas of the US. The failures of roof cover and roof sheathing panels are typical wind damage during hurricanes and draw much attention from researchers (e.g. Ellingwood et al. 2004; Lee & Rosowsky 2005; Li & Ellingwood 2006; van de Lindt & Dao 2009; Rocha et al. 2011). Lee & Rosowsky (2005) conducted a fragility assessment for roof sheathing under wind uplift loading. The fragility of the whole roof was calculated with the wind loading and structural resistance statistics obtained from building codes and experimental tests. Five typical residential structures with different roof shapes, exposures and nail types were used to illustrate their fragility method. van de Lindt & Dao (2009) provides a more detailed assessment of structural response by incorporating a finite element (FE) method to model the nails in roof panel considering both axial and bending effects into their fragility analysis, which enables the evaluation of the statistics of panel uplift capacities under various nailing schedules. The FE method also captures the upward deflection of a panel edge (Dao & van de Lindt 2008) under wind uplift pressure, which allows for further evaluation of rainwater penetration (Dao & van de Lindt 2010) during hurricanes. Rocha et al. (2011) and He & Hong (2012) are another two studies accounting for detailed nail behaviour under wind uplift using FE approach, and the temporal variable wind pressures are also considered in

these studies. The wind damage to wall structures and roof-to-wall connections has been reported in research studies such as Ellingwood et al. (2004), van de Lindt & Rosowsky (2005), Li & Ellingwood (2006), van de Lindt & Dao (2009) and Amini & van de Lindt (2013). More recently, many studies have developed detailed fragility/vulnerability models to assess the damage to wall cladding, windows and doors caused by windborne debris (e.g. Lin et al. 2010; Herbin & Barbato 2012; Grayson et al. 2013). Apart from extensive US studies, Gavanski et al. (2014) and Hong & He (2015) conducted reliability analysis for roof sheathing of Canadian houses subjected to wind suctions. The construction type and method of Canadian houses are similar with those in US. Zhang et al. (2014) evaluated the vulnerability of tile roof for typical Japanese residential buildings exposed to typhoon risk. The windborne debris modelling, wind directionality and shielding effect were incorporated in their study.

2.2.2 Australian houses

Metal roof cladding and tiles are commonly used for houses in Australia. The timber roof trusses are typically connected to wall top plate via truss-to-wall connections using triple grips or straps. Brick veneer or timber weatherboards are typically used for exterior walls. Tropical cyclones and non-cyclonic windstorms such as severe thunderstorms and synoptic windstorms are the major causes of housing damage in Australia. Figure 2.1 shows typical timber-frame contemporary houses in Australia with complex hip-roof geometries.

With distinctive construction methods and practice, it may not be appropriate to apply the fragility/vulnerability models developed for houses in US or other countries directly to houses in Australia. Engineering-based fragility/vulnerability models for Australian housing are scarce in the literature but begin to draw more attention in the recent decade. Henderson & Ginger (2007) developed a reliability-based vulnerability model for a set of structural components and connections of an Australian high-set house. The spatial distribution of wind pressures was not considered in their study and the complex failure mechanism of roof sheeting was simplified by assuming a series system failed by pullout or pullover of the first fastener. Jayasinghe & Ginger (2011) presented a vulnerability analysis of roof connections for contemporary houses built in cyclonic regions of Australia. Their analysis was only conducted for these connections at critical locations without accounting for the overall roof damage. Sivapathasundaram & Mahendran (2016) developed fragility curves for localised pull-through failures of steel roof battens where the structural capacities

of batten to truss/rafter connections were evaluated from experimental tests. Only the first roof batten pull-though failure was considered in their fragility analysis and hence structural redundancy of the entire roofing system may be underestimated. Stewart et al. (2018) proposed a reliability-based fragility model to evaluate the extent of roof cladding damage under spatially varying wind pressures. The progressive failure of roof connections was taken into account by using load redistribution path based on engineering judgement. Konthesingha et al. (2015) and Stewart et al. (2016) have also applied similar approaches to evaluate wind fragility for low-rise industrial buildings in Australia.

Figure 2.1 Typical timber-frame contemporary houses in Australia (photo by Mark Stewart).

2.3 Construction Defects

The modelling of construction defects in housing is a challenging task due to the complex mechanism of human error and a lack of construction defect data. Only a few studies attempt to include construction defects in the reliability/fragility assessment for houses under extreme wind (van de Lindt & Dao 2010; Hong & He 2015; Stewart et al. 2018). van de Lindt & Dao (2010) examined the effect of missing nails on the wind fragility of timber roof

sheathing panels that are commonly used in North American houses. A scenario-based approach was adopted by assuming various missing nail patterns. Hong & He (2015) investigated the effect of missing and/or misaligned nails on the reliability of Canadian timber roof sheathing panels under wind uplift pressure. A constant defect rate was obtained from the construction of a full-scale test house built by students in the laboratory. Stewart et al. (2018) incorporated a preliminary probabilistic model of construction defects into the fragility assessment for metal roof sheeting failure due to extreme wind based on subjective information and defect data inferred from Hong & He (2015). Therefore, most studies considering construction defects rely on a scenario-based approach or subjective judgement for the defect rates. There is a need for a systematic approach to model construction defects.

2.4 Rainwater Intrusion

Rainwater entering houses during a windstorm can damage building interior and contents. The semi-empirical wind-driven-rain (WDR) model and numerical modelling using computational fluid dynamics (CFD) are used to assess the rainwater intrusion through the breaches and gaps in the building envelope. The semi-empirical wind-driven-rain (WDR) models (e.g. Straube & Burnett 2000; Blocken & Carmeliet 2004; ISO 2009) have initially been developed for the assessment of moisture, hygrothermal and durability of building facades. The development of the semi-empirical relationships is based on experimental/field observations that the amount of WDR depositing on buildings increase approximately proportionally with wind speed and rainfall intensity (Blocken & Carmeliet 2004). The formulation of semi-empirical WDR models have some theoretical bases with model parameters to be determined based on experimental and/or field data (Straube & Burnett 2000; Blocken & Carmeliet 2004). Numerical modelling using computational fluid dynamics (CFD) provides an alternative approach for more detailed quantification of WDR (e.g. Choi 1993; Choi 1994a; Blocken & Carmeliet 2002). Dao (2010) and Dao & van de Lindt (2010) employed the CFD approach by Choi (1993) to assess the rainwater penetration via timber roof sheathing panels. Because of the computationally intensive procedure involved in their CFD approach, only the impinging rain on one roof corner was explicitly calculated, and rainfall on other roof areas were estimated based on the calculated values at the roof corner (Dao 2010). The semi-empirical WDR models were adopted by Pita et al. (2012) and Baheru et al (2015) to evaluate rainwater intrusion through roof and wall openings as well as building deficiencies and cracks. The pioneering study by Pita et al.

(2012) proposed the method to assess rainwater intrusion for houses in the US subjected to hurricanes based on event-based hurricane wind and rainfall models as well as the semi-empirical WDR model. Several model parameters in Pita et al. (2012) are assigned with assumed values which are left for estimation and calibration by experiments. Baheru et al. (2014) and Baheru et al (2015) further conducted both wind tunnel and full-scale tests to estimate these parameters in the WDR model for low-rise residential buildings subjected to hurricanes. Johnson et al. (2018) further extended the method by Pita et al. (2012) to account for the effect of varying wind directions during hurricanes. Pant & Cha (2019) also extended the method by Pita et al. (2012) by considering climate change impact on wind speed and rainfall intensity in the event-based hurricane models. These studies are all for hurricanes and US houses with simple gable roofs. A modified method is needed for Australian contemporary houses subjected to non-cyclonic windstorms with metal roof cladding and complex hip-roof geometries.

2.5 Loss Estimation and Risk Assessment

Loss estimation is typically based on empirical loss functions, cost data, insurance loss data and expert opinion (e.g. Huang et al. 2001b; Stewart 2003; Vickery et al. 2006b; Hamid et al. 2010; van de Lindt & Dao 2012; Barbato et al. 2013; Wang & Rosowsky 2017). The monetary loss of residential buildings resulting from wind and rainfall damage is typically classified into two categories, namely, structural (e.g. roof truss and wall, etc) and non-structural (e.g. building envelope, interior and contents) losses. Loss estimation is not an exact science and highly dependent on regional building inventory and cost data. An assembly-based approach (e.g. Porter et al. 2001; HAZUS 2014; Hamid et al. 2010; Stewart et al. 2018) that aggregates losses to individual building components is widely used in loss estimation. Vickery et al. (2006b) estimated the loss of structure components and building contents caused by hurricane in US using empirical loss functions. The indirect loss from additional living cost was also taken into account in their study. van de Lindt & Dao (2012) proposed a general framework incorporating the losses from individual damageable components during hurricanes. Their methodology was illustrated by examining both structural and non-structural losses for a wood-frame house containing four rooms. A detailed assembly-based economic loss estimation is still lacking in the literature for Australian houses.

A full probabilistic risk assessment for housing integrates the hazard and vulnerability models. The majority of studies have focused on the hazard modelling for hurricanes, and fragility and vulnerability models for houses subjected to hurricane winds. The vulnerability models in the literature mostly fall into two categories: empirical vulnerability functions to assess risks for residential communities, and detailed fragility/vulnerability models for individual buildings that are based on structural performance and reliability. For example, Huang et al. (2011b) assessed annual expected hurricane losses for residential buildings in the US using empirical vulnerability functions developed based on insurance loss data. Li & Stewart (2011) and Stewart et al. (2014) used empirical vulnerability models to assess economic losses for Australian houses subjected to tropical cyclones. Wang & Zhang (2018) evaluated losses due to tropical cyclones for buildings in Hong Kong based on historical data considering climate change impact on the intensity and frequency of cyclone winds.

Florida Public Hurricane Loss Model (FPHLM) (Hamid et al. 2010; Hamid et al. 2011; Pinelli et al. 2011) and Hazards U.S. Multi-Hazard (HAZUS-MH) hurricane model (Vickery et al. 2006a; Vickery et al. 2006b) are two major comprehensive loss prediction models for hurricanes that are based on structural performance and reliability. The FPHLM consists of three major model components including an atmospheric science component, a vulnerability analysis component and a loss prediction component. The atmospheric science component utilizes knowledge and methods in meteorology to model the wind field of hurricanes for many Florida zip codes. The vulnerability component provides engineering-based vulnerability curves by using Monte Carlo simulations for various structural types (e.g. timber or masonry) and geographical locations in Florida. The loss prediction component evaluates the expected annual insurance loss for building structure, building interior and contents as well as additional living expenses based on the vulnerability curves. The HAZUS-MH hurricane model is comprised of five components, namely, the hurricane hazard, terrain, wind loading, physical damage and loss models. The hurricane hazard model adopts the approach described in Vickery et al. (2000) to model the intensity, track and wind field of hurricanes. The terrain model provides the ground surface roughness evaluated for different surface types. Unlike FPHLM where wind loading is evaluated based on building standards (e.g. ASCE7 2010), HAZUS-MH has modelled the pressure coefficients for different building components based on large amount of wind tunnel observations. The physical damage model assesses the wind fragility for building components using structural reliability methods, and a detailed mechanics-based model for windborne debris is also

included. The loss prediction model uses empirical loss functions, insurance loss data and engineering judgement to estimate the wind-induced economic losses.

Other examples for risk assessment based on structural reliability and performance include Li & van de Lindt (2012) and Unnikrishnan & Barbato (2017). Li & van de Lindt (2012) conducted risk assessment for residential buildings subjected to hurricanes using engineering-based fragility/vulnerability models. Unnikrishnan & Barbato (2017) employed performance-based hurricane engineering framework to assess annual losses for low-rise residential buildings in the US. There is still a lack of risk assessment for Australian houses using engineering-based fragility/vulnerability models to account for detailed structural reliability and performance, which needs to account for spatially varying wind pressures and damage progression of various structural components.

2.6 Risk-based Decision-making

The cost-benefit analysis or life-cycle cost (LCC) analysis are widely used to evaluate the cost-effectiveness of wind risk mitigation or climate adaptation measures for housing (e.g. Stewart 2003; Li & Ellingwood 2009; Li 2010; Torkian et al. 2014; Unnikrishnan & Barbato 2016; Orooji & Friedland 2017). The selection of optimal mitigation measures is to maximize the expected net benefit/return or minimize the expected LCC. In the recent decade, the cost-effectiveness of mitigation/adaptation measures under a changing climate, has been assessed for housing by many research studies (e.g. Li & Stewart 2011; Bjarnadottir et al. 2011; Stewart et al. 2014; Stewart & Deng 2014; Stewart 2015), and the potential climate change impacts on the cost-benefit analysis were identified and quantified in these studies. The decision analysis for wind risk mitigation based the maximum expected net benefit/return or the minimum expected LCC fails to explicitly account for the magnitude of uncertainty involved in the risk-based decision-making and the risk attitudes of different decision-makers. The expected utility theory (von Neumann & Morgenstern 1944), cumulative prospect theory (Tversky & Kahneman 1992) and stochastic dominance theory (Hadar & Russell 1969; Hanoch & Levy 1969) are decision theories originally developed in the area of economics and finance. These theories have been applied to the decision contexts of civil engineering (e.g. seismic design, operations of nuclear plants, design of energy pipelines, prevention of terrorist attacks and determination of maintenance schedules for ship structures) by many research studies (e.g. Goda & Hong 2006; Goda & Hong 2008a; Stewart et al. 2011; Zhou & Nessim 2011; Cha & Ellingwood 2013; Mahsuli

& Haukaas 2018; Gong & Frangopol 2019), however, only few are available for wind hazard mitigation (Cha & Ellingwood 2014; Cha 2018). Cha & Ellingwood (2014) adopted the cumulative prospect theory to examine the risk preferences reflected in local building code communities in the US, and found that there is a higher degree of risk-acceptance towards wind hazards than earthquakes. Cha (2018) used the cumulative prospect theory to investigate the effect of risk perceptions on hurricane risks under a changing climate. The prospect theory (Kahneman & Tversky 1979) and its modified version the cumulative prospect theory (Tversky & Kahneman 1992) are representative models in behaviour economics to study human behaviour in decision-making. While normative decision-making based on expected utility aims to achieve rationality in the long term, cautions should be taken in the application of prospect theory in civil engineering decision-making as it may lead to systematic biases under bounded rationality. There is a need to explicitly capture the magnitude of uncertainty and risk preferences involved in the decision-making for wind hazard mitigation by applying appropriate decision models.

CHAPTER 3. RELIABILITY-BASED WIND DAMAGE ASSESSMENT FOR ROOF SYSTEM AND WINDOW

3.1 Introduction

The prediction of housing damage caused by extreme winds plays an important role in the development of optimal risk mitigation and climate adaptation measures (e.g. Torkian et al. 2014; Stewart 2016; Stewart et al. 2018). A wind fragility function typically expresses the damage state as a function of wind speed, which offers a convenient and effective metric to forecast the extent of wind damage (e.g. Lee & Rosowsky 2005; Li & Ellingwood 2006; Henderson & Ginger 2007; Stewart et al. 2018), and therefore facilitates the risk assessment and mitigation for housing under extreme winds. Roof cladding and trusses are among the most vulnerable components of timber-frame houses under wind uplift pressure, the failure of which may incur significant economic losses for housing and impose safety threats on building occupants. Post-damage surveys (e.g. Walker 1975; Leitch et al. 2009) have indicated that roof damage typically initiates at and propagates through failures of roof connections that mainly include cladding-to-batten (CTB), batten-to-rafter/truss (BTR) and rafter/truss-to-wall (RTW) connectors. Although the reliability analysis of individual roof components is relatively straightforward, a comprehensive fragility modelling for the roof system is more challenging, and requires stochastic characterizations of spatially varying wind uplift pressure, component resistances, structural response and load redistribution after the failure of one or more roof connections. Windows are a major component of the building envelope. Window damage by high wind pressure or windborne debris has been commonly reported in post-damage surveys (e.g. Henderson & Ginger 2008; Leitch et al. 2009; Ginger et al. 2010), which may lead to significant damage to building interior and contents due to rainwater intrusion. Window breakage may also intensify the internal pressurisation leading to more roof damage. Wind fragility for windows is thus important for the damage assessment and loss estimation.

There have been much research focusing on the reliability/fragility assessment for timber roof sheathing and toe-nail RTW connectors typically used on houses in hurricane-prone regions of North America (e.g. Rosowsky & Cheng 1999; Pinelli et al. 2004; Ellingwood et al. 2004; Lee & Rosowsky 2005; Vickery et al. 2006b; Li & Ellingwood 2006; Rocha et al. 2011; Gavanski et al. 2014; Gavanski & Kopp 2017). However, only limited reliability-

based fragility models are available for Australian timber-framed houses that are commonly installed with metal roof sheeting, steel battens and framing anchors (e.g. triple grip) for RTW connectors (e.g. Henderson & Ginger 2007; Jayasinghe & Ginger 2011; Sivapathasundaram & Mahendran 2016; Stewart et al. 2018). In most of these studies (Henderson & Ginger 2007; Sivapathasundaram & Mahendran 2016), the first connection failure was set as the system limit state similar to many studies for timber roof sheathing panel on North American houses (e.g. Rosowsky & Schiff 1996; Lee & Rosowsky 2005) or only individual roof components at critical locations (Jayasinghe & Ginger 2011) are considered in the fragility analysis. Therefore, the progressive failure after the initiation of local damage has been neglected, and the redundancy of roof system may not have been well addressed. Recently, Stewart et al. (2018) developed a fragility model to evaluate the metal roof sheeting loss for Australian contemporary houses, which takes into account the progressive failure of cladding fasteners by using a simplified load redistribution rule based on engineering judgement that 90% of wind load originally undertaken by one failed fastener would be redistributed to adjacent fasteners on the same crest of the corrugated metal roof sheet. However, this redistribution rule may fail to fully capture various load redistribution scenarios involved in the failure progression of connections. The failures of roof trusses and windows were also not assessed by Stewart et al. (2018).

This chapter aims to develop a reliability-based fragility method to evaluate the roof and window damage for metal-clad contemporary houses in non-cyclonic regions of Australia. The roof of a representative contemporary house mainly consists of corrugated metal roof sheets, metal top-hat battens, timber trusses and roof connections. The overloading of CTB, BTR and RTW connectors was deemed to cause the failure of these roof components. The spatially varying wind uplift pressure was probabilistically modelled based on wind loading standards and wind tunnel testing. Connection capacities were obtained from full-scale tests conducted by James Cook University (JCU) in Australia (Satheeskumar et al 2016a, 2016b). As indicated in AS/NZS 1170.2 (2011), windborne debris is less of a concern in non-cyclonic regions of Australia, and only the window damage by high wind pressure is considered in this study. A Monte Carlo Simulation (MCS) analysis in conjunction with a finite element (FE) approach for the roof system were proposed to evaluate the structural response, load redistribution and failure progression of roof connections under the spatially varying wind uplift pressures. The evolution of internal pressure with increasing roof sheeting loss was also taken into account in the fragility analysis. The MCS analysis was

also used to assess the wind fragility for windows. Fragility analyses were carried out for the representative contemporary house built in Brisbane and Melbourne (non-cyclonic regions as classified in Australian wind loading standard) to illustrate the proposed reliability-based fragility method.

3.2 Representative Contemporary House

Residential construction in non-cyclonic regions of Australia comprises of a large portion of metal-clad contemporary houses, which generally have less wind resistance than houses in cyclonic regions of Australia. The wind damage assessment, risk assessment and decision analysis methods developed in this study are illustrated on the representative contemporary house built in suburbs of Brisbane and Melbourne (classified as non-cyclonic regions in AS/NZS 1170.2 2011). The dimension, shape and construction type of the house were determined by field surveys completed by the Cyclone Testing Station (CTS), James Cook University (JCU) (Parackal et al. 2016). The median values of house plans and features from the survey such as footprint dimensions, roof pitch and wall heights were selected to determine the configuration of the representative contemporary house. Figure 3.1 shows the 3D and plan view of the representative one-story house. It is a timber-framed construction with 21.5° timber roof trusses at 600 mm spacings on a complex hip-end roof. Trusses are arranged with standard trusses in the middle part of the roof and jack trusses connected to truncated girder trusses at the hip ends. Roof cladding is 762 mm wide corrugated metal sheeting. Metal top-hat battens are attached to timber roof trusses at 900 mm spacings. The roof connections include cladding-to-batten (CTB), batten-to-rafter/truss (BTR) and rafter/truss-to-wall connectors. Screw fasteners are used for CTB and BTR connectors, and triple grip framing anchors fastened using nails are adopted for RTW connectors. The representative contemporary house includes 1646 cladding-to-batten (CTB), 532 batten-to-rafter/truss (BTR) and 92 rafter/truss-to-wall (RTW) connectors. Figures 3.2 and 3.3 depict the roof connections for the representative contemporary house. Windows are generally horizontal sliding aluminium or timber awning with a brick on edge or terracotta tiled window sill. More details of the representative contemporary house can be found in Parackal et al. (2016).

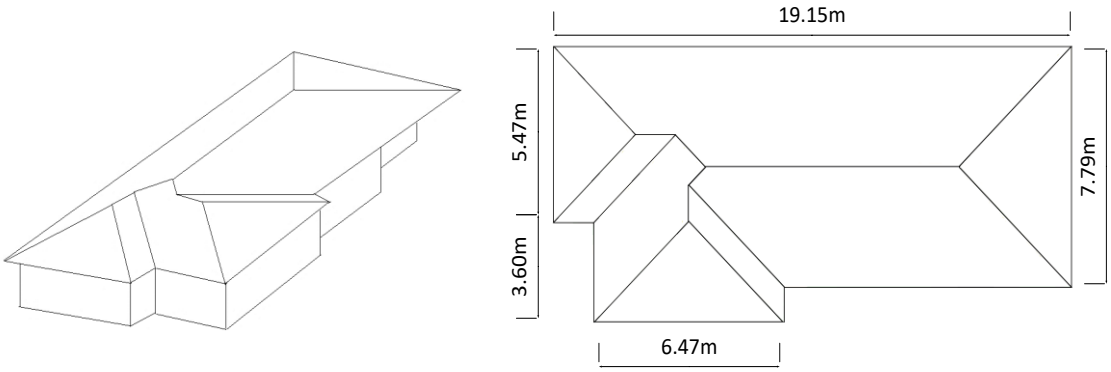

(a) 3D view (b) Plan view

Figure 3.1. One-storey representative contemporary house.

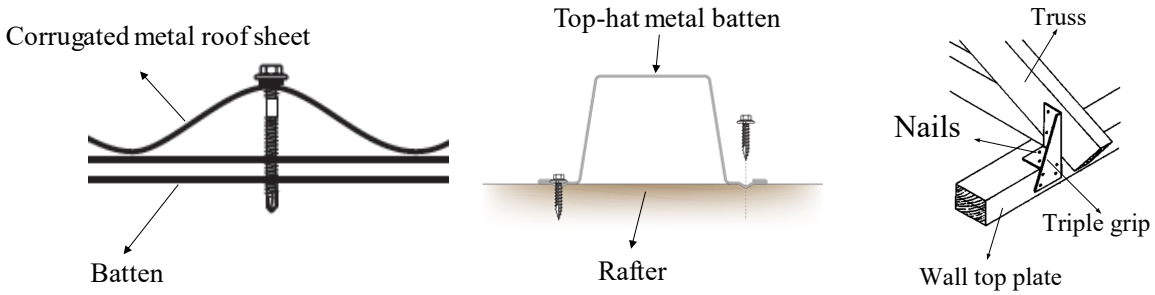

(a) CTB connector (b) BTR connector (c) RTW connector

Figure 3.2. Schematic diagram of the roof connections.

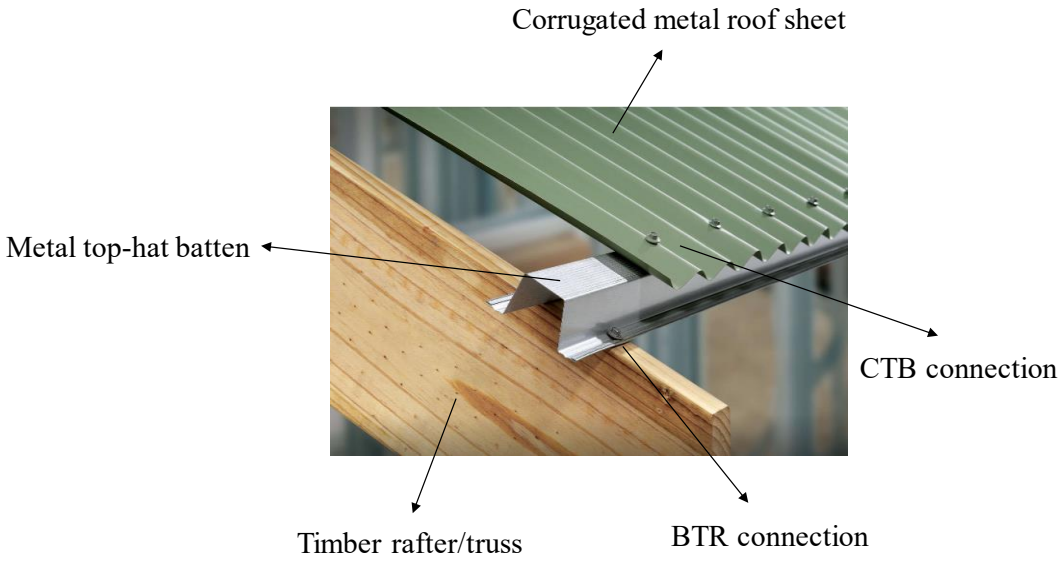

(a) CTB and BTR connections (photo from Stratco 2019).

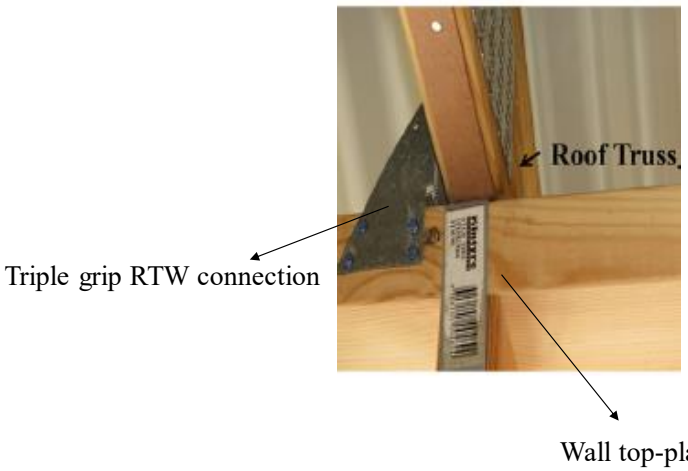

(b) RTW connections (photo from Satheeskumar et al. 2016).

Figure 3.3. Roof connections of the representative contemporary house.

The design of structural members and components for housing subjected to wind loading is based on the design wind classifications specified in AS4055 (2012) for different site conditions. According to AS4055 (2012), most suburban houses in Brisbane have a design wind classification of N2 or N3 excluding those built on the top-third zone of a hill, ridge or escarpment. A higher design wind classification has a higher design wind speed at the roof height. A design wind classification of N1 or N2 is appropriate for most suburban houses in Melbourne. The CTB and BTR connectors are identical for houses in Brisbane and Melbourne, whereas the RTW connectors are different for houses with design wind classifications of N1, N2 and N3. Windows also have different levels of resistance against wind for Brisbane and Melbourne houses with distinct design wind classifications (AS 2047 2014).

3.3 Reliability-based Fragility Method

The fragility of a structural component or system is typically defined as the probability of damage state *DS* conditional on a given hazard *H*. In this study, the damage state for roof is measured by the proportion of the roof sheeting loss and the roof truss failures, and that for window is the likelihood of wind damage. The hazard is corresponding to gust wind speed. The wind fragility for roof is therefore the extent of damage to roof cladding and trusses, R_{loss}, at a given gust wind speed v, expressed as

$$\Pr(DS|H) = \Pr[DS = R_{loss}|H = v] \tag{3.1}$$

The wind fragility for window is the probability of exceeding a window limit state, W_{LS}, conditional on a given gust wind speed v, expressed as

$$\Pr(DS|H) = \Pr[DS \geq W_{LS}|H = v] \tag{3.2}$$

This study considers the failure of roof sheeting and trusses caused by overloading of CTB, BTR and RTW connectors as these connections are deemed as the 'weakest links' of the roof system under wind uplift pressure (Reardon 1996; Henderson & Ginger 2007). Note that fatigue-induced connection failure is neglected in this study as metal roofs in non-cyclonic regions are less sensitive to fatigue, in contrast to cyclonic regions where strong fluctuating winds dominate. The loss of a single roof sheet is assumed to occur when a critical number of cladding fasteners fail as inadequate fixings may lead to a loss of functionality, stability and integrity of the roof sheet. The failure of BTR connectors is also a contributor to the roof sheeting loss. A roof truss is considered to fail if at least one of its RTW connectors is overloaded. The failure of a single CTB, BTR or RTW connector is governed by the following limit state function

$$g = R_c - (W_c - D_L) \tag{3.3}$$

where R_c represents the resistance of the considered roof connection, and W_c is the wind uplift load acting on this connection. The connection resistance and wind uplift loading are both modelled probabilistically which are described in Section 3.4. The dead load arising from the weight of roof components is D_L. A roof connection fails if $g \leq 0$. In this study, the uplift loads acting on roof connections are obtained by using a FE approach. The dead load is considered in the FE modelling by specifying the density of roof components. The failure of a single roof sheet occurs when the number of failed fasteners on the roof sheet N_f exceeds a threshold value N_{cr}. A BTR connection failure is modelled as if all roof fasteners connected to the batten have failed. The sheet failure threshold value (N_{cr}) is equivalent to the sheet failure criterion (SFC) defined in Stewart et al. (2018). A reasonable lower bound for SFC assumes two fasteners cause roof sheet failure in line with Henderson et al. (2013) which represents SFC=10%. The upper bound assumes that 80% of fasteners must fail to cause roof sheet failure (HAZUS 2014). The evidence suggests that failure of a few fasteners will result in sheet failure rather than failure of many fasteners (Konthesingha et al. 2015). Hence, a triangular probability distribution proposed in Stewart et al. (2018) is used to model N_{cr} (expressed as the percentage of the total number of fasteners on a single sheet), see Figure 3.4. The lower and upper bound of the triangular probability distribution are 10%

and 80%, respectively. A sensitivity analysis indicates that the fragility results are not sensitive to N_{cr} assumptions (Stewart et al. 2018). For more details about the triangular distribution model of N_{cr}, see Stewart et al. (2018).

To assess the number of failed CTB, BTR and RTW connectors requires the fragility model to account for the load sharing and redistribution among these roof connections. The wind uplift load acting on a single connection, W_c, is conventionally evaluated using the tributary area approach (e.g. Henderson & Ginger 2007; Stewart et al. 2018) or influence coefficients (e.g. Ji et al. 2018). However, the former approach may not accurately capture the wind loading effects by assuming no load sharing between connections (Kopp et al. 2012), and it is a very complex task to use the latter approach to model the failure progression of roof connections by continuously providing updated influence coefficients for numerous load redistribution scenarios (Smith et al. 2016). Instead, in this study, the uplift forces for roof connections are obtained by using a FE approach, which takes into account the load sharing and redistribution among roof connections under the spatially varying wind uplift pressure. The FE approach models the roof system including metal roof sheets, top-hat battens, timber roof trusses, wall top plates, and CTB, BTR and RTW connections. The details of the FE modelling are described in Section 3.5.

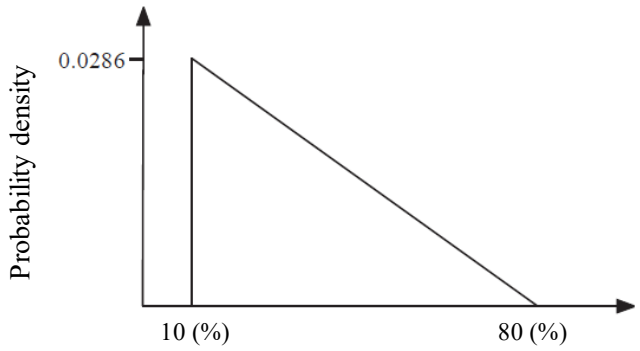

Figure 3.4. Triangular probability distribution of N_{cr} (Stewart et al. 2018).

The damage of windward windows is governed by the limit state function given by

$$g = R_W - W_{win} \tag{3.4}$$

where R_W represents the resistance of windows including ultimate strength and water penetration resistance, and W_{win} is the wind pressure acting on the windward window. Window breakage occurs if the ultimate strength is exceeded, and the exceedance of water

penetration resistance allows for rainwater penetration. The window resistance and wind pressure are both modelled probabilistically that are described in Section 3.4.

A Monte Carlo Simulation (MCS) analysis in conjunction with the FE approach are employed to evaluate the wind fragility for roof cladding and trusses, which enables the stochastic characterization of spatially varying wind uplift pressure, uplift forces in roof connections, failure progression and load redistribution, and evolution of internal pressure with increasing sheeting loss. In each run of the MCS, the spatially distributed wind pressures and structural resistances of roof connections are randomly generated as the input to the FE model of the roof system. The wind uplift loads acting on the roof connections are then obtained from the FE analysis, and the failure of a single connection is checked by the limit state function given by Eq. (3.3). Any overloaded (failed) CTB, BTR and RTW connections are then deactivated in the FE model, and the FE analysis is further conducted to evaluate the load redistribution and failure progression of other connections. It should be noted that, given a short gust duration, the FE analysis of load redistribution and failure progression is only conducted once after the initial failure of connections. The MCS and FE approach proposed in the present study enables the development of two fragility curves for roof: (i) the extent of roof sheeting loss, and (ii) proportion of roof truss failures. The MCS to evaluate wind fragility of windward windows is straightforward that both the window resistances and wind pressures acting on windward windows are randomly generated from corresponding probability distributions. The limit states for windows given by Eq. (3.4) are checked in each simulation run, and fragility curves are then obtained for the windward window.

3.4 Probabilistic Modelling of Wind Loading and Connection Resistance

3.4.1 Wind loading

The wind loading (W) is modelled probabilistically as (e.g. Holmes 1985; Stewart et al. 2018)

$$W = \lambda \cdot M \cdot A_g \cdot (C_P \cdot T \cdot E^2 \cdot D^2 \cdot G_E \cdot \frac{\rho}{2}) \cdot v^2 \tag{3.5}$$

where v is the maximum 0.2 second gust velocity at 10m height in Terrain Category 2 (i.e. open terrain defined in Australian wind loading standard AS/NZS 1170.2 2011); λ is a factor accounting for wind loading modelling inaccuracies and uncertainties; M accounts for wind tunnel modelling inaccuracies such as incorrect Reynolds number, building details, and site

modelling; A_g is the loaded area uncertainty arising from geometric uncertainties of the cladding fastener, batten and truss spacing, and for windows this factor is ignored; C_P is the quasi-steady pressure coefficient, which is a combination of external (C_{Pe}) and internal pressure coefficient (C_{Pi}); T is the shielding factor; E is a terrain height multiplier that accounts for the exposure and height of the building considered; D is a factor accounting for wind directionality effects; G_E is a factor related to area reduction, and ρ is the density of air. These parameters, except for C_P, are assumed to follow a lognormal distribution (Henderson & Ginger 2007) with estimated means and coefficient of variations (COV) listed in Table 3.1 that are derived from the statistics given in Holmes (1985) and Stewart et al. (2018). Note that the subscript 'N' in Table 3.1 denotes the nominal value, which can be obtained from AS/NZS 1170.2 (2011). Random variables, λ, M, E, T, D, G_E, A_g and ρ are statistically independent for each simulated house, but then fully correlated for each roof connection in the simulated house. Sensitivity analyses indicate that, if one or two of the random variables given in Table 3.1 are assumed as deterministic, then fragilities reduce by less than 2%. The spatially variable nature of wind uplift pressure on roof surface is mainly attributed to the spatially distributed external pressure coefficients, which are measured from a wind tunnel test in this study. Note that W is a general notation for wind loading which includes W_c and W_{win} for roof connections and windows respectively.

Table 3.1. Statistical parameters for wind load modelling.

Parameter	Mean	COV
λ/λ_N	1.0	0.10
M/M_N	1.0	0.10
$A_g/A_{g,N}$	1.0	0.05
E/E_N	0.95	0.10
T/T_N	1.0	0.10
D/D_N	1.0	0.00
$G_E/G_{E,N}$	1.0	0.05
ρ/ρ_N	1.0	0.02

3.4.1.1 External pressure coefficients

The external pressure coefficients for windward windows (i.e. external pressure coefficients on windward walls) are not directly measured in wind tunnel testing, and the factor M in Eq. (3.5) is ignored when assessing wind pressure on windows. According to Henderson & Ginger (2007) and AS/NZS 1170.2 (2011), an external pressure coefficient

for windward windows is assumed to follow a normal distribution with a mean of 0.70 and a coefficient of variation (COV) of 0.15.

External pressure coefficients for roof surface provided in wind loading standards are typically based on wind tunnel tests conducted on rectangular hip and gable roofs. As the representative contemporary house has complex hip-roof geometries, wind tunnel testing was carried out to obtain the external pressure coefficients for the entire roof surface. The wind tunnel test was conducted for a scaled model of the representative contemporary house in the Boundary Layer Wind Tunnel at JCU (Parackal et al. 2016). Three hundred and twenty pressure taps were installed on the external roof surface to measure the spatial and temporal variation in external pressure. The fluctuating external pressures on these taps were measured for approaching wind directions of 0° to 350° at intervals of 10°. More details about the wind tunnel test are described in Parackal et al. (2016).

The Gumbel distribution is used to model the spatially varying peak suction pressure coefficients (e.g. Ho et al. 2005; Tieleman et al. 2008) with the location and scale parameters estimated from the wind tunnel observations for each tap location and each wind direction using the maximum likelihood method (e.g. Peng et al. 2014). The use of a Gumbel distribution with no upper limit results in conservative predictions for peak external pressure coefficients, which to some extent compensates for statistical uncertainties given finite wind tunnel data, and uncertainties in applying wind tunnel data to full scale (Holmes & Cochran 2003). Hence, it is reasonable to model the peak pressure coefficients using a Gumbel distribution. The spatially varying external pressure coefficients modelled in this study for different wind directions are illustrated in Fig. 3.5. More details about the interpretation of wind tunnel observations and the modelling of external pressure coefficients can be found in Parackal et al. (2016) and Stewart et al. (2018). Note that the non-simultaneous occurrence of peak suctions across large roof surface is accounted for by the factor G_E given in Eq. (3.5). As wind tunnel testing has shown a very high correlation of peak pressure values between taps in edge zones (Ginger & Letchford 1993), the present fragility analysis assumes a correlation coefficient of 0.9 for the pressure tap data in roof edge. It is noted that the calculated fragilities are not sensitive to assumptions about the pressure tap correlation coefficients (see also Stewart et al. 2018).

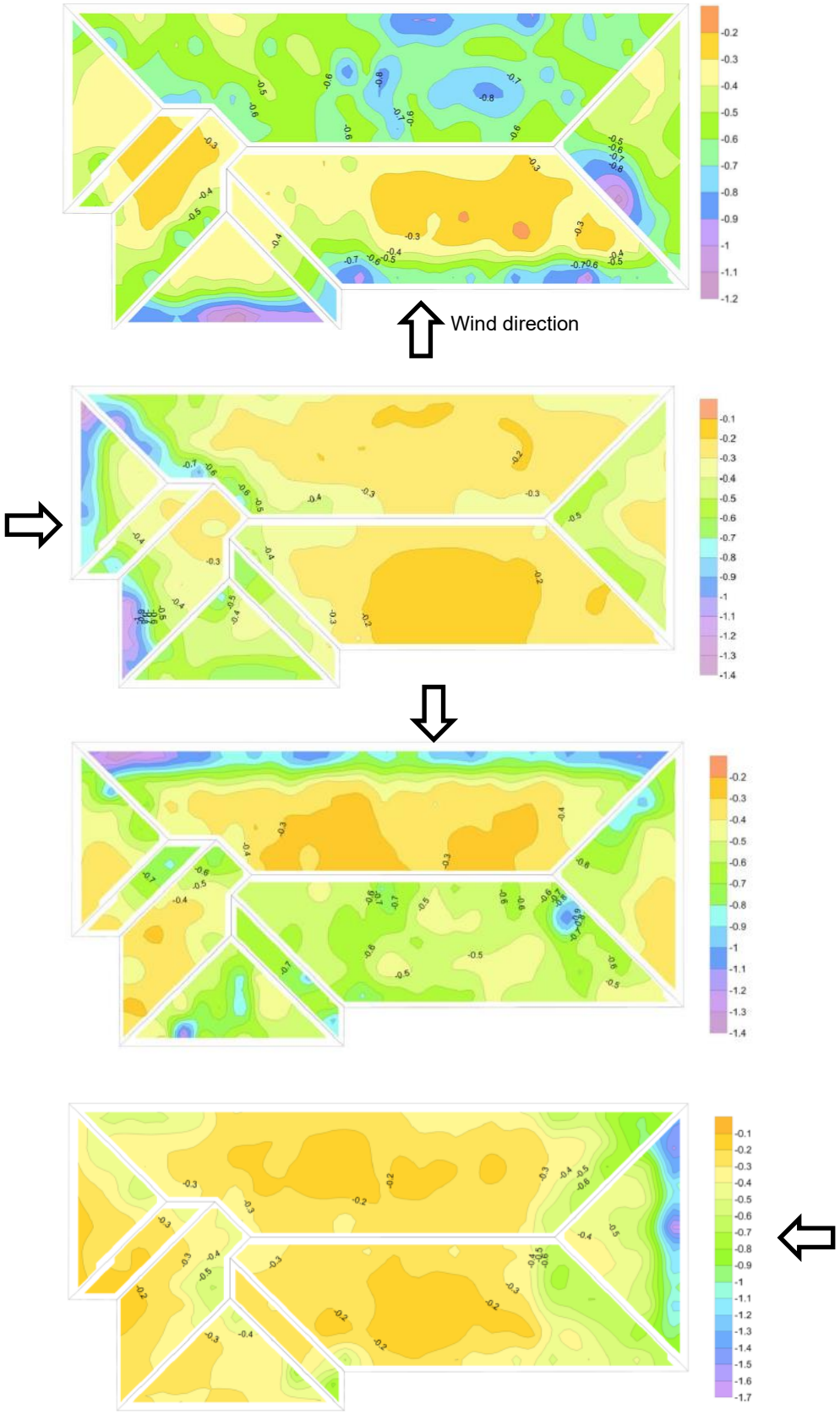

Figure 3.5. Spatially varying external pressure coefficients on the hip roof (Stewart et al. 2018).

3.4.1.2 Internal pressure coefficients

Wind damage and internal pressurisation are interdependent. Internal pressure is an important factor for the assessment of roof uplift and window damage, which combining with external pressure may produce the most adverse effect. The failures of roof cladding and windows also change the internal pressurisation.

Internal pressure is highly dependent on locations and sizes of openings as well as the external pressures around the openings. The progressive failure of windows and roof sheets during an extreme wind event creates multiple openings, which may significantly change the internal pressure and therefore affect the damage assessment. Although the evaluation of internal pressure under multiple wall openings has been reported in the literature (e.g. Kopp et al. 2008; Pan et al. 2012), few studies attempt to investigate the evolution of internal pressure with increasing roof sheeting loss for houses and the consequent effect on roofing fragility.

As internal pressure coefficients were not measured in the wind tunnel test, two typical scenarios are assumed for internal pressure, i.e. (i) dominant openings existing on windward wall and (ii) effectively sealed building without any wall openings. A general equation used to obtain the quasi-steady internal pressure coefficient considering multiple openings is derived from Holmes (2015) by applying mass conservation, which is given by

$$\sum_{j=1}^{N} A_j \sqrt{|C_{Pe,j} - C_{Pi}|} = 0 \tag{3.6}$$

where N is the number of openings in the building envelope; A_j is the size of opening j; $C_{Pe,j}$ is the quasi-steady external pressure coefficient at opening j, and C_{Pi} is the quasi-steady internal pressure coefficient. It should be noted that Eq. (3.6) neglects inertial effects.

To avoid the computational burden involved in solving Eq. (3.6) by numerical methods considering multiple openings, we combine the area for several openings on the windward wall and roof as A_w and A_R, respectively. Then based on Eq. (3.6), the internal pressure coefficient for the windward wall dominant opening scenario is calculated as

$$C_{Pi} = \frac{C_{PW}}{1+(\frac{A_R}{A_W})^2} + \frac{C_{PR}}{1+(\frac{A_W}{A_R})^2} \tag{3.7}$$

where C_{PW} is the average of external pressure coefficients at multiple windward wall openings, C_{PR} is the average of external pressure coefficients at multiple roof openings, A_w

is the total size of wall openings, and A_R is the total size of roof openings. It should be noted that Eq. (3.7) neglects any openings on leeward and side walls.

Windward wall openings due to window breakage is considered in this study. Only roof openings due to the damage progression of metal sheets are considered in this study (i.e. ignoring possible effect of flashings, vents, etc). With windward wall dominant openings, if $C_{PW} = +0.7$ and $C_{PR} = -0.3$ (nominal values in AS/NZS 1170.2), the change of C_{Pi} with increasing loss of roof sheeting (i.e. increasing A_R/A_w), is depicted in Fig. 3.6(a). As shown in Fig. 3.6(a), internal pressure coefficients decrease with increasing A_R/A_w, which suggests that the adverse effect of internal pressure subjected to windward wall dominant openings is relieved with increasing roof sheeting loss. If $A_w = 8$ m^2 (e.g. two 2 m × 2 m windows), the internal pressure evolution with increasing number of failed roof sheets (the size of a typical corrugated sheets used in the representative contemporary house is 3.4 m^2) is depicted in Fig. 3.6(b). Note that Fig. 3.6 is only used to illustrate the approximate trend of internal pressure evolution with increasing roof sheeting loss. In each run of the MCS for fragility assessment, instead of AS/NZS 1170.2 values, C_{PW} and C_{PR} will take values of the average of external pressure coefficients at windward wall openings and roof breaches, respectively. Various sizes of windward wall dominant openings, A_w, that are possible to occur during a windstorm are considered in a sensitivity analysis later in Section 3.6.2.2 to examine the corresponding effects on the fragility assessment.

The internal pressure coefficient is assumed to follow a normal distribution with a COV of 0.33 (e.g. Lee & Rosowsky 2005; Sivapathasundaram & Mahendran 2016) as loss of roof sheeting will result in high variability of internal pressures. A lower COV value is considered later in Section 3.6.2.2 to show the sensitivity of fragility to internal pressure variability. The corresponding mean value of C_{Pi} is calculated by Eq. (3.7) with a 10% reduction when combined with the external pressure coefficient to account for the non-simultaneous occurrence of peak internal and external pressures. For the scenario without any wall openings, the mean value of C_{Pi} would simply be equal to the mean value of C_{PR} and the same COV value is used. When assessing the window damage by wind pressure, the C_{Pi} value used for the windward windows corresponds to the non-dominant opening scenario. Chapter 5 will describe the integration of window damage and roof fragility under the two wall opening scenarios in a probabilistic risk assessment. Note that the effect of porosity on internal pressure is deemed to be negligible when large openings occur (Woods & Blackmore 1995), and therefore is not taken into account in this study.

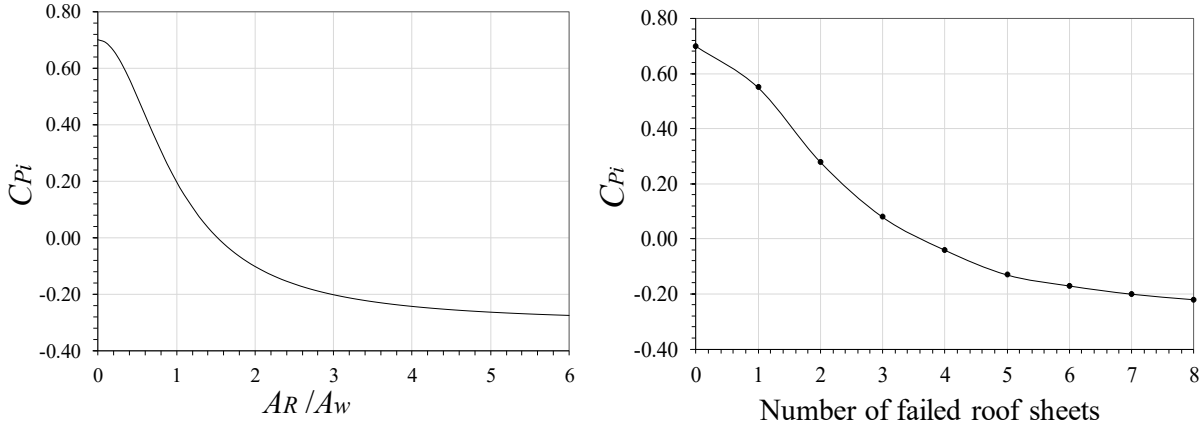

(a) Internal pressure evolution with increasing A_R/A_W ($A_W > 0$)

(b) Internal pressure evolution with increasing number of failed roof sheets (A_w = 8 m^2)

Figure 3.6. Internal pressure evolution with increasing roof sheeting loss with windward wall dominant openings.

3.4.2 Resistances for roof connections and windows

The representative contemporary house is installed with corrugated metal sheeting secured by screw fasteners at every 2nd corrugation of the roof edge and every 3rd or 4th corrugation for other regions of the roof. Metal top-hat battens are used as roof battens and secured to every truss at 900 mm spacings (Parackal et al. 2016). The resistances of the CTB and BTR connectors are modelled as random variables and the failure modes considered are (i) pull-over and (ii) pull-out failures. Both the pull-over and pull-out capacities of CTB and BTR connectors are assumed to follow a lognormal distribution (Henderson & Ginger 2007). The statistical parameters for the resistances of CTB and BTR connectors are listed in Table 3.2, which were derived from laboratory tests and summarized in Stewart et al. (2018). The connection resistances are assumed to be statistically independent and taken as the lower of randomly generated pull-out and pull-over strengths.

Triple grip connections (see Fig. 3.7) are typically used for the rafter/truss-to-wall (RTW) connectors for Australian contemporary houses. The timber species for the truss is typically Australian radiata pine, and two types of fasteners, i.e. hand nails and gun nails, are used for the triple grip connections. The triple grip connection behaviour under uplift loads is captured by a piecewise-linear force-displacement relationship with its model parameters probabilistically characterized based on Australian housing test data in Satheeskumar (2016). Figure 3.8 depicts the piecewise-linear model for the behaviour of triple grip RTW connectors in vertical direction (i.e. y shown in Fig. 3.7). In Fig. 3.8, F_y is the yield load and

the connection has a linear-elastic response when its force $F \leq F_y$, k_0 is the initial secant stiffness, and δ_y is the displacement at yielding. When $F_y < F \leq F_u$, where F_u is the peak load (considered as the uplift capacity for the connection), permanent deformation and load redistribution start to occur. If the displacement of the connection, δ, is greater than the displacement at peak load, δ_u, the separation of triple grip from the top plate is likely to occur, and δ_{max} is the displacement of triple grip connection at complete separation.

Table 3.2. Statistical parameters for resistances of CTB and BTR connectors.

Connection type	Connection failure mode	Mean	COV	Distribution type	Source
Cladding-to-batten (CTB)	Roof sheeting pulling over fastener	1.2kN	0.30	Lognormal	Stewart et al. (2018)
	Roof fastener pulling out of roof batten	1.2kN	0.20		
Batten-to-rafter/truss (BTR)	Roof batten pulling over batten fastener	4.5kN	0.15	Lognormal	Stewart et al. (2018)
	Batten fastener pulling out of rafter/truss	5.5kN	0.20		

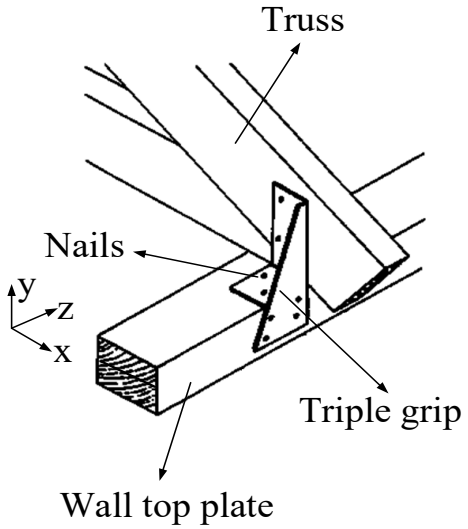

Figure 3.7. Triple grip RTW connector.

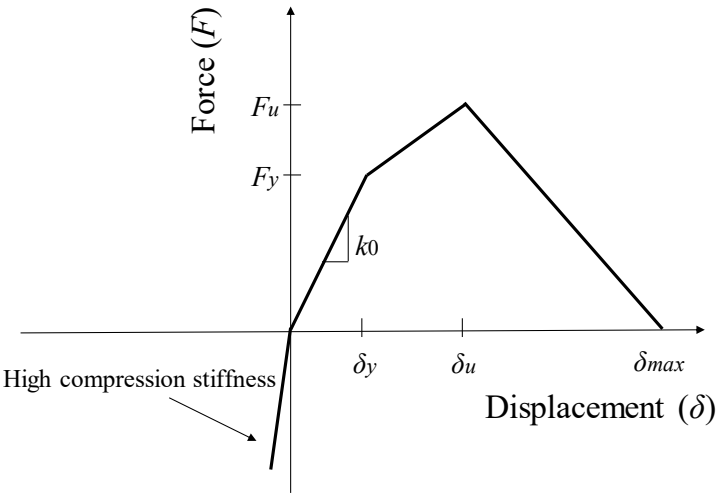

Figure 3.8. Piecewise-linear force-displacement relationship for triple grip RTW connectors.

The overloading of roof connections ($F \geq F_u$) is considered as the limit state for the current reliability-based fragility method. Thus, the connection behaviour after peak load is neglected in the FE analysis and it is assumed that the overloaded RTW connector tends to lose its load carrying capacity very quickly. Clearly, this is a slightly conservative assumption. Another consideration for ignoring the so-called 'negative stiffness' after the peak load is that it can cause non-convergence issues for the FE analysis. A much higher compression stiffness (i.e. 20 kN/mm) is assumed for the RTW connector in the vertical (y) direction. Three major parameters, i.e. k_0, F_u and δ_u, are used to define the piecewise-linear model in Fig. 3.8. All these parameters are assumed to follow lognormal distributions with the mean and COV values obtained from ten individual static tests (Satheeskumar 2016). The statistical parameters of k_0, F_u and δ_u for triple grip connections fastened using hand nails and gun nails are listed in Table 3.3. The yield force (F_y) is defined as two-thirds of F_u based on the averaged ratio of F_y to F_u in the test data. The correlation coefficients between these three model parameters are also obtained from the test data as shown in Table 3.4, and when conducting the fragility analysis, the lognormally correlated parameters are sampled in the MCS using Nataf transformation (Liu & Der Kiureghian 1986) for the calculation of the covariance matrix. Figure 3.9 depicts the force-displacement curves of the test data and the mean piecewise-linear approximation for triple grip fastened using hand nails and gun nails. Note that the descending part in the piecewise-linear curve (i.e. negative stiffness) is arbitrarily assumed for illustration and it is not included in the fragility analysis as explained above. As shown in Fig. 3.9, the piecewise-linear model provides a reasonable approximation for the connection response under uplift loads. Note that the statistical

accuracy can be further improved if more test data is available.

Table 3.3. Statistical parameters of the piecewise-linear model for RTW connectors.

(a) Hand nail triple grip

RTW parameters	Mean	COV	Distribution type
Initial secant stiffness k_0 (kN/mm)	0.44	0.17	Lognormal
Peak load F_u (kN)	4.85	0.11	
Displacement at peak load δ_u (mm)	19.49	0.12	

(b) Gun nail triple grip

RTW parameters	Mean	COV	Distribution type
Initial secant stiffness k_0 (kN/mm)	0.34	0.15	Lognormal
Peak load F_u (kN)	3.80	0.11	
Displacement at peak load δ_u (mm)	19.95	0.18	

Table 3.4. Correlation coefficients between three piecewise-linear model parameters for RTW connectors.

Parameters	Correlation coefficient	
	Hand nail triple grip	Gun nail triple grip
k_0 and F_u	0.63	0.45
k_0 and δ_u	−0.27	−0.16
F_u and δ_u	0.12	0.14

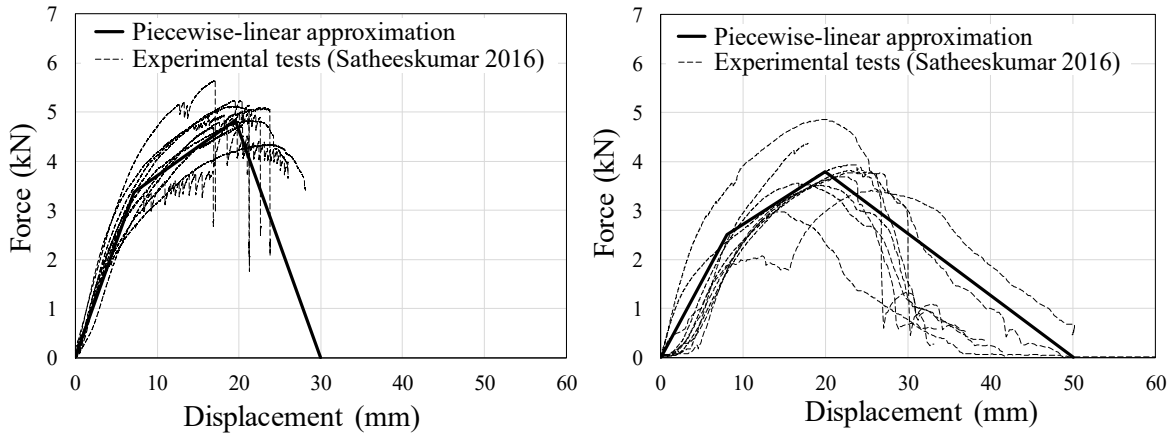

(a) Triple grip fastened using hand nails (b) Triple grip fastened using gun nails

Figure 3.9. Force-displacement curves of the test data and piecewise-linear approximation.

In this study, the window resistance R_W given in Eq. (3.4) includes the ultimate strength (R_{ult}) and water penetration resistance (R_{water}). According to AS 2047 (2014), windows shall

not fail when tested under the ultimate limit state pressure, and shall have no penetration of uncontrolled water when tested under the water penetration resistance test pressure. The ultimate strength and water penetration resistance of windows are assumed to follow a normal distribution (HAZUS 2014). Same as the assumption made in HAZUS (2014), it is assumed that the COV is 0.20 and 20% of the windows do not satisfy the test pressures specified in AS 2047 (2014) to account for the variance of quality in manufacture and installation. In other words, the mean ultimate strength and water penetration resistance are about 1.20 times the test pressures specified in AS 2047 (2014). The ultimate strength and water penetration resistance statistics for windows with different design wind classifications are given in Table 3.5. The probability of a negative window resistance from the normal distributions given in Table 3.5 is no greater than the order of 10^{-7}. This trivial issue is simply addressed by re-generate a positive value from the normal distribution if a negative window resistance occurs in the simulation.

Table 3.5. Ultimate strength and water penetration resistance of windows.

Window rating	R_{ult} (Pa)		R_{water} (Pa)		Distribution type
	Mean	COV	Mean	COV	
N1	720	0.20	180	0.20	Normal
N2	1080	0.20	180	0.20	
N3	1680	0.20	360	0.20	
N4	2400	0.20	360	0.20	

3.5 FE Modelling of Roof System

A FE approach using commercial FE software ANSYS (ANSYS Inc. 2013) is used in this study to evaluate the wind uplift loads acting on roof connections and load redistribution after the failure of one or more connections. The FE approach in conjunction with MCS enables an assessment of wind fragility considering the progressive failure of roof connections.

As shown in Fig. 3.1, the representative contemporary house has a complex hip-roof geometry that requires excessive cost in both FE modelling and computation (e.g. CPU hours) for the reliability-based fragility assessment. For instance, a comprehensive FE model for the roof trusses requires the modelling of several types of trusses (e.g. standard truss, truncated standard truss, truncated girder truss, valley truss, hip truss, jack truss, etc.) with various dimensions as well as many truss-to-truss connections (e.g. hip truss to truncated truss connections, jack truss to truncated girder truss connections, etc.). To reduce

the cost in FE modelling and computation, the FE approach used in this study models the roof cladding and trusses separately, and only critical roof trusses are modelled.

The roof cladding FE model consists of corrugated metal roof sheets, metal top-hat battens, CTB and BTR connectors, which is employed in the MCS analysis to evaluate roof sheeting loss under the spatially varying wind uplift pressure. The details of the roof cladding FE model are described in Section 3.5.1. The roof truss FE model mainly comprises a critical proportion of the timber trusses in the representative contemporary house, which includes 14 standard trusses, 2 truncated standard trusses and 1 truncated girder truss as shown in Fig. 3.10. These modelled trusses cover most of the critical trusses (i.e. trusses that are more likely to fail under wind uplift) in the roof system. Two additional truncated girder trusses depicted in solid line as shown in Fig. 3.10, though not included in the FE modelling, are also considered in the fragility assessment using a simple tributary area approach as they are among the most vulnerable trusses in the roof system. In a single MCS run, the wind uplift loads acting on the BTR connectors obtained from the roof cladding FE model were subsequently applied to the roof truss FE model for truss failure assessment. Satheeskumar et al. (2016b) and JCU have conducted a full-scale test for a subassembly of roof trusses containing five standard trusses from the same representative contemporary house. Material properties and dimensions of the trusses used in the FE models were obtained from this full-scale test. The schematic diagram of this roof structure in the full-scale test is depicted in Fig. 3.11. The details of the roof truss FE model are described in Section 3.5.2.

3.5.1 FE Modelling of Roof Cladding

The FE model of the roof cladding layout containing 75 corrugated metal roof sheets is shown in Fig. 3.12(a). Four-node quadrilateral shell elements including both bending and membrane stiffness are used to model the corrugated metal sheet with six degrees of freedom at each node. The FE model of a typical corrugated metal roof sheet installed on the representative house is depicted in Fig. 3.12(b). A total of 22,792 shell elements are included in a typical metal roof sheet. The corrugated metal sheet has a width of 762 mm, base metal thickness (BMT) of 0.42 mm and crest height of 22 mm. Roof sheets with other shapes are configured by trimming the typical sheets at ridgelines and hips as shown in Fig. 3.12(a).

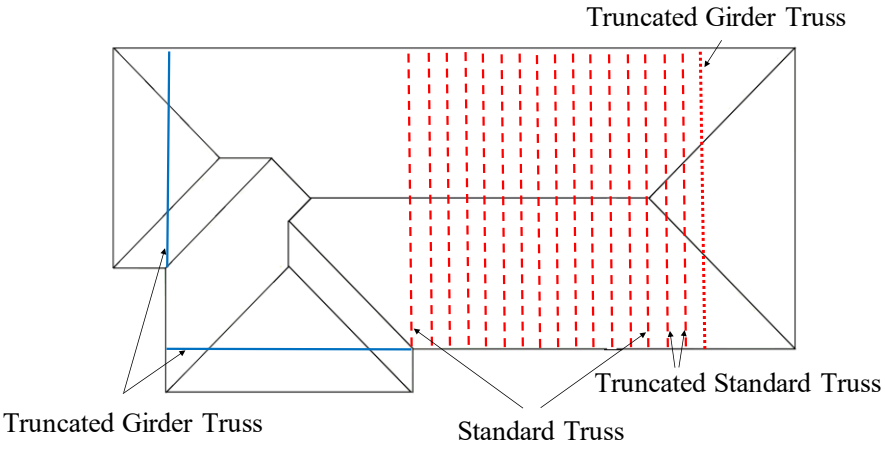

Figure 3.10. The selected trusses modelled in the FE analysis.

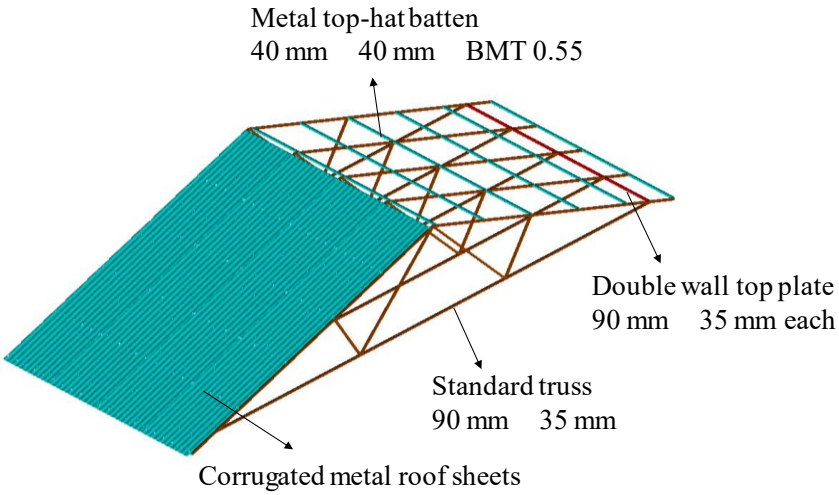

Figure 3.11. Schematic diagram of the roof structure in the full-scale test (Satheeskumar et al. 2016b).

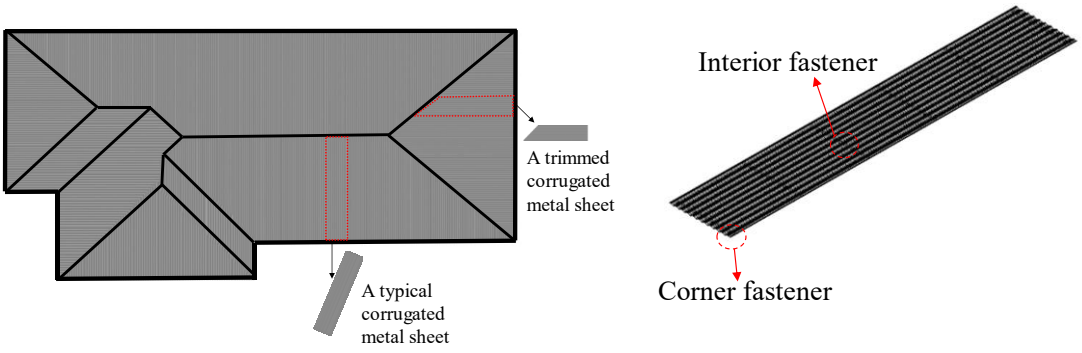

(a) Roof sheeting layout

(b) A typical five-span corrugated metal roof sheet

Figure 3.12. Roof cladding FE model.

As metal roof sheeting loss is primarily due to overloading of CTB and BTR connectors (Reardon 1996; Henderson & Ginger 2007), and for computational efficiency as well, the proposed FE approach does not assess detailed mechanical behaviour of the corrugated metal roof sheets. Instead, the FE approach is mainly aimed at evaluating the wind uplift forces in the roof connections, which in conjunction with the sampled connection resistances are used to assess the roof sheeting loss. To this end, localized dimpling, buckling and fracture of the metal roof sheet are not considered in the proposed FE approach. In addition, according to Xu & Reardon (1992) and Mahendran (1994), the majority of the corrugated metal sheeting are still in the elastic range when the fasteners fail. Thus, the material properties for the corrugated metal sheets are assumed to be isotropic and linear-elastic with a Young's modulus of 220,000 MPa and a Poisson's ratio of 0.3 (Lovisa et al. 2013). Note that the variation in sheet material properties only has a slight effect on the overall cladding response (Lovisa et al. 2013), and therefore deterministic material properties are used.

Two-node beam elements are used to model the metal top-hat roof battens with material and section properties obtained from manufacture's specifications (Lysaght 2014). It is assumed that the CTB and BTR connectors no longer carry any loads when corresponding uplift forces exceed their pull-out and/or pull-over resistances, and the overloaded connections are then deactivated in the roof cladding FE model for further analysis of load redistribution and failure progression. The CTB and BTR connectors are approximately modelled by linear spring elements. The stiffness of the linear spring elements is also assumed to follow a lognormal distribution with a mean value of 300 N/mm and 1800 N/mm (Satheeskumar et al. 2017) for CTB and BTR connectors, respectively. A COV value of 0.20 is assumed for the stiffness variability due to a lack of relevant data. Although the linear spring is not able to capture the actual pull-through and withdrawn behaviour of screw fasteners, it is considered adequate to obtain the connection forces due to wind uplift and evaluate the overloading of roof connections in the context of the current reliability-based fragility method. The roof trusses are not modelled in the roof cladding FE model and flexible supports are assumed to represent the attachment points of batten fasteners to rafters. Using the proposed roof cladding FE model, the failure progression of CTB and BTR connectors can be evaluated. For example, if the corner fastener as shown in Fig. 3.12(b) is the first failed fastener for a typical corrugated metal roof sheet, about 80% of the load originally taken by this fastener is redistributed to neighbouring fasteners in the same corrugation and the remaining 20% redistributes to neighbouring fasteners in adjacent

corrugations. Similarly, if the failure initiates at the interior fastener as shown in Fig. 3.12(b), 90% is the proportion of load redistribution along the corrugation. If more fasteners have failed, different scenarios of load redistribution would occur.

3.5.2 FE Modelling of Roof Trusses

A total of 17 timber roof trusses are modelled in the roof truss FE model, which contains most of the critical trusses in the roof system. The truncated girder truss has a large tributary area (i.e. 10.4 m^2), the failure of which may impact other trusses (e.g. jack trusses) connected to it. The hip trusses and jack trusses typically have the same RTW connector as for a standard truss, while with relatively small tributary areas, they are less vulnerable under wind uplift and therefore are not modelled in the FE approach. This simplification has largely reduced the cost in FE modelling and computation time.

Two-node beam elements with a rectangular section of 90 mm × 35 mm are used to assemble the timber trusses, and the material properties of the truss members are assumed to be isotropic and linear-elastic with a Young's modulus of 10,000 MPa and a Poisson's ratio of 0.37 (Satheeskumar et al. 2017). The same beam elements are used to model the double ribbon wall top plates at each side of the trusses but with a section of 70 mm × 90 mm (twice of each top plate). The wall frame below the top plates are not modelled and flexible supports are assumed to represent the attachment points of top plates to wall studs.

The triple grip connections as shown in Fig. 3.7 are used for the RTW connectors, which are modelled by three non-linear spring elements to characterize the connection behaviour in uplift and shear. The force-displacement relationship for the spring elements in the vertical direction (y direction in Fig. 3.7) is probabilistically characterized by the piecewise-linear model as described in Section 3.4.2. This can account for the variability in connection stiffness and strength as well as the effect of relative stiffness of RTW connectors on the load sharing and redistribution in vertical load paths. The load-deflection behaviour for the spring elements in x (i.e. along the truss) and z (i.e. normal to the truss plane) directions as shown in Fig. 3.7 are assumed to be deterministic as wind uplift is the focus of this study. The mean force-displacement curves depicted in Fig. 3.13 are used for these two spring elements (Satheeskumar et al. 2017). These force-displacement relationships are derived from laboratory tests of triple grip RTW connectors (Satheeskumar 2016) identical to those used for trusses in the representative contemporary house.

The progressive failure of CTB and BTR connectors affects the vertical load transfer for

RTW connectors. For example, the loss of a roof sheet reduces the uplift loads on corresponding RTW connectors. In one MCS run, the uplift forces in BTR connectors obtained from the roof cladding FE model are applied to the roof truss FE model to evaluate the failure of RTW connectors, which accounts for the effect of failure progression of CTB and BTR connectors on the vertical load transfer to RTW connectors. Besides the uplift loads from BTR connectors, additional point loads obtained from the roof cladding FE model in the same MCS run are applied to the bottom chord of the truncated girder truss. These additional loads are derived from the sampled wind uplift loads acting on the hip and jack trusses supported by the truncated girder truss.

The top-hat battens play a major role in load sharing and redistribution of the truss system, and hence the metal battens are assembled in the roof truss FE model as shown in Fig. 3.14. As a secondary roof component for load sharing and redistribution, the metal roof sheeting is also assembled in the roof truss FE model in a simplified manner as opposed to the detailed modelling in the roof cladding FE model. Plane shell elements are used to approximately model the metal roof sheeting, which have the same flexural rigidity (EI = 3.3×10^3 N·m^2 per metre width) with the corrugated metal sheets in the direction along trusses and a much smaller EI value (i.e. 1/10 of the EI value in the direction along trusses) is assumed in the direction along battens (i.e. normal to truss plane).

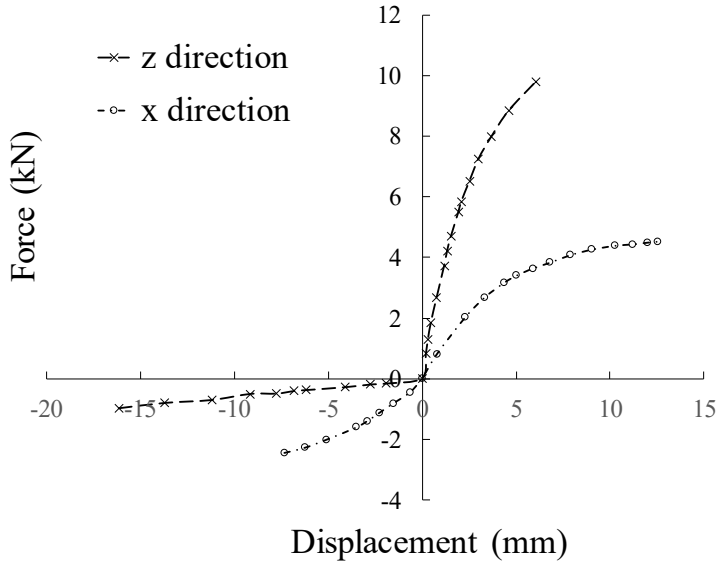

Figure 3.13. Force-displacement relationship for spring elements in x and z directions for RTW connectors (Satheeskumar et al. 2017).

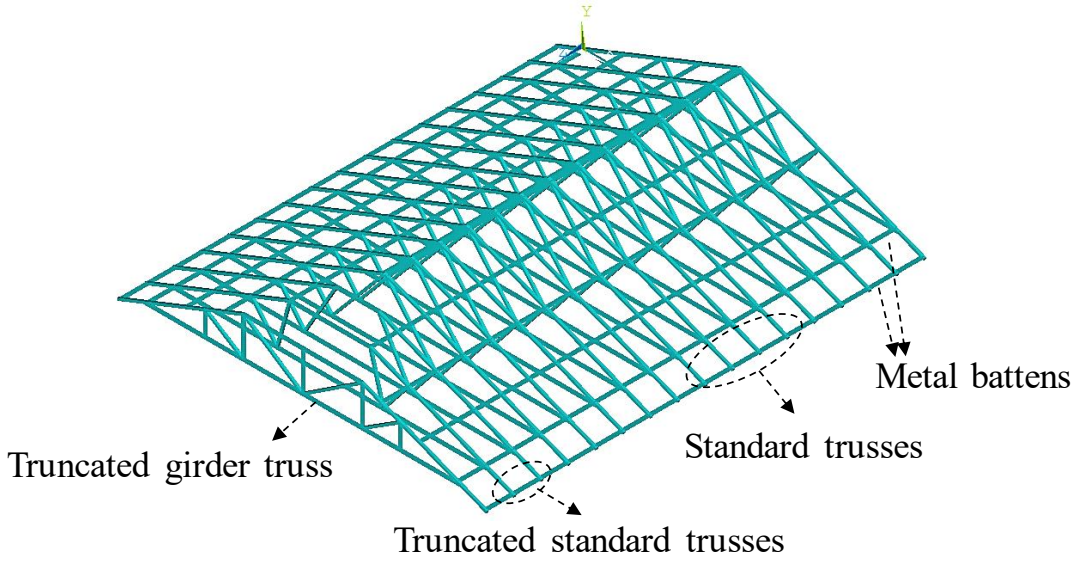

Figure 3.14. Timber trusses and metal battens in the roof truss FE model.

3.5.3 Model Validation

3.5.3.1 Validation of roof cladding FE model

The roof cladding FE model is validated by the test results of a two-span corrugated metal roof sheet (Lovisa et al 2013) that has the same material properties, width and fastener spacings as those used for the representative contemporary house. The same metal sheet has been modelled using the current FE approach. At the central support of the double-span metal sheet, the fastener load (largest fastener reaction) with increasing uniformly distributed uplift pressure yielded by the FE approach is compared with the experimental results as shown Fig. 3.15. In general, the FE analysis results agree well with the experiments in evaluating the wind uplift loads acting on cladding fasteners. The sudden drop of fastener load around 4.8 kPa in the experimental results is due to local dimpling around the fastener, which, as mentioned before, is not considered in the current FE approach for computational efficiency. In addition, the corrugated metal sheeting in non-cyclonic regions are unlikely to experience a wind pressure in excess of 4.8 kPa.

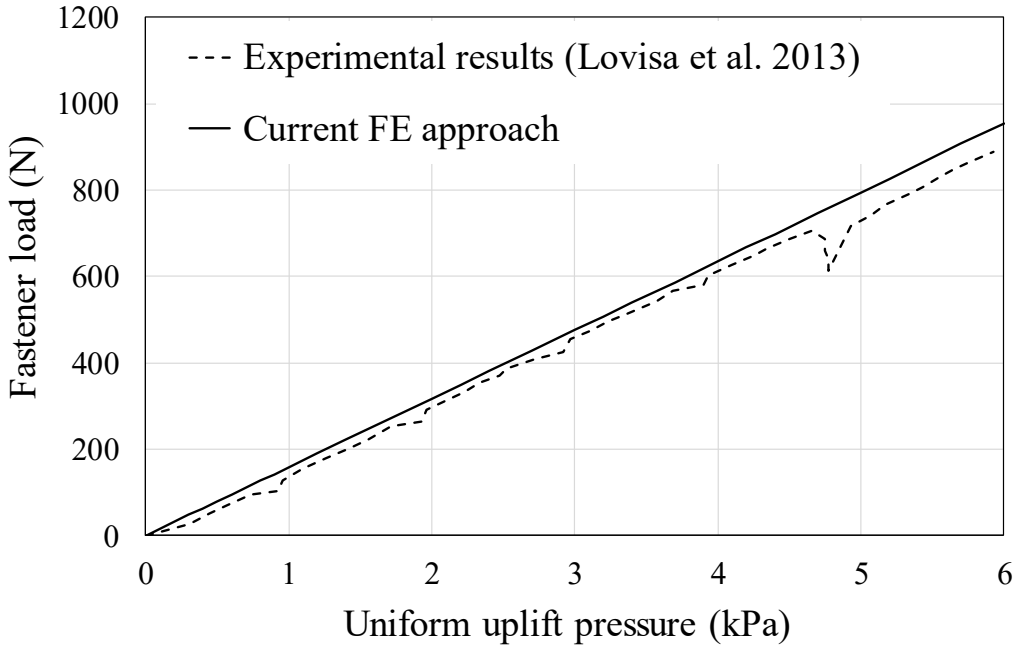

Figure 3.15. Fastener load with increasing uniform uplift pressure.

3.5.3.2 Validation of roof truss FE model

To demonstrate the capability of the roof truss FE model in capturing the complex load sharing mechanism and assessing the uplift forces acting on RTW connectors, the roof structure in the full-scale test by Satheeskumar et al. (2016b) (see Fig. 3.11) is modelled using the current FE approach, and the vertical reaction coefficients (VRCs) of RTW connectors under a static point load obtained from the FE analysis are compared with the full-scale test data. The plan view of the roof trusses and battens is shown in Fig. 3.16. The five trusses are labelled as A, B, C, D and E. The RTW connectors in the left and right side of Truss A are labelled as L_A and R_A, respectively. Similar notations for RTW connectors in the other trusses (L_B, R_B, L_C, R_C, L_D, R_D, L_E, R_E). In the full-scale test, a point load of 1kN was applied normal to the roof surface at the location of BTR connections, and the VRC of a RTW connector is defined as the ratio of the vertical connection reaction to the applied point load. The VRCs of the RTW connectors when the unit point load is applied at six locations are available in Satheeskumar et al. (2016b).

In the FE analysis, the model parameters of the piecewise-linear force-displacement relationship for RTW connectors are randomly sampled using statistics in Tables 3.3 and 3.4, and a total of 1000 simulation runs are carried out. The simulated VRCs of ten RTW connectors are obtained from the probabilistic FE analysis when the point load is applied at six different locations, and the results are then compared with the full-scale test data as

shown in Fig. 3.17. As shown in Fig. 3.18, most of the VRCs of RTW connectors, obtained from the full-scale test, are within the 5% and 95% percentile values of the simulated VRCs. In general, the FE approach used well reproduces the load sharing of the roof system and accurately evaluates the wind uplift loads acting on RTW connectors. Discrepancies between the simulated VRCs by FE analysis and the full-scale test data tend to appear in those RTW connectors sharing a relatively small portion of applied load (i.e. VRCs within ± 0.2). These discrepancies are likely due to the difference in the stiffness of RTW connectors between the FE model and full-scale test structure. The stiffness of RTW connectors in the FE analysis is modelled based on force-displacement relationships obtained from laboratory tests for individual RTW connectors, which may differ from the actual stiffness of a connection serving in a roof system (e.g. having interactions with other roof components).

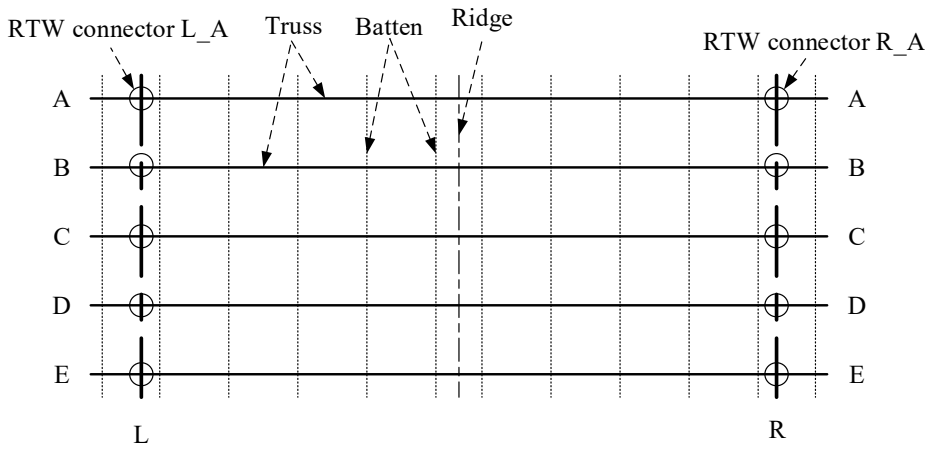

Figure 3.16. Schematic diagram of the roof truss layout.

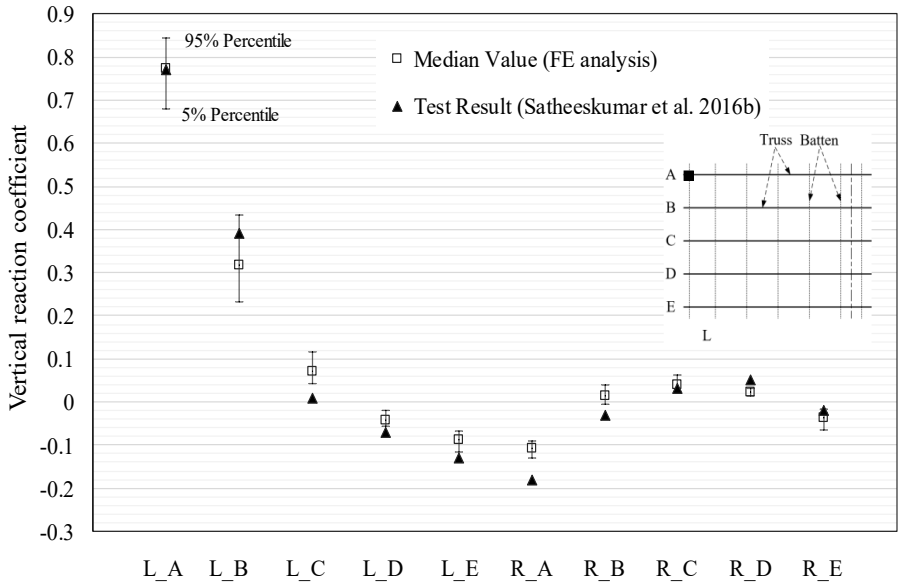

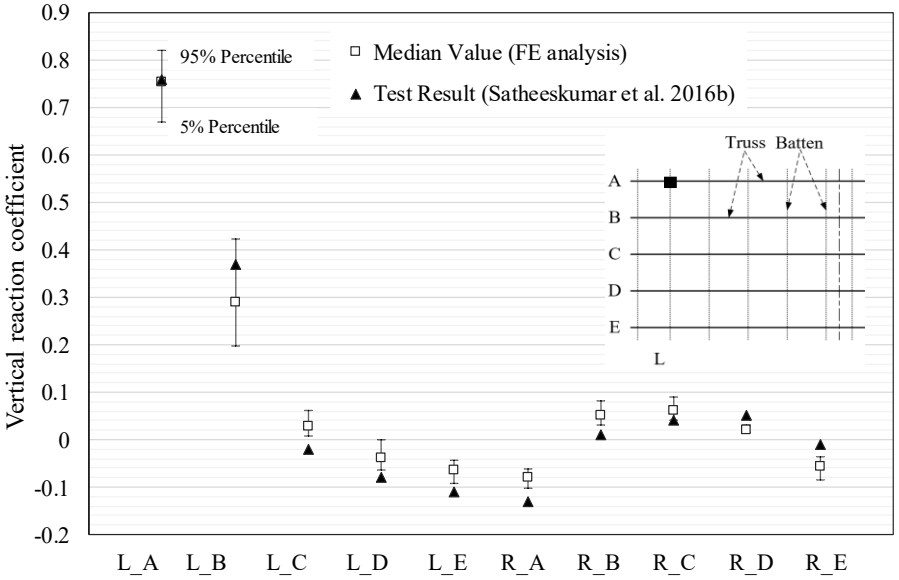
Vertical reaction coefficient
0.9
0.8
0.7
0.6
0.5
0.4
0.3
0.2
0.1
0
-0.1
-0.2
95% Percentile
5% Percentile
Median Value (FE analysis)
Test Result (Satheeskumar et al. 2016b)
Truss
Batten
A
B
C
D
E
L
L_A
L_B
L_C
L_D
L_E
R_A
R_B
R_C
R_D
R_E

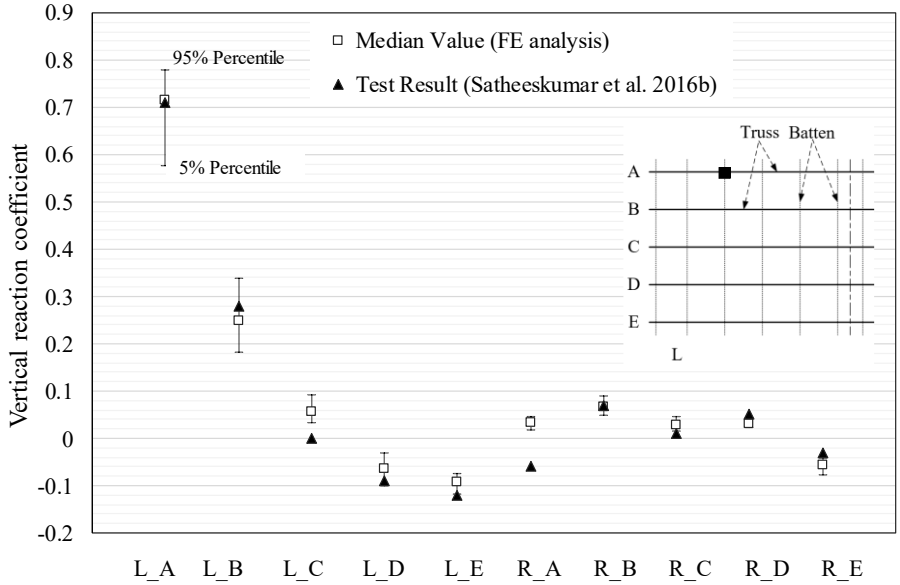
Vertical reaction coefficient
0.9
0.8
0.7
0.6
0.5
0.4
0.3
0.2
0.1
0
-0.1
-0.2
95% Percentile
5% Percentile
Median Value (FE analysis)
Test Result (Satheeskumar et al. 2016b)
Truss
Batten
A
B
C
D
E
L
L_A
L_B
L_C
L_D
L_E
R_A
R_B
R_C
R_D
R_E

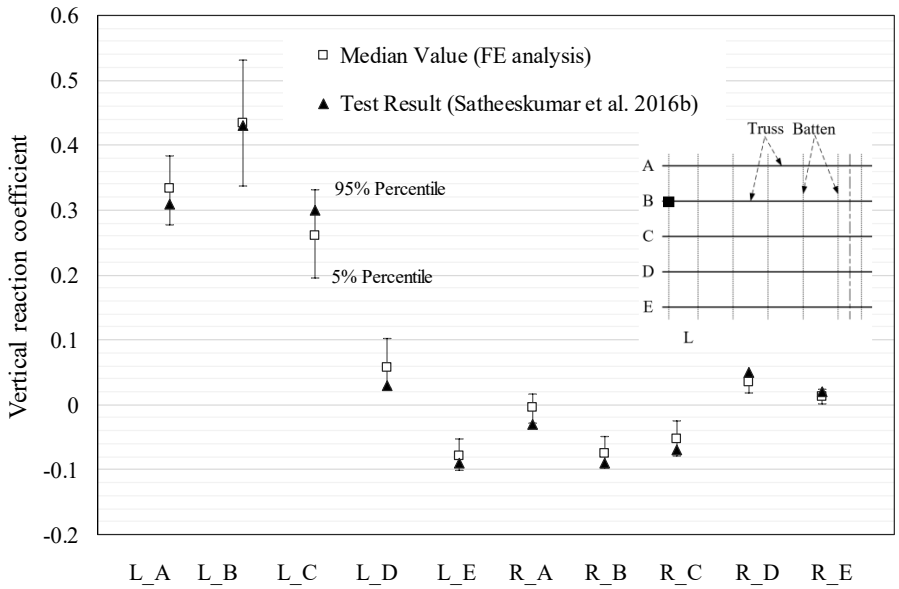
Vertical reaction coefficient
0.6
0.5
0.4
0.3
0.2
0.1
0
-0.1
-0.2
Median Value (FE analysis)
Test Result (Satheeskumar et al. 2016b)
95% Percentile
5% Percentile
Truss
Batten
A
B
C
D
E
L
L_A
L_B
L_C
L_D
L_E
R_A
R_B
R_C
R_D
R_E

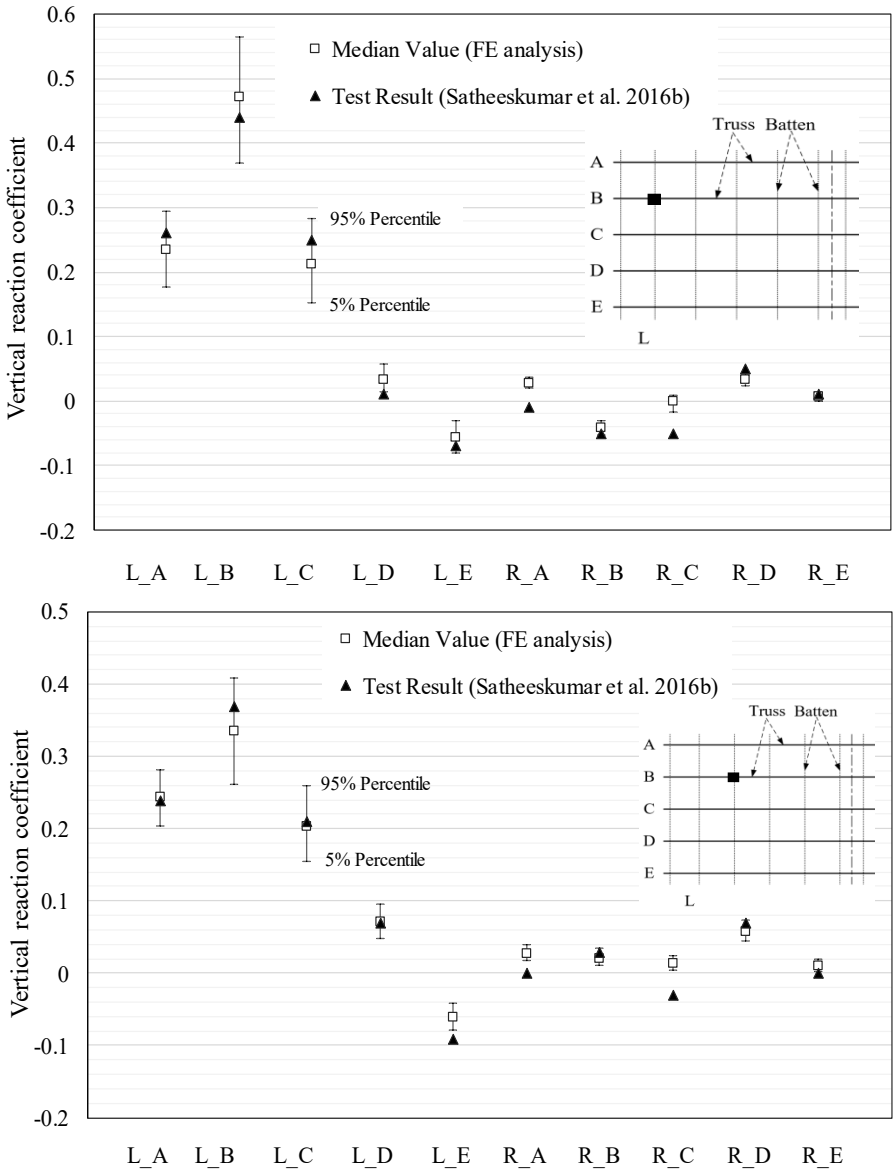

Figure 3.17. Comparison of simulated VRCs with full-scale test data at six point load locations (solid square) represents the location where the point load acts on.

3.6 Fragility Results

3.6.1 Design Considerations and Simulation Procedure

In this section, fragility analyses are conducted for the representative contemporary house using the proposed MCS and FE approach. Wind fragilities up to gust wind speed of 80m/s are calculated for windward windows, metal roof cladding and timber roof trusses. Two wall opening scenarios for internal pressurisation are considered for the fragility analysis of roof cladding and trusses as described in Section 3.4.1.2. It is assumed that potential openings due to window damage are located at all four external walls, and only large openings on the windward wall exist for the dominant opening scenario. This is

because windows on windward wall are most likely to be damaged by wind pressure and/or windborne debris during a windstorm. In the baseline case, a typical size of windward wall openings (i.e. A_w) is assumed to be 8 m^2 (e.g. two 2 m × 2 m windows). The window damage is coupled with the two wall scenarios for roof fragility in a probabilistic risk assessment described later in Chapter 5.

The wind direction was assumed to be uniformly distributed in 10˚ increments from 0˚ to 350˚ to allow for the variability of building orientation – this allows for fragilities to be assessed for a house for a specific wind speed. The wind fragility for roof is expressed by the mean extent of roof sheeting loss and roof truss failures as a function of gust wind speed. A total of 1800 MCS runs are conducted for the roof fragility assessment (50 runs for each 10˚ increment of wind attack angle), which, according to a convergence check, is deemed to be acceptable. To conduct the MCS, a total of 50 sets of connection resistances were randomly generated to represent 50 house samples. For each house sample, a wind speed (starting at 30m/s) and a building orientation (or wind angle relative to building axis, starting at 0˚) were selected. The wind loading parameters in Eq. (3.5) were then randomly generated as inputs to the FE model for damage assessment. For every house sample, this procedure was repeated for each wind speed (30m/s to 80m/s with 1m/s interval). The MCS process was then repeated for each building orientation (0˚ to 350˚ with 10˚ interval). The mean extent of roof damage at a given wind speed was then obtained from aggregated results over all building orientations and house samples. The MCS and the FE approach for the representative contemporary house includes 1646 cladding-to-batten (CTB), 532 batten-to-rafter/truss (BTR) and 38 rafter/truss-to-wall (RTW) connectors. For wind fragility for windward windows, the wind loading parameters in Eq. (3.5) were randomly generated, and the wind pressure was then calculated and compared with the randomly generated window resistance in each simulation run. The failure probabilities of windward windows as a function of gust wind speed (i.e. fragility) are then obtained.

The design and construction considerations for RTW connectors of the representative contemporary house in Brisbane and Melbourne are given in Table 3.6, which conforms to AS 1684.2 (2010). Note that the CTB and BTR connections are generally identical for houses in Brisbane and Melbourne. The design and construction considerations for RTW connections in Table 3.6 is only one option that satisfies housing standards. Other construction practices are not taken into account. The window ratings (consistent with the

design wind classification) for Brisbane and Melbourne houses typically range from N1 to N3, and the corresponding window resistances are given in Table 3.5.

Table 3.6. Design and construction considerations for RTW connectors based on AS4055 (2012) and AS 1684.2 (2010).

Wind classification	Location	RTW connectors	
		Standard/truncated standard truss	Truncated girder truss
N1	Melbourne	One gun nail triple grip	One gun nail triple grip
N2	Melbourne/Brisbane	One gun nail triple grip	Two gun nail triple grips
N3	Brisbane	One hand nail triple grip	Two hand nail triple grips

3.6.2 Results

3.6.2.1 Baseline case

The fragility curves for roof cladding and trusses considering two wall opening scenarios are shown in Fig. 3.18. As indicated in Fig. 3.18, both the roof cladding and truss fragilities corresponding to the windward wall dominant opening scenario are much higher than those without any wall openings. This is expected because the roof suffers much higher internal pressures when large openings appear in the windward wall. The design wind speed corresponding to a 500-year return period for Brisbane is 57 m/s (AS/NZS 1170.2 2011). At this gust wind speed, the mean roof sheeting loss for the representative contemporary house is 4.5% with windward wall dominant openings and only 0.1% for the scenario without any wall openings. While the latter loss is insignificant, the former may result in considerable economic losses. For example, a loss of roughly 15% of the total building and contents value can result from approximately 5% roof sheeting loss as inferred from Stewart et al (2018). The mean proportion of roof sheeting loss at the 500-year gust wind speed of Melbourne, i.e. 45 m/s (AS/NZS 1170.2 2011), is negligible for both wall opening scenarios. Note that the obtained fragility curves in Fig. 3.18 apply to suburban houses located on a flat, level site and subjected to wind coming from the prevailing direction (i.e. the nominal values used for the topographic and directional factor in Eq. (3.5) are unity) with no shielding. However, these fragility curves have the flexibility to account for other wind directions, shielding and topographic conditions. Site-specific wind directional multipliers for eight cardinal directions given in AS/NZS 1170.2 (2011) can be multiplied to the wind speed to account for non-prevailing wind directions, which is to be incorporated in chapter 5 for the risk assessment. The mean roof damage for a different topographic condition can be obtained using the same fragility curves shown in Fig. 3.18. For example, at a wind speed of 55m/s,

the mean roof sheeting loss read from the fragility curve is about 3% (dominant opening scenario). For a house on a slope of a hill, assuming a topographic factor of 1.10 (the exact value can be calculated according to AS/NZS 1170.2 2011 for a specific site condition), then the mean roof sheeting loss is about 8% that is obtained from the fragility curve at the adjusted wind speed, i.e. 55 1.10 = 60.5 m/s. Note that the uncertainty in the topographic factor has already been included as reflected by the mean-to-nominal ratio and COV values given in Table 3.1.

The mean proportion of roof truss failures for the representative contemporary house built in Brisbane at the 500-year design wind speed (i.e. 57 m/s) with windward wall dominant openings is 3.3% and 0.6% for wind classifications N2 and N3, respectively. At the 500-year gust wind speed for Melbourne (i.e. 45 m/s), the mean proportion of roof truss failures for suburban house in Melbourne with windward wall dominant openings is 0.2% and 0.1% for wind classifications N1 and N2, respectively, which is deemed as negligible damage. In the scenarios that no wall openings exist, the mean proportions of roof truss failures for both Brisbane and Melbourne houses at the 500-year design gust wind speed are less than 1%. Table 3.7 shows the mean number of failed CTB, BTR and RTW connectors for the dominant opening scenario at various gust wind speeds. This table suggests that more CTB connectors fail under wind uplift pressure than BTR connectors, which is expected as damage surveys (e.g. Leitch et al. 2009) reveal that roof sheeting loss is mostly due to cladding fastener failures. As expected, the failure of RTW connectors initiates only at relatively higher wind speeds.

The probability of exceeding the ultimate strength and water penetration resistance of the windward window as a function of gust wind speed is shown in Fig. 3.19 for windows with different design wind classifications. Figure 3.19 shows that the probability of window breakage (i.e. exceedance of ultimate strength) is much lower than that of exceeding the water penetration resistance. Given the same site conditions (e.g. same topographic and shielding condition), the probability of window breakage increases with design wind classifications or window ratings. The probability of exceeding the water penetration resistance is the same for N1 and N2 windows, which is expected given the window resistances listed in Table 3.5. Again, note that Fig. 3.19 applies to suburban houses located on a flat, level site and subjected to wind coming from the prevailing direction with no shielding, and can be adjusted to account for shielding and topographic effects, etc. A window damage state with an exceedance of water penetration resistance and a non-

exceedance of ultimate strength is of value in the rainwater intrusion evaluation and risk assessment, which will be discussed in Chapter 5.

Table 3.7. Mean number of failed roof connections for the dominant opening scenario.

Wind speed (m/s)	Cladding-to-batten (CTB)	Batten-to-rafter/truss (BTR)	Rafter/truss-to-wall (RTW)		
			N1	N2	N3
40	0	0	0	0	0
50	8 (0.5%)	1 (0.2%)	1 (2.6%)	0	0
60	62 (3.8%)	4 (0.8%)	4 (10.5%)	3 (7.9%)	0
70	192 (11.7%)	11 (2.1%)	12 (31.6%)	10 (26.3%)	3 (7.9%)

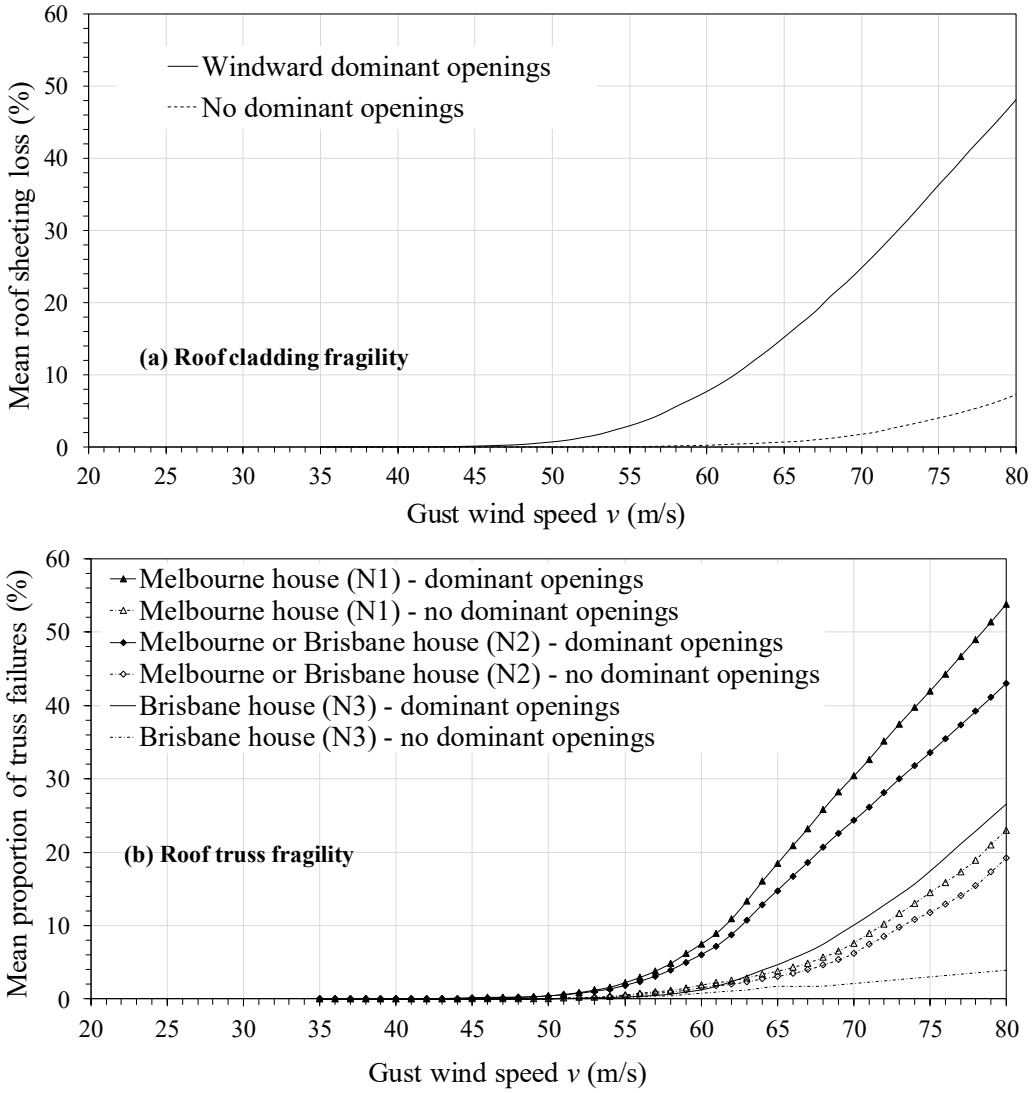

Figure 3.18. Fragility curves for roof cladding and trusses for two wall opening scenarios.

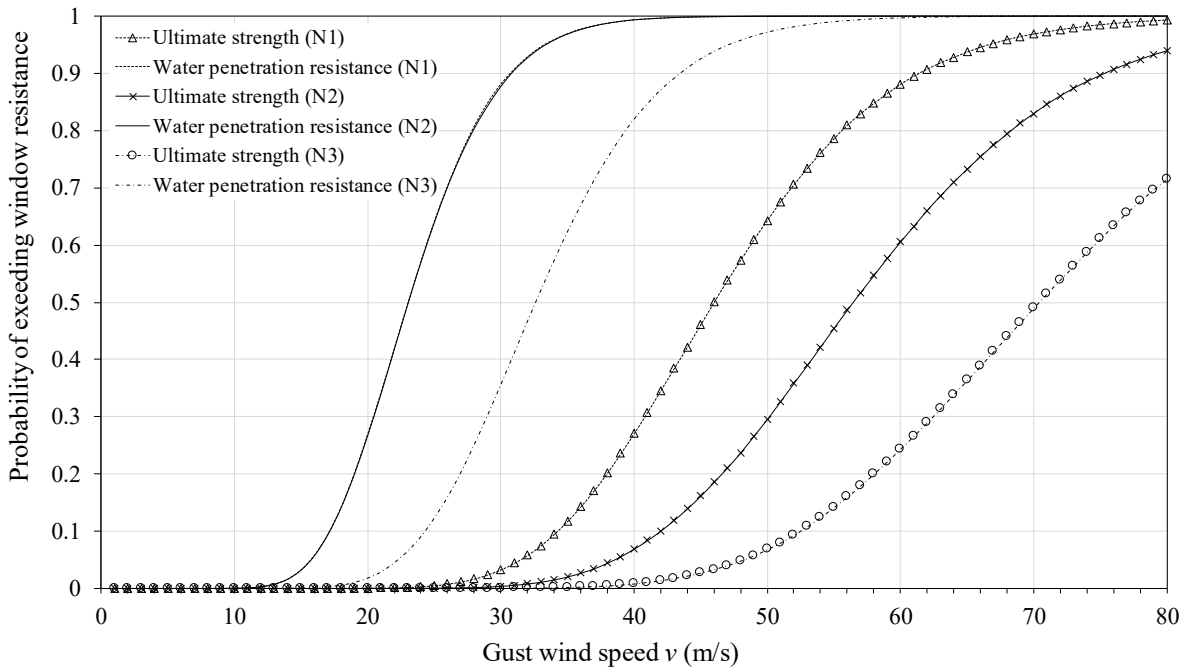

Figure 3.19. Fragility curves for windward windows.

3.6.2.2 Sensitivity analyses

A lower COV value (50% of the value used in the baseline case as mentioned in Section 3.4.1.2) is considered to show the sensitivity of fragilities to internal pressure variability. As illustrated in Fig. 3.20, the mean proportion of roof sheeting loss and roof truss failures decreases slightly as the variability in the internal pressure coefficient reduces. The probability of exceeding the window resistances is not sensitive to the variability in the internal pressure coefficient as shown in Fig. 3.21. The size of windward wall dominant openings can also affect the internal pressure modelling. Hence, A_w = 4 and 12 m^2 are assumed in addition to the baseline case (A_w = 8 m^2). The effects of these dominant opening sizes on roof fragilities for the windward wall dominant opening scenario are shown in Fig. 3.22. It is indicated that a larger size of windward wall openings (A_w) leads to higher wind damage to roof, which is expected as the internal pressure increases with A_w.

The relative stiffness due to variable stiffness of RTW connectors affect the load sharing in a roof truss assembly (Wolfe & McCarthy 1989), and consequently influences the roof truss fragility for the representative contemporary house. Hence, the effect of strength variability and relative stiffness of RTW connectors on the mean proportion of roof truss failures is examined by assuming four scenarios for the connection behaviour. The baseline scenario adopts the probabilistic piecewise-linear model for RTW connectors as described in Section 3.5.2. The second scenario assumes a deterministic piecewise-linear force-

displacement relationship as shown in Fig. 3.9 (the mean curve) for all the RTW connectors (i.e. COV = 0 for k_0, F_u and δ_u). The third scenario assumes that the initial secant stiffness (k_0) and the displacement at peak load (δ_u) for RTW connectors are random variables and the uplift capacity is deterministic (i.e. COV = 0 for F_u). In the fourth scenario, only the uplift capacities for RTW connectors are assumed to be probabilistic (i.e. COV = 0 for k_0 and δ_u). The fragility curves for roof truss failure with windward wall dominant openings are depicted in Fig. 3.23 for these four scenarios. As expected, the fragilities corresponding to the fully deterministic scenario are the lowest, which indicates that ignoring the variability in stiffness and uplift capacity for RTW connectors leads to an underestimation of roof truss failure. The fragility curves corresponding to the third and fourth scenarios suggest that both the variability in stiffness and uplift capacity of RTW connectors influence the roof truss fragilities. The variability in uplift capacity of RTW connectors has more impact on the mean proportion of roof truss failures than the stiffness variability of triple grip connections.

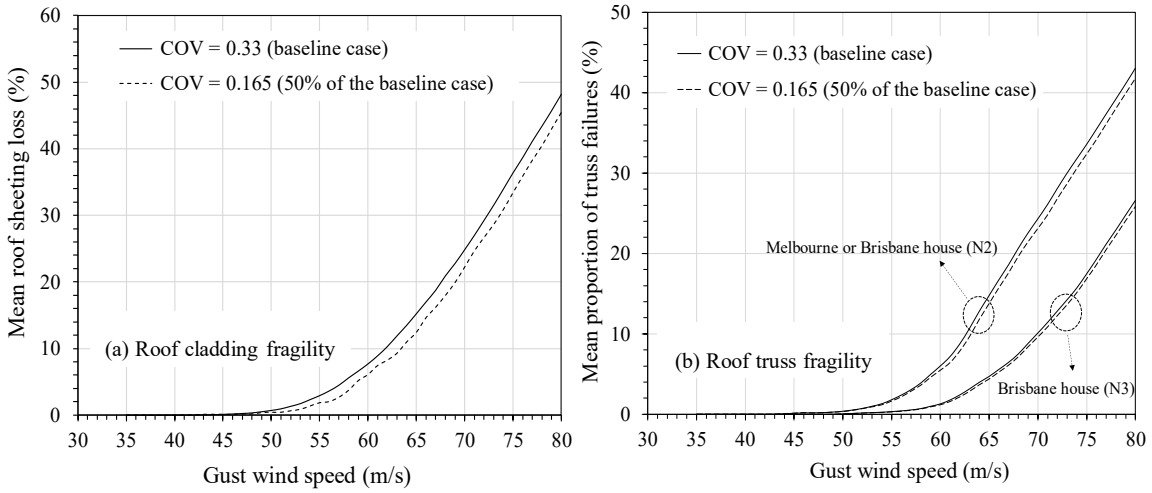

Figure 3.20. Fragility curves for roof considering different degrees of variability in the internal pressure coefficient for the windward wall dominant opening scenario.

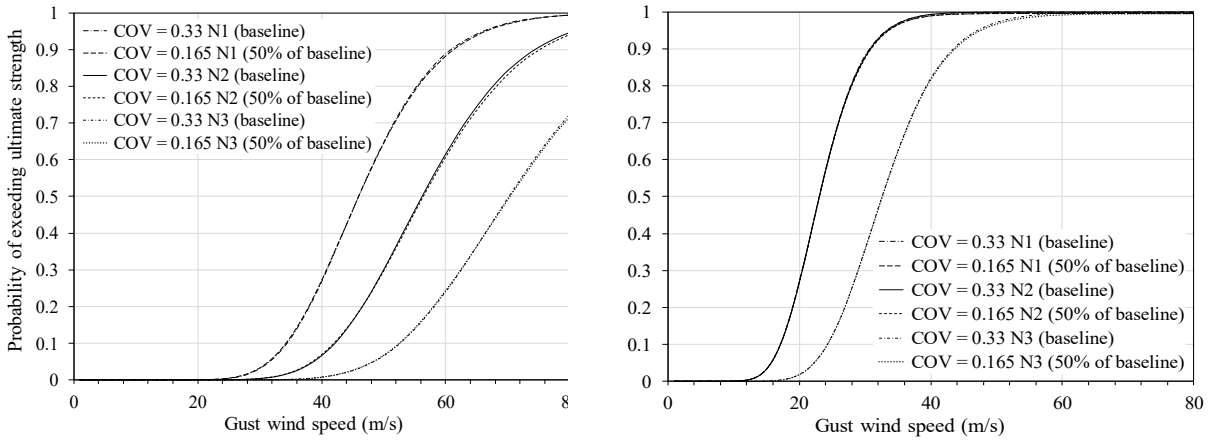

Figure 3.21. Fragility curves for windward windows considering different degrees of variability in the internal pressure coefficient.

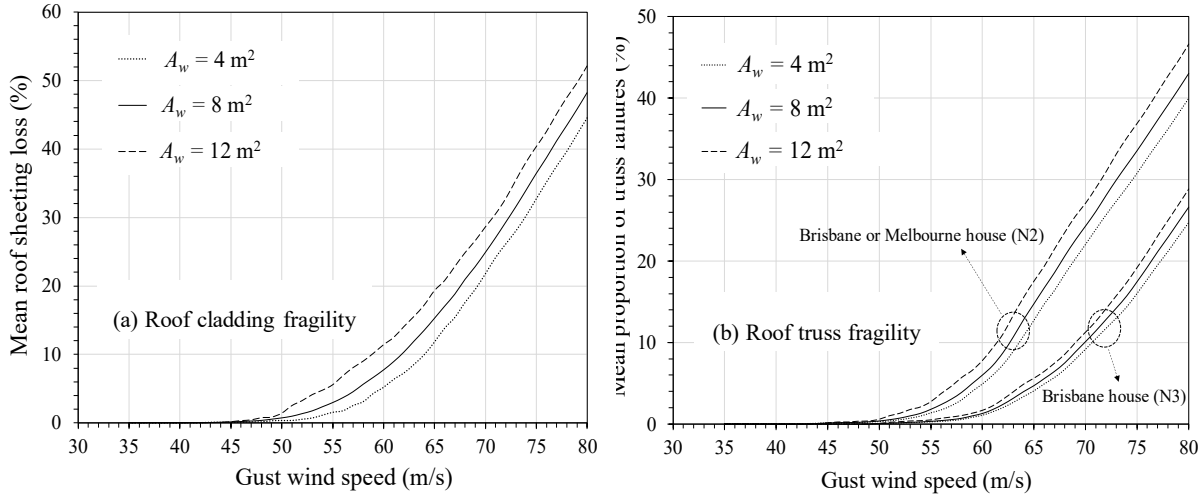

Figure 3.22. Fragility curves for roof considering different opening sizes for the windward wall dominant opening scenario.

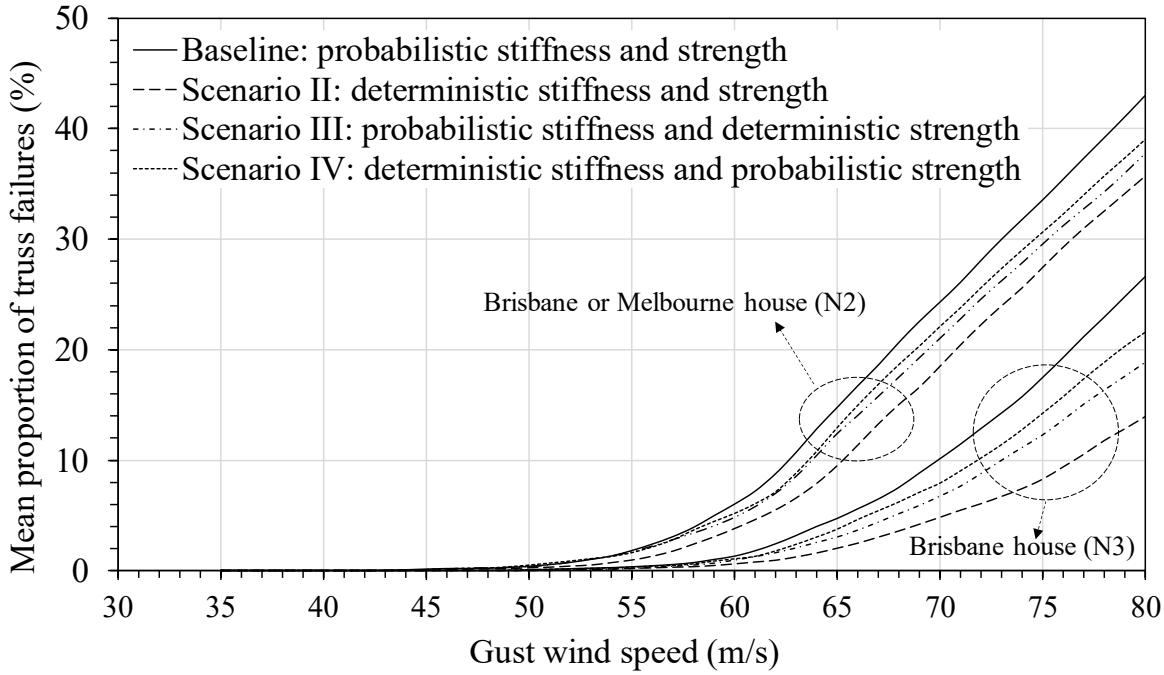

Figure 3.23. Fragility curves for roof truss failure considering different scenarios for stiffness and strength variability of RTW connectors with windward wall dominant openings.

The COV values for connection capacities in Tables 3.2 and 3.3 are considered for a good construction quality when installing roof connections. Poor installation practice often results in a relatively high proportion of improperly installed CTB, BTR and RTW connectors. For example, Boughton et al. (2015) found that over-driving batten fasteners to timber rafter/truss leads to lower withdrawn capacities and higher variability in both withdrawn and pull-through strength. The effect of construction quality on fragility assessment is examined by considering a higher variability in connection resistances. The COV values in Tables 3.2 and 3.3 are increased by 25% to represent a higher variability in connection resistances considering a relatively poor quality in construction practice. The original COV values are considered as a moderate resistance variability for an average construction quality. Figure 3.24 suggests that more roof damage is predicted by the fragility assessment as resistance variability increases. This is expected as higher variability results in a larger number of weak connections with relatively low resistances, and connection failures are more likely to initiate at these 'weakest links'.

The window resistances given in Table 3.5 are estimated based on the engineering judgement that 20% of windows not satisfying the test pressures specified in AS 2047 (2014). It is further assumed that 30% of windows do not satisfy the test pressures to account for a relatively poor quality in installation, which results in approximately 7% decrease in

the mean window resistances given in Table 3.5. The window resistances in Table 3.5 are considered to have moderate construction quality. The fragility curves for windward windows considering different construction quality in window installation are shown in Fig. 3.25. The figure indicates that the construction quality of windows has considerable effect on the probability of window damage, and such effect is higher for the probability of exceeding ultimate strength of windows.

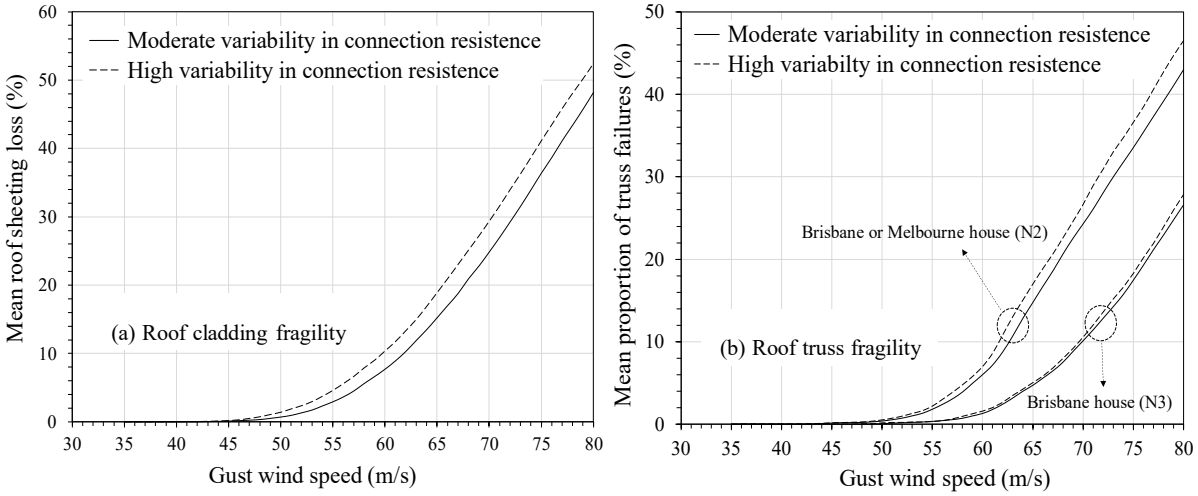

Figure 3.24. Fragility curves for roof considering different degrees of variability in connection resistances for the windward wall dominant opening scenario.

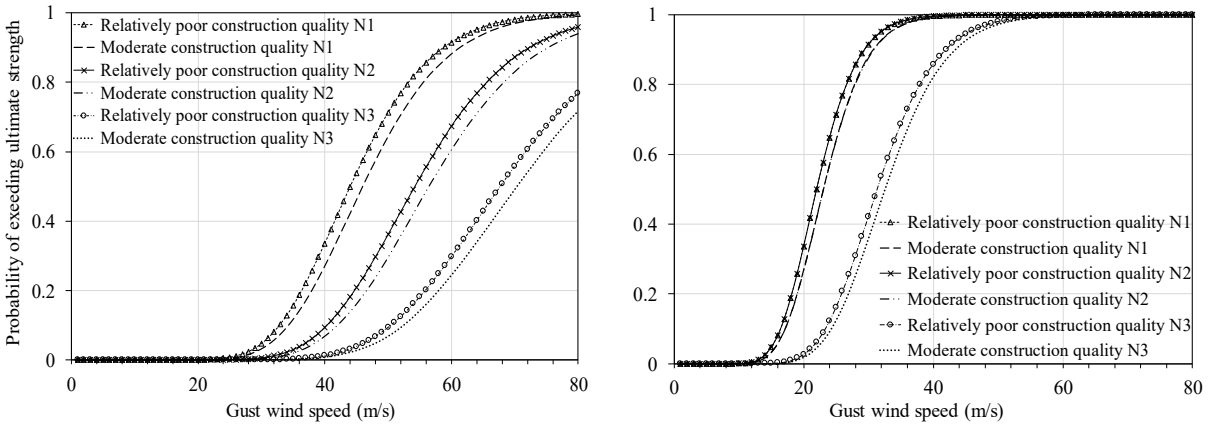

Figure 3.25. Fragility curves for windward windows considering different degrees of variability in window resistances.

3.7 Conclusions

This chapter presents a reliability-based fragility method to evaluate wind damage to roof cladding, trusses and windward windows for contemporary houses in non-cyclonic regions of Australia. The fragility analysis considered the roof damage due to overloading of

cladding-to-batten (CTB), batten-to-rafter/truss (BTR) and rafter/truss-to-wall (RTW) connectors, and window damage by high wind pressure. The spatial variation of wind uplift pressures on the roof was taken into account. The wind loading and structural resistances were probabilistically modelled, and a FE approach was proposed to evaluate the structural response, load redistribution and progressive failure of roof connections. A MCS analysis in conjunction with the FE approach were employed to carry out the fragility assessment. It was found that, if no wall dominant opening exists, the mean proportion of roof sheeting loss and roof truss failures is negligible under a 500-year return period wind speed. When subjected to windward wall dominant openings, considerable roof sheeting loss and roof truss failure are predicted at the 500-year gust wind speed for Brisbane. The probability of window breakage (i.e. exceedance of ultimate strength) is considerably lower than that of exceeding the water penetration resistance at a given wind speed. Given the same site conditions, the probability of window breakage increases with design wind classifications or window ratings.

CHAPTER 4. CONSTRUCTION DEFECTS AND THEIR EFFECTS ON ROOF FRAGILITY

4.1 Introduction

It has been widely acknowledged that the occurrence of human error during design and construction may significantly reduce the reliability of structures (Ellingwood 1987; Stewart & Melchers 1988; Stewart 1992, 1993). In line with this statement, damage surveys have indicated that wind damage to housing in Australia often occurs at peak gust wind speeds below the corresponding design wind speed (e.g. Ginger et al. 2010; Smith et al. 2016). This is mainly due to the commonly observed defects in housing construction (Leitch et al. 2009; Ginger et al. 2010; Ginger et al. 2015) with most defects occurring in tie-down fixings/connections, the effects of which have not been accounted for in most reliability/fragility assessments. Similar findings have been observed in North American houses (e.g. Yazdani et al. 2010) where damage during windstorms are largely due to construction defects. Wind damage is more likely to initiate on defective house components, which causes load redistribution to other components and may trigger a cascading failure. Clearly, ignoring construction defects in wind damage prediction leads to an underestimation of structural failure. Therefore, when conducting fragility/vulnerability assessment for houses subjected to extreme wind, it is essential to include the effects of construction defects (Stewart et al. 2018).

The modelling of construction defects in housing is a challenging task, which requires the quantification of defect rates and their consequent effects on structural performance. Human behaviour and performance are complex in nature, and the occurrence of human error depends on many psychological, physiological and sociological factors. Moreover, data regarding defect rates in housing construction and their corresponding influence on structural resistance are scarce because housing damage is rarely subject to a detailed forensic analysis that records individual defects, their location, and their frequency. Due to the complex error mechanism and a lack of data, it is not surprising that only a few studies attempt to include construction defects in the reliability/fragility assessment for houses under extreme wind (van de Lindt & Dao 2010; Hong & He 2015; Stewart et al. 2018). van de Lindt & Dao (2010) examined the effect of missing nails on the wind fragility of timber roof sheathing panels that are commonly used in North American houses. Their study used

a scenario-based approach by assuming various missing nail patterns. The quantitative estimation of error occurrence was not included in their work. Hong & He (2015) investigated the effect of missing and/or misaligned nails on the reliability of Canadian timber roof sheathing panels under wind uplift loading. This study adopted a constant defect rate which was obtained from the construction of a full-scale test house built by students in the laboratory. The uncertainty and variability involved in the occurrence rate of construction error may not have been well addressed given that there was only a single house specimen and it was constructed in a laboratory environment. Stewart et al. (2018) incorporated a preliminary probabilistic model of construction defects into the fragility assessment for metal roof sheeting failure due to extreme wind. This defect model was built on subjective information and defect data inferred from Hong & He (2015) that may not suit metal roof cladding fastened using screws instead of nails. Construction defects in truss connections are also not taken into account in Stewart et al. (2018).

To improve the modelling of construction defects, it is desirable to address the underlying mechanism of human error, uncertainties in error occurrences and consequences as well as the scarcity of construction error data. To this end, this study proposes a Bayesian approach to probabilistically quantify the defect rates in housing construction. The Bayesian method is appealing for the modelling of construction defects as it enables a systematic integration of expert judgement, human reliability analysis (HRA) models and limited construction defect data. A Cognitive Reliability and Error Analysis Method (CREAM) (Hollnagel 1998), is applied in conjunction with expert judgement to assign the prior distributions for defect rates in a Bayesian framework. CREAM is a HRA technique with the capability to model cognitive aspects in human error (Hollnagel 1998). It provides both qualitative and quantitative predictions of human reliability which can be practically fitted into a probabilistic risk assessment (PRA). In addition, most HRA methods are largely applied to hazardous industries such as nuclear power and aviation (e.g. THERP, SPAR-H). CREAM is a generic approach, and has detailed and appropriate task representation and decomposition based on human cognition. It has been widely used to deal with human error in various engineering fields including operator performance in nuclear power plants (e.g. He et al. 2008; Lee et al. 2011), marine engineering (e.g. Yang et al. 2013; Akyuz & Celik 2015), civil infrastructure management (Nan & Sansavini 2016; Nan & Sansavini 2017) and structural design (De Haan et al. 2013). To be sure, other HRA methods may also be used, however, this chapter presents a framework that can be readily adapted to other HRA

methods. The Bayesian updating is carried out using incomplete and imperfect defect data in housing construction collected from existing literature and field observations. The defect data include the observed occurrence rates of missing and/or improperly installed roof connections in Australian contemporary houses. Wind uplift capacities for defective roof connections are also obtained from experimental studies for housing in Australia.

The fragility model for the roof system presented in Chapter 3 can readily adapt to the change of structural response and the reduction of structural resistance given (i) the occurrence rate and (ii) the magnitude of capacity reduction for five types of construction defects. To this end, the probabilistic defect rates obtained from the Bayesian inference and the weakened roof components due to construction errors are subsequently incorporated into the reliability-based fragility assessment. This provides a rational and systematic method to probabilistically characterise the effects of construction defects on the wind fragility of roof systems for Australian contemporary housing. The combination of HRA methods and sparse human performance data through a Bayesian framework has been originally advocated in the PRA for nuclear power plants (e.g. Hallbert & Kolaczkowski 2007; Podofillini & Dang 2013; Groth et al. 2014), and in this study it is modified to the new application in construction defect modelling and wind fragility assessment for housing.

4.2 Construction Defects in a Metal Roof

Roof connections are generally the 'weakest links' of the roof system (Henderson & Ginger 2007), and damage surveys (e.g. Leitch et al 2009) have revealed that most roof failures occurred to contemporary houses are caused by poor construction details of roof tie-down fixings. In light of this, the construction defects considered herein are missing and/or improperly installed roof connections, which are commonly observed in housing construction (e.g. Ginger et al. 2010).

4.2.1 Typical defect types for roof connections

This study considers the most common types of construction defects in cladding-to-batten (CTB), batten-to-rafter/truss (BTR) and rafter/truss-to-wall (RTW) connectors for the representative contemporary house as described in Section 3.2. Schematic diagrams for the three types of roof connections are depicted in Fig. 3.2. The typical defect types for these roof connections are inferred from various research reports and post-damage surveys (e.g. Leitch et al. 2009; Ginger et al. 2010; Ginger et al. 2015; Boughton et al. 2015; Satheeskumar 2016), and are listed in Table 4.1. For a single BTR connector, it is possible

that one screw fastener is missing and the other is improperly installed. However, this situation is highly unlikely to occur (extremely small probability), and therefore the two defect types considered for BTR connectors are reasonably assumed to be mutually exclusive.

Table 4.1. Typical types of construction defects in roof connections

Connection type	Description	Defect type
Cladding-to-batten (CTB)	Each CTB connector has one screw fastener, connecting corrugated metal roof sheets to top-hat metal battens	Missing (screw not installed) Improper installation (screw unattached to batten or over- and under-driven screws)
Batten-to-rafter/truss (BTR)	Each BTR connector has two screw fasteners, one at each bottom flange of the top-hat batten, connecting metal battens to timber roof trusses	Missing (one or both screws not installed) Improper installation (over- and under-driven screws)
Rafter/truss-to-wall (RTW)	Triple grip framing anchors, fastening timber roof trusses to wall top plates with nails	Missing one or two nails

4.2.2 Construction defect data

The construction error data of interest are the occurrence rates of defects and the reduction of uplift capacities for defective roof connections. However, only limited construction defect data for roof connections are available, which inevitably bases error quantification on insufficient objective information.

A 1.5% defect rate for installing nails on timber roof sheathing panels was obtained in Hong & He (2015) by inspecting a full-scale North American house built by students in the laboratory. This data provides an indication for missing nails on roofing, however, it cannot be directly employed for missing and/or improperly installed CTB connectors (screw fasteners) on Australian contemporary houses because the construction methods are quite different. In this paper, the average occurrence rate of missing cladding fasteners (i.e. CTB connectors) is obtained from field observations of as-built contemporary houses in the suburbs of Newcastle, Australia. It is not unreasonable to assume the average construction quality in Newcastle is similar to those in other Australian cities. A total of ten metal-clad contemporary houses were visually inspected. These houses are newly built with ages less than five years old. Due to the limited accessibility, for each house specimen, only the viewable parts of metal roof cladding were inspected from the street. Figure 4.1 shows sample photos of the inspected roof area with missing screw fasteners. The number of

inspected fastener locations and the number of missing screws were recorded for each house. Fastener locations refer to the positions on metal roof sheeting where a screw fastener is required. Screw fasteners should be used to fix cladding at every 2nd corrugation of the roof edge and every 3rd or 4th corrugation for other regions of the roof. The missing fastener data obtained for the ten randomly selected contemporary houses are shown in Table 4.2. In total, 3,368 fastener locations were visually inspected, and 13 positions were found to have missing screw fasteners. This corresponds to an average defect rate of 0.39% per fastener. As no spatial patterns (e.g. missing screws are more likely to appear in roof edges than other roof areas) were found in the observed data for missing screw fasteners, it is assumed that defects are uniformly distributed across the roof, and the occurrence rate of missing fasteners in the inspected roof area (at least one side of roof) is comparable to the defect rate of the whole roof. An analysis of variance (ANOVA) test on the observed missing fastener data in Table 4.2 is also conducted, which yields a p-value of 0.35 corresponding to the F-test. This implies no significant difference between the means of defect rate for the ten house samples. The collected data are not perfect due to a small number of houses inspected and limited access to the entire roof. However, it provides a reasonable indication of the missing fastener rate for metal roof cladding on Australian contemporary houses. There is a clear need to collect more data with professional housing inspections.

Table 4.2. Visual inspection data for missing CTB connectors

House No.	Number of inspected fastener locations	Number of missing fasteners
1	256	0
2	525	2
3	362	1
4	408	3
5	344	0
6	378	3
7	372	0
8	324	3
9	213	1
10	186	0
Total	3368	13

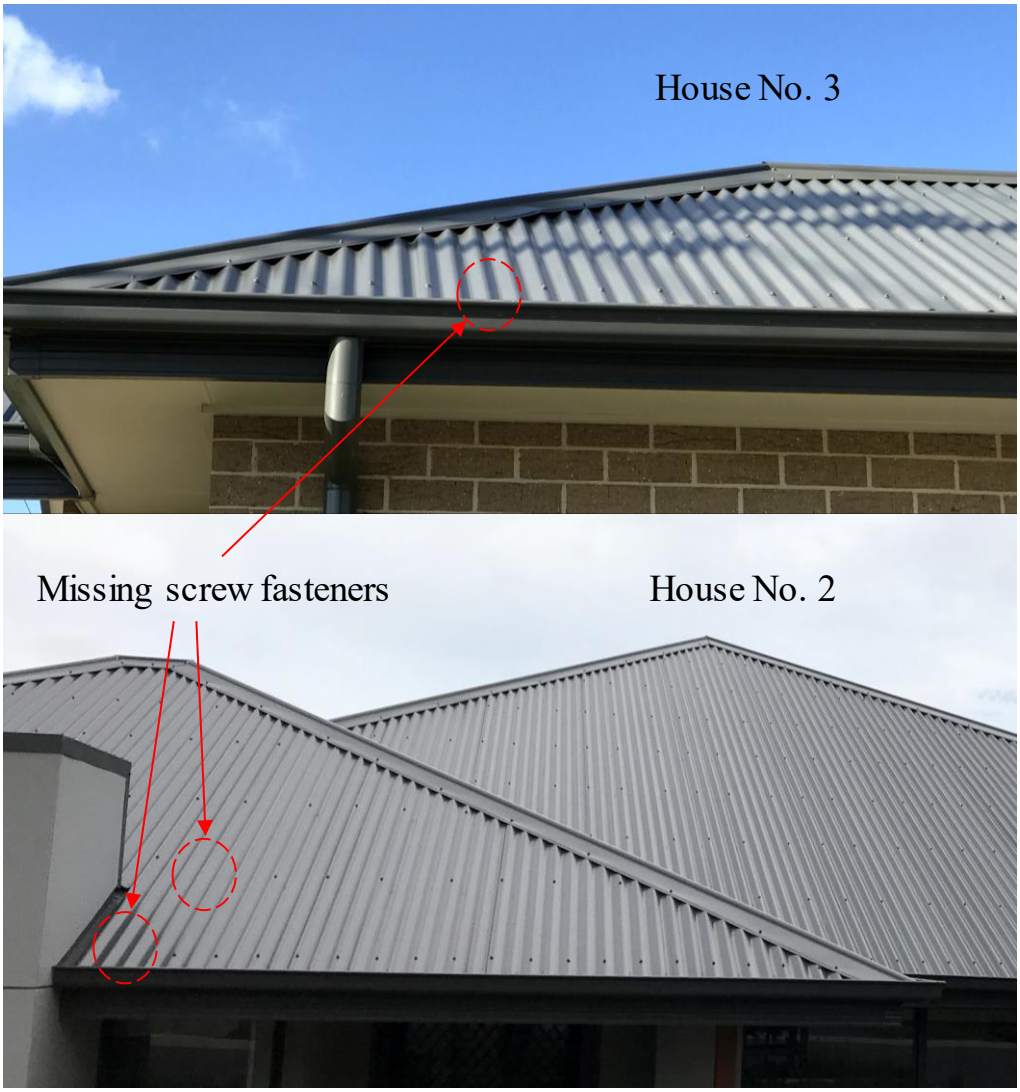

Figure 4.1. Missing cladding fasteners (CTB connectors) on as-built contemporary houses.

The uplift capacities for BTR connectors with under- and over-driven screws are obtained from uplift tests by Boughton et al. (2015) conducted in Australia. It is indicated that over-driving screw fasteners lead to a 50% reduction of withdrawn capacity for BTR connectors, whereas the uplift capacities are similar for BTR connectors with correctly driven or under-driven screws.

Another Australian study (Satheeskumar 2016) found that missing one or two nails in triple grip RTW connectors decreases uplift capacity by up to 40%. This is the most common type of construction defect for triple grip RTW connectors (Satheeskumar 2016), and the present study ignores another less observable type of faults, i.e. grouping nails in triple grip framing anchors. The housing surveys mentioned in Satheeskumar (2016) examined 87 suburban contemporary houses in non-cyclonic regions of Australia and

indicated that about three RTW connectors are defective in most inspected houses but no detailed information are given for each inspected house in the housing surveys. The representative contemporary house considered in this study has 92 triple grip RTW connectors, and then the average defect rate is 3/92 = 3.3% per RTW connector. This inferred data is adopted in the Bayesian updating as anecdotal and indirect evidence with the intention to maximize the use of available information.

All the construction defect data mentioned above are summarized in Table 4.3. As shown in Table 4.3, defect data are incomplete and imperfect due to various limitations. A Bayesian approach is introduced in the next section, which provides a flexible and explicit framework for the quantification of defects in housing construction based on sparse objective information.

Table 4.3. Construction defect data collected from experimental and field observations

Connection type	Defect type	Average defect rate per connection	Capacity reduction per defect
CTB	Missing (screw not installed)	0.39%[a]	100%[b]
	Improper installation (screw unattached to batten or over- and under-driven screw)	Not known	100%[b] (unattached to batten) Not known (over- or under-driven)
BTR	Missing (one or both screws not installed)	Not known	100%[b] (missing both screws) Not known (missing one screw)
	Improper installation (over- and under-driven screws)	Not known	50%[c] (over-driven) 0%[c] (under-driven)
RTW	Missing one or two nails	3.3%[d]	Up to 40%[e]

[a] Based on field observations of as-built metal-clad contemporary houses.
[b] A connection with all screws missing or screws unattached to batten has no capacity.
[c] Based on test results in Boughton et al (2015), reducing withdrawn capacity only.
[d] Inferred data from Satheeskumar (2016).
[e] Based on test results in Satheeskumar (2016).

4.3 Bayesian Method for Defect Rates

4.3.1 Probabilistic model

Suppose that in a house, there are k defect types for a given connection type. For the j^{th} type of roof connection, suppose that there are a total number of n_j connections of this type. To be specific for the representative contemporary house considered in this study, CTB, BTR and RTW connectors are deemed as the first (i.e. j = 1), second (i.e. j = 2) and third

(i.e. j = 3) type of roof connection, respectively. As shown in Table 4.1, two typical defect types (i.e. k = 2) are considered for CTB connectors, whereas BTR and RTW connectors have two (i.e. k = 2) and one (i.e. k = 1) defect types, respectively. The representative contemporary house has a total number of n_1 = 1646 CTB, n_2 = 532 BTR and n_3 = 92 RTW connectors.

The number of a certain type of defects occur in a total number of n_j roof connections of the j^{th} type is assumed to follow a multinomial distribution with a probability mass function (PMF) given as

$$f(x_{1j}, x_{2j}, \ldots, x_{kj}, x_{k+1,j}) = \frac{\Gamma(n_j + 1)}{\prod_{i=1}^{k+1} \Gamma(x_{ij} + 1)} \prod_{i=1}^{k+1} \theta_{ij}^{x_{ij}} = \frac{n_j!}{x_{1j}! \cdots x_{k+1,j}!} \prod_{i=1}^{k+1} \theta_{ij}^{x_{ij}} \tag{4.1}$$

where x_{ij} (i = 1, 2, … , k) and θ_{ij} (i = 1, 2, … , k) are the number and occurrence rate of the i^{th} type of construction defect in the j^{th} type of roof connection, respectively, and $x_{k+1,j}$ and $\theta_{k+1,j}$ represent the number and occurrence rate of correctly installed roof connections of the j^{th} type, respectively, and $\Gamma(\cdot)$ is the gamma function. Note that $\sum_{i=1}^{k+1} x_{ij} = n_j$ (x_{ij} = 0, 1, 2, … , n_j) and $\sum_{i=1}^{k+1} \theta_{ij} = 1$ ($0 \le \theta_{ij} \le 1$). The multinomial distribution is a binomial distribution when k+1=2. Note that the dependence or correlation between defects, i.e. one error or defect is more likely to lead to other errors or defects, is neglected in the proposed defect model.

The defect rate θ_{ij} is inherently variable and uncertain, and in current practice, the defect rates are either assigned using subjective judgement (e.g. Stewart et al. 2018) or estimated from limited construction error data (e.g. Hong & He 2015). Therefore the associated uncertainty and variability may not have been well addressed. The Bayesian method provides an explicit structure to probabilistically infer the defect rates with a combination of expert judgement, HRA techniques and limited objective data, which reduces the degree of uncertainty arising from the complex human behaviour and sparse construction error data.

The subjective beliefs in defect rates $\boldsymbol{\theta_j}$ for the j^{th} type of roof connection are probabilistically expressed by the prior distribution. The data ($\boldsymbol{x_j}$) is used to update the prior information based on the Bayes' rule, and the obtained posterior distribution is then given by

$$f(\boldsymbol{\theta_j}|\boldsymbol{x_j}) = \frac{f(\boldsymbol{\theta_j}, \boldsymbol{x_j})}{f(\boldsymbol{x_j})} = \frac{f(\boldsymbol{x_j}|\boldsymbol{\theta_j}) f(\boldsymbol{\theta_j})}{f(\boldsymbol{x_j})} \tag{4.2}$$

where $f(\boldsymbol{\theta_j}|\boldsymbol{x_j})$ is the posterior distribution of $\boldsymbol{\theta_j}$ with $\boldsymbol{\theta_j} = (\theta_{1j}, \theta_{2j}, \ldots, \theta_{kj}, \theta_{k+1,j})$, $\boldsymbol{x_j} = (x_{1j}, x_{2j}, \ldots, x_{kj}, x_{k+1,j})$ is the observed data for defective and correctly installed roof connections of the j^{th} type, $f(\boldsymbol{x_j}|\boldsymbol{\theta_j})$ is the likelihood function of $\boldsymbol{x_j}$, $f(\boldsymbol{\theta_j})$ is the prior distribution of $\boldsymbol{\theta_j}$, and $f(\boldsymbol{x_j})$ is an integral of the product $f(\boldsymbol{x_j}|\boldsymbol{\theta_j})f(\boldsymbol{\theta_j})$ over all possible values of $\boldsymbol{\theta_j}$, which can be regarded as a normalizing constant to ensure that $f(\boldsymbol{\theta_j}|\boldsymbol{x_j})$ is a proper density.

4.3.2 Prior distributions

4.3.2.1 Dirichlet priors

To account for the uncertainty and variability involved in the defect rates, $\boldsymbol{\theta_j}$ are probabilistically modelled by the Dirichlet distribution, which is a conjugate prior distribution for the multinomial distribution. The Dirichlet distribution is a multivariate generalization of the beta distribution. The probability density function (PDF) of the Dirichlet prior for $\boldsymbol{\theta_j} = (\theta_{1j}, \theta_{2j}, \ldots, \theta_{kj}, \theta_{k+1,j})$ is given by

$$f(\boldsymbol{\theta}_j) = \text{Dirichlet}(\boldsymbol{\theta}_j \mid a_{1j}, a_{2j}, \ldots, a_{kj}, a_{k+1,j}) = \frac{\Gamma(\sum_{i=1}^{k+1} a_{ij})}{\prod_{i=1}^{k+1} \Gamma(a_{ij})} \prod_{i=1}^{k+1} \theta_{ij}^{a_{ij}-1} \tag{4.3}$$

where $\boldsymbol{\alpha_j} = (\alpha_{1j}, \alpha_{2j}, \ldots, \alpha_{kj}, \alpha_{k+1,j})$ are the positive-valued parameters for the Dirichlet distribution for the j^{th} type of roof connection. Let $\alpha_{0j} = \sum_{i=1}^{k+1} \alpha_{ij}$. The marginal mean and variance of θ_{ij} are then given by

$$\mathrm{E}(\theta_{ij}) = \frac{\alpha_{ij}}{\alpha_{0j}} \tag{4.4}$$

$$\mathrm{var}(\theta_{ij}) = \frac{\alpha_{ij}(\alpha_{0j} - \alpha_{ij})}{\alpha_{0j}^{2}(\alpha_{0j}+1)} \tag{4.5}$$

Generally, α_{0j} can be viewed as a measure of the prior informativity. The larger the value of α_{0j} is, the more informative the Dirichlet priors. Further, let $\boldsymbol{\alpha_j} = \alpha_{0j}\boldsymbol{v_j}$, where $\boldsymbol{v_j}$ is a vector of the marginal mean of $\boldsymbol{\theta_j}$ given by $\boldsymbol{v_j} = (v_{1j}, v_{2j}, \ldots, v_{kj}, v_{k+1,j}) = (\alpha_{1j}, \alpha_{2j}, \ldots, \alpha_{kj}, \alpha_{k+1,j})/\alpha_{0j}$, and it satisfies $\sum_{i=1}^{k+1} v_{ij} = 1$. The prior parameters for the defect rates $\boldsymbol{\theta_j}$ for the j^{th} type of roof connection can then be determined by specifying $\boldsymbol{v_j}$ and α_{0j}. In the present Bayesian method, informative prior distributions are proposed to reflect expert's knowledge of the occurrence rates for distinct types of construction defects in CTB, BTR and RTW connectors as listed in Table 4.1.

CREAM (Hollnagel 1998), a widely used HRA technique, which offers a systematic modelling of human error occurrence based on cognitive engineering principles, is

employed to give point estimates of $\boldsymbol{v_j}$. The application of CREAM to the determination of $\boldsymbol{v_j}$ is described in the next section. The parameter, α_{0j}, plays a role of weighing the expert judgement and the sparse data of construction defects. If α_{0j} is much smaller than the data size (e.g. n_1 = 3368 for CTB connectors as shown in Table 4.2), the evidence used in Bayesian updating overwhelms the prior beliefs. In other words, the prior distribution in this scenario can be viewed as a weakly informative prior with limited influence on the posterior distribution. Otherwise, if α_{0j} is much larger than the size of data, the prior dominants the Bayesian inference. Ideally, it is desirable to specify a relatively small value of α_{0j} (i.e. use non-informative or weakly informative priors) and conduct the Bayesian updating based on sufficient objective data. However, due to the scarcity of construction defect data, the selection of α_{0j} depends on the level of confidence towards the prior beliefs and the limited evidence. The analyst may set α_{0j} to be comparable with the data size to give similar weights to the expert opinion and the sparse data of construction defects.

4.3.2.2 Specifying prior parameters

Informative prior distributions are used for the defect rates to reveal experts' subjective knowledge and judgement. HRA techniques offer theoretical models to quantitatively predict human performance under given conditions and/or contexts, which can be used to express the prior beliefs about construction defect rates.

All erroneous human actions are, to some extent cognitive, and cannot be properly modelled or understood without referring to the characteristics of human cognition (Hollnagel 1998). In this study, the HRA approach, CREAM, is employed to provide prior information for the defect rates. Based on cognitive engineering principles, CREAM can reasonably address the underlying mechanism of human error occurrence. The psychological, physiological and sociological factors involved in human error are captured by CREAM through the cognitive functions and common performance conditions. See Hollnagel (1998) for more details. A basic and an extended method are included in the quantitative analysis of CREAM. The purpose of the former is to produce a general assessment of human reliability for a given task, and the latter aims to provide point estimates for specific human error probabilities (i.e. HEP or what we call 'defect rates' in this study).

The task of installing a roof connection is considered to include two main subtasks based on the practical procedures adopted by construction workers: (i) install the roof connection

at the right position, and (ii) visual check if any fastener is missing. The visual check can happen any time during the installation of roof connections, however, herein we consider only an overall check is conducted after the completion of the installation work. It is further assumed that any missing nails or screws that have been detected will be installed immediately, and only missing fasteners can be identified by a visual inspection. In other words, misaligned, over- and under-driven fasteners are deemed to be difficult to detect by a simple visual check. To complete these two subtasks, the builder needs to be equipped with many things such as the rules/procedures for connection installations, tips in fastening using an electric drill, and perceptions for detecting missing fasteners. Hence, the actual actions when conducting these subtasks are only the surface manifestations of the underlying human cognition.

In the basic method of CREAM, (i) common performance conditions (CPCs) and (ii) control modes are determined. CPCs are used to characterize the human interactions with contexts and/or circumstances. The control mode is determined by the CPCs, which provides an overall range of the defect rates. In this study, as the CPCs are not observed during the construction process, a set of neutral CPCs (i.e. no improvement or reduction for performance reliability) are considered as the expected or representative context for typical housing construction. Based on the neutral CPCs, the tactical control mode is then selected, where human performance is based on planning, and more or less follows a known procedure or rule (Hollnagel 1998). This control mode gives an overall evaluation that the defect rates are within 0.1% and 10% (Hollnagel 1998), which is compatible with the average defect rates shown in Table 4.3. The tactical control mode is also consistent with a qualitative view that the installation of roof connections is mostly a rule-based activity. In this study, the main purpose of using CREAM is to produce specific point estimates for construction defect rates. Hence, the basic method of CREAM is only briefly described in this section. More details about the determination of the CPCs and control modes can be found in Hollnagel (1998).

The extended method in CREAM is used to produce specific human action failure probabilities in this study. The cognitive demands associated with a task or subtask can be described by a single or combination of four basic cognitive functions, namely, observation, interpretation, planning, and execution (Hollnagel 1998). The possible failure modes for each cognitive function and corresponding nominal cognitive failure probabilities (i.e. error rates) in CREAM (Hollnagel 1998) are given in Table 4.4. The major cognitive activities

and corresponding cognitive functions are assigned to each subtask for the roof connection installation which is shown in Table 4.5. Table 4.6 lists the main failure modes and nominal defect rates produced by CREAM for distinct types of construction defects in roof connections. For example, the manifestation of a missing CTB connector is due to the situation that the screw fastener is simply not installed (failure type E5) and later this ignorance has not been detected by a simple visual check (failure type O3). Therefore, the nominal defect rate for missing cladding fasteners in Table 4.6 is then calculated as 3% (i.e. nominal error rate for generic failure type E5) 7% (i.e. nominal error rate for generic failure type O3) = 0.21%. As shown in Table 4.6, the nominal defect rates have comparable magnitudes with the available objective information (i.e. average defect rates) listed in Table 4.3, which indicates the compatibility of the elicited prior and defect data.

Table 4.4. Cognitive failure modes and nominal cognitive failure probabilities (Hollnagel 1998).

Cognitive function	Generic failure type	Nominal error rate
Observation (O)	O1. Wrong object observed	0.10%
	O2. Wrong identification	7.0%
	O3. Observation not made	7.0%
Interpretation (I)	I1. Faulty diagnosis	20%
	I2. Decision error	1.0%
	I3. Delayed interpretation	1.0%
Planning (P)	P1. Priority error	1.0%
	P2. Inadequate plan	1.0%
Execution (E)	E1. Action of wrong type	0.30%
	E2. Action at wrong time	0.30%
	E3. Action on wrong object	0.05%
	E4. Action out of sequence	0.30%
	E5. Missed action	3.0%

Table 4.5. Cognitive activities and functions for each subtask for roof connection installation.

Subtask	Description	Cognitive activity	Cognitive function
Install roof connections	Fasten nails or screws for CTB, BTR and RTW connectors	Execute	Execution
Visual check missing nails or screws	Overall visual inspection after installation work	Observe	Observation

Table 4.6. Cognitive failure modes and nominal defect rates produced by CREAM.

Connection type	Typical defect type	Generic failure type	Nominal defect rate	Average defect rate in Table 4.3
CTB (j = 1, k =2)	Missing (i = 1)	E5 and O3	θ_{11} = 0.21%	0.39%
	Improper installation (i = 2)	E1	θ_{21} = 0.30%	Not known
BTR (j = 2, k =2)	Missing (i = 1)	E5 and O3	θ_{12} = 0.42%	Not known
	Improper installation (i = 2)	E1	θ_{22} = 0.60%	Not known
RTW (j = 3, k = 1)	Missing one or two nails (10 nails in total, i = 1)	E5 and O3	θ_{13} = 2.12%	3.30%

The nominal defect rates can be further modified by applying the common performance conditions (CPCs) to characterize the human interactions with working contexts and quantify the improvement or reduction of human reliability due to the working contexts (Hollnagel 1998). For example, inadequate project time and/or unexperienced builders can reduce the human reliability and thus increase the defect rates. The CPCs are analogous to the performance shaping factors (PSFs) in many other HRA methods (e.g. Kirwan 1996; Blackman et al. 2008), and hereafter we use the term PSFs. In this study, as the working contexts are not observed during the construction process, the PSFs are set to unity, indicating no improvement or reduction for human reliability, which is considered as the expected or representative context for typical housing construction. Therefore, the nominal defect rates are adopted as the point estimates produced by CREAM, which can be further used to assign the prior parameters. In a sensitivity analysis in Section 4.5, the potential effects of adverse working contexts (i.e. PSFs > 1.0) are further examined.

The point estimates produced by CREAM are employed to specify the Dirichlet prior parameters. As described in Section 4.3.2.1, the Dirichlet distribution for defect rates can be expressed as Dirichlet ($\boldsymbol{\theta_j}|\alpha_{0j}\boldsymbol{v_j}$). These point estimates for the defect rates of the j^{th} type roof connection are then used as the marginal mean values, $\boldsymbol{v_j}$, in the Dirichlet prior distributions. The value of α_{0j} is determined by subjective judgement to reflect various levels of prior beliefs. The Dirichlet prior distributions assigned for the defect rates for CTB, BTR and RTW connectors are then given in Table 4.7. As only one typical defect type is considered for RTW connectors, the two-dimensional Dirichlet distribution is a beta distribution used as the prior for the defect rate. The prior distributions of construction defect rates for CTB, BTR and RTW connectors considering different $\boldsymbol{\alpha_0}$ values are plotted in Figs. 4.2, 4.3 and

4.4, respectively. Note that $\boldsymbol{\alpha_0} = (\alpha_{01}, \alpha_{02}, \alpha_{03})$ with $j = 1$, 2 and 3 are for CTB, BTR and RTW connectors, respectively. As expected, the larger the $\boldsymbol{\alpha_0}$ value, the smaller the variance and the higher degree of informativity for the prior distribution.

Table 4.7. Dirichlet prior distributions for defect rates.

Connection type	Dirichlet prior distributions for $\boldsymbol{\theta_j}$	α_{0j} value
CTB ($j = 1$)	$\boldsymbol{\theta_1} = (\theta_{11}, \theta_{21}, \theta_{31}) \sim$ Dirichlet $(0.0021\alpha_{01}, 0.0030\alpha_{01}, 0.9949\alpha_{01})$	Express the degree of prior beliefs about the defect rates for the j^{th} type of roof connection, determined by expert judgement
BTR ($j = 2$)	$\boldsymbol{\theta_2} = (\theta_{12}, \theta_{22}, \theta_{32}) \sim$ Dirichlet $(0.0042\alpha_{02}, 0.0060\alpha_{02}, 0.9898\alpha_{02})$	
RTW ($j = 3$)	$\boldsymbol{\theta_3} = (\theta_{13}, \theta_{23}) \sim$ beta $(0.021\alpha_{03}, 0.979\alpha_{03})$ or Dirichlet $(0.021\alpha_{03}, 0.979\alpha_{03})$	

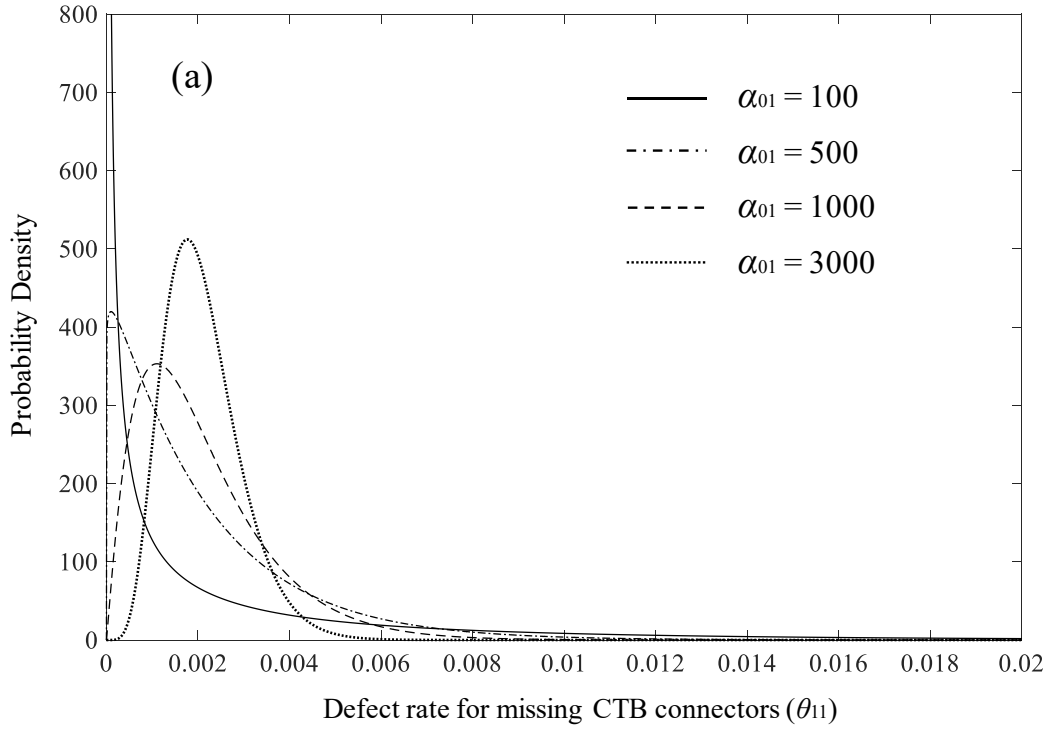

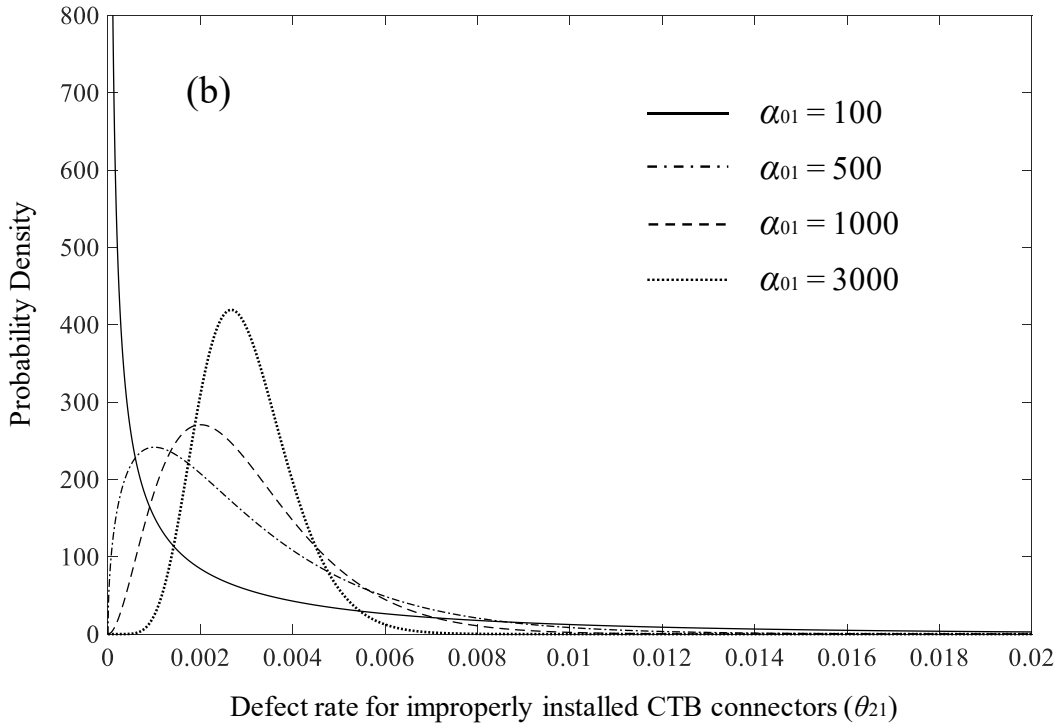

Figure 4.2. Marginal distributions of the Dirichlet prior for defect rates of CTB connectors with different α_{01} values.

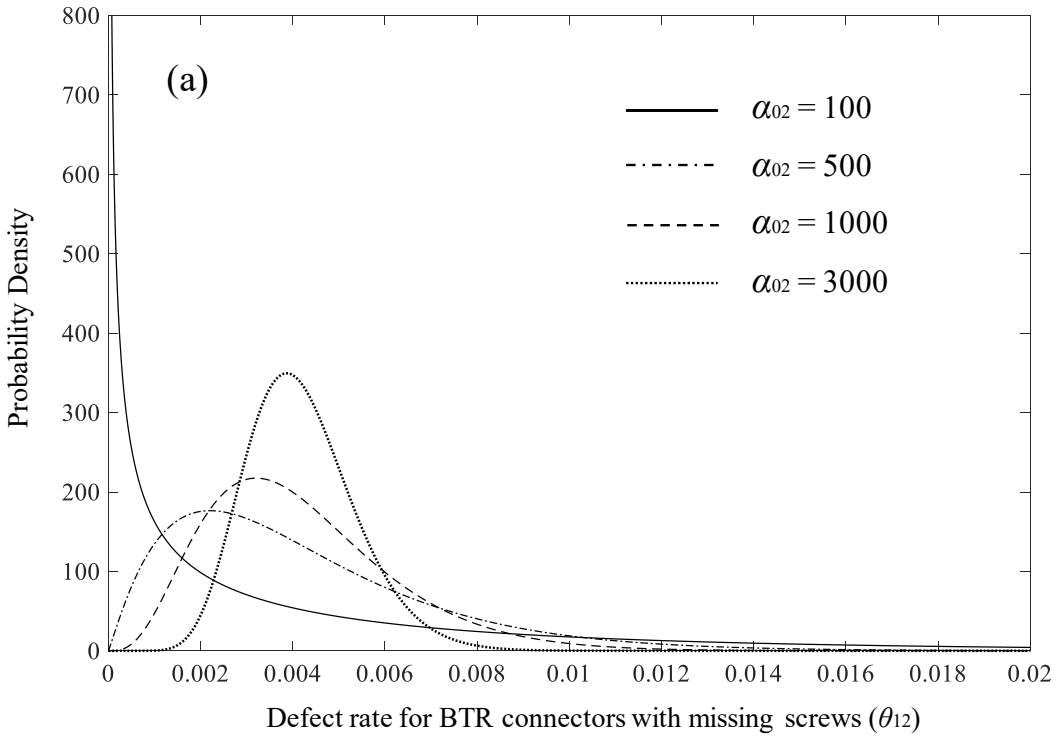

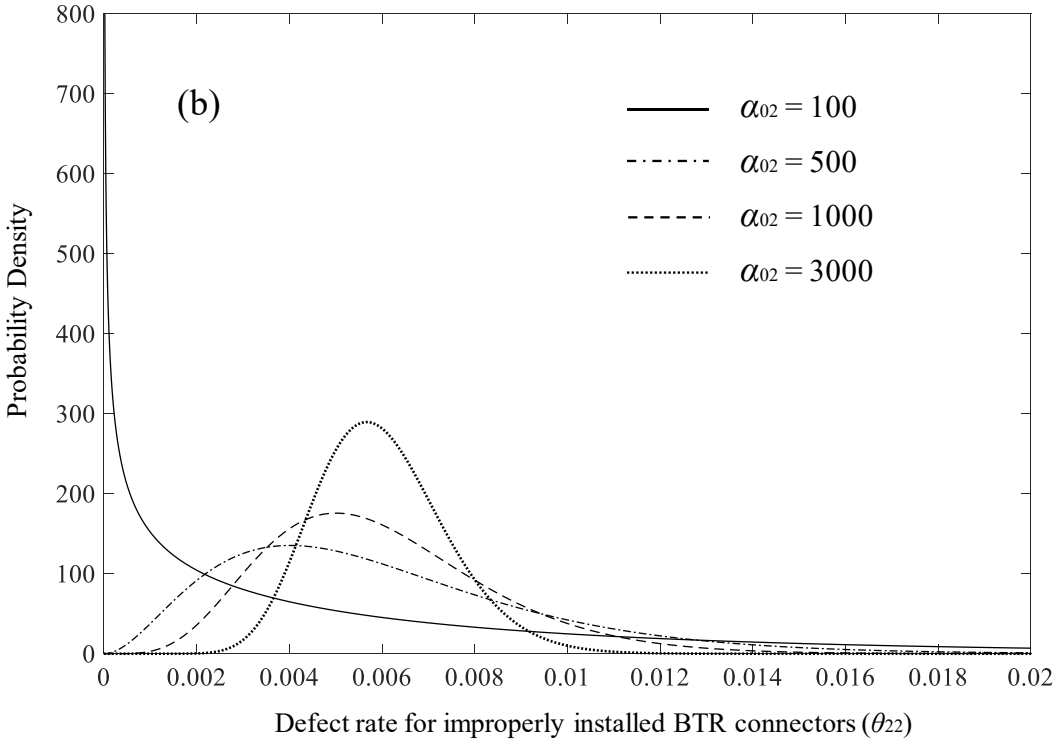

Figure 4.3. Marginal distributions of the Dirichlet prior for defect rates of BTR connectors with different α_{02} values.

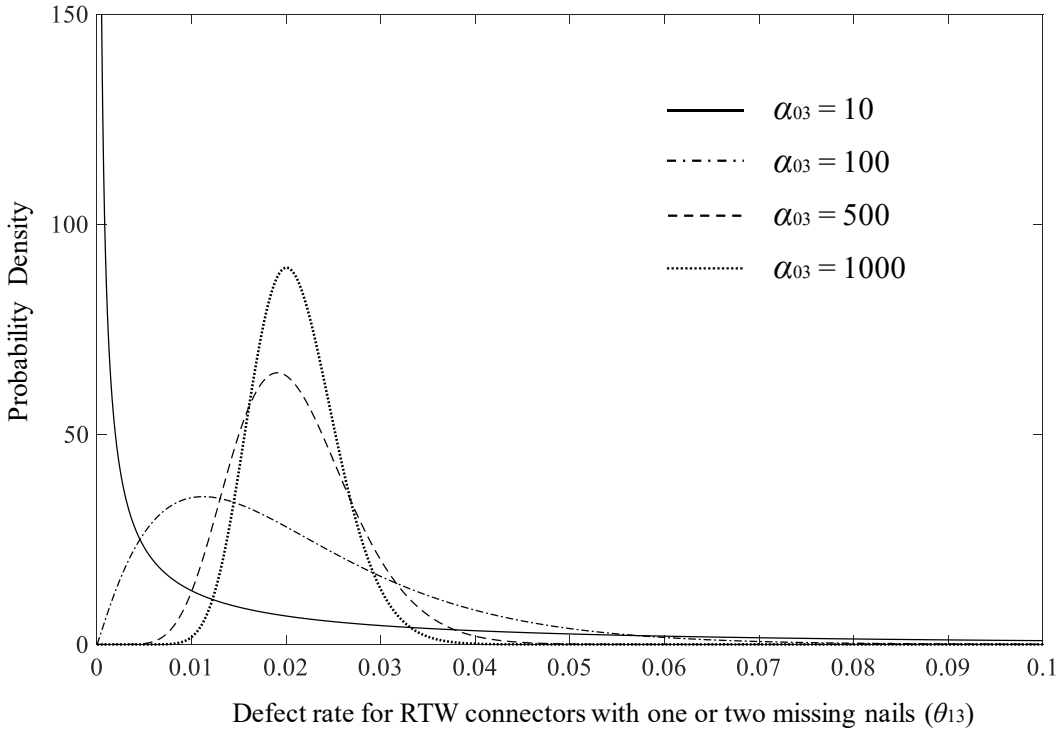

Figure 4.4. Prior distributions for the defect rate of RTW connectors with different α_{03} values.

4.3.3 Posterior distributions

The Dirichlet distribution is a conjugate prior to the multinomial distribution. Suppose a number of n_j roof connections of the j^{th} type have been inspected, and x_{ij} (i = 1, 2, … , k) defective connections are detected for the i^{th} type of construction defect. The posterior distribution for the defect rates $\boldsymbol{\theta_j}$ of the j^{th} type roof connection is also a Dirichlet distribution given by

$$f\left(\boldsymbol{\theta}_j \middle| n_j, \boldsymbol{x}_j\right) = \text{Dirichlet}\ (\boldsymbol{\alpha}_j + \boldsymbol{x}_j) \tag{4.6}$$

where $\boldsymbol{\alpha_j} = (\alpha_{1j}, \alpha_{2j}, \ldots, \alpha_{kj}, \alpha_{k+1,j}) = \alpha_{0j}\boldsymbol{v_j}$, $\boldsymbol{\theta_j} = (\theta_{1j}, \theta_{2j}, \ldots, \theta_{kj}, \theta_{k+1,j})$ and $\boldsymbol{x_j} = (x_{1j}, x_{2j}, \ldots, x_{kj}, x_{k+1,j})$. Note that $x_{k+1,j} = n_j - \sum_{i=1}^{k} x_{ij}$. The Bayesian updating is straightforward with conjugate prior distributions if complete data are given. However, as shown in Table 4.3, data are incomplete and imperfect for the construction defects in roof connections, and therefore more efforts are needed to make the Bayesian inference.

4.3.3.1 CTB connectors

For CTB connectors (the 1st type of roof connection, i.e. j = 1), there are two types of construction defects (i.e. k = 2) considered in this study as shown in Table 4.1. The model parameters of interest are $\boldsymbol{\theta_1} = (\theta_{11}, \theta_{21}, \theta_{31})$, where θ_{11} and θ_{21} are the defect rates for missing and improperly installed CTB connectors, respectively, and $\theta_{31} = 1 - \theta_{11} - \theta_{21}$ is the occurrence rate for correctly installed CTB connectors. If a total of n_1 CTB connectors have been inspected, $\boldsymbol{x_1} = (x_{11}, x_{21}, x_{31})$ then represent the number of missing, improperly installed and correctly installed CTB connectors, where $x_{11} + x_{21} + x_{31} = n_1$. According to Tables 4.2 and 4.3, n_1 = 3368, x_{11} = 13 and x_{21} is not known. The posterior distribution for defect rates of CTB connectors in Eq. (4.6) then transforms into $f\,(\boldsymbol{\theta_1}|\, n_1, x_{11})$, which is proportional to the multiplication of the Dirichlet prior and the observed data (incomplete) likelihood, expressed as

$$f(\boldsymbol{\theta}_1 \mid x_{11}, n_1) \propto \left(\prod_{t=1}^{3} \theta_{t1}^{\alpha_{t1}-1}\right)\theta_{11}^{x_{11}}(\theta_{21}+\theta_{31})^{n_1-x_{11}} = \sum_{t=0}^{n_1-x_{11}} \frac{(n_1-x_{11})!}{t!(n_1-x_{11}-t)!}\left[\theta_{11}^{x_{11}-\alpha_{11}-1}\theta_{21}^{t+\alpha_{21}-1}\theta_{31}^{n_1-x_{11}-t+\alpha_{31}-1}\right] \tag{4.7}$$

The posterior distribution for the defect rates of CTB connectors given by Eq. (4.7) can be numerically evaluated using the Markov Chain Monte Carlo (MCMC) methods (e.g. Gelman et al. 1995). Figure 4.5 depicts the marginal posterior distributions for the defect rates of CTB connectors considering different α_{01} values. The corresponding prior distributions are also plotted in the figure. As shown in Fig. 4.5, the posterior distribution is

getting closer to the prior distribution as α_{01} increases. The smaller the α_{01} value, the more diffuse the posterior distribution. As no defect data is available for improperly installed CTB connectors, the obtained marginal posterior distribution for the defect rate θ_{21} from Bayesian updating is then more spread out to reflect a higher level of uncertainty involved.

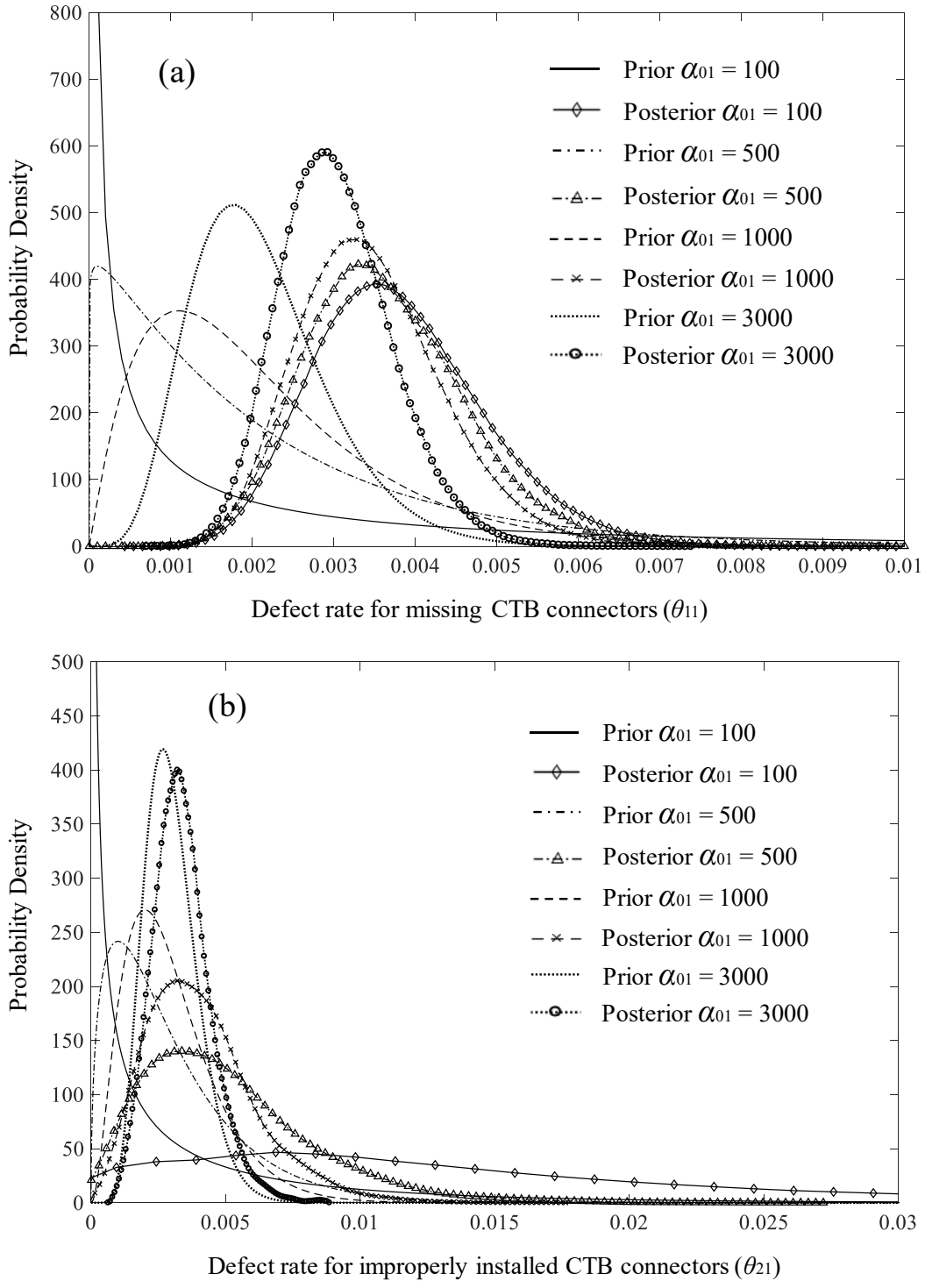

Figure 4.5. Marginal posterior distributions for defect rates of CTB connectors with different α_{01} values.

4.3.3.2 BTR connectors

As shown in Table 4.3, no observed data are available for the two types of construction defects for BTR connectors (the 2nd type of roof connection, i.e. j = 2). Therefore, no Bayesian updating is carried out for BTR connectors, and the prior distribution, i.e. Dirichlet ($0.0042\alpha_{02}$, $0.0060\alpha_{02}$, $0.9898\alpha_{02}$) as shown in Table 4.7 is directly used for the defect rates for BTR connectors.

4.3.3.3 RTW connectors

For RTW connectors (the 3rd type of roof connection, i.e. j = 3), the defect data is inferred from Satheeskumar (2016) that states 87 Australian contemporary houses were inspected in housing surveys and most inspected houses have about three defective triple grip RTW connections with no more details given. This evidence about construction defects for RTW connectors is based on vague descriptions, which is somewhat anecdotal and uncertain. The inferred defect data are then deemed to have three defective triple grip connections in the representative contemporary house with 92 RTW connectors. In other words, only the most representative case for the number of observed defects in a typical contemporary house is considered as the evidence used for Bayesian updating, which may introduce relatively high uncertainties for the defect rate. Given the conjugate prior distribution, i.e. beta ($0.021\alpha_{03}$, $0.979\alpha_{03}$) as shown in Table 4.7, the posterior distribution for the defect rate of RTW connectors θ_{13} is straightforward to obtain through the Bayesian updating, which is given by beta ($0.021\alpha_{03}$ + 3, $0.979\alpha_{03}$ + 89). A relatively higher value of α_{03} (e.g. 200, 500 and 1000) may be used to give more preference to the prior beliefs produced by the HRA method. Figure 4.6 shows the posterior distributions for the defect rate of RTW connectors considering different α_{03} values. The corresponding prior distributions are also plotted in the figure. Smaller α_{03} values lead to more dispersive posterior distributions for the defect rate θ_{13} of RTW connectors, which has similar trends with those shown in Fig. 4.5.

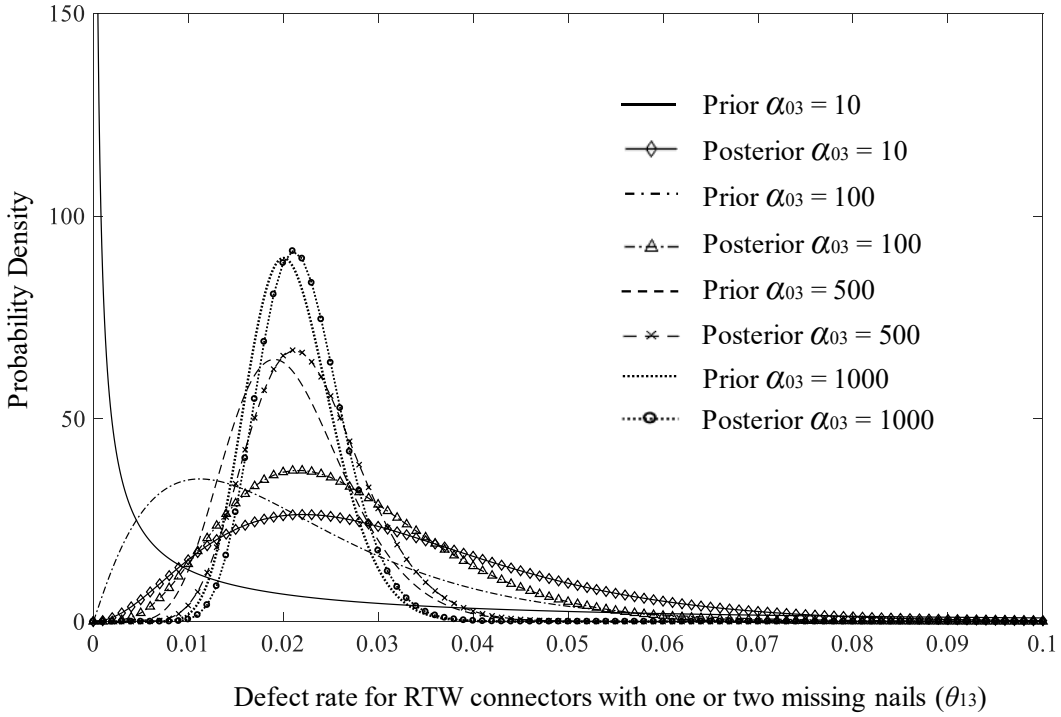

Figure 4.6. Posterior distributions for the defect rate of RTW connectors with different α_{03} values.

4.4 Uplift Capacities for Defective Roof Connections

The uplift capacities for correctly installed (i.e. defect free) roof connections are presented in Section 3.4.2. The pull-over and pull-out capacities of CTB and BTR connectors are assumed to follow a lognormal distribution (Henderson & Ginger 2007) with the statistical parameters listed in Table 3.2. The connection capacities are assumed to be statistically independent and taken as the lower of the randomly generated pull-out and pull-over strengths when conducting a fragility analysis. The uplift capacities for triple grip RTW connectors fastened using hand nails and gun nails are given by Table 3.3 as described in Section 3.4.2.

The data regarding the capacity reduction for roof connections given the occurrence of various types of construction defects are discussed in Section 4.2.2 and summarized in Table 4.3. For missing CTB connectors, it is natural to judge that there is no uplift capacity at the missing fastener location. For improperly installed CTB connectors, if a screw fastener is not attached to the batten, the uplift capacity of the connection is also zero. If a cladding fastener is over- or under-driven, as no uplift capacity data is available, a triangular probability distribution used in Stewart et al. (2018) is employed to model the capacity reduction as shown in Table 4.8.

For BTR connectors, it is assumed that at least 50% capacity reduction with one missing batten screw and 100% capacity reduction if both screws are missing. As the latter has a much smaller occurrence rate than the former, a triangular probability distribution shown in Table 4.8 with a mode of 50% is used. Given the occurrence of an improperly installed BTR connector with over- or under-driven screws, it is considered that the over-driven scenario has a 50% probability of occurrence and reduces the pull-out capacity by about 50% (Boughton et al 2015). Note that there is no capacity reduction for the under-driven scenario. To account for the variability of capacity reduction, a triangular probability distribution given in Table 4.8 with a mode of 50%, a lower bound of 40% and an upper bound of 60% is assumed to model the reduction of pull-out capacity for BTR connectors with over-driven batten screws.

According to the test results in Satheeskumar (2016), approximately 10% capacity reduction was observed for triple grip RTW connectors with one missing nail and 40% reduction of the uplift capacity for those with two missing nails. A triangular probability distribution shown in Table 4.8 is then used to model the capacity reduction for triple grip RTW connectors with one or two missing nails. The piecewise-linear relationship described in Section 3.5.2 is still used to model the load-deflection behaviour of defective RTW connectors. All the three parameters (i.e. initial secant stiffness k_0, peak load F_u and displacement at peak load δ_u) in the piecewise-linear model are also assumed to decrease according to the triangular probability distribution.

The reduction of uplift capacities for defective roof connections are summarized in Table 4.8. Note that all the percentages of reduction mentioned above are compared to the uplift capacities of correctly installed roof connections described in Section 3.4.2.

4.5 Effect of Construction Defects

The construction defect model for roof connections proposed in this chapter is incorporated in the reliability-based fragility assessment for metal roof cladding and timber roof trusses as described in Chapter 3. As mentioned in Chapter 3, two typical opening scenarios are considered, i.e. (i) dominant openings on the windward wall and (ii) effectively sealed building without any wall openings.

Table 4.8. Capacity reduction for defective roof connections.

Connection type	Defect type	Capacity reduction
CTB	Missing (screw not installed)	100%
	Improper installation (screw unattached to batten or over- and under-driven screws)	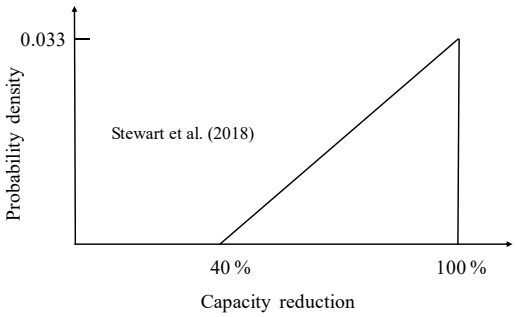
BTR	Missing (one or both screws not installed)	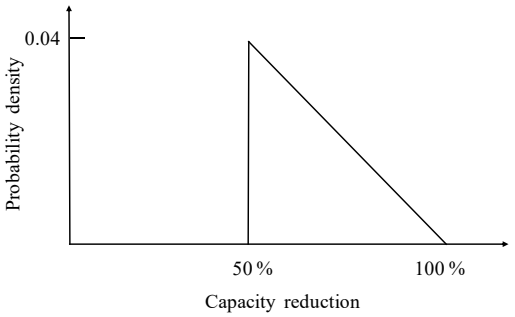
	Improper installation (over- and under-driven screws)	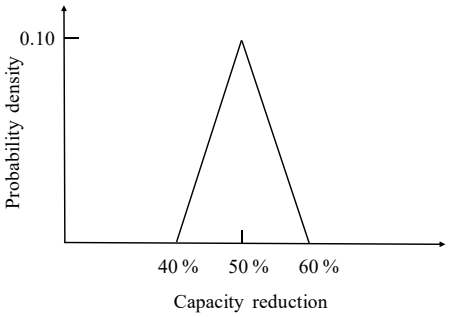 Reduction of pull-out capacity only for those with over-driven screws
RTW	Missing one or two nails	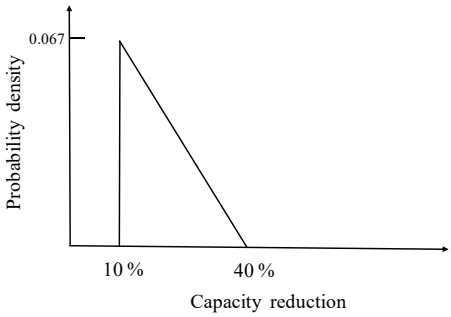

Distinct degrees of prior beliefs about the defect rates are taken into account for the

fragility analysis. The levels of confidence towards the prior are determined by the $\boldsymbol{\alpha_0}$ values as described in Section 4.3.2. The prior distributions are based on both the point estimates yielded by the HRA method (i.e. CREAM in this study) and the selection of $\boldsymbol{\alpha_0}$ values according to expert's opinion. The $\boldsymbol{\alpha_0}$ values selected in this study for the defect rates in CTB, BTR and RTW connectors are listed in Table 4.9. The three sets of $\boldsymbol{\alpha_0}$ values in Table 4.9 reflect relatively strong, moderate and weak prior belief, respectively. The moderate prior is considered as a baseline case, and the strong and weak priors are employed to examine the sensitivity of fragility to the prior beliefs about construction defect rates.

The selection of α_{0j} value for the j^{th} type of roof connection is based on the following subjective judgement. For CTB connectors, as a relatively large data size is available for the defect type of missing cladding fasteners, more preferences are then given to the defect data (i.e. 'let data speak louder'). Thus, a α_{01} value of 1000 is selected in the baseline case, which is roughly one third of the data size (i.e. 3368). The strong prior case has a α_{01} value comparable to the number of observations. In the weak prior case, a α_0 value of 500 is used to ensure that the posterior distribution for the defect rate of improperly installed CTB connectors as shown in Fig. 4.5(b) is not too diffuse. For BTR connectors, as no defect data are available, the prior distributions for the defect rates are directly employed. The selected α_{02} values for the three cases produce reasonable probability distributions for the defect rates of BTR connectors as shown in Fig. 4.3. For RTW connectors, the defect data are inferred from vague descriptions in the literature, which is somewhat anecdotal. Hence, more preferences are given to the prior distribution that are derived from the HRA model (i.e. CREAM). In the weak prior case, the α_{03} value is comparable to the inferred data size (i.e. 92). The moderate and strong prior cases have α_{03} values that are about five and ten times the inferred data size, respectively. The $\boldsymbol{\alpha_0}$ values can be further modified if more expert knowledge and/or objective data about the construction defect rates are available.

As mentioned in Section 4.3.2.2, an average construction quality is assumed in the baseline case, and the working contexts (usually characterized by PSFs) are not explicitly taken into account (i.e. neutral PSFs without improving or reducing human performance are assumed) as no observations for such contexts are available during the construction process. Some adverse working contexts may result in poor construction quality with high defect rates. For example, builders with less experience/training, inadequate time and unclear procedures/plans all have negative effects on the human performance and reliability. Ideally, both the construction defect data and corresponding working contexts need to be collected,

and the probability distribution of the defect rates conditional on PSFs can then be obtained through the Bayesian updating. However, such data are challenging to collect due to many reasons such as restrictive access to construction sites, privacy issues (e.g. people do not like to disclose their mistakes and/or to be monitored while working), etc. A single PSF value ranges from 0.5 to 5.0 in CREAM (Hollnagel 1998). Considering that most contemporary houses are constructed by qualified builders, a relatively low effect of PSFs on defect rates is assumed in a sensitivity analysis. Thus, the negative effects of adverse working contexts are implicitly included and examined by applying a factor of two (close to the average weighting factor of 1.9 to account for effects of PSFs suggested for the tactical control mode in CREAM) to the baseline defect rates obtained from the Bayesian inference. The subsequent effects on the proportion of roof sheeting loss and roof truss failures are then examined by conducting the fragility assessment with the adjusted defect rates.

Table 4.9. Degree of prior beliefs for each defect type.

Connection type	Typical defect type	α_{0j} value reflecting the level of confidence towards prior beliefs		
		Strong	Moderate (baseline case)	Weak
CTB (j = 1)	Missing Improper installation	3000	1000	500
BTR (j = 2)	Missing Improper installation	3000	1000	500
RTW (j = 3)	Missing one or two nails	1000	500	100

The construction defects are often correlated or dependent, i.e. one error or defect is more likely to lead to other errors or defects, which is not included in the model formulation as described in Section 4.3. In a sensitivity analysis, the effect of correlation between defects on the wind fragility is simply examined by applying an empirical equation to the defect rates in the baseline case. The probability of a defect given a defect occurs in the previous task is obtained from the following equation (Kirwan 1994)

$$\Pr(\text{defect} \mid \text{defect occurs in previous task}) = \left(\frac{1+A\cdot\text{defect rate}}{A+1}\right) \tag{4.8}$$

where A = 19, 6 and 1 for low, moderate and high dependence, respectively. A moderate correlation is assumed in the present analysis.

The fragility results for the representative contemporary house with construction defects, expressed as the mean proportion of roof sheeting loss and roof truss failures, are shown in

Figs. 4.7 and 4.8, respectively, with the consideration of distinct degrees of prior beliefs, the effects of adverse working contexts and dependence between defects. As shown in Fig. 4.7, the effect of construction defects on the roof cladding fragility is significant. For example, compared to the fragility results ignoring construction defects, the predicted mean proportion of roof sheeting loss in the baseline case increases by up to eight times when gust wind speed is smaller than 55m/s, and up to 52% higher, when gust wind speed is larger than 55m/s with the presence of windward wall dominant openings. At the design wind speed for Brisbane (i.e. 57m/s) and for the dominant opening scenario, the mean proportion of roof sheeting loss increases from 4.5% to 6.5% when considering the construction defects in the baseline case. At the design wind speed for Melbourne (i.e. 45m/s) and for the dominant opening scenario, the mean proportion of roof sheeting loss increases five-fold from 0.1% to 0.5% when considering the construction defects in the baseline case. Accounting for the potential influence of adverse working contexts can increase the roof cladding fragility by approximately six times on average. The consideration of dependence between defects on average leads to approximately a threefold increase in the predicted mean proportion of roof sheeting loss. The predicted mean proportion of roof sheeting loss increases with decreasing degrees of prior beliefs. This is expected as a weak prior distribution results in a relatively high variance for the posterior distributions of the defect rates as shown in Fig. 4.5.

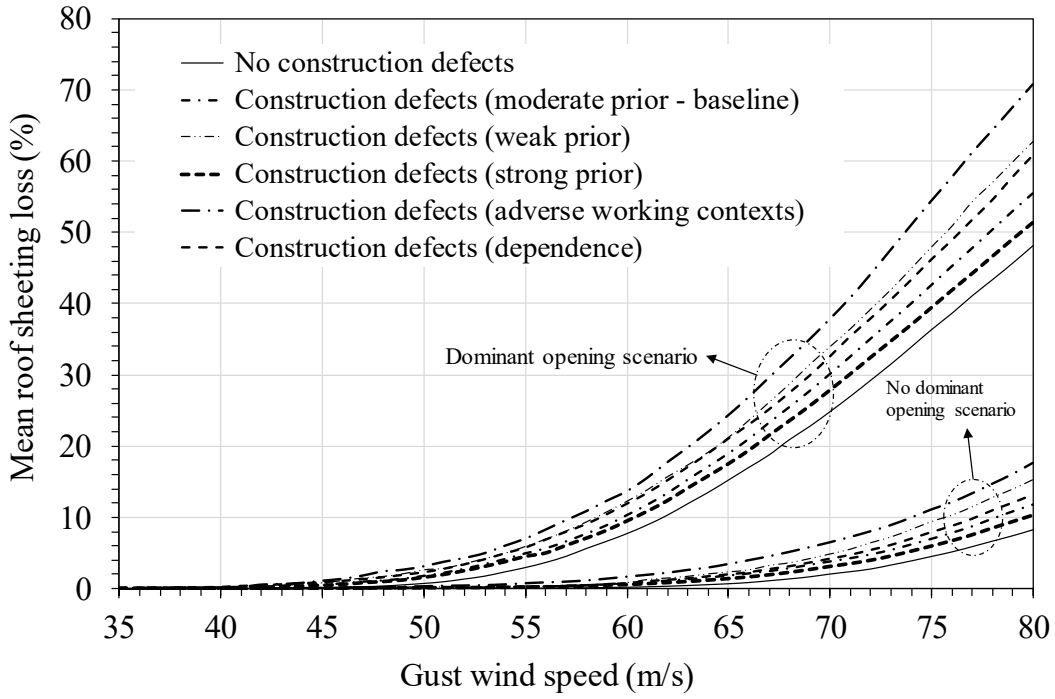

Figure. 4.7. Fragility curves for metal roof cladding considering construction defects.

Figures 4.8(a) and (b) indicate that the predicted mean proportion of roof truss failures increase only slightly when considering the effect of construction defects. This is likely due to a relatively low reduction of the uplift capacities given the occurrence of a typical construction defect for RTW connectors. As shown in Table 4.8, the uplift capacity of a RTW connector decreases by only 10-40% and 20% on average, which is a much lower consequence compared to the effects of construction defects on CTB and BTR connectors (e.g. a missing CTB connector is equivalent to a 100% capacity reduction). In addition, the weakened RTW connector tends to receive less wind uplift load due to the load sharing of the roof truss system, which, to some extent, compensates the adverse effect of the defective RTW connectors.

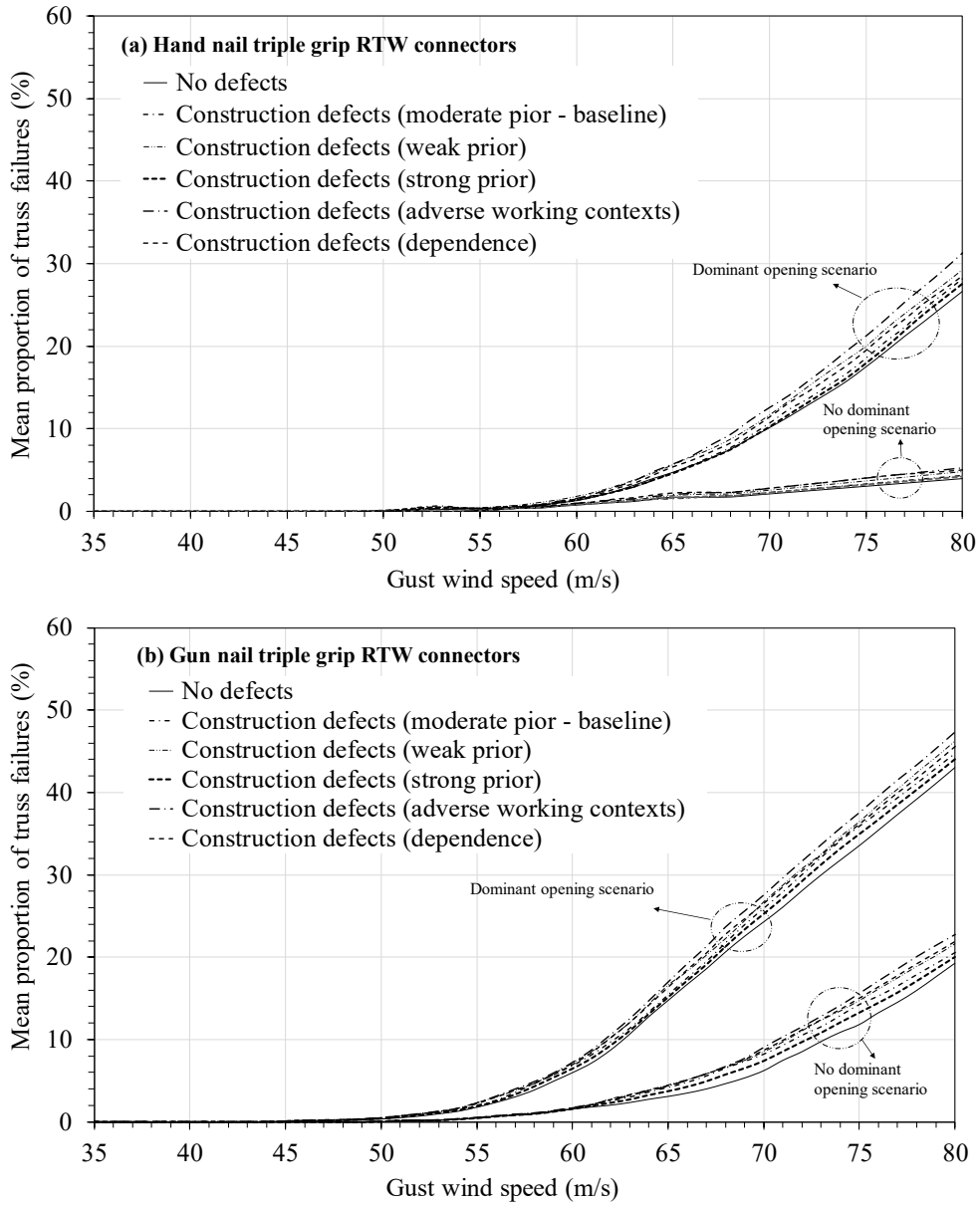

Figure. 4.8. Fragility curves for timber roof trusses considering construction defects.

4.6 Conclusions

A Bayesian approach combining expert opinion, HRA method and limited construction defect data was developed in this chapter to probabilistically characterize the construction defect rates in roof connections. The capacity reductions of roof connections given the occurrence of distinct types of construction defects were also probabilistically modelled based on engineering judgement and available experimental evidence. A total of five types of construction defects in roof connections were modelled. The proposed construction defect model was then integrated into a reliability-based fragility method to assess the wind damage to metal roof cladding and timber roof trusses for contemporary houses in Australia.

The fragility results were expressed as the mean proportion of roof sheeting loss and roof truss failures. It was found that the effect of construction defects on the roof cladding fragility is significant. Compared to the fragility results ignoring construction defects, the predicted mean proportion of roof sheeting loss in the baseline case increases by up to eight times when gust wind speed is lower than 55m/s, and up to 52% when gust wind speed is higher than 55m/s with the presence of windward wall dominant openings. The influence of construction defects can further increase if adverse working contexts and dependence between defects are taken into account. The roof truss fragility is only marginally affected by construction defects.

CHAPTER 5. ECNOMIC LOSS ESTIMATION AND PROBABILISTIC RISK ASSESSMENT

5.1 Introduction

Non-cyclonic windstorms (e.g. synoptic storms associated with low-pressure systems; severe thunderstorms) are the major causes of wind and rainfall damage to housing in Southeast Australia (Ginger et al. 2010). The three states, Victoria, Queensland and New South Wales, in the southeastern region have more than half of the population of Australia. Loss estimation and risk assessment for housing in these non-cyclonic regions are evidently essential and the key to assessing the cost-effectiveness of relevant wind mitigation measures to reduce the economic losses. Losses and risks to housing during severe windstorms often accrue to damage to the building envelope (Henderson & Ginger 2008; Stewart et al. 2018). The breaches of roof cladding and windows/doors may subsequently induce significant losses to building interior and contents due to rainwater intrusion (e.g. Henderson & Ginger 2008; Leitch et al. 2009; Ginger et al. 2010). Rainfall often concurs with extreme winds. Subsequent interior and contents losses due to rainwater intrusion through the breaches of building envelope (roof and windows) can be evaluated based on the wind damage (fragility) assessment described in Chapter 3, where a rainwater intrusion model is proposed herein.

The semi-empirical wind-driven-rain (WDR) models (e.g. Straube & Burnett 2000; Blocken & Carmeliet 2004; ISO 2009) have initially been developed for the assessment of moisture, hygrothermal and durability of building facades. The development of the semi-empirical relationships is based on experimental and/or field observations that the amount of WDR depositing on buildings increases approximately proportionally with wind speed and rainfall intensity (Blocken & Carmeliet 2004). Numerical modelling using computational fluid dynamics (CFD) provides an alternative approach for more detailed quantification of WDR (e.g. Choi 1994a; Blocken & Carmeliet 2002). Recently, these WDR methods have been extended to evaluate the amount of rainwater intrusion through building envelope breaches during hurricanes for timber-framed houses in the US (Dao 2010; Dao & van de Lindt 2010; Pita et al. 2012; Baheru et al. 2015; Johnson et al. 2018; Pant & Cha 2019). Although the CFD approach provides a more detailed assessment of WDR, it increases the complexity and cost in both modelling and computation (Blocken & Carmeliet

2010). This may not be suitable for roofs of Australian contemporary houses with large dimensions and complex geometries. The semi-empirical WDR model is thus employed in this study for a convenient and fast evaluation of rainwater intrusion. In this study, the semi-empirical WDR model is modified to suit metal-clad contemporary houses in Australia subjected to non-cyclonic windstorms. Rainwater intrusion through damaged windows and gaps around undamaged windows that are commonly reported in post-damage investigations (Henderson & Ginger 2008; Ginger et al. 2010; Henderson et al. 2017) is also considered in this study.

The loss estimation and risk assessment for houses in the US are based on existing wind and rainfall models for hurricanes (e.g. Pita et al. 2012; Mudd et al. 2016; Johnson et al. 2018; Pant & Cha 2019). However, there is a lack of hazard models for rainfall associated with non-cyclonic extreme winds. Thus, this study newly develops a probabilistic model to characterize the duration and the average rainfall intensity for non-cyclonic windstorms using regional wind and rainfall data of Brisbane and Melbourne. This model can be used for the subsequent rainwater intrusion evaluation after wind damage. Loss estimation is conducted based on cost data obtained from Australian housing cost guides (Rawlinsons 2015). The loss functions depend on the extent of damage to housing components and the volume of rainwater intrusion yielded by the wind fragility analysis and the rainwater intrusion model, respectively, and are developed according to the loss modelling in HAZUS (2014) and Wang & Rosowsky (2017) as well as engineering judgement. By integrating the hazard model for extreme wind and associated rainfall, wind damage and rainwater intrusion assessment, and loss modelling, this chapter conducts a probabilistic risk assessment (PRA) for the representative contemporary house in Brisbane and Melbourne. The construction defect model presented in Chapter 4 are also incorporated to examine the effect of construction defects on annual risks. This chapter presents the annual economic losses evaluated from the PRA. The cumulative losses over the building service life and the climate change impact are further described and discussed in Chapter 6. The obtained annual losses can facilitate the risk mitigation and climate adaptation for housing in non-cyclonic regions of Australia, which is demonstrated in Chapter 6 and 7.

5.2 Hazard Modelling

5.2.1 Extreme wind speed

Non-cyclonic extreme winds (winds not associated with tropical cyclones) dominate in South-East Queensland, and further south in Sydney and Melbourne. The peak non-cyclonic gust wind speed, v (m/s), is modelled by the Gumbel distribution (Wang et al. 2013; Stewart et al. 2018). The cumulative distribution function (CDF) for annual maximum non-cyclonic gust wind speed is then given by

$$F_V(v) = e^{-e^{-\frac{v-v_g}{\sigma_g}}} \tag{5.1}$$

where v_g and σ_g are the location and scale parameter, respectively. The gust wind speed v is the maximum 0.2 second gust velocity at 10 m height in Terrain Category 2 (open terrain defined in AS/NZS 1170.2 2011). Figure 5.1 shows the relationship between gust wind speed and return period. The location and scale parameters are given as v_g=26.0326, σ_g=4.0488 for Brisbane and v_g=27.7777, σ_g=1.664 for Melbourne (Wang et al. 2013; Stewart et al. 2018).

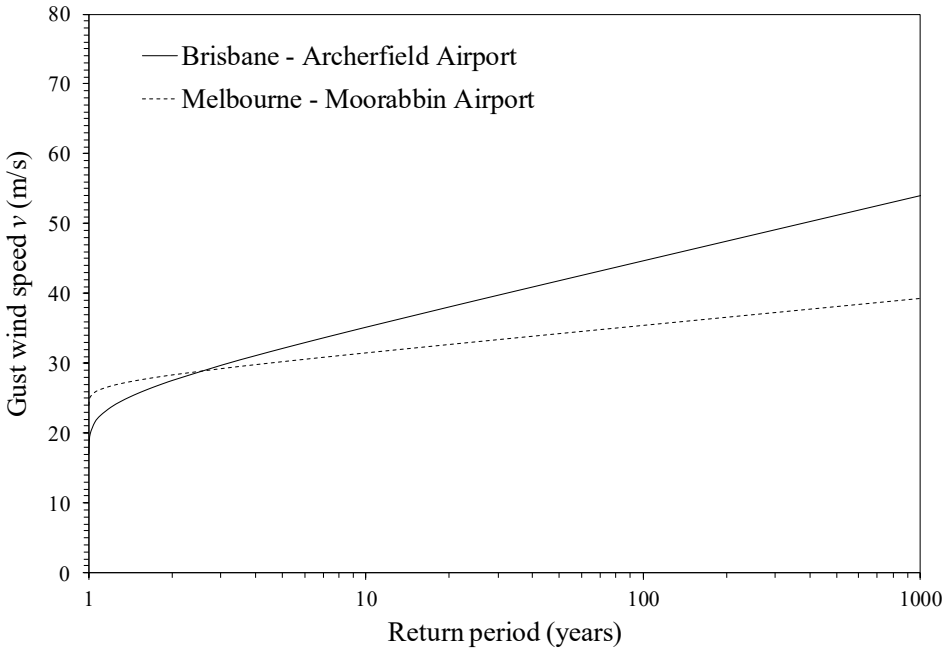

Figure 5.1. Extreme gust wind speed corresponding to return periods.

5.2.2 Rainfall associated with extreme winds

An extreme wind event is often associated with rainfall. When assessing rainwater intrusion and the consequent damage to building interior and contents, it is ideal to have the

joint probability of wind speed and rainfall intensity (e.g. Mudd et al. 2016; Wang & Rosowsky 2017) rather than treating these two weather variables independently. In addition, the average rainfall intensity (R_h) during a windstorm is typically dependent on the duration, e.g. intense burst of rainfall is more likely to occur in a short event.

The exponential distribution is connected to the Poisson arrival process, and commonly used to model the storm duration (e.g. Eagleson 1972; Koutsoyiannis & Georgiou 1993; Lambert & Kuczera 1998). A two-parameter exponential distribution is adopted in this study to model the windstorm duration (D_{ur}) with the CDF given by

$$F(D_{ur}) = 1 - e^{-\kappa(D_{ur}-\mu)} \tag{5.2}$$

where κ and μ are the rate and location parameter, respectively.

A gamma distribution is used to model the average rainfall intensity during an extreme windstorm. The probability density function (PDF) of the gamma distribution is given by

$$g_a(R_h) = \frac{R_h^{\gamma-1} e^{\frac{R_h}{\beta(D_{ur})}}}{\Gamma[\gamma]\beta(D_{ur})^{\gamma}} \tag{5.3}$$

where $\Gamma(\cdot)$ is the gamma function, γ is the shape parameter, and $\beta(D_{ur}) = a_0 + a_1(1/D_{ur})$ is the scale parameter which is assumed to have a linear relationship with the reciprocal of D_{ur}. Note that R_h in Eq. (5.3) is greater than zero, and hence the gamma distribution is only used when rainfall occurs simultaneously with strong winds. Accounting for the probability of no rain (P_{no}) during a windstorm, the CDF of R_h ($R_h \geq 0$) is given by

$$F(R_h) = P_{no} + (1 - P_{no})G_a(R_h) \tag{5.4}$$

where $G_a(R_h)$ is the CDF of the gamma distribution given by Eq. (5.3) to model the non-zero R_h, and P_{no} can be estimated from the meteorological data.

The model parameters of the exponential and gamma distribution are estimated using the meteorological data from two weather stations, i.e. Archerfield airport in Brisbane and Moorabbin airport in Melbourne. A twenty-year length of half hourly wind and rainfall data from 1996 to 2015 for these two weather stations are obtained from the Australian Bureau of Meteorology (BoM). A windstorm with the maximum gust wind speed greater than 36 knots (i.e. 18.5 m/s or 66.7 km/hr) is considered as an extreme wind as strong wind warnings can be issued at this wind speed by BoM. A total of 86 and 364 severe windstorms from 1996 to 2015 are then extracted from the meteorological data for Archerfield and Moorabbin

airports, respectively, and for each storm event, the duration and average rainfall intensity (accumulative rainfall depth divided by storm duration) are obtained. The number of storm events with no rain (i.e. $R_h = 0$) is also obtained to estimate P_{no}.

Figure 5.2 shows the exponential probability plots for D_{ur}, which suggests that the two-parameter exponential distribution given by Eq. (5.2) fits well to the storm duration data. It is estimated that P_{no} = 25.6% and 45.9% for Brisbane and Melbourne, respectively. The model parameters in the gamma regression formulation given by Eq. (5.3) are estimated using the generalized linear model in the **R** software package (R Core Team 2019). Figure 5.3 shows the mean and quantile values of R_h produced by the gamma model as a function of D_{ur}. The average rainfall intensity data is also plotted in the same figure, which indicates that Brisbane tends to have shorter windstorms with more intense rainfall (e.g. thunderstorms), whereas windstorms in Melbourne are generally longer with lower average rainfall intensity. Figure 5.3 suggests a good predictability of the gamma model to capture the average rainfall intensity during windstorms. Note that the estimated model parameters for D_{ur} and R_h can only be rigorously applied to the risk assessment for houses in the surrounding or nearby suburbs of Archerfield airport and Moorabbin airport, however it can be further extended to incorporate more weather stations in Brisbane and Melbourne, and account for the spatial variations and patterns of rainfall across the entire urban areas. The gamma distribution is a widely used parent distribution for the rainfall intensity during a storm (e.g. Sivapalan & Blöschl 1998; Koutsoyiannis et al. 2003). Other probability distributions, e.g. Weibull, lognormal, Generalized Pareto, have also been reported in the literature to model rainfall intensity (e.g. Heneker et al. 2001; Koutsoyiannis et al. 2003; Mudd et al. 2016), however, it is out of the scope of this study to examine which is the best fit to the local meteorological data. The accuracy of estimation can be further improved by incorporating more years of data, if available.

This section presents a new statistical approach to characterize extreme wind speed and associated rainfall for non-cyclonic windstorms using regional meteorological data. This approach is data-driven instead of building on physical mechanisms of the natural phenomena. This is because the physical mechanisms of non-cyclonic windstorms are generally less understood than hurricanes or tropical cyclones. The hurricane models used to simulate the concurrence of wind and rainfall are typically based on the physical process of hurricanes or tropical cyclones (e.g. Pita et al. 2012; Mudd et al. 2016), which do not apply to non-cyclonic windstorms. For example, the duration of a hurricane may be

characterized by a decay function depending on factors such as central pressure, transitional speed, etc, and the rainfall intensity may be expressed as a function of the radius and maximum wind speed of the hurricane and calculated using the R-CLIPER model (e.g. Tuleya et al. 2007). However, such existing models generally do not exist or practically available to model non-cyclonic windstorms in the context of this study.

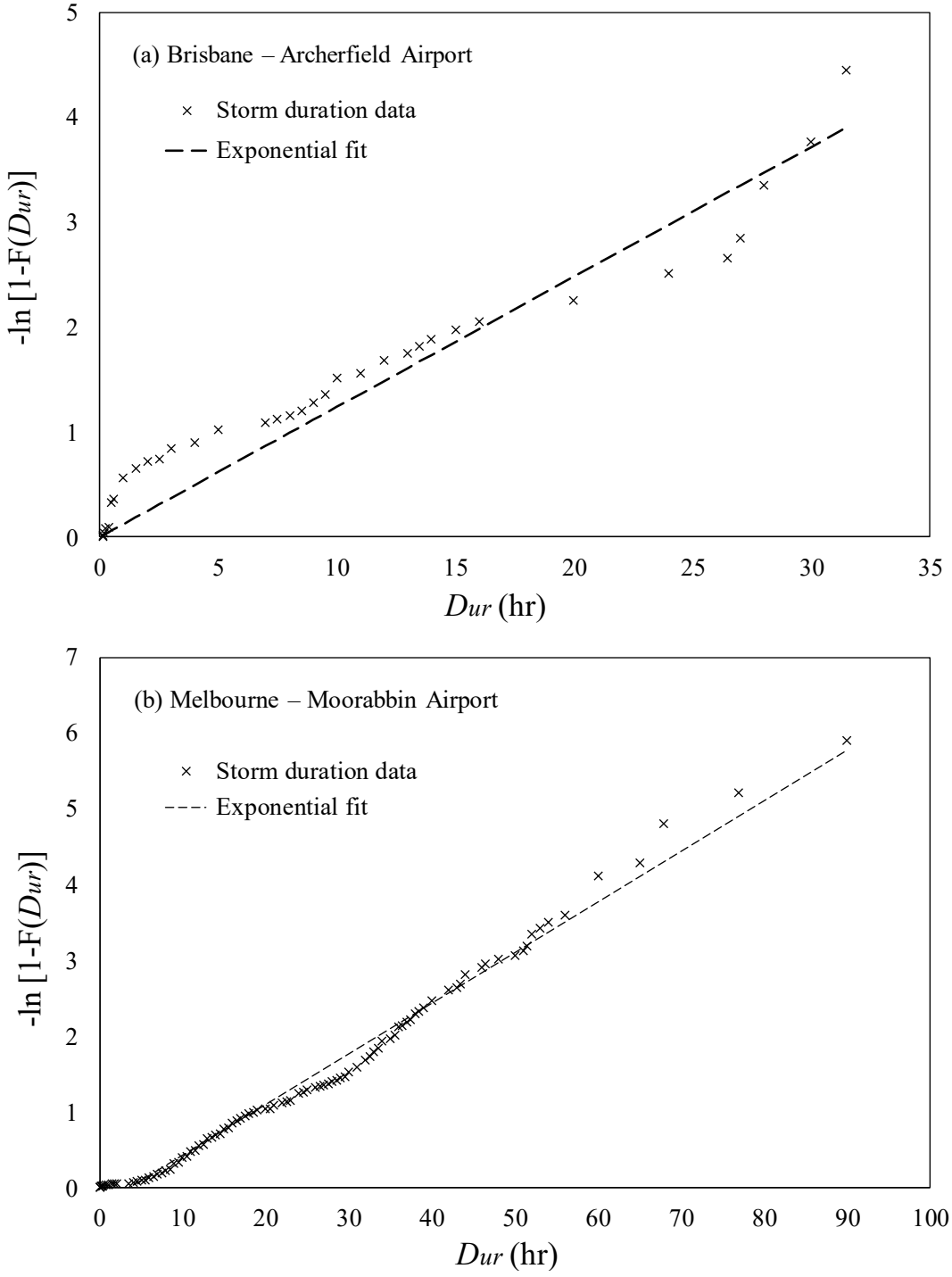

Figure 5.2. Exponential probability plots for storm duration D_{ur}.

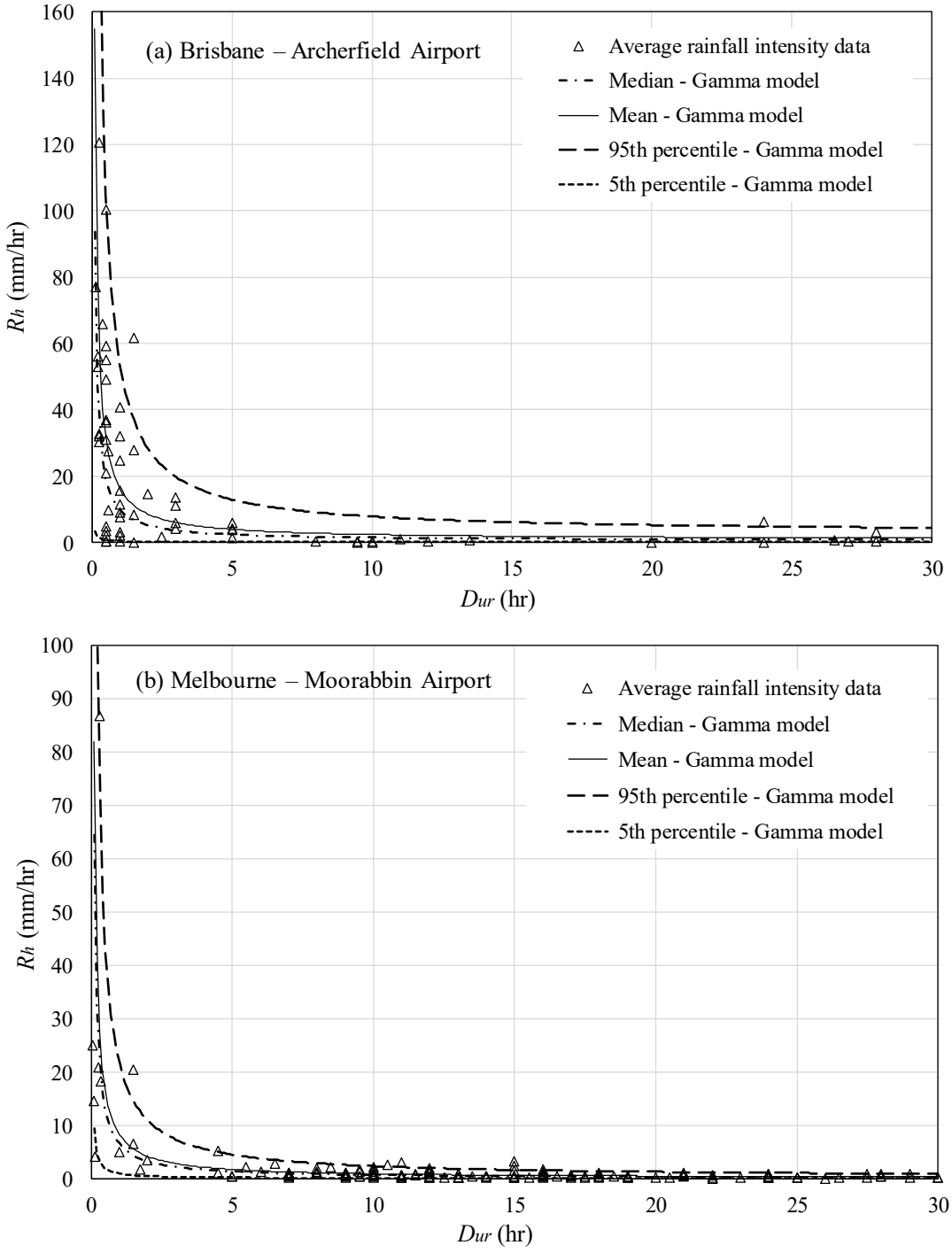

Figure 5.3. Average rainfall intensity R_h from the observed data and gamma regression model.

5.3 Wind Damage

Post-damage surveys (e.g. Leitch et al. 2009; Parackal et al. 2015) reveal that the majority of losses to contemporary houses result from wind damage to roof and fenestrations (especially windows), and the subsequent rainwater intrusion. The damage to other housing

components (e.g. walls) is rare for contemporary houses in non-cyclonic regions of Australia. To this end, the economic losses in this study are considered to arise from direct wind damage to the building envelope (roof and windows) and subsequent rainwater intrusion through the building envelope. The reliability-based wind damage assessment for metal roof cladding, timber roof trusses and windward windows are described in detail in Chapter 3, which is incorporated in the PRA framework to assess wind and rainfall losses. The incorporation of construction defects in the fragility assessment is described in Chapter 4, and thus the effect of construction defects can also be accounted for in the PRA framework. The limit states for windward windows are related to the internal pressurisation and rainwater intrusion. The limit states used for windward windows are given in Table 5.1. The notations in Table 5.1 are described in Section 3.4.2.

Table 5.1. Limit states for the windward window.

Limit states	Internal pressurisation scenario	Water entry
$W_{win} \geq R_{ult}$	Windward dominant opening	Via window breakage
$W_{win} \geq R_{water} \cap W_{win} < R_{ult}$	No dominant opening	Via small gaps around the window
$W_{win} < R_{water}$	No dominant opening	No entry via window

5.4 Rainwater Intrusion

Same as the roof fragility assessment described in Chapter 3, the quantification of rainwater intrusion in this section is also conducted under two wall opening scenarios: (i) presence of windward dominant openings (with window breakage) and (ii) absence of any wall openings (without window breakage). In the PRA, the window damage model is coupled to distinguish these two wall opening scenarios in a MCS analysis (see details in Section 5.6). For the windward dominant opening scenario, the main source of rainwater intrusion considered is water entering from roof and window breaches. Due to high wind pressures acting on the windward wall during an extreme wind event, water entry through undamaged windows has also been commonly reported in post-damage surveys (Henderson & Ginger 2008; Ginger et al. 2010). This is likely because the high differential pressures across windows exceed the water penetration resistances of windows. For the scenario without any wall openings, rainwater is thus considered to enter through roof breaches and gaps around undamaged windward windows. The rainwater intrusion via any gaps and cracks on undamaged roof cladding is neglected because the metal roof is mostly subjected to suction pressures, and is generally more watertight.

Given the occurrence of strong wind, the rain is given a significant horizontal velocity component by the wind and then falls obliquely. The vertical component of the oblique rainfall passing through a horizontal plane is typically measured at the meteorological stations, while the horizontal component passing through a vertical plane, defined as wind-driving rain (WDR), is not measured and needs to be quantified by relevant WDR methods. A semi-empirical WDR model (e.g. Straube & Burnett 2000; Blocken & Carmeliet 2004; ISO 2009) is employed in this study to assess the amount of driving rain entering the breaches and gaps in the building envelope. An empirical runoff model is also applied to assess the water ingress due to rainwater runoff from upstream undamaged building envelope.

5.4.1 Free-field WDR intensity

It is assumed that the wind flow is uniform, steady and horizontal, and the horizontal velocity of the raindrops is equal to the wind speed. Then the free-field WDR intensity (unobstructed by the building), R_{WDR} (mm/hour), passing through an imaginary vertical plane can be expressed as (Straube & Burnett 2000; Blocken & Carmeliet 2004)

$$R_{WDR} = DRF \cdot R_h \cdot U \tag{5.5}$$

where U (m/s) is the mean wind speed, R_h (mm/hr) is the average rainfall intensity, $DRF = 1/V_t$ is the driving rain factor, and V_t (m/s) is the terminal velocity of raindrops (i.e. vertical falling speed of raindrops). The driving rain factor DRF is a function of the rainfall intensity R_h, and is evaluated using the approach given by Choi (1994b). Table 5.2 shows the DRF values corresponding to various rainfall intensities.

Table 5.2. DRF values corresponding to various rainfall intensities.

R_h (mm/hr)	10	20	30	40	50	60	80	100
DRF	0.209	0.186	0.175	0.168	0.163	0.159	0.153	0.149

The mean wind speed, U, can be linked to the maximum gust wind speed, v, by the following equation

$$U = (E \cdot D \cdot T) \cdot v/G_u \tag{5.6}$$

where E, D, T are described in Section 3.4.1, and G_u is the velocity gust factor used to approximately convert a peak gust wind speed to corresponding mean wind speed. The factors E, D and T are assumed to follow a lognormal distribution with the mean-to-nominal ratios and coefficient of variation (COV) values given in Table 3.1. The corresponding

nominal values of these factors can be obtained from AS/NZS 1170.2 (2011) for different site conditions. For an hourly mean wind speed, a gust duration of 0.2s and a turbulence intensity of 0.20 (open terrain), a value of 1.77 is calculated for G_u (ESDU 2002). Table 5.3 shows the G_u values corresponding to different averaging periods estimated according to ESDU (2002).

Table 5.3. Gust factors corresponding to different averaging periods (gust duration of 0.2s).

Averaging periods (hr)	0.5	1	2	3	6	9	12	18	24
Gust factor (G_u)	1.73	1.77	1.80	1.82	1.85	1.87	1.88	1.90	1.91

5.4.2 Driving rain intrusion

5.4.2.1 Roof breaches

The volumetric rate of oblique driving rain intrusion (litre/hr) via a roof opening is

$$VOL_R = RAF_R \cdot R_{WDR} \cdot A_{SV} \tag{5.7}$$

where RAF_R is the rain admittance factor (Straube & Burnett 2000) for roof which is the ratio of the rainwater intrusion intensity to the free-field WDR intensity, R_{WDR} is the free-field WDR intensity given by Eq. (5.5), A_{SV} is the vertical projection area of a metal roof sheet opening with $A_{SV} = A_S \sin(\omega)$, where A_S is the area of the damaged metal sheet and ω is the roof slope (21.5˚ for the representative contemporary house). The RAF_R mainly depends on building geometries and aerodynamics to account for the building disturbance to the free-field WDR.

The RAF_R value is estimated based on limited experimental evidence (Baheru et al. 2014). The RAF_R for roof openings on the windward side is assumed to follow a truncated normal distribution with a mean of 0.30 and a standard deviation of 0.20 (truncated to an interval of 0 to 1), whereas the RAF_R value for roof openings on the leeward side is zero. For roof openings parallel to the wind direction, the RAF_R is assumed to follow a truncated normal distribution with a mean of 0.05 and a standard deviation of 0.05 (truncated to an interval of 0 to 1). For oblique wind angles, it can be approximately accounted for by projecting onto directions normal and parallel to the building facades (Straube & Burnett 2000; Blocken & Carmeliet 2004). As the building geometries and wind conditions in Baheru et al. (2014) do not exactly match those for the representative contemporary house examined in this study, a relatively large standard deviation is selected for the truncated normal distribution of RAF_R values to implicitly account for the uncertainties involved. The

statistical parameters for RAF_R are summarized in Table 5.4. There is a clear need to modify the estimation of RAF_R values with more evidence from experiments and/or CFD studies to better inform the semi-empirical model, and hence improve the accuracy of the rainwater intrusion model.

5.4.2.2 Window breaches

Only the horizontal component of the oblique driving rain enters window breaches. The volumetric rate of driving rain intrusion via a window opening is

$$VOL_W = RAF_W \cdot R_{WDR} \cdot A_W \tag{5.8}$$

where A_W is the area of the window opening, and RAF_W is the rain admittance factor for window. The value of RAF_W is only non-zero for window openings on the windward wall, which is assumed to follow a truncated normal distribution with a mean of 0.50 and a standard deviation of 0.20 (truncated to an interval of 0 to 1) as inferred from Straube & Burnett (2000) and Baheru et al. (2014) as shown in Table 5.4. A cosine projection (Straube & Burnett 2000; Blocken & Carmeliet 2004) can be used to approximately account for the rain driven by oblique wind (i.e. wind angle is non-normal to the wall/window).

5.4.2.3 Gaps around windows

The volumetric rate of driving rain intrusion via gaps around the window is given by

$$VOL_G = f_v \cdot RAF_W \cdot R_{WDR} \cdot A_G \tag{5.9}$$

where A_G is the area of the gap (mm^2), and f_v is a velocity ratio that accounts for the speed change of air as it passes through small gaps, cracks and openings on buildings (Baheru et al. 2015). As shown in Table 5.4, the f_v value is assumed to follow a normal distribution with a mean of 2.50 and a standard deviation of 0.30 which is estimated based on the environmental design guide CIBSE (2015) for air infiltration driven by wind through small gaps in buildings. A gap width of 0.5 mm is assumed for windows in the representative contemporary house.

5.4.3 Rainwater runoff

The rainwater runoff is another source of rainwater intrusion through breaches and gaps in the building envelope. A portion of the oblique driving rain deposited on the upstream undamaged building envelope can run into the damaged roof sheets and windows. The volumetric rate of rainwater runoff into a roof or window opening (VOL_{RO}) is simply calculated by applying a reduction factor, f_r, to the volumetric rate of driving rain impinging

on the upstream surface of undamaged building envelope. Figure 5.4 shows an example of the upstream runoff surface of a roof opening. This reduction factor accounts for the loss of rainwater amount due to splashing, evaporation, absorption and adhesion, which is assumed to follow a truncated normal distribution with a mean of 0.25 and a standard deviation of 0.15 (truncated to an interval of 0 to 1) as shown in Table 5.4. This estimation is based on the engineering judgement that the representative contemporary house only experiences a small portion of runoff water. The basis of this engineering judgement are given herein. A brick veneer wall has great capacity for water absorption to reduce rainwater runoff through windows. Windows on Australian contemporary houses are typically positioned very close to the eave with limited area of upstream surface for rainwater runoff. The corrugation of metal roof sheets reduces rainwater runoff through roof openings. Sensitivity analyses for the factors listed in Table 5.4 are conducted in Section 5.6.2.3 to examine their effects on the probabilistic risk assessment.

Table 5.4. Random variables in the semi-empirical rainwater intrusion model.

Parameters	Location applied	Mean	Standard deviation	Distribution	Source
RAF_R	Windward roof	0.30	0.20	Truncated normal[a]	Inferred from Baheru et al. (2014)
	Sideward roof	0.05	0.05		
	Leeward roof	0.00	0.00		
RAF_W	Windward window	0.50	0.20	Truncated normal[a]	Inferred from Straube & Burnett (2000) Baheru et al. (2014)
f_v	Gaps around windward window	2.50	0.30	Truncated normal[a]	Inferred from CIBSE (2015)
f_r	Upstream undamaged surface	0.25	0.15	Truncated normal[a]	Assumed based on engineering judgement

[a]Truncated to an interval of 0 to 1.

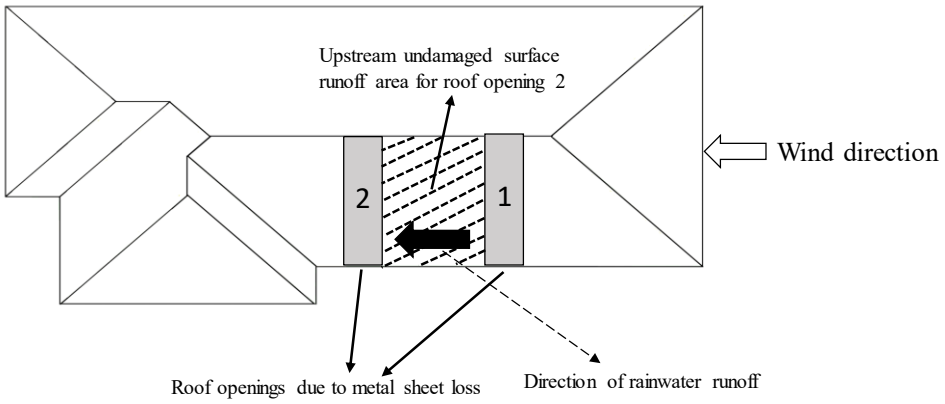

Figure 5.4. Upstream undamaged surface runoff area for a roof opening due to metal sheet loss.

5.4.4 Volumetric rate of rainwater intrusion

A MCS analysis is employed to evaluate the total volumetric rate of rainwater intrusion VOL_T (litre/hr) through roof and window breaches, and gaps around the window (i.e. VOL_R, VOL_W, VOL_G, and VOL_{RO} for all building envelope breaches and gaps). For the dominant opening scenario, the total size of openings due to window breakage on a windward wall is estimated to be 4m^2. A sensitivity analysis is conducted in Section 5.6.2.3 for a different opening size. The MCS used for wind fragility analysis is extended to assess the subsequent rainwater intrusion by applying the semi-empirical model. The volumetric rates of rainwater intrusion are dependent on the number and locations of failed roof sheets obtained from the wind damage assessment, and also a function of gust wind speed and rainfall intensity.

Construction defects in metal roof cladding can cause more roof sheeting loss, which may incur more rainwater intrusion through roof breaches. Figure 5.5 shows the mean VOL_T as a function of gust wind speed and rainfall intensity for the two wall opening scenarios with/without construction defects. As expected, the mean VOL_T increases with wind speed and rainfall intensity. The nonlinearity of rainwater intrusion with increasing wind speed is because there is more roof sheeting loss at a higher wind speed allowing for more rainwater intrusion. The mean rainwater intrusion rate is up to 25% higher when construction defects are considered in the roof damage assessment.

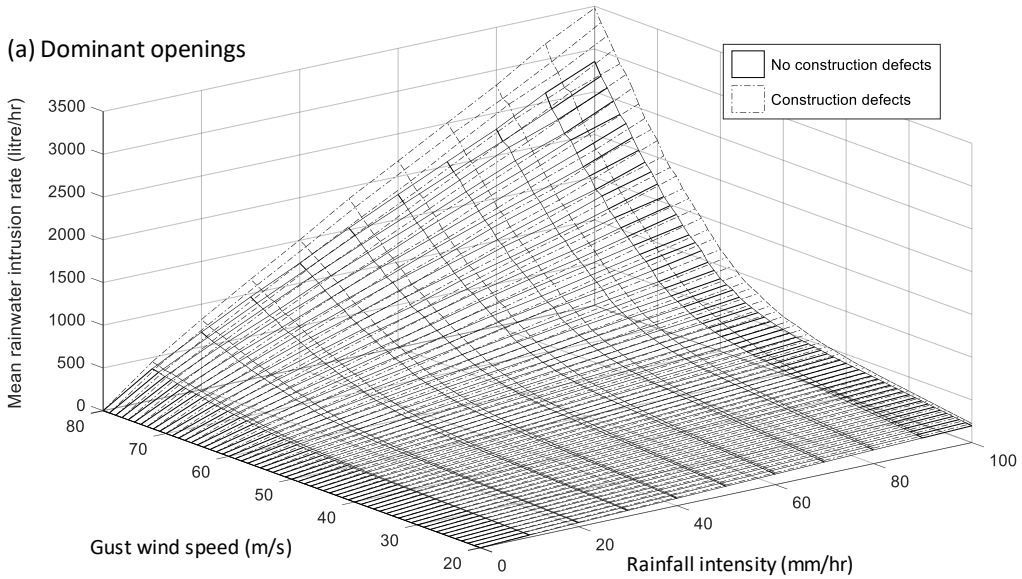

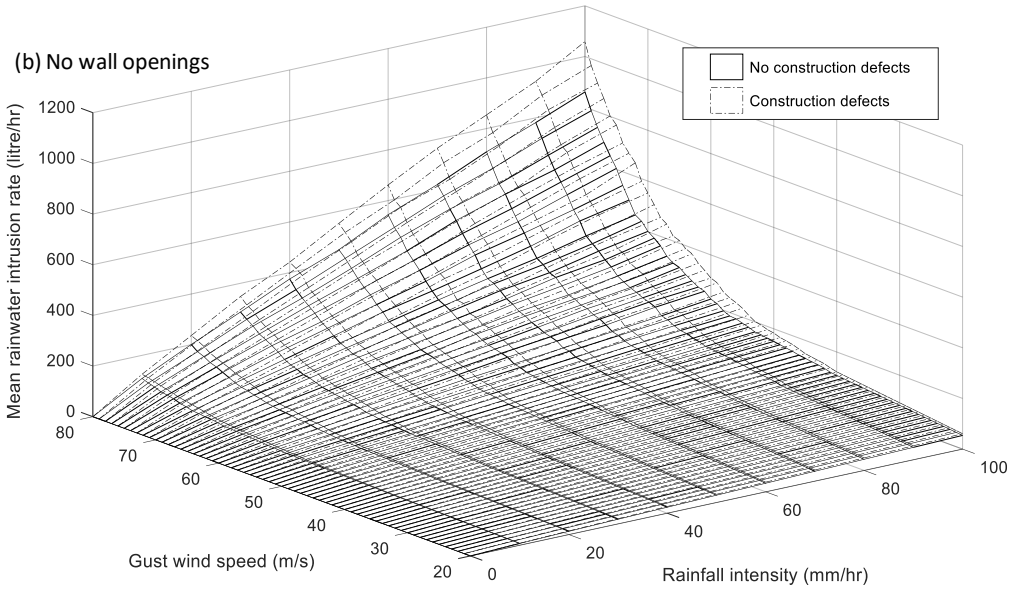

Figure 5.5. Mean VOL_T of rainwater intrusion with/without construction defects.

Figure 5.6 shows the mean volumetric rates of rainwater intrusion through roof and window, respectively, under the two wall opening scenarios at the rainfall intensity of 10 mm/hr. As shown in Fig. 5.6, the rainwater intrusion via window is higher than that through roof openings for relatively lower wind speeds. With an increasing wind speed, more roof openings tend to occur due to increasing metal roof sheeting loss, which results in more rainwater intrusion via roof breaches.

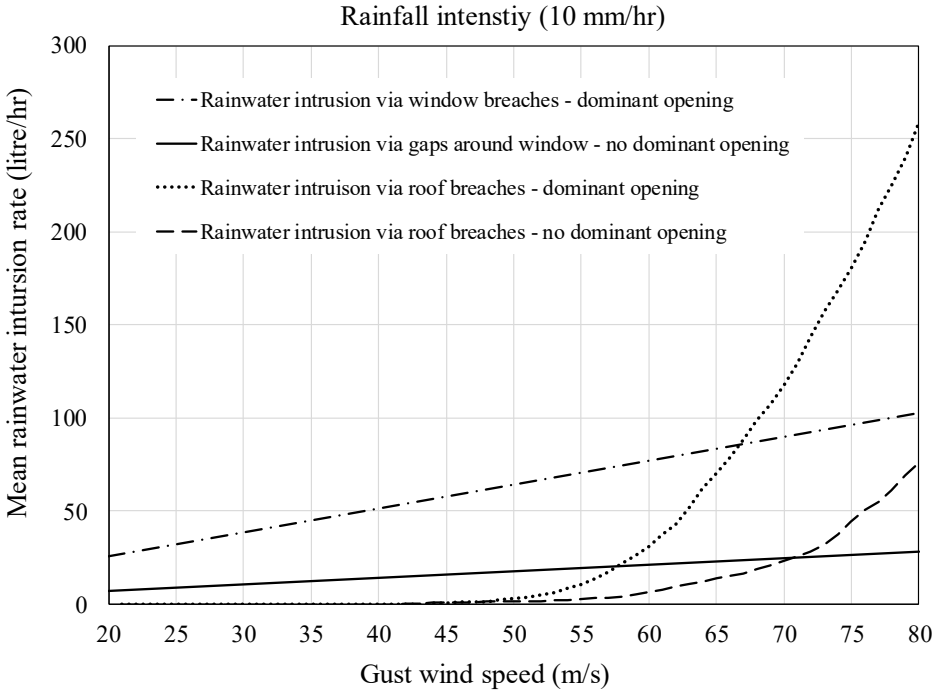

Figure 5.6. Mean volumetric rate of rainwater intrusion via roof and window respectively under the two wall opening scenarios at a rainfall intensity of 10 mm/hr.

5.4.5 Volume of rainwater intrusion

The evolution of internal pressurisation and load redistribution due to the progressive failure of the building envelope are explicitly accounted for in the wind damage assessment (see Chapter 3 for more details), however, the temporal damage progression of the building envelope is not explicitly considered. It is assumed that the roof damage and the exceedance of limit states for windward windows given by Table 5.1 all happen at the occurrence time of the maximum gust wind speed (T_M) during a windstorm. The volume of rainwater intrusion (VOL) through all breaches and gaps in the building envelope is then given by

$$VOL = VOL_T \cdot T_R \tag{5.10}$$

where $T_R = D_{ur} - T_M$ is the length of time after the wind damage to the building envelope, and T_M is assumed to follow a uniform distribution with a lower bound of zero and an upper bound of $D_{ur.}$ Note that VOL_T evaluated in Section 5.4.4 is based on the average rainfall intensity R_h. This is another approximation that the temporal variation of rainfall intensity during a windstorm is not explicitly taken into account, and hence the assessment of rainwater intrusion volume in this study is not fully event-based.

5.5 Loss Modelling

5.5.1 Subassembly cost ratios

The loss estimation uses an assembly-based approach (e.g. Porter et al. 2001; HAZUS 2014; Hamid et al. 2010; Stewart et al. 2018). The entire house is divided into components/subassemblies based on specific building details. Then the total loss is equal to the sum of repair or replacement costs of every housing components. The loss estimation takes into account housing components/subassemblies that are related to the failure of roof cladding and trusses, windward windows, and those susceptible to rainwater damage. The representative contemporary house described in Section 3.2 is then divided into subassemblies as shown in Table 5.5. The subassemblies (e.g. site preparations, foundations, wall structures, etc.) that are not explicitly included in the loss estimation are categorized under ‘other’.

The losses are estimated in terms of cost ratios. Herein, the cost ratio of a subassembly is defined as the ratio of the cost to complete the subassembly (i.e. newly build, upgrade, repair or replace) to the building value. The estimated total cost to build a new contemporary house with an approximate floor area of 150 m^2 is $L_{building}$ = \$300,000 Australian Dollars

(HIA 2018 and RLB 2019). Based on cost data provided by Australian housing cost guides (Rawlinsons 2015) and subjective judgement, the subassembly cost ratios are estimated for a representative contemporary house built to an average standard as shown in Table 5.5. Note that the cost ratios in Table 5.5 are estimated for new construction that includes material and labour costs plus contractor's overhead and profit. In the context of this study, cost ratios for repair and/or replacement of damaged components/subassemblies are needed, which can be obtained by adjusting the cost ratios in Table 5.5 using a factor of 1.25 to account for the additional costs associated with removal, repair and remodelling of an existing house (HAZUS 2014), and a factor of 1.05 to account for increased contractor's overhead and profit for repair and/or replacement work (Rawlinsons 2015). The adjusted cost ratios are also given in Table 5.5.

Table 5.5. Subassembly cost ratios for the representative contemporary house.

Subassembly		Description	Cost ratio	Adjusted cost ratio
Roof	Roof cladding	Mainly including corrugated metal roof sheets, metal top-hat battens and insulation	4.1%	L_1 = 5.4%
	Roof framing	Timber trusses, rafters, ceiling joists, fixings, etc.	15.9%	L_2 = 20.9%
Windows on one wall		Single glazed, aluminum sliding or awning windows	0.8%	L_3 = 1.0%
Internal finishes, fittings	Wall	Mostly plasterboard, also include ceramic tiles and painting	6.8%	L_4 = 51.2% (building interior)
	Floor	Mixed use of timber, carpet and ceramic tiles	3.5%	
	Ceiling	Mostly plasterboard, also including painting	4.7%	
	Fittings and fixtures	Built-in wardrobes/cupboards, kitchen units, bathroom suites, shelving, internal doors, etc.	10.0%	
Mechanical		Air conditioning, heaters, ventilation, etc.	10.0%	
Electrical		Lighting, conduits, cables, etc.	4.0%	
Other		Site preparation, foundation, wall framing, other fenestrations, plumbing, etc.	37.0%	n/a

5.5.2 Loss functions

5.5.2.1 Roof cladding loss

Australian insurance data suggests that the metal roof is likely to be entirely replaced if the proportion of roof sheeting damage exceeds 20% (Smith & Henderson 2015), hence,

$$\Pr(L_1|DS = R_{clad}) = \begin{cases} R_{clad} & R_{clad} \leq 20\% \\ 1.0 & R_{clad} > 20\% \end{cases} \quad (5.11)$$

where R_{clad} is the proportion of metal roof cladding damage and L_1 = 5.4% is the cost ratio for full replacement of roof cladding.

5.5.2.2 Roof framing loss

The cost ratio for a full roof framing replacement is L_2 = 20.9%. The roof framing for the representative contemporary house with complex hip-roof geometries includes timber roof trusses, jack and hip rafters, ridgeboard, valley rafters, struts and ties, ceiling joists, fixings and connections, etc. In the wind fragility assessment, only the failures of critical roof trusses are explicitly evaluated. It is assumed that the failure of a critical truss causes damage to other framing elements directly and/or indirectly linked to this truss. In this study, a threshold value of 20% is assumed for a full replacement of the roof framing based on existing loss functions and damage states used in the literature (e.g. Li et al. 2011; van de Lindt & Dao 2012). In other words, if the damage proportion of the critical roof trusses exceeds this threshold value, a full replacement of the entire roof framing is then required, leading to

$$\Pr(L_2|DS = R_{truss}) = \begin{cases} R_{truss} & R_{truss} \leq 20\% \\ 1.0 & R_{truss} > 20\% \end{cases} \quad (5.12)$$

where R_{truss} is the damage proportion of the critical roof trusses.

5.5.2.3 Windward windows

The ratio of windward window loss caused by high wind pressure is expressed as

$$\Pr(L_3|DS) = \begin{cases} 0 & W_{win} < R_{ult} \\ 1.0 & W_{win} \geq R_{ult} \end{cases} \quad (5.13)$$

where L_3 = 1.0%.

5.5.2.4 Interior loss

The building interior considered in the loss estimation includes internal finishes and fittings, mechanical and electrical systems. The cost ratio for a full replacement of interior

is L_4 = 51.2%. The interior loss is modelled as a function of rainwater intrusion, and it is assumed that the interior losses increase linearly with an increasing amount of rainwater intrusion until exceeding a threshold value to cause a complete loss (Pita et al. 2012; HAZUS 2014). The proportion of interior loss due to rainwater damage is

$$\Pr(L_4|DS = h_I) = \begin{cases} \frac{h_I}{h_T} & h_I \le h_T \\ 1.0 & h_I > h_T \end{cases} \tag{5.14}$$

where h_I (mm) is the accumulated water depth calculated as the total rainwater intrusion volume *VOL* given by Eq. (5.10) divided by the floor area of the entire house, and h_T (mm) is a threshold value of water depth that leads to total interior loss. A threshold value of h_T = 25 mm given by Pita et al. (2012) is used in this study. A sensitivity analysis for h_T is presented in Section 5.6.2.3 to examine its effect on annual expected losses.

5.5.2.5 Contents loss

The contents loss is also modelled as a function of rainwater intrusion. The contents loss is directly related to rainwater entering from windows, and it is assumed that the contents can only be damaged by rainwater entering from the roof if the ceiling leaks (e.g. due to local damage of a ceiling). In this case, a weighting factor, w_0 = 0.6, is assumed for the proportion of water depth resulting from a damaged roof that causes contents loss. A sensitivity analysis is conducted in Section 5.6.2.3 for this weighting factor. Using the same threshold value of water depth, h_T = 25 mm, the proportion of contents loss due to rainwater damage is

$$\Pr(L_5|DS = w_0h_R + h_W) = \begin{cases} \frac{w_0h_R+h_W}{h_T} & w_0h_R + h_W \le h_T \\ 1.0 & w_0h_R + h_W > h_T \end{cases} \tag{5.15}$$

where h_R and h_W are the accumulated water depth due to rainwater intrusion via roof and windows, respectively. Based on the statistics of the average value of a household's home contents in Australia (ABS 2011), it is estimated that L_5 = 25.0%.

5.5.2.6 Loss of use

The annual likelihood of loss of use arising from a damaged building is (HAZUS 2014)

$$\Pr(L_6 \mid DS) = \frac{\mathrm{N_{lou}}\left(\Pr(L_{building} \mid DS)L_{building}\right) \cdot \mathrm{Mod}\left(\Pr(L_{building} \mid DS)L_{building}\right)}{365} \tag{5.16}$$

where N_{lou} is the loss of use (days) taking into account delays in decision-making, financing,

inspection, etc., and Mod is a loss of use multiplier to account for the fact that homeowners can remain in their homes when damage is not severe (HAZUS 2014). Both N_{lou} and Mod are modelled as a function of the expected total building loss, i.e. $\Pr(L_{building}|DS)L_{building}$, which is a summation of all the subassembly losses (excluding contents loss) considered in this study (i.e. $\sum_{i=1}^{4} \Pr(L_i|DS)\, L_i$). According to HAZUS (2014), N_{lou} = 0, 5, 120, 360 and 720 days and Mod = 0.0, 0.0, 0.5, 1.0 and 1.0, for total expected loss of 0%, 2%, 10%, 50% and 100%, respectively. The annual loss of use (365 days) corresponds to a cost ratio of L_6 = 16.3% based on an estimated additional living cost of $1,000 per week (e.g. rent, hotel costs, relocation and increased transportation fees, furniture rental costs, etc.).

5.6 Economic Losses and Risks

5.6.1 Risk analysis method

The annual risk (expressed as annual expected loss) is given by

$$E_{annual}(L) = \int\int\int f(R_h \mid v, D_{ur}) f(v) f(D_{ur}) \frac{1}{n_d} \sum_{j=1}^{n_d} \left[\Pr(DS \mid D_{Nj} T_N v, R_h, D_{ur}) \sum_{i=1}^{n_c} \Pr(L_i \mid DS) L_i \right] dv dR_h dD_{ur} \tag{5.17}$$

where $f(v)$ is the probability distribution of the annual maximum gust wind speed, $f(R_h|v, D_{ur})$ is the probability distribution of the average rainfall intensity of a severe windstorm corresponding to a given duration D_{ur}, $f(D_{ur})$ is the probabilistic distribution of the windstorm duration, n_d = 8 is the number of cardinal wind directions considered in this study, n_c = 6 is the number of components/subassemblies considered in the loss estimation as described in Section 5.5, D_N is the nominal wind speed directionality factor for the eight cardinal directions, and T_N is the nominal value of the shielding factor, $\Pr(DS|v, R_h, D_{ur})$ is the probability of damage state (e.g. extent of roof damage, amount of rainwater intrusion) given the gust wind speed, rainfall intensity and storm duration, $\Pr(L_i|DS)$ is the loss likelihood for the i^{th} component/subassembly as described in Section 5.5.2, and L_i is the maximum probable loss for the i^{th} component/subassembly.

The probabilistic models for $f(v)$, $f(D_{ur})$ and $f(R_h|v, D_{ur})$ are described in Section 5.2. The D_N and T_N values are obtained from AS/NZS 1170.2 (2011) for suburban houses in Brisbane and Melbourne with different site conditions and design wind classifications (see Table 5.6). Note that Eq. (5.17) assumes that damage is caused by the largest wind event in any calendar year, which will slightly underestimate damage risks in the event of a lesser

damaging windstorm in the same year. An alternative way is the adoption of a Poisson distribution to model the number of severe windstorms in a calendar year, and a Generalized Pareto distribution for the maximum gust wind speed in each windstorm (i.e. method of 'peaks over threshold'). This is subjected to further examination if more meteorological data are accessible.

Table 5.6. Nominal values of T and D for suburban houses with different design wind classifications.

	Design wind classification	T_N (shielding factor)	D_N (directionality factor)
Brisbane house	N2	0.90	1.0
	N3	1.0	1.0
Melbourne house	N1	0.90	See Table 3.2 in AS/NZS 1170.2 (2011)
	N2	1.0	

The probabilistic risk assessment conducted using a MCS analysis consists of four major components, i.e. (i) hazard modelling for wind and rainfall, (ii) reliability-based wind damage assessment, (iii) evaluation of rainwater intrusion, and (iv) loss estimation. Figure 5.7 shows an outline to illustrate the risk analysis method to assess the annual economic losses for the representative contemporary house subjected to non-cyclonic extreme winds and associated rainfall.

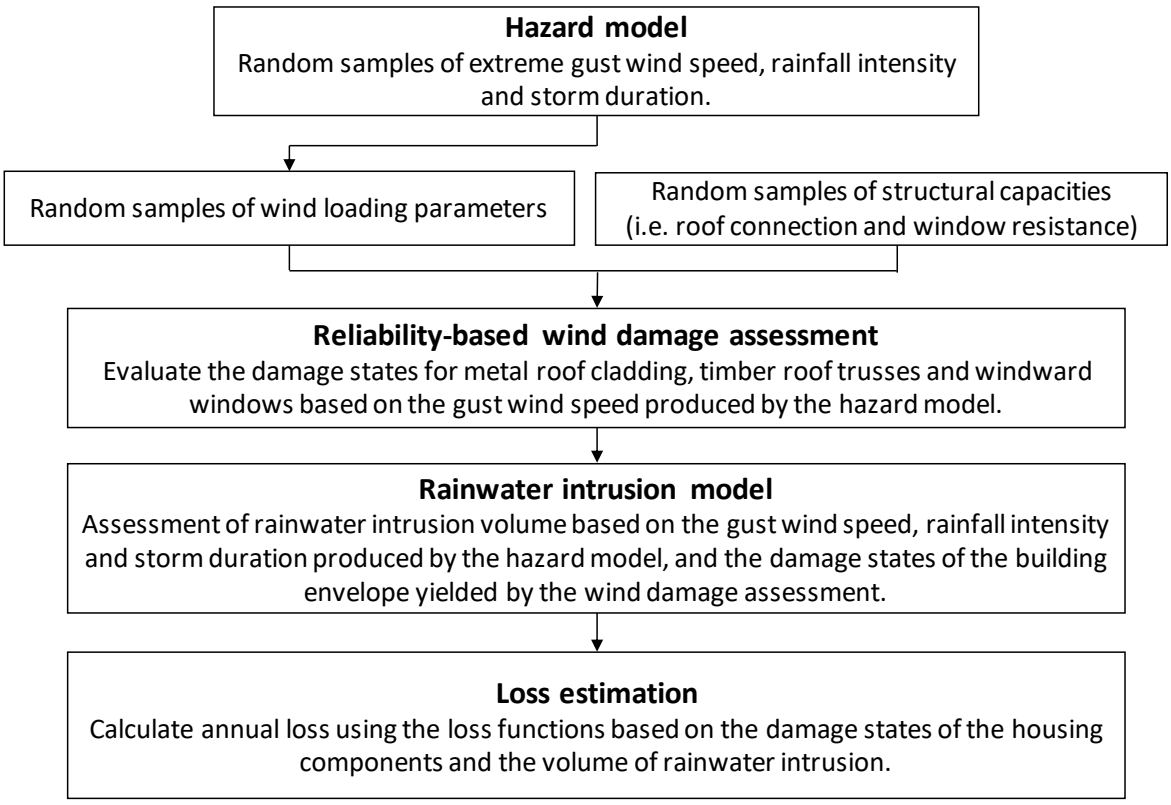

Figure 5.7. Outline of the risk analysis method.

5.6.2 Results

The risk analysis is conducted for the representative contemporary house built in suburbs of Brisbane and Melbourne. The Brisbane house is considered to have design wind classifications of N2 and N3, and the Melbourne house has design wind classifications of N1 and N2. The CTB and BTR connections are considered to be identical for houses with different design wind classifications, whereas the RTW connections and window strengths are different. The higher the design wind classification, the stronger the RTW connections and windows (i.e. with higher ultimate strength against wind pressure). However, this is not the case for the water penetration resistance of windows (see Table 3.5).

5.6.2.1 Annual losses

Table 5.7 shows the total annual expected losses (normalized by the building value) including the loss of use (i.e. L_6) for the representative contemporary house in Brisbane and Melbourne with different design wind classifications and with/without the consideration of construction defects. The annual expected losses to each housing component/subassembly (L_1 to L_5 described in Section 5.5.2) and the average days for loss of use in a calendar year are also given in Table 5.7. As shown in this table, building interior and contents losses are the major contributor to the annual risks (i.e. more than 90% of the total loss), which is much larger than the direct losses to metal roof cladding, timber roof framing and windward windows. This is because the annual expected damage proportions of roof and windows are small. In addition, the costs to repair or replace roof and windows are much less than those for building interior and contents. Although the economic losses directly caused by roof sheeting loss and window breakage are not significant, a small portion of such building envelope breaches may allow for rainwater intrusion and induce significant losses to building interior and contents. The annual expected losses for the representative contemporary house in Brisbane with construction defects are considerably higher (up to 24%) than that without considering construction defects, whereas the effect of construction defects on the calculated annual risk is slight for the Melbourne house. This is expected because the metal roof sheeting loss is negligible for the Melbourne house even with the consideration of construction defects, and there is not much increase in subsequent rainwater intrusion from roof breaches.

Table 5.7. Annual expected losses for the representative contemporary house.

(a) No construction defects

	Design wind classification	Annual expected losses (%)						
		Roof clad	Roof framing	Windward window	Building interior	Contents	Total	Loss of use (days)
Brisbane house	N2	0.004	0.003	0.003	0.069	0.030	0.109	0.22
	N3	0.006	0.002	0.001	0.053	0.023	0.085	0.17
Melbourne house	N1	0.000	0.000	0.000	0.024	0.011	0.035	0.04
	N2	0.000	0.000	0.000	0.032	0.014	0.046	0.06

(b) With construction defects

	Design wind classification	Annual expected losses (%)						
		Roof clad	Roof framing	Windward window	Building interior	Contents	Total	Loss of use (days)
Brisbane house	N2	0.005	0.003	0.003	0.085	0.037	0.133	0.29
	N3	0.008	0.002	0.001	0.066	0.028	0.105	0.24
Melbourne house	N1	0.000	0.000	0.000	0.026	0.011	0.037	0.04
	N2	0.000	0.000	0.000	0.034	0.015	0.049	0.06

As indicated in Table 5.7, window breakage is rare, and hence the non-dominant opening scenario is more likely to occur. Since the proportion of roof sheeting loss is small under the non-dominant opening scenario as shown in Fig. 3.18(a), considerable rainwater enters through gaps around windward windows when the water penetration resistance is exceeded (see Fig. 5.6). For example, the Brisbane house with a wind classification of N2 suffers more losses from rainwater intrusion than the house with a wind classification of N3, mainly due to a lower water penetration resistance of the windward wall window (see Table 3.5). Melbourne houses with a design wind classification of N2 are subjected to higher wind pressure than those with a design wind classification of N1 but the water penetration resistances of the windward window are comparable. This results in slightly higher building interior and contents losses for Melbourne houses with a design wind classification of N2. Table 5.7 also indicates that houses in Brisbane are generally subjected to higher losses than houses in Melbourne because the extreme wind speed and rainfall intensity are higher in Brisbane, though Brisbane houses have been designed to resist higher wind speed.

Table 5.8 shows the mean proportions of wind damage to metal roof cladding and timber roof trusses, and the mean depth of rainwater intrusion at the 50-year and 500-year gust

wind speed (i.e. V_{50} and V_{500}). Table 5.8 suggests that the metal roof cladding and timber roof trusses are subjected to negligible damage at the 50-year wind speed, which is expected. At the wind speed V_{50} = 35 m/s for Melbourne and V_{50} = 43 m/s for Brisbane, houses are more likely under the non-dominant opening scenario, and the proportions of roof sheeting loss and roof truss failures are close to zero (see Fig. 3.18). The losses at V_{50} are mainly due to the rainwater intrusion through gaps around windward windows. At the 500-year wind speed, Brisbane houses with a design wind classification of N2 are subjected to more damage to roof trusses than those with a design wind classification of N3, because the former has weaker RTW connections (see Fig. 3.18b). Slight roof truss damage is predicted for Melbourne houses at V_{500}. The amount of rainwater intrusion increases at V_{500} due to the increasing building envelope breaches and wind speed.

Table 5.8. Mean damage states under extreme wind speed with 50 and 500 year return periods.

	Design wind classification	V_{50}			V_{500}		
		R_{clad} (%)	R_{truss} (%)	h_I (mm)	R_{clad} (%)	R_{truss} (%)	h_I (mm)
Brisbane house	N2	0.00	0.00	0.10	0.73	1.01	0.22
	N3	0.00	0.00	0.08	1.22	0.56	0.16
Melbourne house	N1	0.00	0.00	0.02	0.00	0.00	0.04
	N2	0.00	0.00	0.03	0.00	0.00	0.05

The annual losses presented in Table 5.7 are expected losses. Statistical information other than the mean (e.g. quantile values) is also of interest to better capture the severe consequences from extreme wind events (i.e. right tail of the loss distribution). The random samples of annual losses with/without the consideration of construction defects are obtained from the PRA using MCS. Table 5.9 shows the 90th percentile of annual losses (normalized by building value) with/without the consideration of construction defects. It is suggested that the 90th percentile of annual losses are much larger than the annual expected losses given in Table 5.7, which implies a high dispersion in wind damage risks yielded by the PRA. The 90th percentile of annual losses for the representative contemporary house in Brisbane with construction defects are up to 50% higher than that without considering construction defects. Although construction defects have negligible effect on the annual expected losses for Melbourne houses, the 90th percentile of annual losses with construction defects are up to 35% higher than that without considering construction defects. The results in Table 5.9 indicate a much higher influence of construction defects on severe storm losses (i.e. damage events with low probability but high consequences).

Table 5.9. 90th percentile of annual loss for the representative contemporary house.

	Design wind classification	90th percentile of annual loss (%)	
		Construction defects	Without construction defects
Brisbane house	N2	0.389	0.259
	N3	0.288	0.204
Melbourne house	N1	0.110	0.082
	N2	0.154	0.116

5.6.2.2 Implications for insurance premium

According to Goda & Hong (2008b), the annual insurance premium (*INP*) charged by an insurer for a building is

$$INP = (1 + \eta) \cdot E[I(ML)] \tag{5.18}$$

where $E[I(ML)]$ is the annual expected value of indemnity $I(ML)$, and η is the insurance loading factor. As inferred from Walker et al. (2016), η is typically greater than 0.3 to account for administration costs and profits, and could be considerably large for high exposure areas. The indemnity $I(ML)$ is expressed as a function of the monetary loss *ML* (Goda & Hong 2008b), given by

$$I(ML) = \begin{cases} 0 & ML \leq EX \\ CO \cdot (ML - EX) & EX < ML < INV \\ CO \cdot (INV - EX) & ML \geq INV \end{cases} \tag{5.19}$$

where *CO* is the co-insurance factor that typically equals to 1.0 for home insurance in Australia, *EX* is the excess fee or deductibles, and *INV* is the sum insured value of the house. If *EX* equals to zero and *INV* is infinity, $E[I(ML)]$ is the annual expected loss given by Table 5.7.

For a typical building and contents insurance policy for the representative contemporary house with an *EX* of \$600, the annual insurance premium *INP* ranges from \$1,000 to \$1,500 for houses in Brisbane and \$600 to \$1,000 for houses in Melbourne, which includes risks from windstorms, theft, impact, earthquake, fire, accidental damage, etc. The flood coverage is usually optional and not initially included in *INP*. It is further assumed that *INV* is 30% higher than the total building and contents value (i.e. \$375,000 as described in Section 5.5). By substituting the random samples of *ML* (i.e. annual monetary loss) yielded by the PRA using MCS analysis into Eq. (5.19), $E[I(ML)]$ is estimated to be \$260 and \$210 for the Brisbane house with a design wind classification of N2 and N3, respectively. For the Melbourne house with a design wind classification of N1 and N2, $E[I(ML)]$ is estimated to

be \$75 and \$100, respectively. These estimates seem to be reasonable insurance premiums for wind and rainfall damage compared to the typical *INP* values for Brisbane and Melbourne houses including all perils.

5.6.2.3 Sensitivity analysis

The parameters of the semi-empirical rainwater intrusion model given by Table 5.4 are subjected to considerable uncertainties due to limited experimental and field monitoring evidence. A sensitivity analysis is conducted by varying the mean values of the parameters in Table 5.4 by ±50% and adjusting the corresponding standard deviations accordingly to keep the COV values unchanged. Table 5.10 shows the respective effects of RAF_R, RAF_W, f_v and f_r on the annual expected losses. The variations of the mean RAF_R and f_v have limited effects on the estimated annual expected losses, whereas the risk analysis is relatively sensitive to changes in RAF_W. Varying the mean f_r considerably changes the estimated annual expected losses by up to 10%, and hence more detailed evaluation of rainwater runoff by either experiments or numerical methods (e.g. Blocken & Carmeliet 2012; Blocken & Carmeliet 2015) for the building material of the representative contemporary house are needed to better estimate this reduction factor in the future work.

The threshold of water depth h_T leading to a total loss of building interior and contents, and the weighting factor w_0 in Eq. (5.14) and (5.15) are varied by ±50%. The corresponding changes in the calculated annual expected losses are also shown in Table 5.10. While the effect of w_0 is negligible, the estimated annual expected losses are very sensitive to a −50% decrease in h_T. This threshold value may depend on the materials of building interior and contents as well as many local factors in pricing and claim evaluation. Hence, a revision of h_T is needed if relevant insurance data in Australia becomes available and accessible.

A sensitivity analysis suggests that the annual expected losses increase by up to 70% if the windward window area (A_W) is doubled to 8m^2 as also shown in Table 5.10. Therefore, a contemporary house with a higher window-to-floor ratio (i.e. window area divided by the floor area, typically less than 25% for Australian housing) is more susceptible to wind and rain losses. However, the determination of window-to-floor ratio depends on many other factors such as natural lighting, ventilation, energy efficiency and architectural appearance, etc. The mean window resistances (i.e. R_{ult} and R_{water}) given by Table 3.5 are varied by ±20%. Table 5.10 shows the sensitivity of the risk analysis to the changes in window resistances. The annual expected losses for Melbourne houses are relatively less sensitive

to a 20% change in window resistances and it implies that strengthening windows for housing in Brisbane offers more reduction in economic losses due to extreme wind and associated rainfall.

Table 5.10. Sensitivity of annual expected losses to various uncertain parameters.

Parameters	Variations for sensitivity analysis	Approximate changes in annual expected losses	
		Brisbane house	Melbourne house
RAF_R	±50% of the mean values given in Table 5.4 and COV values unchanged	±5%	±5%
RAF_W		±30%	±30%
f_v		±1%	±1%
f_r		±10%	±40%
h_T	±50% of the values given in Section 5.5.2	−30% and +60%	−30% and +70%
w_0		±1%	±1%
A_W	Doubled to 8m^2	+70%	+70%
R_{ult} and R_{water}	±20% of the mean window resistances given in Table 3.5	−20% and +25%	−10% and +15%

5.7 Conclusions

In this chapter, a probabilistic risk assessment framework was developed to evaluate the wind and rain losses for contemporary houses subjected to non-cyclonic windstorms. The components included are (i) a hazard model accounting for the simultaneous occurrence of extreme wind and associated rainfall, (ii) a reliability-based wind damage assessment for roof and windows, (iii) a semi-empirical model for rainwater intrusion, and (iv) a loss estimation model. The risk analysis results suggest that the annual expected losses are mainly attributed to the rainwater damage to building interior and contents. Although houses in Brisbane have a stronger design, they are generally subjected to higher losses than Melbourne houses because the extreme wind speed and rainfall intensity are higher in Brisbane. The annual expected losses for the representative contemporary house in Brisbane with construction defects are considerably higher than that without considering construction defects, whereas the effect of construction defects on the calculated expected losses is slight for the Melbourne house. It was also found a much higher influence of construction defects on severe storm losses (i.e. damage events with low probability but high consequences).

CHAPTER 6. COST-BENEFIT ANALYSIS OF RISK MITIGATION AND CLIMATE ADAPTATION MEASURES

6.1 Introduction

Climate change impact on the intensity of windstorm and associated rainfall impose more uncertainty on housing damage risks. Risk mitigation and climate adaptation measures are of significant importance for the improvement of building resilience to windstorms, and the reduction of economic losses associated with wind and rainfall damage under a changing climate. However, the adoption of a specific mitigation/adaptation measure is still in question if its cost-effectiveness is unclear, and therefore there is a need to quantify the costs and benefits associated with mitigation/adaptation measures to assess their economic viability.

Many cost-benefit studies have been reported in the literature for houses subjected to tropical cyclones or hurricanes in the United States (e.g. Li & Ellingwood 2009; Torkian et al. 2014; Unnikrishnan & Barbato 2016; Orooji & Friedland 2017) and Australia (e.g. Stewart 2003; Stewart et al. 2014). New South Wales, Victoria and southeast Queensland have most of Australia's population, and are classified as non-cyclonic regions in AS/NZS 1170.2 (2011). Only about 5% of Australia's population live in cyclonic regions. Residential construction in non-cyclonic regions of Australia comprises of a large portion of metal-clad contemporary houses, which generally have less wind resistance than houses in cyclonic regions of Australia, and differ from North American houses in materials, construction techniques and building design. Quantitative studies regarding wind risk mitigation and climate adaptation for Australian contemporary houses subjected to non-cyclonic windstorms are scarce in the literature. The development of feasible mitigation/adaptation measures and the quantification of their cost-effectiveness are still needed to improve the resilience of residential communities in Australia against wind hazards.

Wind risk mitigation and climate adaptation include measures to either enhance the design during initial construction or retrofit (i.e. upgrade or strengthen) an existing house. Chapter 5 presents a probabilistic risk assessment for Australian contemporary houses subjected to wind and rainfall damage, and found that most losses result from damage to building interior and contents caused by rainwater intrusion through breaches (e.g. openings due to metal roof sheeting loss and window breakage) and gaps in the building envelope. A

set of mitigation/adaptation measures are thus proposed in this study to reinforce the building envelope against wind and improve the water resistance of building interior: (i) strengthening connections for metal roof cladding, (ii) installing shutters for windows, (iii) improving window resistance, and (iv) using water-resistant materials for the building interior.

Most studies regarding the cost-benefit analysis of wind mitigation or climate adaptation measures for housing in Australia are based on empirical vulnerability models to quantify the wind and rainfall damage (e.g. Li & Stewart 2011; Stewart et al. 2014; Stewart 2015; Smith & Henderson 2015). For example, Stewart (2015) employed expert-elicited wind vulnerability curves to assess the housing losses with enhanced building design. Smith & Henderson (2015) used insurance data to estimate the cost and benefit of various retrofit and mitigation solutions for houses in cyclonic regions of Australia. However, these empirical vulnerability models have very limited ability to assess the performance of detailed mitigation or adaptation measures applied to specific housing components for wind risk reduction (Walker 2011). To overcome this limitation, the cost-benefit analysis in this study is conducted based on the probabilistic risk assessment method described in Chapter 5, which systematically integrates engineering judgement, data-driven and engineering-based models for the quantification of extreme wind and associated rainfall, wind damage to housing, rainwater intrusion and economic losses. Such cost-benefit analysis provides a better risk-based performance assessment and decision support for the proposed mitigation/adaptation measures.

Construction defects may also affect the cost-effectiveness of mitigation/adaptation measures. For example, a mitigation/adaptation measure may provide little reduction in economic losses for houses with a good construction quality, but it might be worthwhile for houses that have defective components. The influence of construction defects on the evaluation of cost effectiveness for risk mitigation and climate adaptation measures has not yet been taken into account in existing cost-benefit studies. The construction defect model described in Chapter 4 is thus incorporated into the cost-benefit analysis to examine the effect of construction defects.

The cost-effectiveness of a mitigation/adaptation measure is evaluated in terms of net present value (NPV) that is equal to the benefit minus the cost. A mitigation/adaptation measure is considered to be economically viable if NPV > 0, which is analogous to the

benefit-to-cost ratio (BCR) or life-cycle cost analysis used in many other studies (e.g. Li & Stewart 2011; Torkian et al. 2014; Orooji & Friedland 2017; Bastidas-Arteaga & Stewart 2019). A break-even economic assessment (e.g. Stewart 2015) is also adopted in this chapter to assess the conditions under which a mitigation/adaptation measure is cost-effective. The break-even analysis is conducted when considerable uncertainties are involved in the assessment of risk reduction and mitigation/adaptation cost due to either the model limitations and/or a lack of data. As the climate projections for many regions of Australia are under great uncertainty, a scenario-based approach is used in this study to examine the climate change impacts on the cost-benefit analysis.

6.2 Climate Change Projections

Climate change influences extreme wind speed and associated rainfall intensity and thus affect the risk assessment, mitigation and climate adaptation for housing. The latest projections (Dowdy et al. 2015; Grose et al. 2015) for changes in extreme wind speed in Brisbane and Melbourne are summarised in Table 6.1 for medium and high CO_2 emission scenarios RCP 4.5 and RCP 8.5, respectively, to 2090. Note that climate projects are relative to 1995 levels (1986-2005 average). Extreme wind projections for Melbourne are only available for RCP 8.5 (changes are not available for RCP 4.5). A drying trend with declining annual average rainfall is predicted Brisbane and Melbourne, while extreme rainfall is projected to become more intense due to increasing water-holding capacity of the atmosphere under a warmer climate (Dowdy et al. 2015; Grose et al. 2015). However, the quantitative projections for rainfall concurred with strong winds in a future climate are not available because the climate change impacts considering compound events (e.g. simultaneous occurrence of extreme wind and rainfall) in Australia remains unclear (Zscheischler et al. 2018). A high level of uncertainty is also involved in the projected magnitudes of change in wind speed due to the limitation of general circulation models (Stewart & Bastidas-Arteaga 2019). To this end, a scenario-based analysis is conducted in this study to examine the climate change impacts on the cost-benefit analysis. While there may be scenarios with no change in climate, and even a reduced climate hazard, risk mitigation and climate adaptation measures may still be recommended as there is no surety that current codes of practice are optimised for the current climate.

Table 6.1. Climate projections for extreme wind speed (percentage change relative to 1995 levels) to 2090 under two CO_2 emission scenarios.

	RCP4.5			RCP8.5		
	10th	Median	90th	10th	Median	90th
Brisbane	-8.0%	-1.5%	+1.0%	-5.0%	-2.0%	+2.0%
Melbourne	n/a	n/a	n/a	-4.0%	-1.0%	+5.0%

6.3 Cost-benefit analysis

The cost-effectiveness of a mitigation/adaptation measure is evaluated based on the NPV, which is calculated as

$$\text{NPV} = E(L)\Delta R + \Delta B - C_M \tag{6.1}$$

where ΔR is the reduction in risk due to the mitigation/adaptation measure, $E(L)$ is the risk for the house without any mitigation/adaptation measures (i.e. 'business as usual'), ΔB is the co-benefit of mitigation/adaptation such as reduced losses to other hazards, increased energy efficiency, etc., and C_M is the cost for risk mitigation and climate adaptation. For a mitigation/adaptation measure, ΔR can vary from 0 to 100%. If the mitigation/adaptation measure is applied at the initial design/construction stage, C_M is the extra money spent on a stronger design/construction. For retrofitting, C_M is the cost to remove the old housing component, if applicable, plus the cost to upgrade the component. All the mitigation/adaptation measures (see Section 6.4) considered in this study only require a one-off expense. The present study focuses on the wind risk mitigation, and therefore explicit quantification of ΔB is not included. The NPV calculated in this study is a dependent variable mainly due to the variability of ΔR. The confidence bounds of NPV or the probability of NPV > 0 may also be calculated. However, the cost-benefit analysis in this chapter is based on a maximum expected net benefit/return criterion, only the mean NPV is of interest. Note that Eq. (6.1) can be generalised for any time period, discounting of future costs and detailed time-dependent cost and damage consequences.

In addition to the NPV, a break-even analysis is also employed in this chapter as a decision tool when significant uncertainties are involved in the estimation of ΔR and C_M due to the limitation of relevant models and/or a lack of information. The break-even analysis can be viewed as a type of retrospective analysis, the output of which is the condition that enables the mean of NPV to be zero. A mitigation/adaptation measure is not cost-effective if the risk reduction provided by the measure is lower than, or the mitigation/adaptation cost

is higher than the predicted break-even value. Decision-makers can then judge whether a mitigation/adaptation measure meets these break-even values.

6.4 Mitigation and Adaptation Measures

The mitigation/adaptation measures proposed in this study for the representative contemporary house mainly aim to reduce the rainwater damage to building interior and contents. The estimated total cost to build a new contemporary house with an approximate floor area of 150 m^2 is $L_{building}$ = \$300,000 Australian Dollars as described in Section 5.5. The fragility and risk analysis show that wind damage to roof cladding is highly likely to occur for the representative contemporary house in Brisbane. The failure of metal roof sheets can further incur rainwater intrusion through the roof breaches, though the direct loss from roof cladding damage is limited due to a small cost ratio as shown in Table 5.5. Window breakage by high wind pressure creates windward dominant openings, which allows for more rainwater intrusion and roof damage due to significantly increased internal pressure. Rainwater intrusion via small gaps around undamaged windows may also occur when the water penetration resistance of window is exceeded. Strengthening roof cladding and windows not only decreases the direct losses from wind damage to the building envelope, but also reduce the amount of rainwater intrusion. In addition to reinforcing the building envelope, the use of water-resistant materials for building interior can also reduce the rainwater damage.

To this end, four mitigation/adaptation measures are proposed herein: (i) increase of uplift capacities for cladding-to-batten (CTB) connections (RF), (ii) protection of windows by shutters (WS), (iii) improvement of window resistances (WR), and (iv) use of water-resistant materials for ceiling and internal wall finishes (IW).

The fragility analysis in Chapter 3 reveals that the damage proportions of BTR and RTW connections are considerably less than the failures of CTB connections, and hence RF is to strengthen CTB connections by (i) increasing the base metal thickness (BMT) of metal roof cladding from 0.42 mm to 0.48 mm, and (ii) upgrading the screw fastener for CTB connections from M6-11 (diameter of 6.0 mm and 11 threads per inch) to 14-12 (diameter of 6.3 mm and 12 threads per inch). This improves the mean pull-over and pull-out capacities of CTB connections by 25% and 7%, respectively.

In WS, cyclone-rated steel roller shutters tested for wind pressure up to 2,500 Pa are used. The shutter strength against wind pressure is assumed to follow a normal distribution

with a mean of 3,000 Pa and a COV of 0.20, which implies that 20% of the shutters cannot satisfy the test pressure to account for the variance of quality in manufacture and installation. A triangular distribution with a lower bound of 50% and an upper bound of 100% as shown in Fig. 6.1 is assumed for the reduction of wind pressure and wind-driven rain on windows due to the installation of shutters, if not damaged. HAZUS (2014) assumes the reduction is 50% which is considered as a lower bound for a cyclone-rated roller shutter.

Window resistances may be increased by using a higher window rating (i.e. N1 to N2, N2 to N3 and N3 to N4). Note that improving window ratings does not necessarily increase the water penetration resistances of windows as shown in Table 3.5. By adding some additives in manufacture, the water absorption rate of plasterboard can be reduced. Gypsum plasterboard with specified water-resistant grade given by AS/NZS 2588 (2018) may be used as the internal linings for ceiling and wall. Water-resistant gypsum plasterboard is required to have an average water absorption of less than 5% of self-weight after two-hour immersion under a minimum of 25mm of water (AS/NZS 2588 2018), and a triangular probability distribution given by Fig. 6.2 is assumed to model the reduction of rainwater damage to internal linings. The internal linings (i.e. ceiling and wall finishes) consist of 30% of the building interior value as shown in Table 5.5.

The proposed mitigation/adaptation measures are summarized in Table 6.2. The mitigation/adaptation cost (normalized by building value) and the improved performance due to the mitigation/adaptation measure (i.e. benefit in Table 6.2) are also shown in Table 6.2. The mitigation/adaptation measures applied at the initial design and construction are RF, WR and IW, whereas window shutters (WS) can be installed at any time during the service life to retrofit an existing house. The cost is the additional money spent on the mitigation/adaptation measure, which is considered as a one-off expense. The mitigation/adaptation costs presented in Table 6.2 are estimated from an Australian housing construction cost guide (Rawlinsons 2015). The effect of variations in such costs on the cost-benefit analysis is examined through a break-even analysis presented in Section 6.5.2.

Table 6.2. Mitigation/adaptation measures for contemporary housing.

Housing component	Mitigation/adaptation measure	Description	Cost	Benefit
Roof cladding	**RF.** Strengthen CTB connections	Increase BMT of metal roof sheets from 0.42mm to 0.48mm, and upgrade the screw fastener from M6-11 to 14-12.	0.7%	Improve the uplift capacities of CTB connections with the mean pull-over and pull-out capacity increased by 25% and 7% respectively.
Window	**WS.** Install shutters	Cyclone-rated steel roller shutters tested for wind pressure up to 2,500 Pa.	2.0%	Reduce wind pressure and the amount of wind-driven rain acting on windows as shown in Fig. 6.1, and hence decrease the probability of windward dominant openings.
	WR. Higher window rating	Increase the window rating to a higher level (e.g. N2 to N3).	0.4%	Increase the ultimate strength and water penetration resistance of windows according to Table 3.5.
Building interior	**IW.** Water resistant materials	Use water-resistant plasterboard for ceiling and internal wall finishes.	1.0%	Improve water resistance of building interior and reduce rainwater damage as shown in Fig. 6.2.

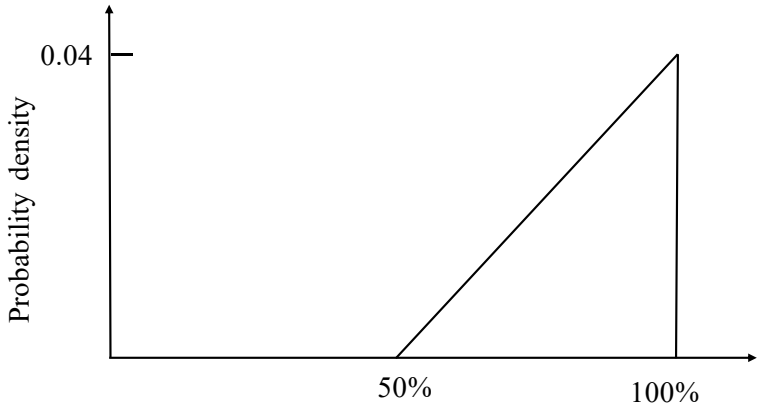

Figure 6.1. Reduction of wind pressure and wind-driven rain on windward windows due to cyclone shutters.

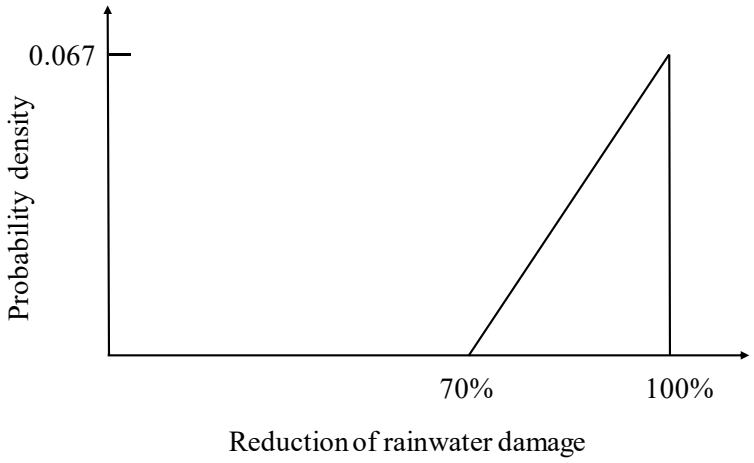

Figure 6.2. Reduction of water damage to internal linings by using water-resistant plasterboard.

6.5 Results

6.5.1 Cumulative risks

The cumulative expected loss (or risks) over the 50-year service life of the representative contemporary house from 2020 to 2070 is given by

$$E(L) = \sum_{t=2020}^{2070} E_{annual}(t) / (1+r)^{(t-2020)} \tag{6.2}$$

where $E_{annual}(t)$ is the annual expected loss in year t, and r is the discount rate. As derived from Eq. (5.17), $E_{annual}(t)$ considering the climate change impact is given by

$$E_{annual}(t) = \iiint f(R_h, t \mid v, D_{ur}) f(v,t) f(D_{ur}) \frac{1}{n_d} \sum_{j=1}^{n_d} \left[\Pr(DS \mid D_{Nj} T_N v, R_h, D_{ur}) \sum_{i=1}^{n_c} \Pr(L_i \mid DS) L_i \right] dv dR_h dD_{ur} \tag{6.3}$$

where $f(v, t)$ is the probability distribution of the annual maximum gust wind speed in year t, $f(R_h, t|v, D_{ur})$ is the probability distribution of the average rainfall intensity of a severe windstorm corresponding to a given duration D_{ur} in year t. The other notations in Eq. (6.3) are described in Section 5.6.1. In this study, the cumulative economic risks are presented in 2020 Australian dollars and a discount rate of r = 4% is used (Stewart et al. 2018). A sensitivity analysis is conducted in Section 6.5.4 using different discount rates.

Figure 6.3 shows the cumulative expected losses to 2070 considering construction defects. A constant climate is assumed in this section (i.e. no climate change impacts on wind and rainfall), and the climate change impacts are examined in Section 6.5.3. The cumulative expected losses to 2070 and risk reductions (shown in bracket) provided by the

mitigation/adaptation measures are shown in Table 6.3. In this section, it is assumed that the mitigation/adaptation measure WS is applied at the new construction (i.e. Year 2020) to maximise its benefits (i.e. risk reduction). Figure 6.3 and Table 6.3 suggest that installing window shutters (WS) is the most effective mitigation/adaptation measure that provides over 96% risk reduction. Strengthening roof connections (RF) provides up to 8% risk reduction for Brisbane houses but it is not effective for Melbourne houses, which is expected as roof failure is rare and most losses for houses in Melbourne are attributed to rainwater intrusion through windward windows. Improving window ratings (WR) offers more risk reduction when both the ultimate strength and water penetration resistance of windows are increased (i.e. N2 to N3), whereas less risk reduction is achieved if only the ultimate strength is increased (i.e. N1 to N2, N3 to N4). Using water-resistant materials for internal linings (IW) is generally effective, and provides about 20% risk reduction. As expected, considerably higher cumulative risks are predicted for houses in Brisbane with construction defects compared to those without construction defects, whereas the effect of construction defects on cumulative expected losses for Melbourne houses is slight.

Table 6.3. Cumulative expected losses to 2070 with no climate change.

(a) No construction defects

	Design wind classification	Cumulative expected losses $E(L)$ and risk reduction ΔR (in brackets)				
		No mitigation/ adaptation	RF	WS	WR	IW
Brisbane	N2	\$7,364	\$6,807 (8%)	\$292 (96%)	\$3,260 (56%)	\$5,870 (20%)
	N3	\$5,738	\$5,387 (6%)	\$191 (97%)	\$4,997 (13%)	\$4,905 (15%)
Melbourne	N1	\$2,381	\$2,270 (5%)	\$8 (99%)	\$2,153 (10%)	\$2,009 (16%)
	N2	\$3,069	\$2,926 (5%)	\$10 (99%)	\$1,344 (56%)	\$2,567 (16%)

(b) With construction defects

	Design wind classification	Cumulative expected losses $E(L)$ and risk reduction ΔR (in brackets)				
		No mitigation/ adaptation	RF	WS	WR	IW
Brisbane	N2	\$8,995	\$8,512 (5%)	\$337 (96%)	\$3,875 (57%)	\$7,456 (17%)
	N3	\$7,106	\$6,707 (6%)	\$267 (96%)	\$6,335 (11%)	\$5,904 (17%)
Melbourne	N1	\$2,475	\$2,409 (3%)	\$8 (99%)	\$2,331 (10%)	\$2,062 (17%)
	N2	\$3,251	\$3,162 (3%)	\$12 (99%)	\$1,481 (55%)	\$2,648 (18%)

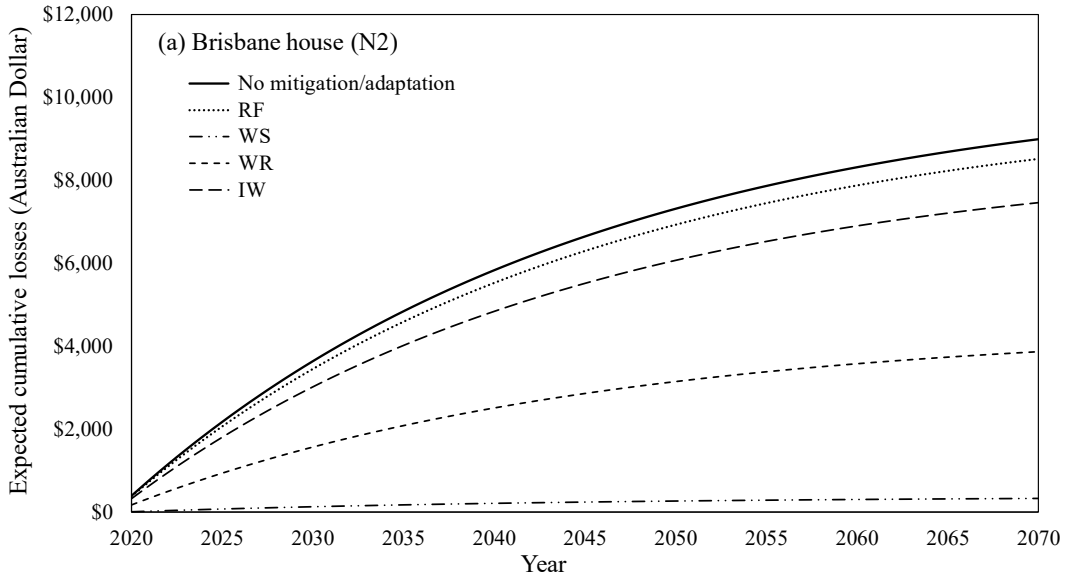
(a) Brisbane house (N2)
No mitigation/adaptation
RF
WS
WR
IW
Expected cumulative losses (Australian Dollar)
$12,000
$10,000
$8,000
$6,000
$4,000
$2,000
$0
2020
2025
2030
2035
2040
2045
2050
2055
2060
2065
2070
Year

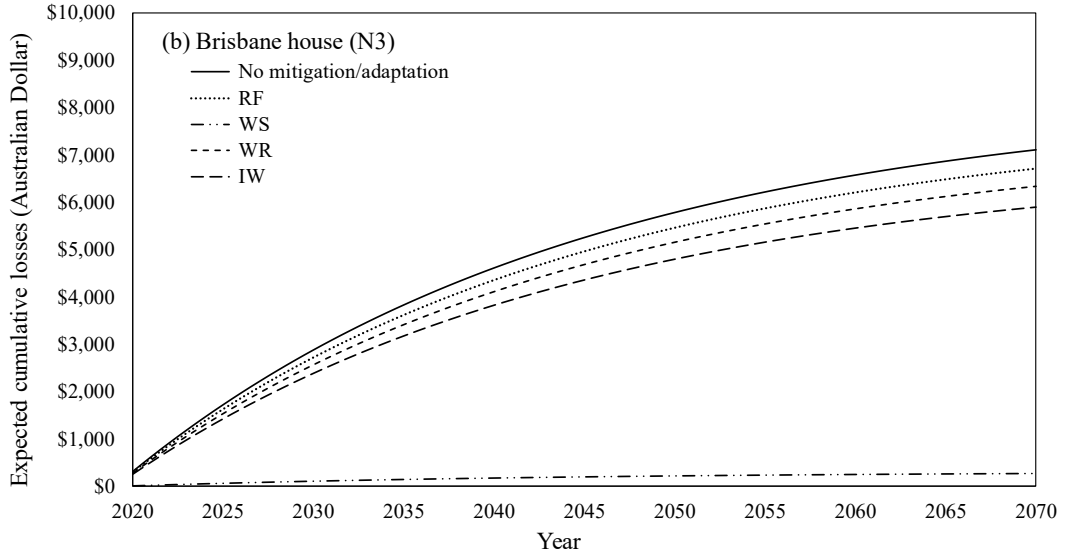
(b) Brisbane house (N3)
No mitigation/adaptation
RF
WS
WR
IW
Expected cumulative losses (Australian Dollar)
$10,000
$9,000
$8,000
$7,000
$6,000
$5,000
$4,000
$3,000
$2,000
$1,000
$0
2020
2025
2030
2035
2040
2045
2050
2055
2060
2065
2070
Year

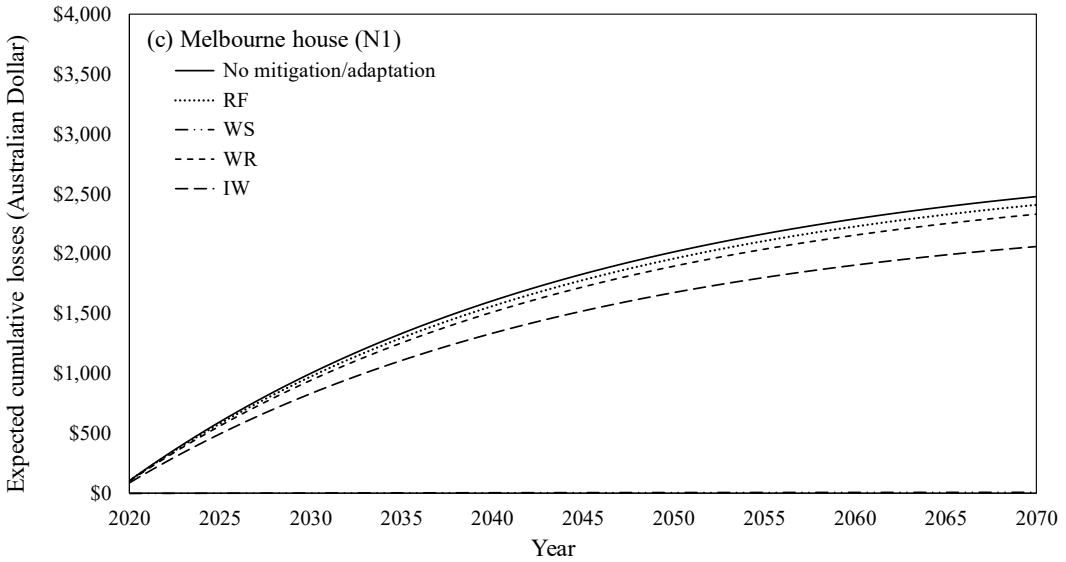
(c) Melbourne house (N1)
No mitigation/adaptation
RF
WS
WR
IW
Expected cumulative losses (Australian Dollar)
$4,000
$3,500
$3,000
$2,500
$2,000
$1,500
$1,000
$500
$0
2020
2025
2030
2035
2040
2045
2050
2055
2060
2065
2070
Year

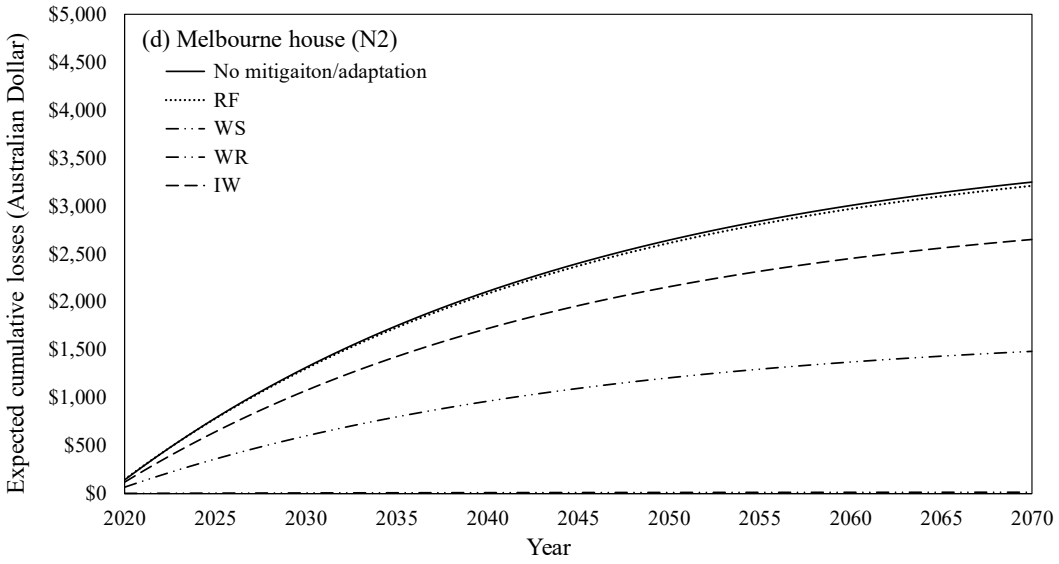

Figure 6.3. Cumulative expected losses for houses with construction defects and no climate change.

6.5.2. Evaluation of cost-effectiveness

The cost-benefit analysis is conducted using the annual and cumulative expected losses evaluated from the PRA described in Chapter 5. The procedures for the cost-benefit analysis are summarized as:

(i) Calculate the annual expected loss in year t for the considered house without mitigation/adaptation using the PRA method, and then calculate the cumulative expected loss for the 50-year building service life using Eq. (6.2);

(ii) Calculate the annual expected loss in year t for the considered house with a given mitigation/adaptation measure using the PRA method, and then calculate the cumulative expected loss for the 50-year building service life using Eq. (6.2);

(iii) Calculate the reduced cumulative expected loss due to the mitigation/adaptation measure, i.e. $E(L)\Delta R$, in Eq. (6.1);

(iv) Implement (ii) and (iii) for all considered mitigation/adaptation measures, and then calculate the mean NPVs corresponding to these measures using Eq. (6.1);

(v) Decision-making based on the mean NPVs corresponding to different mitigation/adaptation measures. Mitigation/adaptation measures with the mean NPV greater than zero are deemed as cost-effective, and those with a higher mean NPV is more preferred by assuming a risk neutral decision-maker whose primary goal is economic efficiency.

Table 6.4 shows the mean NPVs to 2070 for the representative contemporary house with/without construction defects and no climate change is assumed. Table 6.4 suggests that, in most cases, the mean NPVs of mitigation/adaptation measures with the consideration of construction defects are higher than those without considering construction defects. This is expected because construction defects result in higher cumulative risks and a specific mitigation/adaptation measure can generally offer more reduction in monetary losses (i.e. $E(L)\cdot\Delta R$) at a given cost. For the Brisbane house with a design wind classification of N2, the mitigation/adaptation measures yielding a positive mean NPV are WS and WR. No mitigation/adaptation measure is cost-effective for the Brisbane house with a design wind classification of N3 without considering construction defects, however, WS turns to a positive mean NPV when construction defects are taken into account. This illustrates the effect of construction defects on the cost-benefit analysis. None of the mitigation/adaptation measures may be recommended for the Melbourne house with a design wind classification of N1 as the corresponding mean NPVs are negative. Table 6.4 also shows that WR is the only cost-effective measure for the Melbourne house with a design wind classification of N2.

Table 6.4. Mean NPVs to 2070 with no climate change.

(a) No construction defects

	Design wind classification	Mean NPV			
		RF	WS	WR	IW
Brisbane	N2	-$1,543	$1,072	$2,904	-$1,506
	N3	-$1,749	-$453	-$460	-$2,167
Melbourne	N1	-$1,989	-$3,628	-$972	-$2,629
	N2	-$1,957	-$2,941	$525	-$2,499

(b) With construction defects

	Design wind classification	Mean NPV			
		RF	WS	WR	IW
Brisbane	N2	-$1,618	$2,657	$3,920	-$1,461
	N3	-$1,701	$839	-$429	-$1,798
Melbourne	N1	-$2,034	-$3,533	-$955	-$2,586
	N2	-$2,011	-$2,761	$570	-$2,398

The mitigation/adaptation costs given in Table 6.2 are estimated according to the average cost data given by Australian housing construction cost guide (Rawlinsons 2015). However,

the costs may vary among different locations, contractors and labourers. A break-even analysis is thus conducted to calculate the maximum mitigation/adaptation cost that enables the mean NPV to be zero with the consideration of construction defects, see Table 6.5. It is indicated from Table 6.5 that a mitigation/adaptation measure may turn to be cost-effective with reasonable discounts on the cost given by Table 6.2. For example, only a 13% discount on the cost makes WR cost-effective for the Brisbane house with a design wind classification of N3, whereas a 50% reduction in cost is needed to enable IW to be cost-effective for the Brisbane house with a design wind classification of N2. A few mitigation/adaptation measures can remain cost-effective even with significantly increased costs. For example, WR is still cost-effective for the Brisbane house with a design wind classification of N2, if the anticipated cost of WR given by Table 6.2 increases by 300%.

Table 6.5. Break-even costs (normalized by the building value) for different mitigation/adaptation measures to be cost-effective (with construction defects).

	Design wind classification	Break-even cost			
		RF	WS	WR	IW
Brisbane	N2	0.16%	2.89%	1.71%	0.51%
	N3	0.13%	2.28%	0.26%	0.40%
Melbourne	N1	0.03%	0.82%	0.08%	0.14%
	N2	0.03%	1.08%	0.59%	0.20%

6.5.3. Climate change impact and adaptation

A mitigation measure may provide more risk reduction (benefit) if the climate scenario becomes worse, and hence affect the cost-effectiveness. A scenario-based analysis is conducted to examine the cost-effectiveness of the mitigation/adaptation measures under a changing climate. The median, 10^{th} and 90^{th} percentile projections for wind speed change under RCP 4.5 and RCP 8.5 as shown in Table 6.1 are adopted, and the changes in rainfall intensity to 2090 conditional on an extreme wind climate scenario are assumed to be –20%, –10%, 0%, +10% and +20%. Information is scarce to non-existent on time-dependent changes in extreme wind speed and associated rainfall for Australia. A time-dependent linear change (Stewart et al. 2018) is then assumed for both wind speed and rainfall intensity. Based on the cumulative expected losses evaluated for the considered climate change scenarios, the mean NPVs for different mitigation/adaptation measures to 2070 can then be calculated. Figure 6.4 shows the mean NPVs corresponding to different climate scenarios for Brisbane and Melbourne houses with a design wind classification of N2. The error bars

in Fig. 6.4 represent the 10th and 90th percentile projections for wind speed change under RCP 4.5 and RCP 8.5. It is observed that, in general, the larger the wind speed and the associated rainfall intensity in a future climate, the higher the mean NPVs produced by the mitigation/adaptation measures. Climate change tends to have higher influences on the cost-effectiveness of mitigation/adaptation measures applied to houses in Brisbane. However, in general, climate change has a limited influence on the cost-benefit analysis.

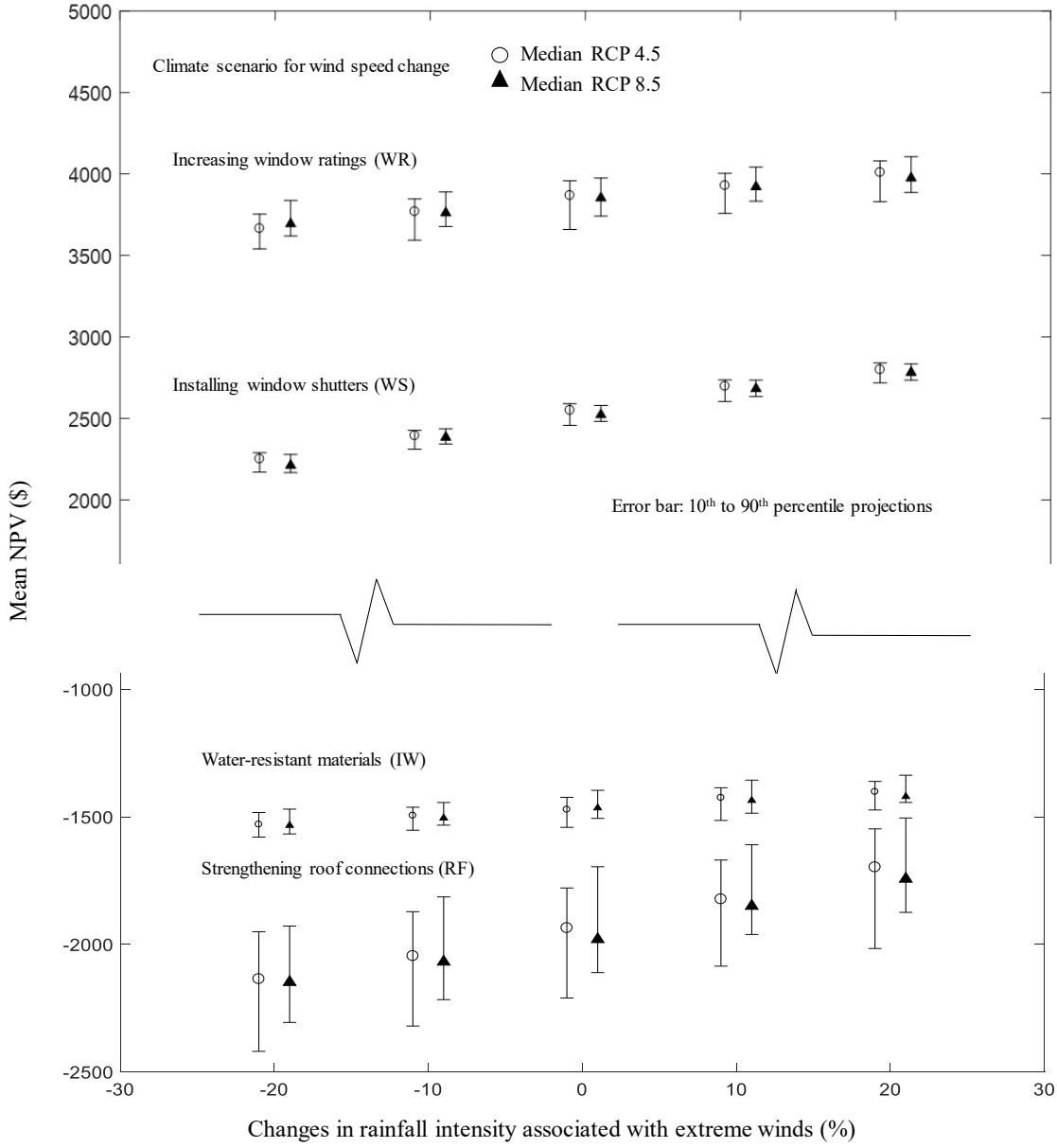

(a) Brisbane house N2

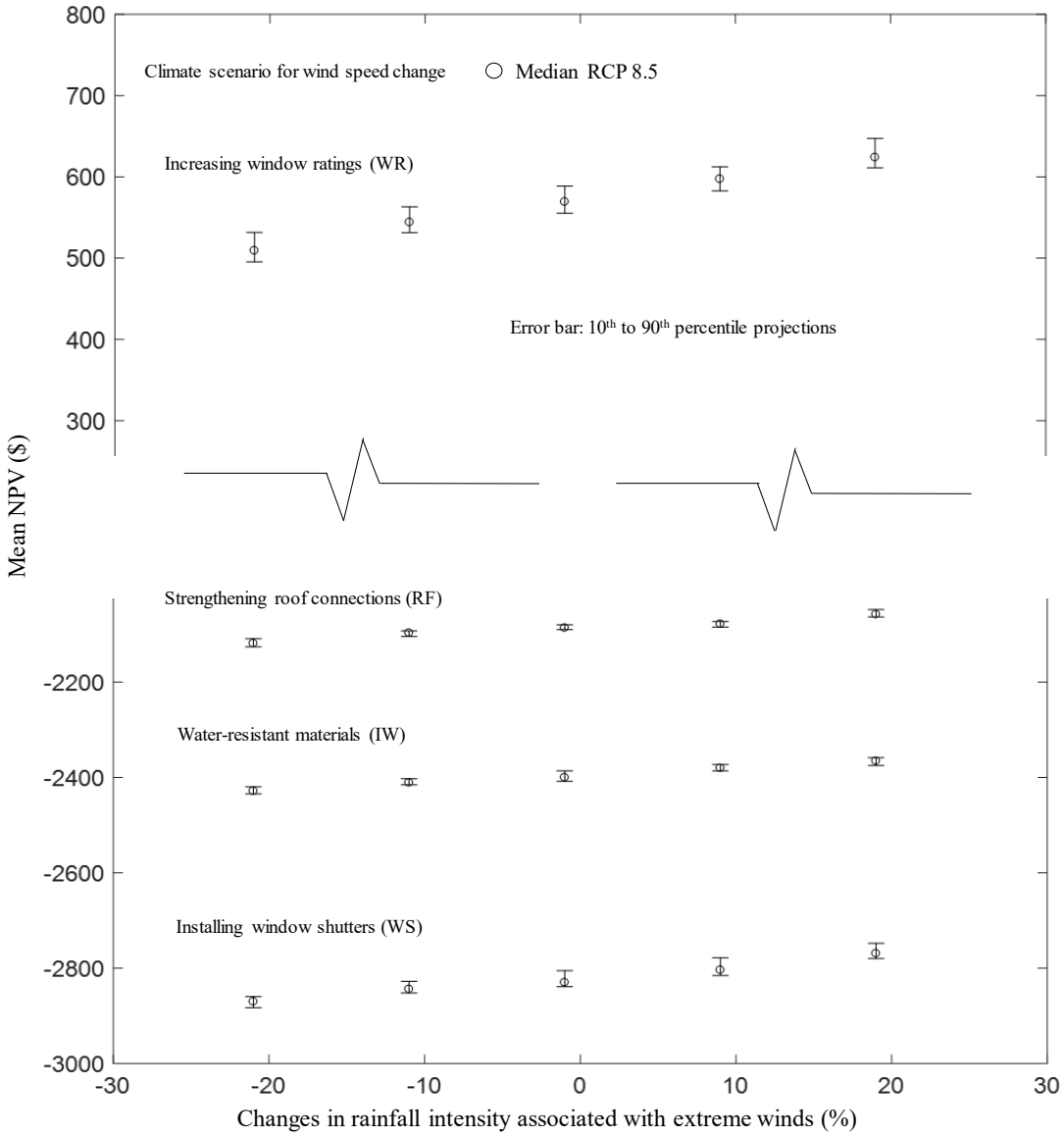

(b) Melbourne house N2

Figure 6.4. Climate change impacts on mean NPVs for different mitigation/adaptation measures.

Installing window shutters (WS) and increasing window ratings (WR) remain cost-effective for the Brisbane house (N2), and WR is cost-effective for the Melbourne house (N2) under all the considered climate scenarios. For the most adverse climate scenario considered in this study (i.e. 90th percentile projection for extreme wind speed under RCP 8.5 and a 20% increase in rainfall intensity), the mean NPVs increase by approximately 15% and 10% respectively for WS and WR compared to the scenario with no climate change. Strengthening roof connections (RF) and using water-resistant materials (IW) are not cost-effective under all the considered climate change scenarios. In addition, the co-benefits (ΔB given in Eq. (6.1)) associated with RF and IW are negligible, whereas considerable co-

benefits exist for WS and WR. Using a higher window rating (WR) provides energy efficiency due to increased glass thickness. Shutters (WS) can offer more co-benefits such as noise reduction, prevention of heat loss, light control and home security. Although the mean NPV of WR is higher than that corresponding to WS for the Brisbane house (N2) under a changing climate, WS is still a competitive option for wind risk mitigation and climate adaptation due to considerable co-benefits. In terms of implications for insurance premium, an insurer may offer incentives by a discount in annual insurance premium for homeowners who decide to retrofit their houses by installing window shutters.

6.5.4. Sensitivity analysis

The mitigation/adaptation measure WS is considered as a retrofit that can be applied at any year during the service life. Figure 6.5 shows the mean NPV to 2070 for houses with no climate change when installing window shutters at different points in time. It is indicated that WS is cost-effective for houses in Brisbane if applied no later than 2048 for N2 houses and 2035 for N3 houses. The mean NPVs to 2070 increase for houses in Melbourne if window shutters are installed in a later year. Climate change has limited influences on these results.

Two discount rates (i.e. 2% and 7%) are further adopted in the cost-benefit analysis, and the corresponding mean NPVs with the consideration of construction defects and no climate change are given in Table 6.6. As expected, the mean NPV increases for a lower discount rate, and decreases for a higher discount rate. Installing window shutters (WS) for Brisbane houses with design wind classifications of N2 and N3 is no longer cost-effective under a discount rate of 7%. Increasing window ratings (WR) for the Brisbane house with a design wind classification of N3 turns to be cost-effective under a discount rate of 2%.

Table 6.6. The effect of discount rate on mean NPV.

(a) Discount rate of 2%

	Design wind classification	Mean NPV			
		RF	WS	WR	IW
Brisbane	N2	-$1,404	$6,485	$6,184	-$781
	N3	-$1,524	$3,864	$13	-$1,267
Melbourne	N1	-$2,005	-$2,442	-$892	-$2,404
	N2	-$1,969	-$1,328	$1,352	-$2,131

(b) Discount rate of 7%

	Design wind classification	Mean NPV			
		RF	WS	WR	IW
Brisbane	N2	-$1,782	-$301	$2,171	-$1,987
	N3	-$1,837	-$1,497	-$692	-$2,209
Melbourne	N1	-$2,056	-$4,376	-$1,105	-$2,728
	N2	-$2,042	-$3,868	-$35	-$2,603

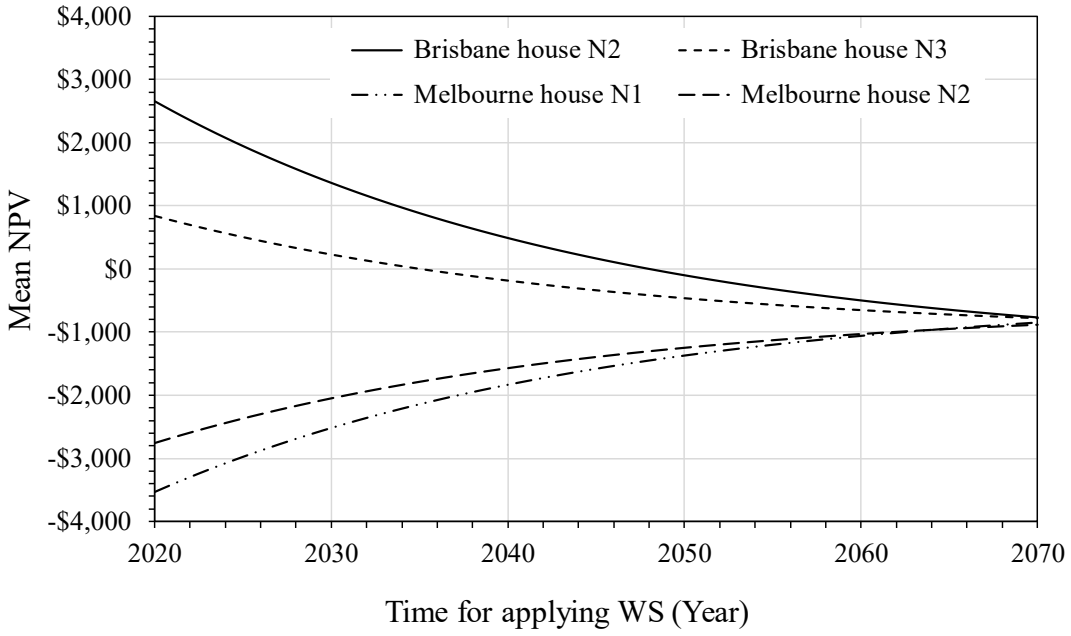

Figure 6.5. Effect of the time for installing window shutters (WS) on the mean NPV.

Although Australian standard AS2047 (2014) specifies the design window ratings for housing with different site conditions, it was found that many window manufacturers do not provide detailed window ratings for their products. Window manufacturers are only required to publish energy data, but the structural performance data is non-mandatory in Australia. This may lead to construction error in practice that windows with unsatisfied or mislabeled window ratings are installed. A scenario-based approach is used herein to examine the effects of mislabelled windows on the cost-benefit analysis. It is assumed that N1-rated windows are incorrectly installed on Brisbane and Melbourne houses with a design wind classification of N2, and N2-rated windows are incorrectly installed on Brisbane houses with a design wind classification of N3. This increases the cumulative expected losses to 2070 by 32%, 4% and 96% for the Brisbane house (N2), Melbourne house (N2) and

Brisbane house (N3), respectively. Table 6.7 shows the mean NPVs for mitigation/adaptation measures RF, WS and IW if the mislabelled windows are installed. It is suggested that RF and IW is still not cost-effective, and WS is cost-effective for Brisbane houses. When mislabelled windows are installed, there is an approximately twofold and tenfold increase of the mean NPV yielded by WS for Brisbane houses with a design wind classification of N2 and N3, respectively, compared to that without such construction error. This implies that the adverse effects of construction defects can be largely counter-balanced by installing shutters.

Table 6.7. Mean NPV when mislabeled windows are installed.

	Design wind classification	Mean NPV		
		RF	WS	IW
Brisbane	N2	-$1,439	$5,531	-$1,016
	N3	-$1,365	$8,063	-$1,073
Melbourne	N2	-$1,994	-$2,062	-$2,357

6.6 Conclusions

In this chapter, several wind risk mitigation or climate adaptation measures are adopted for Australian contemporary houses subjected to non-cyclonic windstorms to either reinforce the building envelope or increase water resistance of the building interior. A cost-benefit analysis is conducted to evaluate the cost-effectiveness of these mitigation/adaptation measures. It reveals that strengthening windows by increasing window ratings (e.g. N1 to N2, N2 to N3) is cost-effective for Brisbane houses and Melbourne houses with a design wind classification of N2. Installing shutters significantly reduces economic risks incurred by wind and rainfall damage, and is cost-effective for houses in Brisbane with a design wind classification of N3. The adverse effects of construction defects can be largely counter-balanced by installing shutters. Installation of window shutters as a retrofit also provides many co-benefits and has the potential to attract incentives in annual insurance premium, which makes it a promising candidate for wind risk mitigation and climate adaptation. Climate change has limited impacts on the cost-benefit analysis.

CHAPTER 7. RISK PREFERENCES AND DECISION-MAKING FOR WIND HAZARD MITIGATION UNDER UNCERTAINTY

7.1 Introduction

The probabilistic risk assessment (PRA) presented in Chapter 5 includes the probabilistic quantification of non-cyclonic extreme winds and associated rainfall, structural response and system performance, construction defects, structural damage states and consequences. The outputs of PRA can be used to evaluate the probability distribution of net present value (NPV) and life-cycle cost for further decision analysis. The cost-benefit analysis presented in Chapter 6 is based on the mean NPV, which is equivalent to rank the mitigation/adaption measures by either maximizing the expected net benefit/return or minimizing the expected life-cycle cost (MELC). Hereafter, MELC is used to represent this type of decision analysis. Although economic efficiency is achieved by MELC, statistical information other than the mean in the probability distribution of life-cycle cost is neglected in such decision analysis.

A rational decision maker may be risk-neutral given the perfect modelling and understanding of the occurrence rate and magnitude of natural and man-made hazards, structural response and performance, the direct and indirect consequences. However, a decision-maker who is originally risk-neutral may turn to be risk-averse because substantial uncertainties, both aleatory and epistemic, are involved in the PRA for housing under extreme winds developed in this study, or similarly, risk assessment for other civil facilities exposed to low-probability, high-consequence events. For example, the wind and rainfall hazard modelling is subjected to statistical uncertainty due to a relatively short length of historical weather records, and model uncertainty resulting from a partial understanding of the natural phenomenon and a lack of knowledge regarding the climate change impact. The uncertainties of human error and its influence on structural reliability and performance may arise from the partial understanding of error mechanism and a shortage of statistical information for error rates. To this end, it is not surprising that risk averseness is found to be prevalent in civil engineering decisions associated with extreme events (Stewart et al. 2011; Cha & Ellingwood 2012; Cha & Ellingwood 2013), and decision-making under uncertainty tends to invest more resources to avoid high consequences from natural and man-made hazards. The MELC is adequate for risk-neutral decision-makers but fails to

capture other risk preferences, especially risk averseness. Therefore, the cost-benefit analysis presented in Chapter 6 needs to be further extended to consider different risk preferences.

Rather than decision analysis solely based on the expected life-cycle cost, several decision models can capture risk preferences involved in the wind mitigation decisions under uncertainty, and provide more risk-informed decision support. The utility theory (UT) by von Neumann & Morgenstern (1944) is widely employed to explicitly factor risk preferences into the decision process (e.g. Stewart et al. 2011; Mahsuli & Haukaas 2018), where nonlinear utility functions are used to incorporate a subjective evaluation of the consequences to account for risk-seeking and risk-averse attitudes. The UT provides a normative model that prescribes rational decisions by maximizing the expected utility associated with different risk attitudes. However, the elicitation of a widely accepted utility function is not an easy task. It is very likely that a decision-maker has difficulties in expressing his/her preferences explicitly (i.e. only partial information of risk preference is available), or multiple decision-makers with different risk preferences cannot reach an agreement, which could happen even when all decision-makers are risk-averse but with varying degrees of risk-averseness.

The stochastic dominance (SD) criteria (Hadar & Russell 1969; Hanoch & Levy 1969) provides an alternative approach for decision-making under uncertainty in civil engineering applications, for example, the selection of design levels for buildings and pipelines (e.g. Goda & Hong 2006; Zhou & Nessim 2011). The SD conforms to the principle of maximum expected utility, and can rank decision alternatives based on probability distributions of the associated life-cycle cost without explicitly specifying any utility functions. Despite the advantages, the SD often fails to offer a full ranking of all decision alternatives due to its rigorous rules that are frequently violated by some 'pathological' preferences (Levy 2016), for example, extremely risk-averse or risk-seeking. Thus, SD is often used in an initial screen to exclude inefficient or suboptimal alternatives. The almost stochastic dominance (ASD) is an extension of SD to provide a relaxation of SD's strict conditions (Leshno & Levy 2002), which is firstly introduced by the present study in a context of civil engineering decision-making. Compared to SD, ASD has an improved capability to rank decision alternatives. The superquantile value, also called conditional-value-at-risk (Rockafellar & Uryasev 2000; Rockafellar & Royset 2015), offers another approach to account for risk averseness in engineering decision-making with the convenience that utility functions are

not needed. Compared to the commonly used quantile values (or value-at-risk), the superquantile better captures the extreme tail of the life-cycle cost distribution, and conforms theoretical axioms such as coherency and regularity (Rockafellar & Royset 2015).

The normative UT model presumes a decision-maker to be an expected utility maximizer that behaves rationally, and ignores the decisional behaviour under bounded rationality that is common in reality (Simon 1955; Kahneman & Tversky 1979). The descriptive decision models in behaviour economics such as rank-dependent utility theory (RDUT) (Quiggin 1982) and cumulative prospect theory (CPT) (Tversky & Kahneman 1992) are then developed to describe the actual behaviour of decision-makers, which have been applied in the context of civil engineering decision-making to either identify the risk attitudes in existing engineering decisions (e.g. Cha & Ellingwood 2013; Cha & Ellingwood 2014) or predict decision-makers' preferred choices under bounded rationality (e.g. Goda & Hong 2008a; Gong & Frangopol 2019). Goda & Hong (2008b) also examined the decision-makers' preferences for seismic design levels with the consideration of insurance protection using CPT. These descriptive decision models in behaviour economics may have limited usefulness in decision support for large corporations or government agencies who tend to be risk-neutral and favour to have rational basis in their long-term decisions if all direct and indirect consequences including societal and political effects are properly taken into account. Instead, the descriptive decision models are more useful for the prediction of individual's preferred choices, for example, homeowners' choices in purchasing insurance and reinforcing their houses to reduce wind damage.

This chapter presents a set of decision models to account for the magnitude of uncertainty and risk preferences involved in mitigation decisions for housing under extreme winds. These models have different features, and can address various issues in the decision context (e.g. risk attitudes, extreme tail of life-cycle cost distribution, elicitation of utility functions, the role of behaviour economics and bounded rationality, etc) to better inform and support decision-making. This study also employs the descriptive decision models to predict homeowners' preferences in implementing mitigation measures for their home with the consideration of insurance purchasing. The predicted decisional behaviour is useful for devising economic incentives to motivate homeowners to install window shutters for the protection of their homes against windstorms, which has the potential to substantially reduce insurance losses and improve the resilience of residential communities in Australia.

7.2 Life-cycle Cost and Insurance

The life-cycle cost (LCC) for the considered house without insurance subjected to extreme winds is

$$LCC = C_D + C_M \tag{7.1}$$

where C_D is the damage/failure cost resulting from wind and rainfall hazards during the considered time horizon, and C_M is the mitigation cost. This study focuses on the wind mitigation decisions for houses, thus the initial construction cost or any maintenance cost is not included.

The costs for the four mitigation measures proposed in this study are considered to be deterministic as given in Table 6.2. A service life of 50 years from 2020 to 2070 is considered for the representative contemporary house, and C_D is then the cumulative losses over the 50-year building service life, given by

$$C_D = \sum_{t=2020}^{2070} C_A(t) / (1+r)^{(t-2020)} \tag{7.2}$$

where $C_A(t)$ is the annual loss in year t, and r is the discount rate. The probability distribution of $C_A(t)$ can be obtained from the PRA using MCS described in Chapter 5. The expected value of $C_A(t)$ is the annual expected loss in year t, i.e. $E_{annual}(t)$, given by Eq. (6.3). The damage cost or cumulative loss over the 50-year building service life, C_D, is thus a random variable. The expected value of C_D is the cumulative expected loss over the 50-year building service life, $E(L)$, given by Eq. (6.2).

For homeowners who purchase home and contents insurance, C_D is partially or fully transferred to the insurer depending on the excess fee and sum insured. The life-cycle cost for homeowners with insurance, LCC_{HO}, is calculated as

$$LCC_{HO} = \sum_{t=2020}^{2070} [C_A(t) - I(C_A(t))] / (1+r)^{(t-2020)} + C_M + \sum_{t=2020}^{2070} INP(t) / (1+r)^{(t-2020)} \tag{7.3}$$

where $I(C_A(t))$ is the annual indemnity paid by the insurer (or annual insurance loss) in year t, and $INP(t)$ is the annual insurance premium for windstorms at year t. For a fully insured homeowner, $I(C_A(t))$ is calculated as

$$I(C_A(t)) = \begin{cases} 0 & C_A(t) \le EX \\ C_A(t) - EX & C_A(t) > EX \end{cases} \tag{7.4}$$

where EX is the excess fee to avoid any small claims. The damage cost for homeowners who are fully insured results from small losses no greater than the excess fee and excess fee paid when making claims given the occurrence of considerable losses. The ratio of annual expected insurance loss to annual insurance premium, i.e. the expected value of $I(C_A(t))/INP(t)$, is typically around 60% for home insurance in Australia (AGA 2014), which measures the potential business cost and profit for the insurer. In insurance industry, the annual premium $INP(t)$ is typically determined based on the regional loss data and other factors (e.g. customer information, market competition, business goals, etc.) considered by the insurer (e.g. Suncorp 2013). Climate change is generally not considered in calculating insurance premium, but the premium may increase in a future year because of, for example, an increased number of storm claims in previous years.

The insurance loss or claim cost for the insurer, L_{INS}, during the 50-year building service life is given by

$$L_{INS} = \sum_{t=2020}^{2070} [I(C_A(t))] / (1+r)^{(t-2020)} \tag{7.5}$$

7.3 Decision Models

7.3.1 Superquantile

The α-superquantile of the life-cycle cost, LCC ($0< \alpha <1$), also called conditional value-at-risk, is given by (Rockafellar & Royset 2015)

$$\bar{q}_\alpha(LCC) = \frac{1}{1-\alpha}\int_\alpha^1 q_\beta(LCC)d\beta \tag{7.6}$$

where $q_\beta(LCC)$ is the β-quantile value of LCC, also called value-at-risk. The α-superquantile, $\bar{q}_\alpha(LCC)$, is the average of quantiles $q_\beta(LCC)$ with $\alpha < \beta < 1$. In practice, given the random samples of LCC obtained from the PRA using MCS, $\bar{q}_\alpha(LCC)$ can be calculated as the conditional expectation of LCC equal or greater the α-quantile value, given by

$$\bar{q}_\alpha(LCC) = E[LCC \mid LCC \geq q_\alpha(LCC)] \tag{7.7}$$

Compared to quantile values, the superquantile better captures the extreme tails of the life-cycle cost distribution, which is generally of interest in decision-making for civil structures and infrastructure systems subjected to low-probability high-consequence events. The superquantile also holds some attractive mathematical properties such as coherency and

regularity (see Rockafellar & Royset 2015 for details). Note that the larger the considered α value, the higher the degree of risk aversion.

7.3.2 Utility theory

Utility measures the desirability of consequences. The utility theory (UT) is a normative decision tool that prescribes the rational decisions by maximizing the expected utility. For a random variable x of the consequence containing n outcomes, $x_1, x_2, \ldots, x_n$, the expected utility (EU) of x is given by

$$\mathrm{EU}(x) = \sum_{i=1}^{n} p_i u(x_i) \tag{7.8}$$

where $u(x)$ is the utility function, and p_i is the probability of x_i. Note that $\sum_{i=1}^{n} p_i = 1$. The utility functions are used to reflect decision-makers' risk attitudes. When a linear utility function is adopted to represent the risk-neutral attitude, the decisions yielded by UT are equivalent to those dictated by the MELC criteria. Nonlinear utility functions are used to characterize risk-seeking or risk-averse attitudes. Generally speaking, the more nonlinearity in the utility function, the higher the degree of risk proneness or risk aversion. Consider a power utility function $u(x) = -(-x)^l$ where $x = -LCC$ is a negative value to frame the life-cycle cost as a loss, and to ensure $u(x)$ is a monotonic and increasing function. In other words, a lower life-cycle cost with a higher utility is preferred. The scaled shape of $u(x)$ with different l values is plotted in Fig. 7.1, where $l = 1$, $l < 1$ and $l > 1$ stand for risk-neutral, risk-seeking and risk-averse attitudes, respectively.

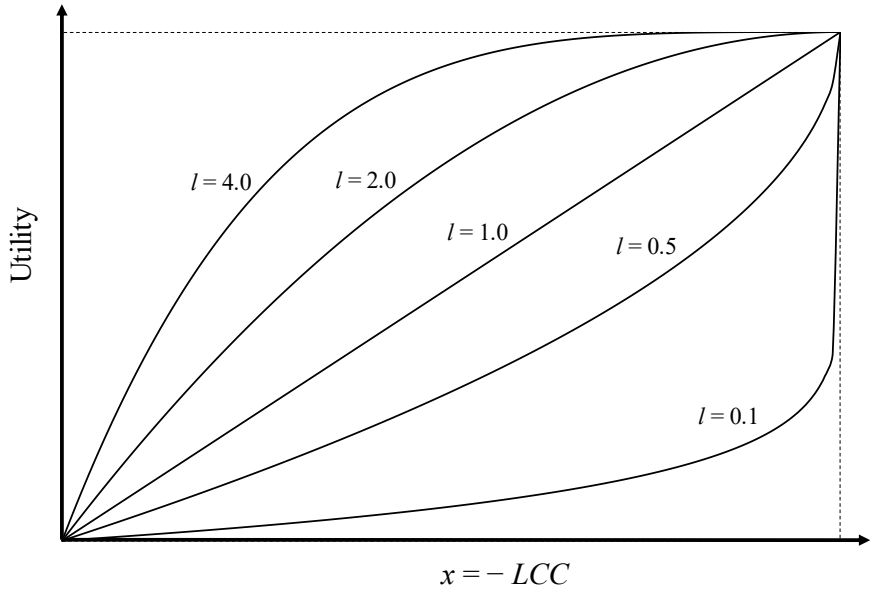

Figure 7.1. Power utility functions to reflect different risk attitudes.

7.3.3 Almost stochastic dominance

The stochastic dominance (SD) ranks two decision alternatives by checking if one is superior to the other without explicitly specifying a utility function. In the context of this study, suppose F and G are two mitigation measures. Let $F(x)$ and $G(x)$ denote the cumulative distribution function (CDF) of x where $x = -LCC$ is a random variable associated with the life-cycle cost of a mitigation measure. Then for any decision-maker with a non-decreasing utility function $u(x)$ (i.e. $u'(x) \geq 0$, generally one prefers a larger value of x or a smaller life-cycle cost), F dominates G by the first-degree stochastic dominance rule (FSD) if and only if $F(x) \leq G(x)$ for all values of x with a strong inequality for at least one value of x (Levy 2016). If F dominates G by FSD, F is always preferred to G, and the expected utility associated with F is always no smaller than that of G regardless of the risk attitudes of decision-makers (i.e. the non-decreasing utility function of x can be linear, concave or convex). Figure 7.2 illustrates the CDFs of F and G when F dominates G by FSD. Other higher degree SD rules are not used in this study, see Levy (2016) for more details.

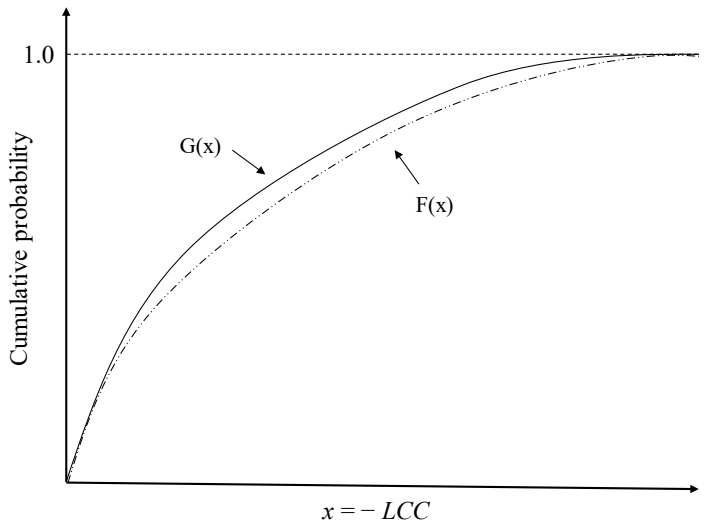

Figure 7.2. Graphical illustration of FSD.

In practical applications, the SD often cannot rank two decision alternatives due to its strict conditions (e.g. $F(x) \leq G(x)$ for all values of x for FSD). For example, the FSD adopted by Goda & Hong (2006) and Zhou & Nessim (2011) failed to rank any design alternatives, and only a partial rank was achieved by screening out a few inferior alternatives when higher degree SD rules were adopted. The almost stochastic dominance (ASD) provides a relaxation of SD's condition to better rank the decision alternatives. The almost first-degree stochastic dominance (AFSD) allows a relatively small portion of x at which the condition of FSD does not hold, i.e. $F(x) > G(x)$. Define S_1 is a subset of x that contains x values where

$F(x) > G(x)$. For $0 < \varepsilon < 0.5$, F dominants G by AFSD for all values of x if and only if (Levy 2016)

$$\int_{S_1} [F(x) - G(x)]dx \le \varepsilon \int |G(x) - F(x)|\, dx \tag{7.9}$$

Figure 7.3 illustrates the CDFs of F and G when F dominates G by AFSD. The ε value is calculated as the violation area enclosed between $F(x)$ and $G(x)$ when $F(x) > G(x)$ as shown in Fig. 7.3 (i.e. $\int_{S_1} [F(x) - G(x)]dx$) divided by the total area enclosed under the two CDFs (i.e. $\int |G(x) - F(x)|dx$). It is also referred as F dominates G by ε-AFSD. Note that if there is no violation area, AFSD coincides with FSD. If F dominants G by ε-AFSD and ε is sufficiently small, then F is preferred to G, and the expected utility associated with F is no smaller than that of G except for some 'pathological' defined utility functions (Levy 2016), for example, overly convex or concave (i.e. extremely risk-averse or risk-seeking attitude). In other words, the rank of alternatives dictated by AFSD would satisfy most decision makers who are expected utility maximizers with non-decreasing utility functions. The ε value in AFSD has a broad range, i.e. $0 < \varepsilon < 0.5$, that provides a full rank of all decision alternations, however, caution is needed when selecting the ε value in practice. The smaller the ε value, the stronger the dominance. It may need subjective judgement to determine the largest allowed violation area or ε value that can vary depending on the decision context. Section 7.4 discusses the discretion for ε value in the wind mitigation decisions. Refer to Leshno & Levy (2002) and Tzeng et al. (2013) for higher degree ASD rules.

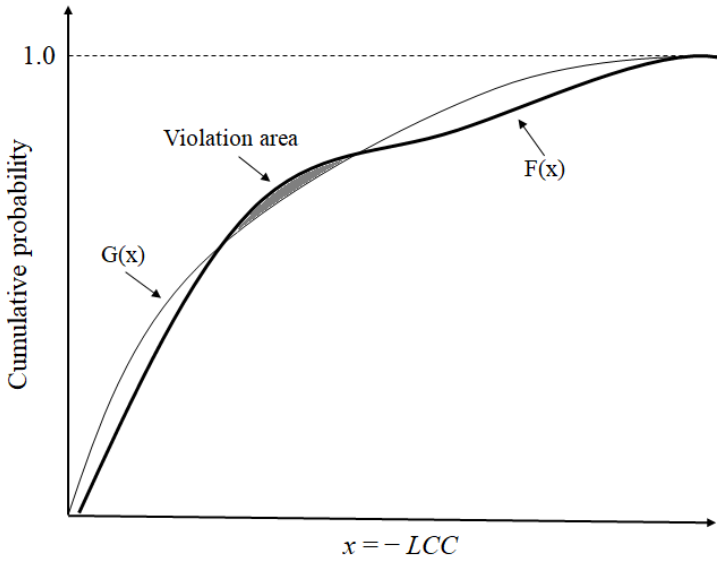

Figure 7.3. Graphical illustration of AFSD.

7.3.4 Descriptive decision models

While UT as a normative decision model prescribes the rational decisions, the descriptive decision models in behaviour economics attempt to predict the actual behaviour of decision-makers under bounded rationality that the maximum expected utility rule is often violated. The rank-dependent utility theory (RDUT) (Quiggin 1982) and cumulative prospect theory (CPT) (Tversky & Kahneman 1992) are two well-known descriptive models. These descriptive decision models in behaviour economics can be used to predict individual's preferences, for example, homeowners' choices and willingness in adopting mitigation measures for their houses.

The RDUT distinguishes from UT by replacing the objective probabilities (p_i) in Eq. (7.8) with subjectively evaluated probabilities to account for some psychological and cognitive aspects in decisional behaviour. Suppose x is a random variable of the consequence containing n outcomes $x_1, x_2, \ldots, x_n$ with a non-descending order (i.e. $x_1 \leq x_2 \leq \ldots \leq x_n$), and x_i is with a probability of p_i, the rank-dependent expected utility (RDEU) of x is given by

$$\mathrm{RDEU}(x) = \sum_{i=1}^{n} \pi_i u(x_i) \tag{7.10}$$

where π_i is the decision weights with $\pi_i = w(\sum_{k=i}^{n} p_i) - w(\sum_{k=i+1}^{n} p_i)$ for $i \leq n-1$ and $\pi_n = w(p_n)$. Note that the decision weights sum to one, i.e. $\sum_{i=1}^{n} \pi_i = 1$. The probability weighting function w is a strictly increasing function from 0 to 1 with $w(0) = 0$ and $w(1) = 1$ to model the subjective evaluation of probabilities, for example, people may overestimate the probability of extreme events. A probability weighting function given by Tversky & Kahneman (1992) is adopted in this study, which is

$$w(p) = p^{\varphi} / [p^{\varphi} + (1-p)^{\varphi}]^{1/\varphi} \tag{7.11}$$

Figure 7.4 shows the shape of this probability weighting function when $\varphi < 1.0$, $\varphi = 1.0$ and $\varphi > 1.0$. An inverse S-shape of $w(p)$ when $\varphi < 1.0$ overweights low-probability events and underweights high-probability events which reflects risk aversion in the context of civil engineering decision-making associated with extreme events. The opposite is represented by an S-shape of $w(p)$ when $\varphi > 1.0$. An inverse-S shape of $w(p)$ is typically adopted based on empirical evidence in gambling and financial activities (e.g. Tversky & Kahneman 1992; Abdellaoui 2000). However, the actual shape of $w(p)$ may vary in a different decision context. The RDUT coincides with UT if $w(p) = p$ (i.e. $\varphi = 1.0$). In RDUT, the risk attitudes

are encoded in both the utility function and the probability weighting function to better describe the decisional behaviours in real life. Other forms of probability weighting function may also be used (e.g. Prelec 1998).

The CPT is a modified version of the prospective theory (PT) by Kahneman & Tversky (1979). In addition to subjective probability weighting, CPT has more descriptive power for the decisional behaviour than RDUT by further incorporating more psychological and cognitive principles from PT. The value function (analogous to utility function) in CPT frames the outcomes as gains and losses relative to a reference point that captures several observed phenomena in decision-making (e.g. framing effects, loss aversion, diminishing sensitivity, etc.). The value function and the corresponding probability weighting function in CPT are thus defined separately for gains and losses. See details in Tversky & Kahneman (1992). As the life-cycle cost is typically treated as losses in civil engineering decision-making, the CPT with one-sided value functions is mathematically equivalent to the RDUT.

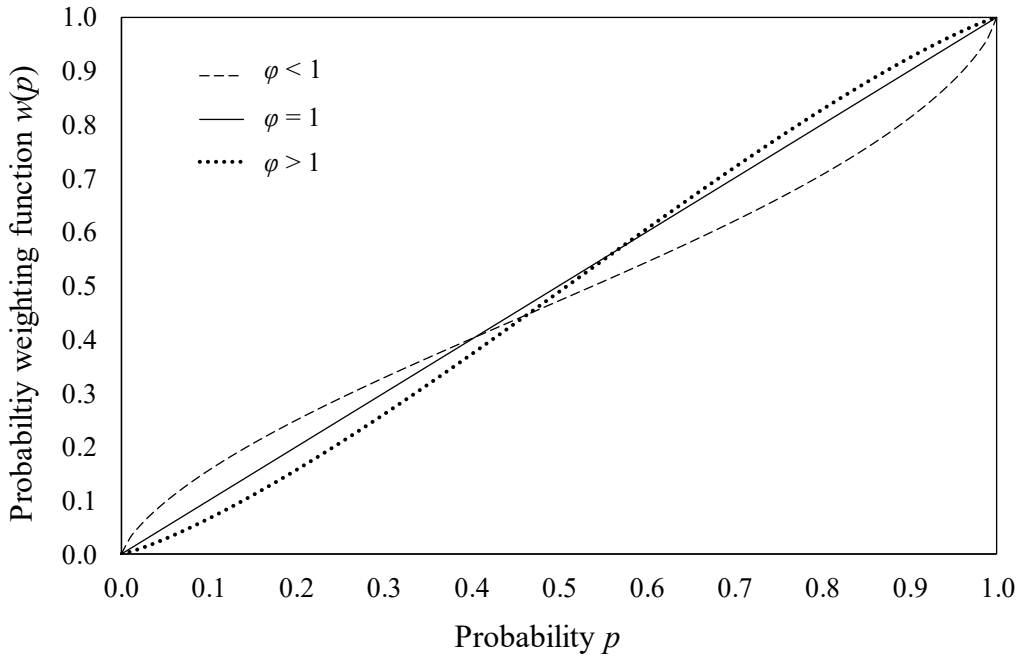

Figure 7.4. Probability weighting function $w(p)$.

7.4 Wind Mitigation Decisions without Insurance

The mitigation measures proposed in chapter 6 and 'business as usual (BAU)' are considered as decision alternatives in this section, summarized as

(1) No mitigation (BAU).

(2) Strengthening the roof by upgrading cladding fasteners and batten thickness (RF).

(3) Installing shutters to protect windows (WS).

(4) Increasing window resistance by improving window ratings (WR).

(5) Using water-resistant material for building interior to reduce rainwater damage (IW).

7.4.1 Life-cycle cost analysis

The life-cycle costs without considering insurance, *LCC*, for a building service life of 50 years from 2020 to 2070 associated with the five decision alternatives are calculated according to Eq. (7.1) and a discount rate of $r = 4\%$. The annual damage cost (i.e. the annual loss) in Eq. (7.2) is evaluated based on the PRA using MCS as described in Chapter 5 with the consideration of construction defects. Figure 7.5 shows the expected life-cycle costs corresponding to the five decision alternatives for Brisbane and Melbourne houses with different design wind classifications, and the cumulative probability functions (CDF) of the life-cycle cost are shown in Fig. 7.6. As shown in Fig. 7.5, the rank of the decision alternatives dictated by the MELC criteria is equivalent to that given by the cost-benefit analysis based on mean NPV as described in Chapter 6. A decision alternative with the lower expected life-cycle cost is more preferred. Figure 7.6 implies the tail behaviour of the life-cycle cost distribution, which indicates that the MELC may not well capture extremely high consequences that are of concern for risk-averse decision-makers. Figure 7.6 also indicates that Brisbane houses are likely to suffer more severe consequences than Melbourne houses.

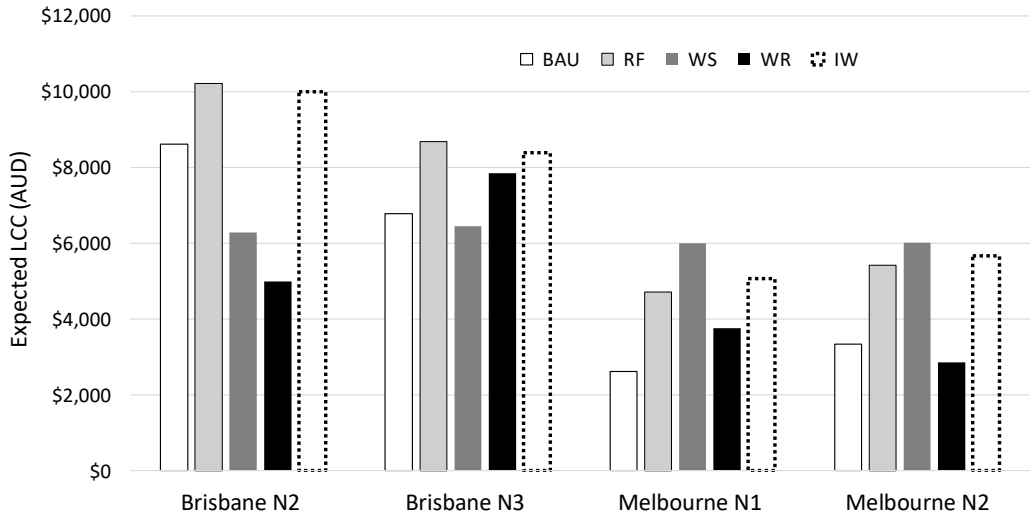

Figure 7.5. Expected life-cycle cost.

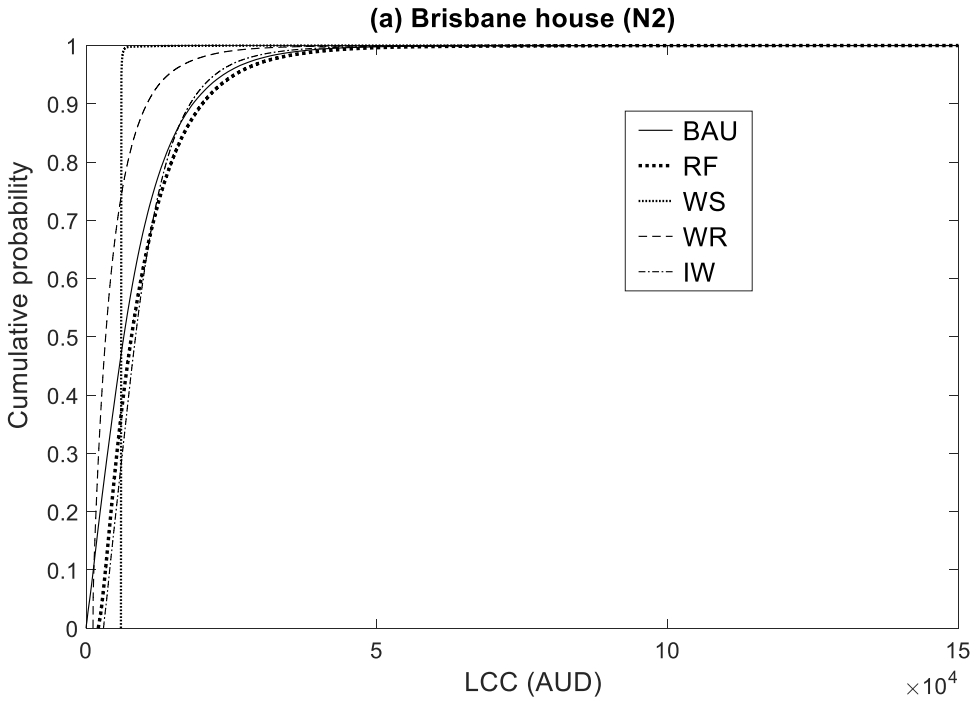
(a) Brisbane house (N2)
Cumulative probability
LCC (AUD)
×10^4
BAU
RF
WS
WR
IW

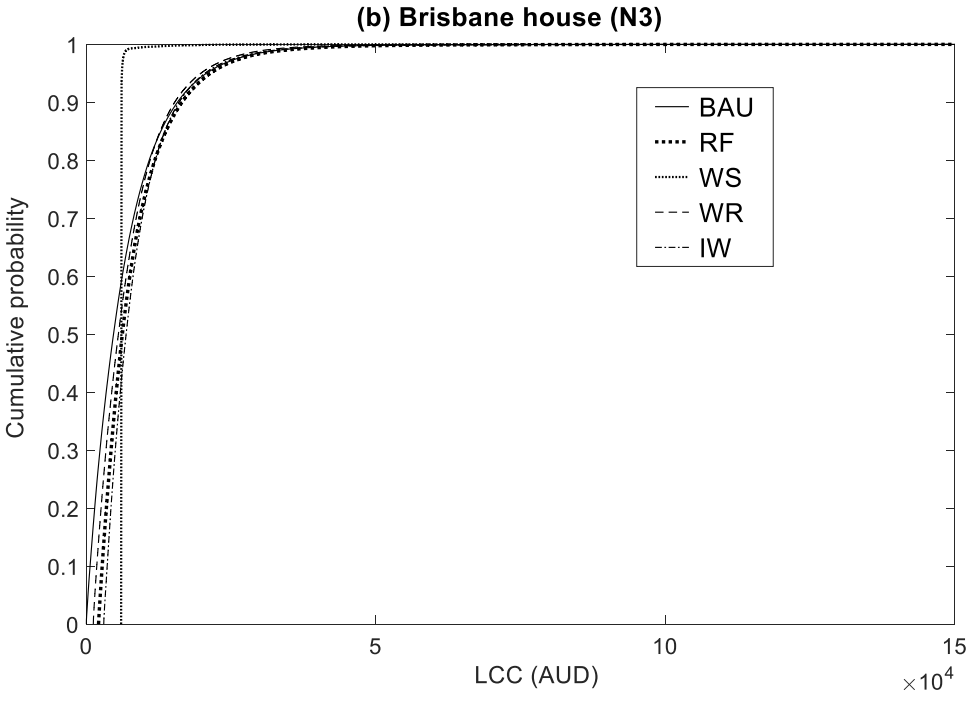
(b) Brisbane house (N3)
Cumulative probability
LCC (AUD)
×10^4
BAU
RF
WS
WR
IW

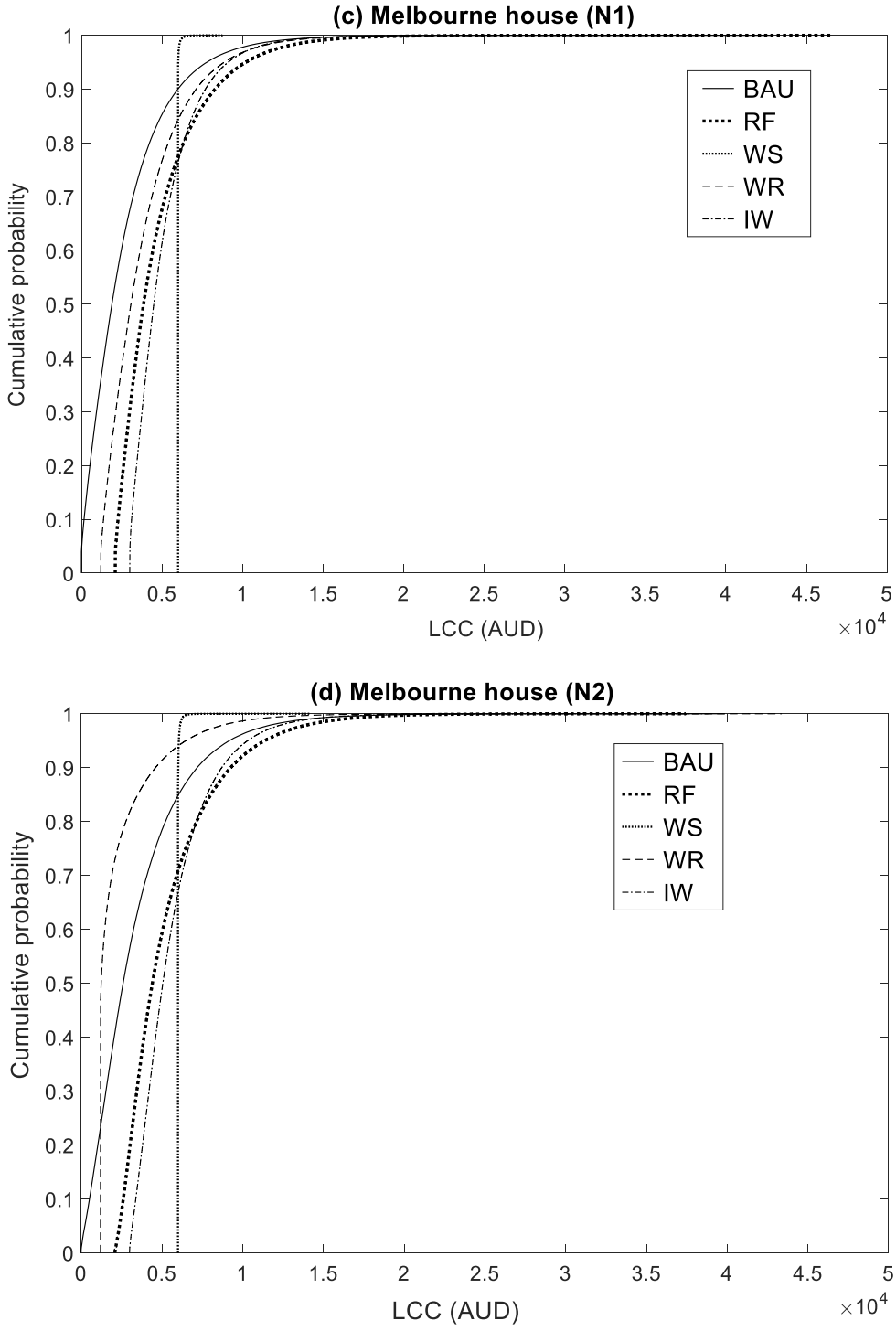

Figure 7.6. Cumulative probability of life-cycle cost.

7.4.2 Risk attitudes and decision-making under uncertainty

This section describes the application of superquantile, utility theory and almost stochastic dominance in decision-making for housing mitigation. Such decision-making is based the random variable *LCC* without insurance purchasing, and considers different risk attitudes.

7.4.2.1 Decisions based on superquantile

The superquantile of the life-cycle cost offers a risk index giving more weight to high consequences, which can be adopted by risk-averse decision-makers to rank decision alternatives. Figure 7.7 shows the α-superquantile values (α = 0.05, 0.25, 0.50, 0.75 and 0.95) of the life-cycle cost (*LCC*) corresponding to the five decision alternatives for Brisbane and Melbourne houses with different design wind classifications. As shown in Fig. 7.7, the superquantile values of life-cycle cost increase with the α value. An alternative with the lower α-superquantile value is preferred by a risk-averse decision-maker. The larger the considered α value, the higher the degree of risk aversion involved. The rank of alternatives when α = 0.05 is same as that based on the expected life-cycle cost as shown in Fig. 7.5. However, the rank of the five decision alternatives can vary with other α values considered. For example, increasing window ratings (WR) is preferred to installing window shutters (WS) for Brisbane houses with a design wind classification of N2 when α = 0.05, whereas a lower superquantile value of the life-cycle cost is associated with WS than WR for other α values (i.e. WS is preferred to WR). No mitigation measure is preferred to business as usual for Melbourne houses with a design wind classification of N1 when α = 0.05, 0.25 and 0.50, however, for α = 0.75 and 0.95, WS would be chosen. The superquantile values of the life-cycle cost associated with WS only slightly increase with the α value, which implies that installing shutters significantly reduces both the magnitude and likelihood of severe consequences. This is also indicated by the CDFs as shown in Fig. 7.6. In general, the selection of a higher α value in decision-making implies the decision-maker is more risk-averse and willing to choose mitigation measures that can provide more risk reduction, even at a high mitigation cost (e.g. installing window shutters).

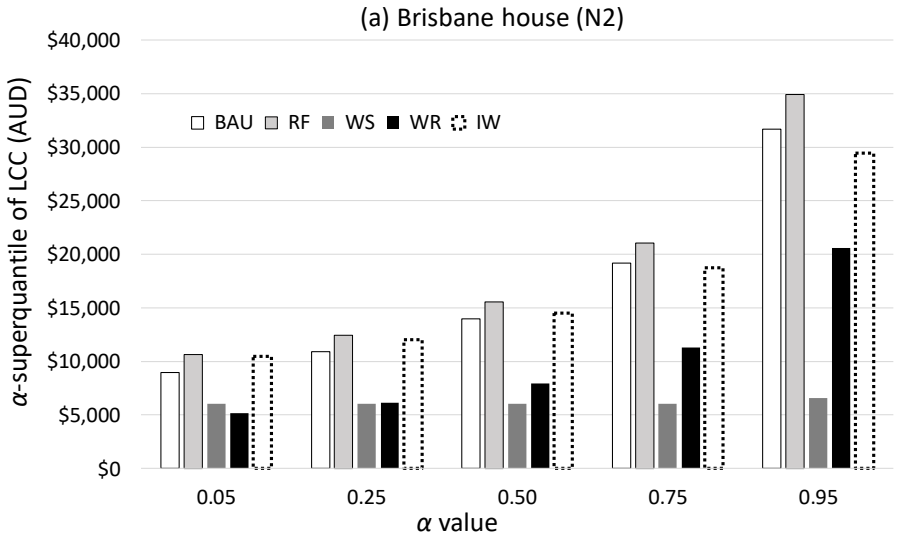

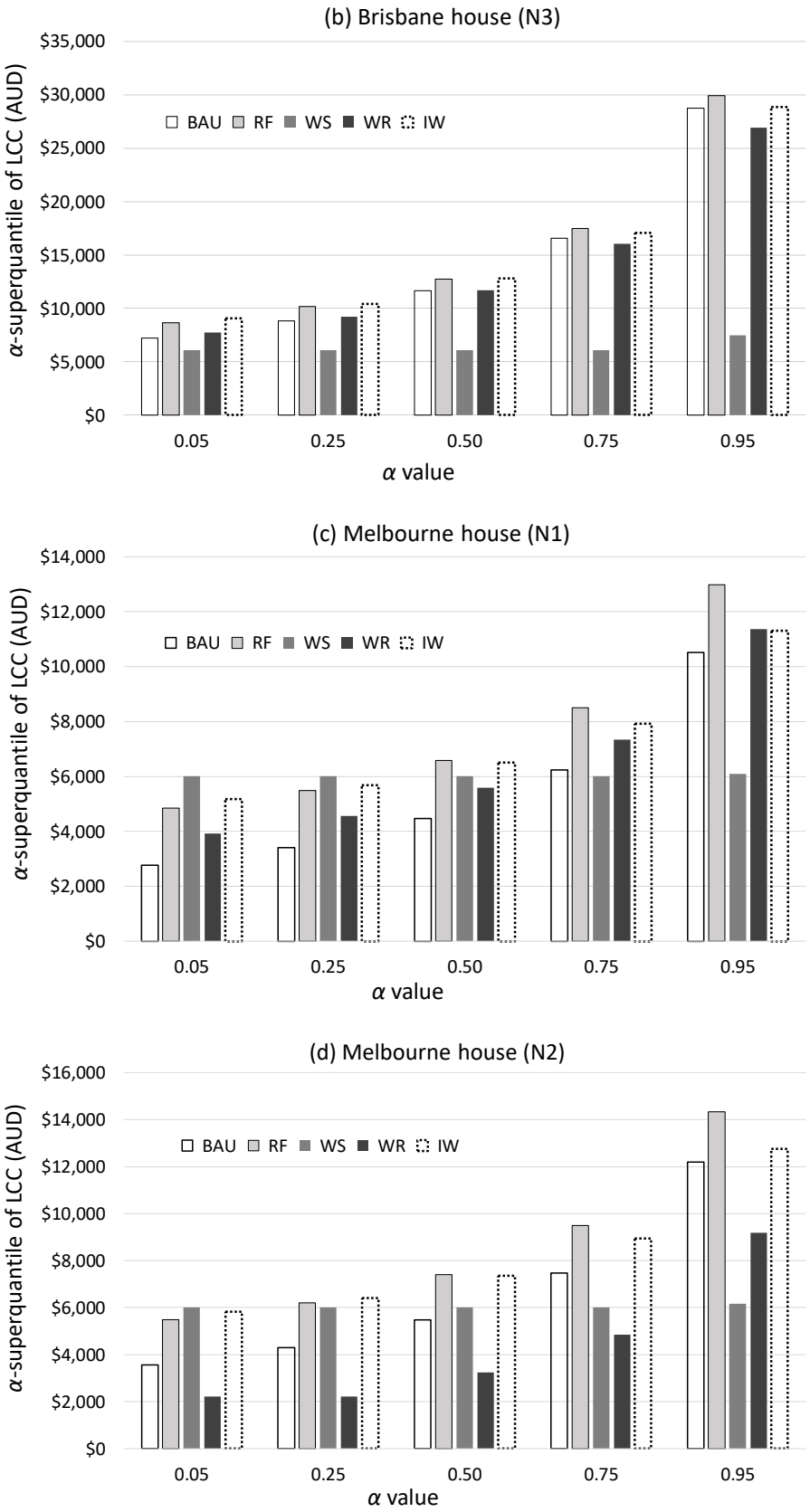

Figure 7.7. Superquantile values of the life-cycle cost.

7.4.2.2 Decisions based on expected utility

To consider a wider variety of risk attitudes, the decision analysis is further conducted by comparing the expected utility associated with the five decision alternatives. The power utility function described in Section 7.3.2 is used, i.e. $u(x) = -(-x)^l$, where $x = -LCC$ to ensure $u(x)$ is a monotonic and increasing function. The expected utilities are then evaluated for the l value ranging from 0.1 to 4.0 with an increment of 0.1 to represent a variety of risk attitudes. For the risk-neural attitude, the rank of decision alternatives based on expected utility is equivalent to those based on the expected life-cycle cost (i.e. an alternative with a higher expected utility or lower life-cycle cost is preferred). The general findings from the expected utility analysis are (i) the higher the degree of risk aversion (i.e. the larger l value with $l > 1.0$), the more willingness of decision-makers to adopt mitigation measures; (ii) the higher the degree of risk proneness (i.e. the smaller l value with $l < 1.0$), the more likely decision-makers would keep business as usual; (iii) some mitigation measures are not preferred even for decision-makers with extremely risk-averse attitudes (e.g. $l = 4.0$); (iv) some mitigation measures are still preferred even for an extremely risk-seeking attitude (e.g. $l = 0.1$).

Specifically, for Brisbane house with a design wind classification of N2, installing window shutters (WS) is preferred to business as usual (BAU) for most decision-makers except those with an extremely risk-seeking attitude (i.e. $l = 0.1$). Improving window ratings (WR) is always preferred to BAU for all the risk attitudes considered (i.e. $0.1 \leq l \leq 4.0$), whereas strengthening roof (RF) is always not preferred to BAU. Using water-resistant internal linings (IW) is only preferred to BAU for decision-makers with a relatively high degree of risk-averse attitude (i.e. $l \geq 2.8$). WR is preferred to WS for all considered risk-seeking, risk-neutral and a portion of risk-averse decision-makers (i.e. $1.0 < l \leq 1.5$), whereas WS is preferred to WR for a considerable portion of risk-averse decision-makers (i.e. $l \geq 1.6$). This is consistent with the decisions based on superquantile values that WS is preferred to WR for certain degrees of risk aversion when $\alpha \geq 0.25$ as described in Section 7.4.2.1. The rank of the five decision alternatives with l = 0.1, 1.0, 1.6, 2.8 and 4.0 for Brisbane houses with a design wind classification of N2 is summarized in Table 7.1(a) to show the above findings.

For Brisbane house with a design wind classification of N3, RF and IW are always not preferred to BAU for all considered risk attitudes (i.e. $0.1 \leq l \leq 4.0$). WS is preferred to BAU

for all risk-neutral, risk-averse and a small portion of risk-seeking decision-makers (i.e. $0.8 \leq l < 1.0$), whereas BAU is preferred to WS for most risk-seeking decision-makers (i.e. $0.1 \leq l \leq 0.7$). WR is only preferred to BAU for some risk-averse decision-makers (i.e. $l \geq 1.9$), and preferred to WS for only a small portion of decision-makers who are highly risk-seeking (i.e. $0.1 \leq l \leq 0.3$). Table 7.1(b) summarizes the rank of the five decision alternatives with l = 0.1, 0.3, 0.7, 1.0, 1.9 and 4.0 for Brisbane houses with a design wind classification of N3.

For Melbourne house with a design wind classification of N1, BAU is preferred to all mitigation measures for all considered risk attitudes (i.e. $0.1 \leq l \leq 4.0$). Table 7.1(c) shows the rank of the five decision alternatives with l = 0.1, 1.0 and 4.0 for Melbourne houses with a design wind classification of N1. For Melbourne house with a design wind classification of N2, BAU is always preferred to RF and IW for all considered risk attitudes (i.e. $0.1 \leq l \leq 4.0$). WR is preferred to BAU and WS for all considered risk attitudes (i.e. $0.1 \leq l \leq 4.0$). WS is preferred to BAU only for a small portion of decision-makers who are highly risk-averse (i.e. $l \geq 3.4$). Table 7.1 (d) shows the rank of the five decision alternatives with l = 0.1, 1.0, 3.4 and 4.0 for Melbourne houses with a design wind classification of N2.

Table 7.1. Rank of decision alternatives based on expected utility.

(a) Brisbane house (N2)

l value	Rank based on expected utility				
	No.1	No.2	No.3	No.4	No.5
l = 0.1	WR	BAU	WS	RF	IW
l = 1.0	WR	WS	BAU	IW	RF
l = 1.6	WS	WR	BAU	IW	RF
l = 2.8	WS	WR	IW	BAU	RF
l = 4.0	WS	WR	IW	BAU	RF

(b) Brisbane house (N3)

l value	Rank based on expected utility				
	No.1	No.2	No.3	No.4	No.5
l = 0.1	BAU	WR	WS	RF	IW
l = 0.3	BAU	WR	WS	RF	IW
l = 0.7	BAU	WS	WR	RF	IW
l = 1.0	WS	BAU	WR	RF	IW
l = 1.9	WS	WR	BAU	RF	IW
l = 4.0	WS	WR	BAU	RF	IW

(c) Melbourne house (N1)

l value	Rank based on expected utility				
	No.1	No.2	No.3	No.4	No.5
l = 0.1	BAU	WR	RF	IW	WS
l = 1.0	BAU	WR	RF	IW	WS
l = 4.0	BAU	WS	WR	IW	RF

(d) Melbourne house (N2)

l value	Rank based on expected utility				
	No.1	No.2	No.3	No.4	No.5
l = 0.1	WR	BAU	RF	IW	WS
l = 1.0	WR	BAU	RF	IW	WS
l = 3.4	WR	WS	BAU	IW	RF
l = 4.0	WR	WS	BAU	IW	RF

7.4.2.3 Decisions based on almost stochastic dominance

The almost first-degree stochastic dominance (AFSD) is used in this study to identify mitigation measures that would be preferred by most decision-makers who are expected utility maximizers without explicitly specifying any utility functions. Given the random samples of x ($x = -LCC$) associated with two alternatives produced by the PRA using MCS, the ε value for one dominating the other by AFSD can be calculated according to Eq. (7.9). The approach given by Levy (2012) is employed to solve Eq. (7.9) when x is a discrete random variable. The AFSD relationships of the five decision alternatives for Brisbane and Melbourne houses with different design classifications are summarized in Table 7.2.

For Brisbane houses with a design wind classification of N2, WR and WS dominates BAU by AFSD with ε = 0.02 and 0.21, respectively. These ε values are deemed to be small enough for most decision-makers with non-decreasing utility functions to choose mitigation measures of WR and WS over BAU. This is consistent with the decision analysis based on expected utility as described in Section 7.4.2.2 that WR is preferred to BAU for a wide range of risk attitudes, and WS is preferred to BAU by most decision-makers except for those are extremely risk-seeking. Among these two preferred mitigation measures, WR dominates WS by AFSD with ε = 0.36. This ε value may not be small enough to choose WR over WS

for most decision-makers, which is consistent with the expected utility analysis described in Section 7.4.2.2 that WS would be preferred to WR by a considerable portion of risk-averse decision-makers. RF and IW would not be selected because BAU dominants RF and IW by FSD (i.e. BAU is always preferred to RF by decision-makers with any non-decreasing utility functions) and AFSD ($\varepsilon = 0.09$ is sufficiently small in the current decision context), respectively. For Brisbane houses with a design wind classification of N3, WS is the only alternative that dominates BAU by AFSD with $\varepsilon = 0.35$, however, this ε value may not be sufficiently small to choose WS over BAU as shown in the expected utility analysis described in Section 7.4.2.2 that BAU would be preferred to WS for a considerable portion of convex utility functions (i.e. risk-seeking attitudes). For Melbourne houses with a design wind classification of N1, no mitigation measures would be selected over BAU because BAU dominants the other alternatives either by FSD or AFSD with a small ε value. For Melbourne houses with a design wind classification of N2, WR dominates BAU by AFSD with $\varepsilon = 0.10$ and thus WR would be preferred to BAU by most decision-makers which is shown in the expected utility analysis described in Section 7.4.2.2 that WR is preferred to BAU for a wide range of risk attitudes.

Table 7.2. AFSD relationships of the decision alternatives.

Brisbane house (N2)	Brisbane house (N3)	Melbourne house (N1)	Melbourne house (N2)
WR AFSD BAU ($\varepsilon = 0.02$)	WS AFSD BAU ($\varepsilon = 0.35$)	BAU AFSD WR ($\varepsilon = 0.02$)	WR AFSD BAU ($\varepsilon = 0.10$)
WS AFSD BAU ($\varepsilon = 0.22$)	BAU AFSD WR ($\varepsilon = 0.17$)	BAU AFSD WS ($\varepsilon = 0.06$)	BAU AFSD WS ($\varepsilon = 0.12$)
BAU FSD RF	BAU FSD RF	BAU FSD RF	BAU FSD RF
BAU AFSD IW ($\varepsilon = 0.09$)	BAU AFSD IW ($\varepsilon = 0.01$)	BAU AFSD IW ($\varepsilon = 0.01$)	BAU AFSD IW ($\varepsilon = 0.01$)
WR AFSD WS ($\varepsilon = 0.36$)			

By specifying a threshold for ε value (i.e. the maximum ε value), the AFSD can be used to identify mitigation measures that would be preferred to BAU or to screen out mitigation measures that would not be selected over BAU for most decision-makers if the corresponding ε value does not exceed the threshold. This threshold value is determined by subjective judgement and can vary depending on the decision problem of interest. In the

current decision context, a threshold value around 0.25 might be appropriate according to the discussions in this section.

7.5 Incentive for Homeowners with Insurance

The decision analysis results in this chapter and Chapter 6 suggest that installing window shutters (WS) is the most effective mitigation measure that provides the highest risk reduction, and significantly decreases both the magnitude and likelihood of severe consequences. The homeowner can install window shutters to retrofit an as-built house at any time. Installing window shutters is therefore ideal for homeowners to protect their homes against wind hazard, despite its cost is the highest among the four mitigation measures proposed in this study. In light of this, the use of economic incentives is helpful to motivate homeowners to install window shutters. The incentives considered in this study are (i) a discount in insurance premium, and (ii) a government rebate to reduce cost for shutter installation.

7.5.1 Devise of incentive based on MELC

The life-cycle cost for a homeowner who purchases insurance, LCC_{HO}, is calculated using Eq. (7.3). In Eq. (7.3), the mitigation cost C_M for installing window shutters is treated as deterministic and a one-off expense in 2020 (i.e. shutters are installed in 2020). The annual insurance premium *INP* for windstorms is loosely assumed to be deterministic and time-invariant as the prediction of premium in the future is unlikely due to many unknown factors involved as described in Section 7.2. The premium in a future year is converted to the present value in 2020 dollars by a discount rate of 4%. The average annual premium for home and contents insurance considering all perils is estimated to be $1,300 and $800 for homeowners in Brisbane and Melbourne, respectively (Canstar 2016). This estimation is consistent with the data in AGA (2014) that the premium rate (i.e. premium charged per $1,000 sum insured value) in Melbourne is about 60% of that in Brisbane. As inferred from AGA (2014), non-cyclonic windstorms accounts for approximately 32% and 27% of the total annual insurance loss in Brisbane and Melbourne, respectively. Then the annual insurance premium for windstorms is estimated to be *INP* = $416 and $216 for homeowners in Brisbane and Melbourne, respectively. Note that such estimation doesn't account for other factors such as business goals and market competition that can vary greatly among different insurers.

The random samples of the annual loss due to non-cyclonic windstorm in year t, $C_A(t)$, can be evaluated from the PRA using MCS as described in Chapter 5, and the annual insurance loss in year t, $I[C_A(t)]$, is calculated using Eq. (7.4) by assuming homeowners are fully insured. The total insurance losses, L_{INS}, during the 50-year building service life are calculated by Eq. (7.5). Assuming the excess fee is \$600, the expected values of LCC_{HO} and L_{INS} associated with WS and BAU for Brisbane and Melbourne houses with different design wind classifications are given in Table 7.3. For homeowners who keep business as usual (BAU), LCC_{HO} includes the insurance premium paid to the insurer, small losses less than the excess fee, and excess fee paid for any claims. For homeowners who install window shutters (WS), LCC_{HO} also includes the mitigation cost. Note that the co-benefits associated with window shutters (e.g. noise reduction, home security, light control, etc.) are not included in the quantification.

Table 7.3 suggests that the expected LCC_{HO} is larger than the expected LCC for homeowners without purchasing insurance as shown in Fig. 7.5. This is anticipated as the premium paid by homeowners not only transfers most financial risks to the insurer, but also covers insurer's business cost and profit. As shown in Table 7.3, installing window shutters significantly reduce the expected insurance losses for the insurer. However, the expected LCC_{HO} for homeowners who install shutters will increase if no incentives are offered. Note that there might be other insurance losses associated with windstorms, for example, windborne debris, hail and fallen tree damage, which are not taken into account in this study. Based on the MELC criteria, Table 7.4 shows the minimum discount in annual insurance premium (INP) and the minimum rebate for shutter installation that ensure the expected LCC_{HO} associated with WS is no greater than that of BAU. Table 7.4 implies that it is worth for the insurer to offer a 30-40% or other reasonably higher discounts (e.g. 50%) in the annual premium to encourage homeowners in Brisbane to install window shutters, which can significantly reduce insurance losses for the insurer. The discounts in Table 7.4 may be too high for the insurer to offer to homeowners in Melbourne because the other losses associated with windstorms (e.g. windborne debris, hail and fallen tree damage) are not quantified in this study and it is necessary to make sure the premium charged for windstorm accounts for all storm-related losses as well as insurer's costs and profits. Government may also offer rebates for shutter installation. Table 7.4 suggest that, for homeowners in Brisbane and Melbourne, government may respectively offer a more than 47% and 68% rebate for the shutter cost as an incentive.

Table 7.3. Expected value of life-cycle cost for fully insured homeowners and insurance losses.

Design wind classification	LCC_{HO}		L_{INS}	
	BAU	WS	BAU	WS
Brisbane N2	\$12,556	\$15,371	\$5,335	\$89
Brisbane N3	\$11,586	\$15,362	\$4,338	\$68
Melbourne N1	\$6,428	\$10,860	\$1,698	\$2
Melbourne N2	\$6,783	\$10,864	\$2,256	\$5

Table 7.4. The minimum discount in annual insurance premium and rebate for shutter installation based on MELC.

Design wind classification	Discount (%) in annual insurance premium	Rebate (%) for shutter installation
Brisbane N2	30%	47%
Brisbane N3	40%	63%
Melbourne N1	93%	74%
Melbourne N2	81%	68%

7.5.2 Devise of incentive based on descriptive decision models

Homeowners generally dislike severe damage occurring to their home and contents due to psychological and emotional factors as well as disruptions and inconvenience incurred by the damage. In addition, homeowners still need to pay the excess fee if they make claims, which increases the life-cycle cost LCC_{HO} for homeowners. Moreover, an adverse claim history may increase the premium or cause the cancellation and refusal of policy, which is not explicitly quantified in this study. Installing window shutters can reduce the likelihood of severe storm-rated losses and the number of claims for homeowners during the 50-year building service life. In real life, many homeowners have misperceptions about the likelihood of home and contents damage caused by windstorms due to, for example, previous unpleasant experience with severe storm damage, overly exposed to media coverage of wind hazard and unawareness of risks from windstorm. It is more likely for homeowners who overestimate the occurrence rate of severe storm damage and the likelihood of making claims to install shutters, whereas those insensitive or unaware of storm risks may need more incentives for them to install shutters.

The minimum discount and rebate based on MELC in Table 7.4 are for homeowners who are risk-neutral, and behave rationally to achieve economic efficiency. The descriptive

models given in Section 7.3.4 are further employed to model the decisional behaviour of homeowners under bounded rationality, and the minimum discount in premium and rebate for shutter installation are then re-estimated based on the predicted preferences of homeowners. In particular, the rank-dependent utility theory (RDUT) is adopted in this section, which is a special case of the cumulative prospect theory (CPT) given one-sided utility/value functions (i.e. the life-cycle cost for homeowners with insurance is framed as a loss, $x = -LCC_{HO}$). A linear utility function, i.e. $u(x) = x$, is considered in Eq. (7.10) for homeowners because severe losses would be mostly covered by the insurer. The probability weighting function $w(p)$ given by Eq. (7.11) is used to model homeowners' misperceptions about the likelihood of severe damage by windstorms. The selected φ values in Eq. (7.11) are 0.6 for homeowners who overestimate the occurrence rate of severe damage and claims, and 1.4 for homeowners who underestimate such likelihood. A $w(p)$ with $\varphi < 1.0$ as shown in Fig. 7.4 implies that the high LCC_{HO} with small probability would be overweighed in the assessment of rank-dependent expected utility (RDEU) as described in Section 7.3.4. A high LCC_{HO} with small probability is very likely associated with large storm damage and a high number of claims. This is illustrated in Fig. 7.8, which shows the histogram of LCC_{HO} associated with BAU and WS for Brisbane house (N3). As shown in Fig. 7.8(a), high LCC_{HO} has low frequency, whereas high frequency is associated with relatively small and moderate LCC_{HO} that are mostly comprised of some small losses and the insurance premium paid during the building service life. Installing window shutters significantly reduces the frequency of high LCC_{HO} implying the potential reduction of large storm damage and the number of claims, though the overall LCC_{HO} increases for homeowners due to the mitigation cost spent if no incentive is offered (see Fig. 7.8(b)). The moderate LCC_{HO} containing some small losses less than the excess fee can also be significantly reduced by installing shutters as shown in Fig. 7.8(b).

Given the random samples of $x = -LCC_{HO}$ in a non-descending order, the RDEU of x associated with BAU and WS are then calculated by Eq. (7.10), where the decision weights in Eq. (7.10) is evaluated using the cumulative probabilities of x and the probability weighting function as described in Section 7.3.4. Table 7.5 shows the calculated RDEU of x associated with BAU and WS for homeowners in Brisbane and Melbourne. If no incentive offered, WS would not be preferred by homeowners given a lower RDEU suggested by Table 7.5. Table 7.6 shows the minimum discount in annual insurance premium and the minimum rebate for shutter installation that ensure the RDEU associated with WS is no

smaller than that of BAU. It is suggested that offering discount in premium to homeowners in Melbourne is still not a viable option for the insurer. For homeowners in Brisbane who are considered as risk-averse (i.e. overestimate the likelihood of severe damage and making claims), less discount in annual insurance premium would be needed to motivate them to install window shutters as compared with those in Table 7.4. On the other hand, more discount in premium would be needed for homeowners in Brisbane who underestimate storm damage probability to install window shutters. Similar findings are also suggested by Table 7.6 for rebates to reduce cost of window shutters that less rebate would be needed for homeowners who overestimate the likelihood of severe storm damage and the number of claims. Note that this study uses φ = 0.6 and 1.4 just to illustrate the effect of different types of judgemental distortion or misperception on the devise of incentives for homeowners to implement mitigation measures. In real applications, quantitative surveys are needed to select appropriate probability weighting functions for different groups of homeowners. Proper risk communication is also needed to inform homeowners about the storm damage risks and the benefits of installing window shutters. This is left for future research. The adoption of economic incentives in practice is related to policy-making and involves multiple stakeholders, which is a complex issue and out of the scope of this study.

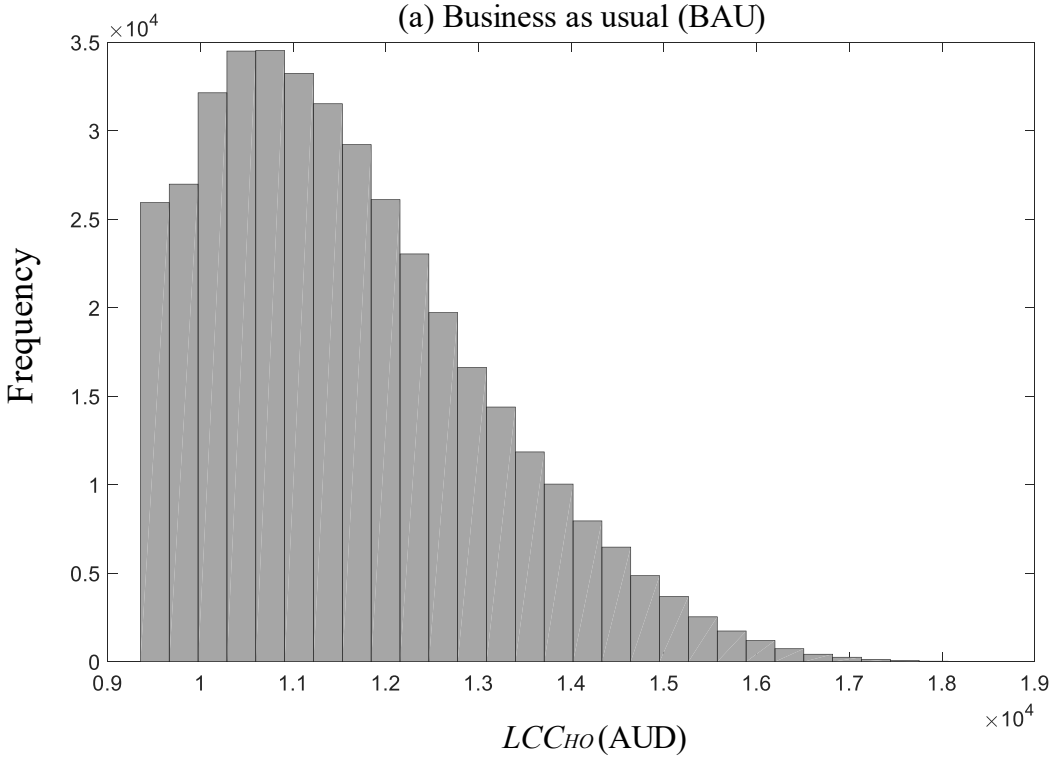

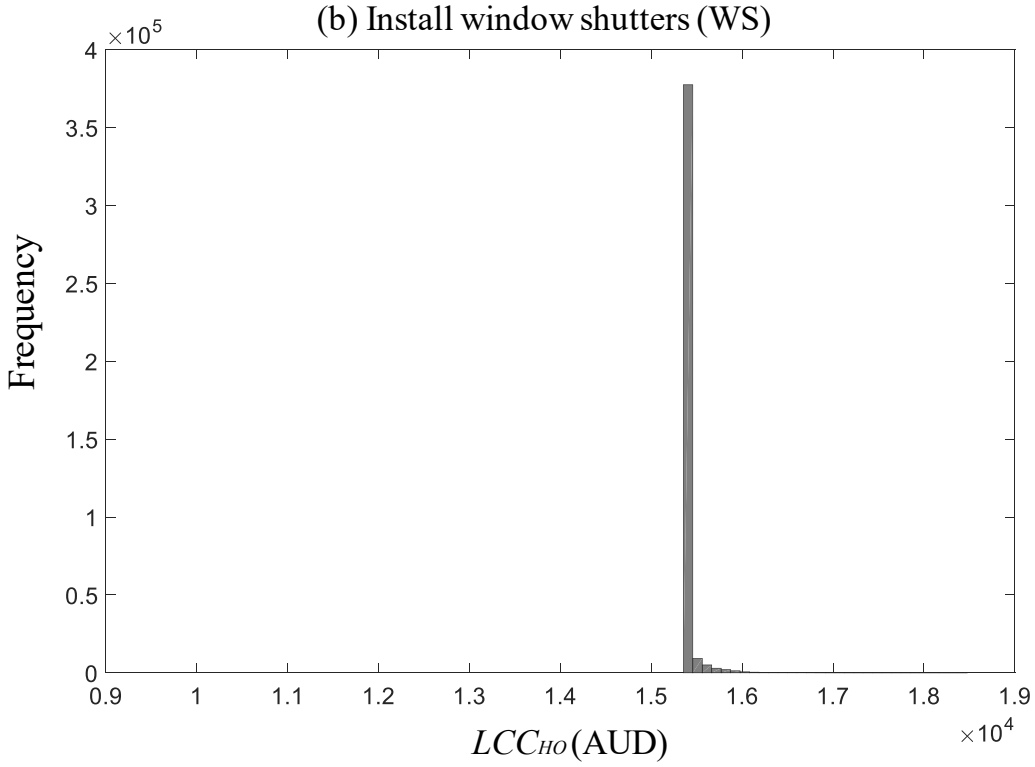

Figure 7.8. Histogram of LCC_{HO}.

Table 7.5. RDEU for homeowners with misperceptions about objective probabilities.

Design wind classification	Overestimate likelihood of severe damage (φ = 0.6)		Underestimate likelihood of severe damage (φ = 1.4)	
	BAU	WS	BAU	WS
Brisbane N2	−13,202	−15,449	−12,577	−15,364
Brisbane N3	−12,306	−15,481	−11,638	−15,365
Melbourne N1	−6,901	−10,900	−6,487	−10,859
Melbourne N2	−7,171	−10,906	−6,860	−10,861

Table 7.6. The minimum discount in annual insurance premium and rebate for shutter installation based on RDEU.

Design wind classification	Discount (%) in annual insurance premium		Rebate (%) to reduce shutter cost	
	φ = 0.6	φ = 1.4	φ = 0.6	φ = 1.4
Brisbane N2	24%	33%	41%	49%
Brisbane N3	34%	45%	53%	66%
Melbourne N1	81%	95%	67%	77%
Melbourne N2	77%	83%	62%	70%

7.5.3 Time horizon

The analyses in Section 7.5.1 and 7.5.2 are based on a time horizon of 50 years. In this section, time horizons of 10 and 30 years are further taken into account. As the time horizon becomes shorter, the risk reduction provided by window shutters decreases, which indicates higher incentives would be needed for homeowners to install shutters. This section considers that discount in annual insurance premium and rebate to reduce shutter cost are both offered to homeowners in Brisbane. Figure 7.9 shows several pairs of discount and rebate for 10- and 30-year time horizons which are minimal incentives that ensure WS and BAU would be equally preferred based on MELC and RDEU. Figure 7.9 suggests that higher incentives are needed to motivate homeowners in Brisbane to install window shutters if a shorter time horizon (i.e. 10 years) is considered. Lower incentives are needed for risk-averse homeowners who overestimate the likelihood of severe damage events (modelled by probability weighting function with φ = 0.6), whereas higher incentives are needed to motivate homeowners who are unaware or insensitive to storm damage risks to install window shutters (modelled by probability weighting function with φ = 1.4).

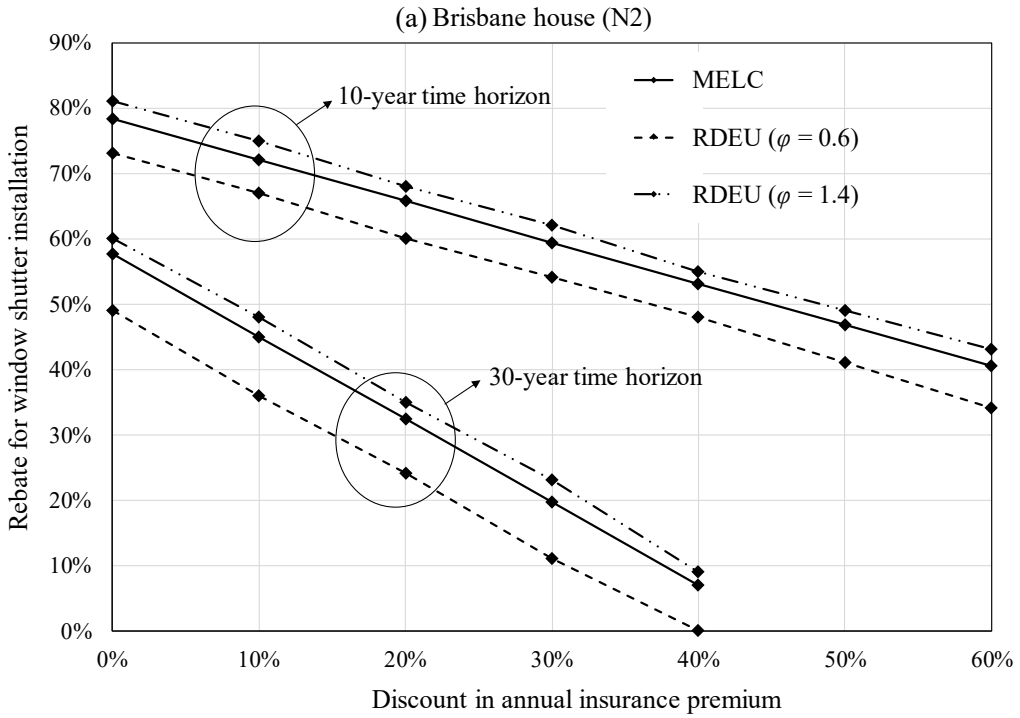

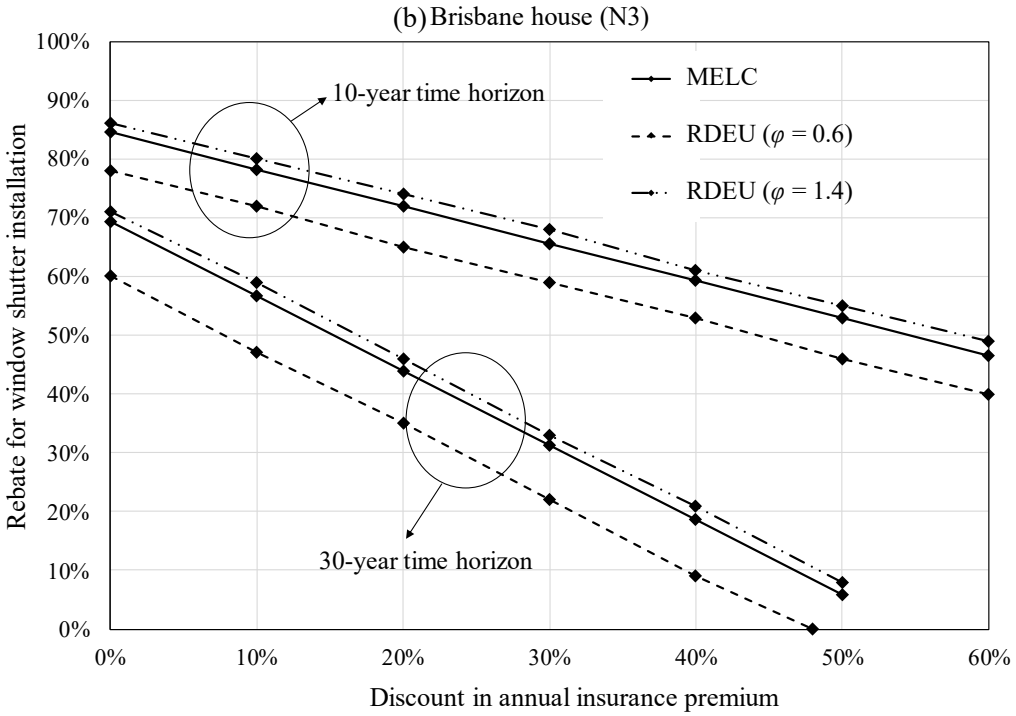

Figure 7.9. Minimal incentives for 10- and 30-year time horizon based on MELC and RDEU.

7.6 Conclusions

This chapter presents a variety of decision models to account for risk preferences in civil engineering decision-making under uncertainty. The superquantile, utility theory (UT) and almost stochastic dominance (ASD) were employed to provide decision support in selecting alternatives for housing mitigation under extreme winds. The superquantile offers an effective risk index for risk-averse decision-makers, which well captures the extreme tails of life-cycle cost distributions. The UT was applied to fully rank mitigation alternatives for decision-makers with different risk attitudes that are encoded in utility functions. The ASD does not require the explicit elicitation of utility functions, and therefore it can be used prior to a detailed expected utility analysis to identify preferred or screen out disliked mitigation measures for most decision-makers who are expected utility maximizers. The decision analysis using UT and ASD reveals that, in general, the higher the degree of risk aversion, the more willingness of decision-makers to implement mitigation measures. Strengthening roof cladding would always not be preferred even for extremely risk-averse decision-makers. Installing window shutters for Brisbane houses would be preferred by risk-neutral and risk-averse decision-makers as well as a considerable portion of risk-seeking decision-makers. The descriptive decision models aim to predict the decisional behaviour under

bounded rationality. This study proposes a potential application of descriptive decision models in devising incentives that can motivate homeowners to install window shutters for the protection of their home against storm damage. The storm-related losses can be significantly reduced if homeowners are encouraged to install window shutters. It was found that, lower discount in annual insurance premium and rebate for shutter installation would be needed to motivate risk-averse homeowners who overestimate the occurrence rate of severe storm damage and the likelihood of making claims.

CHAPTER 8. CONCLUSIONS AND FUTURE WORK

8.1 Summary and Conclusions

This thesis presents a probabilistic risk assessment (PRA) framework to evaluate economic losses for individual houses subjected to non-cyclonic windstorms. The PRA framework includes (i) a hazard model accounting for the simultaneous occurrence of extreme wind and associated rainfall, (ii) a reliability-based wind damage assessment for a roof system and windows, (iii) a semi-empirical model for rainwater intrusion, and (iv) a loss estimation model. The developed PRA framework was illustrated on representative metal-clad contemporary houses in Brisbane and Melbourne − capital cities of Queensland and Victoria within non-cyclonic regions of Australia. The economic risks are considered to result from (i) damage to metal roof cladding, timber roof trusses and windward windows by high wind pressure, (ii) damage to building interior and contents by rainwater entering from damaged roof and windows as well as gaps around undamaged windows, and (iii) loss of use and additional living costs. A probabilistic construction defect model for the roof was also developed, which can be readily integrated into the PRA framework to account for the reduced roof reliability and performance due to construction defects. The climate change impact on extreme wind speed and associated rainfall can also be accounted for by the PRA through a scenario-based approach.

Risk-based decision analyses were further conducted in this thesis to identify cost-effective measures for risk mitigation and climate adaptation. Based on the outputs of the PRA, i.e. economic risks, decision variables such as net present value (NPV) and life-cycle cost were calculated for different mitigation/adaptation alternatives. The cost-benefit analysis based on mean NPV was conducted to evaluate the cost-effectiveness of the mitigation/adaptation measures for risk-neutral decision-makers aiming to achieve economic efficiency. A sets of decision models were also employed to capture the magnitude of uncertainty and decision-makers' risk preferences (i.e. risk aversion, risk-neutrality and risk proneness) in decision-making. The implications for mitigation/adaptation decisions with the consideration of insurance and economic incentives were also discussed in this thesis.

The specific methods and models for the proposed PRA and decision support framework in this thesis are summarized in the following:

1) Probabilistic models for extreme wind speed and associated rainfall are described in Chapter 5. Statistical inferences for the model parameters were conducted using historical wind speed and rainfall records in Brisbane and Melbourne.
2) Wind damage/fragility assessment for metal roof cladding, timber roof trusses and windward windows for representative contemporary houses in Brisbane and Melbourne is described in Chapter 3. Overloading of roof connections was considered to cause roof cladding and truss failures. A Monte Carlo Simulation analysis in conjunction with a finite element method were developed to conduct the fragility assessment for roof cladding and trusses, which enables the probabilistic characterization of spatially variable wind loads, structural resistances, structural response, load redistribution and failure progression. Damage to windward windows by high wind pressure was also considered, and exceedance probabilities of ultimate strength and water penetration resistances of windows were calculated.
3) Probabilistic modelling for construction defects in roof connections is described in Chapter 4. A Bayesian approach integrating engineering judgement, human reliability analysis technique and limited defect data was developed to model the occurrence rate for five types of construction defects. The uplift capacities for defective roof connections were also probabilistically modelled based on engineering judgement and experimental data. The effect of construction defects on wind fragility for metal roof cladding and timber roof trusses was examined.
4) A semi-empirical rainwater intrusion model is described in Chapter 5 to estimate the amount of rainwater entering roof and window breaches as well as gaps around undamaged windows. The volumetric rate of rainwater intrusion was assessed based on wind speed, rainfall intensity, and the damage states of roof cladding and windows. The effect of construction defects in roof connections on rainwater intrusion was also examined in Chapter 5.
5) Assembly-based loss estimation is described in Chapter 5. Cost ratios of housing components/subassemblies were estimated according to Australian construction cost guides. Empirical loss functions are presented in Chapter 5 to calculate the loss given a specific damage state for each housing component.
6) A Monte Carlo simulation (MCS) approach was employed for the PRA that integrates the hazard analysis, wind damage analysis, rainwater intrusion evaluation and loss estimation. The output of the PRA is the random samples of annual economic loss

yielded by the MCS. The construction defect model can be readily incorporated in the simulation-based PRA framework. The annual economic loss in a future year can be evaluated by incorporating projected or hypothetical climate change scenarios for wind and rainfall.

7) Four risk mitigation and climate adaptation measures for the representative contemporary house were proposed in Chapter 6, including (i) strengthening connections for metal roof cladding, (ii) installing shutters for windows, (iii) improving window resistance, and (iv) using water-resistant materials for the building interior. These measures aim to reduce wind and rainfall losses by either reinforcing the building envelope or improving water resistance of building interior. The cumulative economic losses associated with 'business as usual' and different mitigation/adaptation measures were evaluated for a 50-year time horizon based on the annual losses obtained from the PRA. Decision variables such as NPV and life-cycle cost were then obtained for decision-making. A cost-benefit analysis based on mean NPV were conducted in Chapter 6 to assess the cost-effectiveness of the proposed mitigation/adaptation measures for risk-neutral decision-makers.
8) A set of decision models are described and employed in Chapter 7 to account for different risk preferences and the magnitude of uncertainty involved in the wind hazard mitigation decisions. These decision models have different features, and can address various issues in the current decision context (e.g. risk attitudes, extreme tail of life-cycle cost distribution, elicitation of utility functions, the role of behaviour economics and bounded rationality, etc) to better inform and support decision-making.
9) The descriptive decision models in behaviour economics were adopted in Chapter 7 to predict individual homeowners' preferred choices for window shutter installation. A potential application based on the predicted decisional behaviour was proposed in Chapter 7 to devise economic incentives to motivate homeowners to install window shutters.

The main conclusions and findings of this PhD study are summarized in the following:

1) The statistical analysis for extreme wind and associated rainfall suggests that Brisbane tends to have shorter windstorms with more intense rainfall (e.g. severe

thunderstorms), whereas windstorms in Melbourne are generally longer with lower average rainfall intensity.

2) Wind fragility of the roof system significantly increases given the presence of windward dominant openings (e.g. broken windows). Metal roof cladding is more susceptible to wind damage than roof trusses.
3) The probability of window breakage (i.e. exceedance of ultimate strength) is considerably lower than that of exceeding the water penetration resistance at a given wind speed.
4) Rainwater intrusion via window breaches or gaps around undamaged windows is higher than that through roof openings for relatively lower wind speeds. With an increasing wind speed, more roof openings tend to occur due to increasing metal roof sheeting loss, which results in more rainwater intrusion via roof openings.
5) Construction defects in roof connections considerably increase the wind fragility of metal roof cladding, whereas such effect on roof truss fragility is lower. When construction defects in roof connections are taken into account, there are more rainwater entering via roof breaches due to increased metal roof sheeting failures.
6) Annual economic losses for Australian contemporary houses are mainly attributed to rainwater damage to building interior and contents. Brisbane houses are generally subjected to higher losses than Melbourne houses. The annual expected losses for the representative contemporary house in Brisbane with construction defects are considerably higher than that without considering construction defects, whereas the effect of construction defects on the calculated expected losses is slight for the Melbourne house. Construction defects have a much higher influence on severe storm losses (i.e. damage events with low probability but high consequences).
7) The cost-benefit analysis based on mean NPV or expected life-cycle cost for risk-neutral decision-makers suggests that strengthening windows by increasing window ratings (e.g. N1 to N2, N2 to N3) is cost-effective for Brisbane houses and Melbourne houses. Installing window shutters significantly reduces economic risks incurred by wind and rainfall damage, and is cost-effective for houses in Brisbane. The adverse effects of construction defects can be largely counter-balanced by installing window shutters. Climate change impact on the cost-benefit analysis is marginal.

8) The decision analysis based on mean NPV or expected life-cycle cost fails to capture the magnitude of uncertainty and risk preferences involved in the wind mitigation decisions for housing. The superquantile, utility theory and almost stochastic dominance can serve as decision support tools to explicitly account for risk preferences in decision-making under uncertainty. The decision analysis using these decision models reveals that, in general, the higher the degree of risk aversion, the more willingness of decision-makers to implement mitigation measures. Strengthening roof cladding would always not be preferred even for extremely risk-averse decision-makers. Installing window shutters for Brisbane houses would be preferred by risk-neutral and risk-averse decision-makers as well as a considerable portion of risk-seeking decision-makers.
9) The incentives devised based on the predicted homeowners' preferences have the potential to motivate homeowners to install window shutters for the protection of their houses against storm damage. The storm-related losses can be significantly reduced if homeowners are encouraged to install window shutters. Lower discounts in annual insurance premiums and rebates for shutter installation would be needed to motivate risk-averse homeowners who overestimate the occurrence rate of severe storm damage and the likelihood of making claims.

8.2 Recommendations for Future Work

Many parameters in the probabilistic and statistical models developed in this study were estimated based on limited observed data and evidence that are available publicly. Subjective engineering judgement was inevitably used to give the best estimates of these parameters. Therefore, more numerical studies, experimental tests and field observations may be further introduced to improve the accuracy of the models and methods developed in this PhD study. The PRA and decision support framework developed in this PhD study are for individual houses. The major extension of this study is to further assess economic risks for multiple houses in a residential community.

Specific suggestions for the improvement and extension of this PhD study are given as follows:

1) Wind and rain data in Brisbane and Melbourne from more weather stations can be further incorporated in statistical analysis for the hazard models by accounting for spatial variations and patterns of rainfall across the entire urban areas.

2) Damage accumulation during a windstorm with varying wind directions or from multiple windstorms need to be further incorporated in the wind damage assessment. This may require event-based wind hazard modelling and detailed analyses for structural response such as fatigue and permanent deformation of structural components beyond the elastic stage.
3) Wind Damage/fragility assessment can be extended to account for other vulnerable housing components during windstorms (e.g. garage doors, gutters, flashings, etc). This requires more information regarding the spatially varying wind loading on these components and the corresponding structural resistances.
4) Although the effect of correlation between defects is practically examined in a sensitivity analysis in Chapter 4, further inclusion of the defect dependence in the theoretical model formulation is needed. This requires modified mathematical models and more statistical information about the correlations.
5) A challenging task is to collect more construction defect data and corresponding information regarding working contexts, which is essential for the improvement of the damage and risk assessment for housing. It is challenging due to many reasons such as restrictive access to construction sites, privacy issues (e.g. people do not like to disclose their mistakes and/or to be monitored while working), etc. It might be beneficial if authorized or permitted professional inspectors were introduced in some stages of the construction process to have detailed inspections on the construction quality and obtain the statistics for the occurrence rate of construction defects.
6) The parameters of the semi-empirical rainwater intrusion model need a revisit when more experimental evidence and computational fluid dynamics (CFD) studies are available. Full-scale and wind tunnel testing for rainwater intrusion may be conducted for buildings with generic geometries. Corresponding CFD models can be calibrated using the test data and then extended to a wider range of building geometries.
7) The threshold of water depth leading to a total loss of building interior and contents used in the empirical loss functions can be further modified when more field observations and insurance data are available.
8) Further validations of the wind damage and risk assessment results using post-damage observations and insurance data, if available, are needed.

9) The proposed application of descriptive decision models in devising incentives for homeowners to install window shutters is illustrated in Chapter 7 based on assumed risk perceptions of homeowners. Quantitative surveys are needed to identify different homeowners' attitudes and preferences as well as the associated influencing factors (e.g. socioeconomic status). Proper risk communication is also needed to inform different groups of homeowners about the storm damage risks and the benefits of installing window shutters.
10) The PRA and decision support framework can be extended to consider a residential community. Different types of houses in a community need to be further considered (e.g. houses with tile roof). Interactions and correlations between multiple houses need to be taken into account. This may require the explicit modelling of shielding effects and windborne debris.
11) There is a need to account for other perils associated with windstorms that may cause housing damage such as hail, windborne debris, flood and fallen tree damage.
12) The climate change projections for compound events (e.g. simultaneous occurrence of extreme wind and rainfall) in Australia are not available. Thus, the climate change impact on wind and rainfall losses needs a revisit when consistent and accurate projections become available for the change in extreme wind speed and associated rainfall, which requires further inputs from climate scientists.
13) The proposed risk assessment and mitigation framework can be extended to other metal-roofed buildings such as warehouses and residential buildings with multiple storeys. When applied to a different type of building, detailed wind loads, building geometries and structural resistances need to be adapted to the new application accordingly.
14) The proposed risk assessment and mitigation framework can also be extended to houses in cyclonic regions of Australia. The wind and rainfall modelling is subjected to change for cyclonic winds. The wind loads, structural design and resistances also need to change accordingly for houses under cyclonic winds. The cost-effectiveness of relevant mitigation measures to reduce damage risks from tropical cyclones also needs to be examined based on an engineering and reliability-based approach, which is currently absence in the literature for Australian housing subjected to cyclonic winds. Such future study may provide unique recommendations for mitigating

Australian houses in cyclonic regions compared with the recommendations made in this study for housing in non-cyclonic regions.

REFERENCES

Abdellaoui, M. (2000). Parameter-free elicitation of utility and probability weighting functions. *Management science*, 46(11), 1497-1512.

ABS (2011). *Australian Social Trends December 2011: Components of household wealth*. Australian Bureau of Statistics, Canberra, Australia.

Akyuz, E., & Celik, M. (2015). Application of CREAM human reliability model to cargo loading process of LPG tankers. *Journal of Loss Prevention in the Process Industries*, 34, 39-48.

Amini, M. O., & van de Lindt, J. W. (2013). Quantitative insight into rational tornado design wind speeds for residential wood-frame structures using fragility approach. *Journal of Structural Engineering*, 140(7), 04014033.

AGA (2014). *Report on Home and Contents Insurance Prices in North Queensland*. Australian Government Actuary, Canberra, Australia.

ANSYS Inc (2013). *ANSYS Mechanical APDL Introductory Tutorials*. Canonsburg, PA, USA.

AS 1684.2 (2010). *Residential timber-framed construction*. Standards Australia, Sydney.

AS 2047 (2014). *Windows and external glazed doors in buildings*. Standards Australia, Sydney.

AS 4055 (2012). *Wind Loads for Housing*. Standards Australia, Sydney.

AS/NZS 1170.2 (2011). *Structural Design Actions, Part 2: Wind Actions*, Standards Australia, Sydney.

AS/NZS 2588 (2018). *Gypsum plasterboard*. Standards Australia, Sydney.

ASCE (2010). *Minimum design loads for buildings and other structures*. ASCE7-10, Reston, VA, USA.

Baheru, T., Chowdhury, A. G., & Pinelli, J. P. (2015). Estimation of wind-driven rain intrusion through building envelope defects and breaches during tropical cyclones. *Natural Hazards Review*, 16(2), 04014023.

Baheru, T., Chowdhury, A. G., Pinelli, J. P., & Bitsuamlak, G. (2014). Distribution of wind-driven rain deposition on low-rise buildings: Direct impinging raindrops versus surface runoff. *Journal of Wind Engineering and Industrial Aerodynamics*, 133, 27-38.

Barbato, M., Petrini, F., Unnikrishnan, V. U., & Ciampoli, M. (2013). Performance-based hurricane engineering (PBHE) framework. *Structural Safety*, 45, 24-35.

Bastidas-Arteaga, Emilio, Stewart, Mark. G. (2019). *Climate Adaptation Engineering: Risks and Economics for Infrastructure Decision-Making*. 1st edition. Butterworth-Heinemann, Elsevier, Oxford, UK.

BITRE (2008). *About Australia's regions*. Bureau of Infrastructure, Transport and Regional Economics, Canberra, Australia.

Bjarnadottir, S., Li, Y., & Stewart, M. G. (2011). A probabilistic-based framework for impact and adaptation assessment of climate change on hurricane damage risks and costs. *Structural Safety*, 33(3), 173-185.

Blackman, H. S., Gertman, D. I., & Boring, R. L. (2008). Human error quantification using performance shaping factors in the SPAR-H method. *Proceedings of the human factors and ergonomics society annual meeting*, Los Angeles, CA, USA.

Blocken, B., & Carmeliet, J. (2002). Spatial and temporal distribution of driving rain on a low-rise building. *Wind and Structures*, 5(5), 441-462.

Blocken, B., & Carmeliet, J. (2004). A review of wind-driven rain research in building science. *Journal of wind engineering and industrial aerodynamics*, 92(13), 1079-1130.

Blocken, B., & Carmeliet, J. (2010). Overview of three state-of-the-art wind-driven rain assessment models and comparison based on model theory. *Building and Environment*, 45(3), 691-703.

Blocken, B., & Carmeliet, J. (2012). A simplified numerical model for rainwater runoff on building facades: possibilities and limitations. *Building and Environment*, 53, 59-73.

Blocken, B., & Carmeliet, J. (2015). Impact, runoff and drying of wind-driven rain on a window glass surface: numerical modelling based on experimental validation. *Building and Environment*, 84, 170-180.

Boughton, G.N., Falck, D.K., Vinh Nghi Duong, A., Pham, S. & Nguyen, A. (2015). *Static Testing of Batten Connections at University of Western Australia*. Technical Report No.62. Cyclone Testing Station, James Cook University.

Canstar (2016). *Home and Contents Insurance Star Ratings Report*. Canstar, Brisbane, Australia.

Cha, E. J. (2018). Discrepancy in Perceived Hurricane Risks in a Changing Climate. *Natural Hazards Review*, 19(2), 04018002.

Cha, E. J., & Ellingwood, B. R. (2012). Risk-averse decision-making for civil infrastructure exposed to low-probability, high-consequence events. *Reliability Engineering & System Safety*, 104, 27-35.

Cha, E. J., & Ellingwood, B. R. (2013). The role of risk aversion in nuclear plant safety decisions. *Structural Safety*, 44, 28-36.

Cha, E. J., & Ellingwood, B. R. (2014). Attitudes towards acceptance of risk to buildings from extreme winds. *Structure and Infrastructure Engineering*, 10(6), 697-707.

Choi, E. C. C. (1994a). Determination of wind-driven-rain intensity on building faces. *Journal of Wind Engineering and Industrial Aerodynamics*, 51(1), 55-69.

Choi, E. C. C. (1994b). Characteristics of the co-occurrence of wind and rain and the driving-rain index. *Journal of wind engineering and industrial aerodynamics*, 53(1-2), 49-62.

CIBSE (2015). *GVA/15 CIBSE Guide A: Environmental Design 2015*. The Chartered Institution of Building Services Engineers, London, UK.

CSIRO & BOM (2015). *Climate Change in Australia Information for Australia's Natural Resource Management Regions*: *Technical Report*. CSIRO and Bureau of Meteorology, Australia.

CTS (2018). *North Queensland Study into Water Damage from Cyclones*. A summary of report TS1124, Cyclone Testing Station, James Cook University.

Dao, T. N. (2010). *The development of performance-based wind engineering for residential structures: From concept to application*. Ph.D. dissertation, Colorado State University, Fort Collins, CO, USA.

Dao, T. N., & van de Lindt, J. W. (2008). New nonlinear roof sheathing fastener model for use in finite-element wind load applications. *Journal of structural engineering*, 134(10), 1668-1674.

Dao, T. N., & van de Lindt, J. W. (2010). Methodology for wind-driven rainwater intrusion fragilities for light-frame wood roof systems. *Journal of Structural Engineering*, 136(6), 700-706.

De Haan, J., Terwel, K. C., & Al-Jibouri, S. H. S. (2013). Design of a Human Reliability Assessment model for structural engineering. *Proceedings of the 22nd European Safety and Reliability Conference*, Amsterdam, The Netherlands.

Dowdy, A. et al. (2015). *East Coast Cluster Report, Climate Change in Australia Projections for Australia's Natural Resource Management Regions: Cluster Reports*. eds. Ekström, M. et al., CSIRO and Bureau of Meteorology, Australia.

Eagleson, P. S. (1972). Dynamics of flood frequency. *Water Resources Research*, 8(4), 878-898.

Ellingwood, B. (1987). Design and construction error effects on structural reliability. *Journal of structural engineering*, 113(2), 409-422.

Ellingwood, B. R., Rosowsky, D. V., Li, Y. & Kim, J. H. (2004). Fragility assessment of light-frame wood construction subjected to wind and earthquake hazards. *Journal of Structural Engineering*, 130(12), 1921-1930.

ESDU (2002). *Strong winds in the atmospheric boundary layer. II: Discrete gust speeds*. Engineering Science Data Unit, Item No. 83045, London, UK.

Gavanski, E. & Kopp, G. A. (2017). Fragility assessment of roof-to-wall connection failures for wood-frame houses in high winds. *ASCE-ASME Journal of Risk and Uncertainty in Engineering Systems, Part A: Civil Engineering*, 3(4), 04017013.

Gavanski, E., Kopp, G. A. & Hong, H. P. (2014). Reliability analysis of roof sheathing panels on wood-frame houses under wind loads in Canadian cities. *Canadian Journal of Civil Engineering*, 41(8), 717-727.

Gelman, A., Carlin, J. B., Stern, H. S., & Rubin, D. B. (1995). *Bayesian data analysis*. London: Chapman and Hall/CRC.

Georgiou, P.N. (1985). *Design Wind speeds in Tropical Cyclone-Prone Regions*. Ph.D. Thesis, Faculty of Engineering Science, University of Western Ontario, London, Ontario, Canada, 1985.

Ginger J., Henderson D., Humphreys, M., and Parackal, K. (2015). *Climate Adaptation Engineering for Extreme Events (CAEX), Project 1.1 Progress report 4*. Cyclone Testing Station, James Cook University, Australia.

Ginger, J. D. & Letchford, C. W. (1993). Characteristics of large pressures in regions of flow separation. *Journal of Wind Engineering and Industrial Aerodynamics*, 49(1), 301-310.

Ginger, J., Henderson, D., Edwards, M. and Holmes, J. (2010). Housing damage in windstorms and mitigation for Australia. *Proceedings of 2010 APEC-WW and IG-WRDRR Joint Workshop: Wind-Related Disaster Risk Reduction Activities in Asia-Pacific Region and Cooperative Actions*, 1-18.

Goda, K., & Hong, H. P. (2006). Optimal seismic design considering risk attitude, societal tolerable risk level, and life quality criterion. *Journal of Structural engineering*, 132(12), 2027-2035.

Goda, K., & Hong, H. P. (2008a). Application of cumulative prospect theory: Implied seismic design preference. *Structural Safety*, 30(6), 506-516.

Goda, K., & Hong, H. P. (2008b). Implied preference for seismic design level and earthquake insurance. *Risk Analysis: An International Journal*, 28(2), 523-537.

Gong, C., & Frangopol, D. M. (2019). Preferred dry-docking interval of corroded ship hull girders based on cumulative prospect theory. *Ocean Engineering*, 192, 106440.

Grayson, J. M., Pang, W., & Schiff, S. (2013). Building envelope failure assessment framework for residential communities subjected to hurricanes. *Engineering Structures*, 51, 245-258.

Grose, M. et al. (2015). *Southern Slopes Cluster Report, Climate Change in Australia Projections for Australia's Natural Resource Management Regions: Cluster Reports*. eds. Ekström, M. et al., CSIRO and Bureau of Meteorology, Australia.

Groth, K. M., Smith, C. L., & Swiler, L. P. (2014). A Bayesian method for using simulator data to enhance human error probabilities assigned by existing HRA methods. *Reliability Engineering & System Safety*, 128, 32-40.

Hadar, J., & Russell, W. R. (1969). Rules for ordering uncertain prospects. *The American economic review*, 59(1), 25-34.

Hallbert B, Kolaczkowski A. (2007). *The employment of empirical data and Bayesian methods in human reliability analysis: a feasibility study*. US Nuclear Regulatory Commission, Washington DC.

Hamid, S. S., Pinelli, J. P., Chen, S. C., & Gurley, K. (2011). Catastrophe model-based assessment of hurricane risk and estimates of potential insured losses for the State of Florida. *Natural Hazards Review*, 12(4), 171-176.

Hamid, S., Kibria, B. G., Gulati, S., Powell, M., Annane, B., Cocke, S., ... & Chen, S. C. (2010). Predicting losses of residential structures in the state of Florida by the public hurricane loss evaluation model. *Statistical methodology*, 7(5), 552-573.

Hanoch, G. & H. Levy (1969). The Efficiency Analysis of Choices Involving Risk. *Review of Economic Studies*, 36(3), 335–346.

HAZUS (2014). *Multi-hazard Loss estimation methodology - hurricane model*. Hazus-MH 2.1 Technical Manual, Federal Emergency Management Agency, Mitigation Division, Washington, DC.

He, W. X., & Hong, H. P. (2012). Probabilistic characterization of roof panel uplift capacity under wind loading. *Canadian Journal of Civil Engineering*, 39(12), 1285-1296.

He, X., Wang, Y., Shen, Z., & Huang, X. (2008). A simplified CREAM prospective quantification process and its application. *Reliability Engineering & System Safety*, 93(2), 298-306.

Henderson D, Smith D, Boughton G, Falck D and Ginger J (2017). Damage and losses in engineered buildings from wind and rain. *24th Australasian Conference on the Mechanics of Structures and Materials*. 6-9 December 2016, Perth, Australia.

Henderson, D. J. & Ginger, J. D. (2007). Vulnerability model of an Australian high-set house subjected to cyclonic wind loading. *Wind and Structures*, 10(3), 269-285.

Henderson, D., & Ginger, J. (2008). Role of building codes and construction standards in windstorm disaster mitigation. *Australian Journal of Emergency Management*, 23(2), 40-46.

Heneker, T. M., Lambert, M. F., & Kuczera, G. (2001). A point rainfall model for risk-based design. *Journal of Hydrology*, 247(1-2), 54-71.

Herbin, A. H., & Barbato, M. (2012). Fragility curves for building envelope components subject to windborne debris impact. *Journal of Wind Engineering and Industrial Aerodynamics*, 107, 285-298.

HIA (2018). *Window into Housing 2018*. The Housing Industry Association, Canberra, Australia.

Ho, T. C. E., Surry, D., Morrish, D. & Kopp, G. A. (2005). The UWO contribution to the NIST aerodynamic database for wind loads on low buildings: Part 1. Archiving format and basic aerodynamic data. *Journal of Wind Engineering and Industrial Aerodynamics*, 93(1), 1-30.

Hollnagel, E. (1998). *Cognitive reliability and error analysis method (CREAM)*. Oxford: Elsevier.

Holmes, J. D. (1985). Wind loads and limit states design. *Civil Engineering Transactions*, Institution of Engineers Australia, CE27(1): 21-26.

Holmes, J. D. (2002). A re-analysis of recorded extreme wind speeds in region A. *Australian Journal of Structural Engineering*, 4(1), 29-40.

Holmes, J. D., & Moriarty, W. W. (1999). Application of the generalized Pareto distribution to extreme value analysis in wind engineering. *Journal of Wind Engineering and Industrial Aerodynamics*, 83(1-3), 1-10.

Holmes, J. D., & Oliver, S. E. (2000). An empirical model of a downburst. *Engineering structures*, 22(9), 1167-1172.

Holmes, J.D., (2015). *Wind loading of structures*. 3rd Edition, CRC Press Boca Raton, Florida, USA.

Hong, H. P., & He, W. X. (2015). Effect of human error on the reliability of roof panel under uplift wind pressure. *Structural Safety*, 52, 54-65.

Huang, Z., Rosowsky, D. V., & Sparks, P. R. (2001a). Hurricane simulation techniques for the evaluation of wind-speeds and expected insurance losses. *Journal of wind engineering and industrial aerodynamics*, 89(7-8), 605-617.

Huang, Z., Rosowsky, D. V., & Sparks, P. R. (2001b). Long-term hurricane risk assessment and expected damage to residential structures. *Reliability engineering & system safety*, 74(3), 239-249.

ISO (2009). *Hygrothermal performance of buildings – calculation and presentation of climatic data – Part 3: calculation of a driving rain index for vertical surfaces from hourly wind and rain data*. International Organization for Standardization 2009, 15927-3.

Jayasinghe, N. C. & Ginger, J. D. (2011) Vulnerability of roofing components to wind loads. *Wind and Structures*, 14 (4). pp. 321-335.

Ji, X., Huang, G., Zhang, X. & Kopp, G. A. (2018). Vulnerability analysis of steel roofing cladding: Influence of wind directionality. *Engineering Structures*, 156, 587-597.

Johnson, T., Pinelli, J. P., Baheru, T., Chowdhury, A. G., Weekes, J., & Gurley, K. (2018). Simulation of Rain Penetration and Associated Damage in Buildings within a Hurricane Vulnerability Model. *Natural Hazards Review*, 19(2), 04018004.

Kahneman, D., & Tversky, A. (1979). Prospect theory: An analysis of decision under risk. *Econometrica*, 47(2), 363-391.

Khanduri, A. C., & Morrow, G. C. (2003). Vulnerability of buildings to windstorms and insurance loss estimation. *Journal of wind engineering and industrial aerodynamics*, 91(4), 455-467.

Kirwan, B. (1994). *A guide to practical human reliability assessment*. London: Taylor & Francis.

Kirwan, B. (1996). The validation of three Human Reliability Quantification techniques—THERP, HEART and JHEDI: Part 1—technique descriptions and validation issues. *Applied ergonomics*, 27(6), 359-373.

Konthesingha, K. C., Stewart, M. G., Ryan, P., Ginger, J., & Henderson, D. (2015). Reliability based vulnerability modelling of metal-clad industrial buildings to extreme wind loading for cyclonic regions. *Journal of Wind Engineering and Industrial Aerodynamics*, 147, 176-185.

Kopp, G. A., Morrison, M. J. & Henderson, D. J. (2012). Full-scale testing of low-rise, residential buildings with realistic wind loads. *Journal of Wind Engineering and Industrial Aerodynamics*, 104, 25-39.

Kopp, G. A., Oh, J. H. & Inculet, D. R. (2008). Wind-induced internal pressures in houses. *Journal of structural engineering*, 134(7), 1129-1138.

Koutsoyiannis, D., & Foufoula-Georgiou, E. (1993). A scaling model of a storm hyetograph. *Water Resources Research*, 29(7), 2345-2361.

Koutsoyiannis, D., Onof, C., & Wheater, H. S. (2003). Multivariate rainfall disaggregation at a fine timescale. *Water Resources Research*, 39(7).

Lambert, M., & Kuczera, G. (1998). Seasonal generalized exponential probability models with application to interstorm and storm durations. *Water Resources Research*, 34(1), 143-148.

Lee, K. H. & Rosowsky, D. V. (2005). Fragility assessment for roof sheathing failure in high wind regions. *Engineering Structures*, 27(6), 857-868.

Lee, S. M., Ha, J. S., & Seong, P. H. (2011). CREAM-based communication error analysis method (CEAM) for nuclear power plant operators' communication. *Journal of Loss Prevention in the Process Industries*, 24(1), 90-97.

Leitch C, Ginger J, Harper B, Kim P, Jayasinghe N, & Somerville L (2009). *Investigation of performance of housing in Brisbane following storms on* 16 *and* 19 *November* 2008, Technical Report No. 55. Cyclone Testing Station, James Cook University.

Leshno, M., & Levy, H. (2002). Preferred by "all" and preferred by "most" decision makers: Almost stochastic dominance. *Management Science*, 48(8), 1074-1085.

Levy, H. (2016). *Stochastic dominance: Investment decision making under uncertainty*. Springer International Publishing, Switzerland.

Levy, M. (2012). Almost stochastic dominance and efficient investment sets. *American Journal of Operations Research*, 2(03), 313.

Li, Y. (2010). Assessment of damage risks to residential buildings and cost–benefit of mitigation strategies considering hurricane and earthquake hazards. *Journal of Performance of Constructed Facilities*, 26(1), 7-16.

Li, Y., & Ellingwood, B. R. (2006). Hurricane damage to residential construction in the US: Importance of uncertainty modeling in risk assessment. *Engineering structures*, 28(7), 1009-1018.

Li, Y., & Ellingwood, B. R. (2009). Risk-based decision-making for multi-hazard mitigation for wood-frame residential construction. *Australian Journal of Structural Engineering*, 9(1), 17-26.

Li, Y., & Stewart, M. G. (2011). Cyclone damage risks caused by enhanced greenhouse conditions and economic viability of strengthened residential construction. *Natural Hazards Review*, 12(1), 9-18.

Li, Y., & van de Lindt, J. W. (2012). Loss-based formulation for multiple hazards with application to residential buildings. *Engineering Structures*, 38, 123-133.

Li, Y., van de Lindt, J. W., Dao, T., Bjarnadottir, S., & Ahuja, A. (2011). Loss analysis for combined wind and surge in hurricanes. *Natural hazards review*, 13(1), 1-10.

Lin, N., Vanmarcke, E., & Yau, S. C. (2010). Windborne debris risk analysis—Part II. Application to structural vulnerability modeling. *Wind and Structures*, 13(2), 207.

Liu, P. L. & Der Kiureghian, A. (1986). Multivariate distribution models with prescribed marginals and covariances. *Probabilistic Engineering Mechanics*, 1(2), 105-112.

Lovisa, A. C., Wang, V. Z., Henderson, D. J. & Ginger, J. D. (2013). Development and validation of a numerical model for steel roof cladding subject to static uplift loads. *Wind and Structures*, 17(5), 495-513.

Lysaght (2014), *TOPSPAN Design and Installation Guide for Building Professionals*, Bluescope Lysaght, Australia, 23 July 2014.

Mahendran, M. (1994). Behaviour and design of crest-fixed profiled steel roof claddings under wind uplift. *Engineering Structures*, 16(5), 368-376.

Mahsuli, M., & Haukaas, T. (2018). Risk minimization for a portfolio of buildings considering risk aversion. *Journal of Structural Engineering*, 145(2), 04018241.

Mudd, L., Rosowsky, D., Letchford, C., & Lombardo, F. (2016). Joint Probabilistic Wind–Rainfall Model for Tropical Cyclone Hazard Characterization. *Journal of Structural Engineering*, 143(3), 04016195.

Nan, C., & Sansavini, G. (2016). Developing an agent-based hierarchical modeling approach to assess human performance of infrastructure systems. *International Journal of Industrial Ergonomics*, 53, 340-354.

Nan, C., & Sansavini, G. (2017). A quantitative method for assessing resilience of interdependent infrastructures. *Reliability Engineering & System Safety*, 157, 35-53.

Orooji, F., & Friedland, C. J. (2017). Cost-benefit framework to generate wind hazard mitigation recommendations for homeowners. *Journal of Architectural Engineering*, 23(4), 04017019.

Palutikof, J. P., Brabson, B. B., Lister, D. H., & Adcock, S. T. (1999). A review of methods to calculate extreme wind speeds. *Meteorological applications*, 6(2), 119-132.

Pan, F., Cai, C. S. & Zhang, W. (2012). Wind-induced internal pressures of buildings with multiple openings. *Journal of Engineering Mechanics*, 139(3), 376-385.

Pant, S., & Cha, E. J. (2019). Wind and rainfall loss assessment for residential buildings under climate-dependent hurricane scenarios. *Structure and Infrastructure Engineering*, 15(6), 771-782.

Parackal, K. I., Humphreys, M. T., Ginger, J. D. & Henderson, D. J. (2016). Wind Loads on Contemporary Australian Housing. *Australian Journal of Structural Engineering*, 17(2), 136-150.

Parackal, K. I., Mason, M., Henderson, D., Stark, G., Ginger, J., Somerville, L., Harper, B., Smith, D., & Humphreys, M. (2015). *Investigation of Damage: Brisbane, 27 November 2014 Severe Storm Event*, Technical Report No. 60. Cyclone Testing Station, James Cook University.

Peng, X., Yang, L., Gavanski, E., Gurley, K. & Prevatt, D. (2014). A comparison of methods to estimate peak wind loads on buildings. *Journal of Wind Engineering and Industrial Aerodynamics*, 126, 11-23.

Pinelli, J. P., Pita, G., Gurley, K., Torkian, B., Hamid, S., & Subramanian, C. (2011). Damage characterization: Application to Florida public hurricane loss model. *Natural Hazards Review*, 12(4), 190-195.

Pinelli, J. P., Simiu, E., Gurley, K., Subramanian, C., Zhang, L., Cope, A. ... & Hamid, S. (2004). Hurricane damage prediction model for residential structures. *Journal of Structural Engineering*, 130(11), 1685-1691.

Pita, G., Pinelli, J. P., Cocke, S., Gurley, K., Mitrani-Reiser, J., Weekes, J., & Hamid, S. (2012). Assessment of hurricane-induced internal damage to low-rise buildings in the Florida Public Hurricane Loss Model. *Journal of Wind Engineering and Industrial Aerodynamics*, 104, 76-87.

Podofillini, L., & Dang, V. N. (2013). A Bayesian approach to treat expert-elicited probabilities in human reliability analysis model construction. *Reliability Engineering & System Safety*, 117, 52-64.

Porter, K. A., Kiremidjian, A. S., & LeGrue, J. S. (2001). Assembly-based vulnerability of buildings and its use in performance evaluation. *Earthquake spectra*, 17(2), 291-312.

Powell, M., Soukup, G., Cocke, S., Gulati, S., Morisseau-Leroy, N., Hamid, S., ... & Axe, L. (2005). State of Florida hurricane loss projection model: Atmospheric science component. *Journal of wind engineering and industrial aerodynamics*, 93(8), 651-674.

Prelec, D. (1998). The probability weighting function. *Econometrica*, 66, 497–527.

Quiggin, J. (1982). A theory of anticipated utility. *Journal of Economic Behavior & Organization*, 3(4), 323-343.

R Core Team (2019). *R: A language and environment for statistical computing*. R Foundation for Statistical Computing, Vienna, Austria. URL: http://www.R-project.org/.

Rawlinsons (2015). *Rawlinsons Construction Cost Guide 2015*. Rawlinsons Publishing, Perth, Australia.

Reardon, G. F. (1996). Simulated wind loading of full size houses. In *Proc. Int. Seminar: The Role of Large and Full Scale Testing*, Inst. of Struct. Eng. City University, London, UK.

RLB (2019). *Riders Digest 47th Edition*. Rider Levett Bucknall, Australia.

Rocha, D., Eamon, C. D. & Murphy, J. F. (2011). Reliability analysis of roof sheathing panels exposed to a hurricane wind. *Structural Safety*, 33(1), 74-81.

Rockafellar, R.T., & Royset, J. O. (2015). Engineering decisions under risk averseness. *ASCE-ASME Journal of Risk and Uncertainty in Engineering Systems, Part A: Civil Engineering*, 1(2), 04015003.

Rockafellar, R. T., & Uryasev, S. (2000). Optimization of conditional value-at-risk. *Journal of risk*, 2, 21-42.

Rosowsky, D. V. & Cheng, N. (1999). Reliability of light-frame roofs in high-wind regions. I: Wind loads. *Journal of Structural Engineering*, 125(7), 725-733.

Rosowsky, D. V., & Ellingwood, B. R. (2002). Performance-based engineering of wood frame housing: Fragility analysis methodology. *Journal of Structural Engineering*, 128(1), 32-38.

Rosowsky, D. V., & Schiff, S. D. (1996). Probabilistic modeling of roof sheathing uplift capacity. *Proceedings of ASCE Specialty Conference on Probabilistic Mechanics & Structural Reliability*, Worcester, MA, USA.

Satheeskumar, Navaratnam (2016) *Wind load sharing and vertical load transfer from roof to wall in a timber-framed house*. PhD thesis, James Cook University, Australia.

Satheeskumar, N., Henderson, D. J., Ginger, J. D. & Wang, C. H. (2016a). Wind uplift strength capacity variation in roof-to-wall connections of timber-framed houses. *Journal of Architectural Engineering*, 22(2), 04016003.

Satheeskumar, N., Henderson, D. J., Ginger, J. D., Humphreys, M. T. & Wang, C. H. (2016b). Load sharing and structural response of roof–wall system in a timber-framed house. *Engineering Structures*, 122, 310-322.

Satheeskumar, N., Henderson, D. J., Ginger, J. D. & Wang, C. H. (2017). Three-Dimensional Finite-Element Modeling and Validation of a Timber-Framed House to Wind Loading. *Journal of Structural Engineering*, 143(9), 04017112.

Simiu, E. & Scanlan, R. H. (1986). *Wind Effects on Structures: an Introduction to Wind Engineering*. Wiley-Interscience, New York.

Simon, H. A. (1955). A behavioral model of rational choice. *The Quarterly Journal of Economics*, 69(1), 99-118.

Sivapalan, M., & Blöschl, G. (1998). Transformation of point rainfall to areal rainfall: Intensity-duration-frequency curves. *Journal of Hydrology*, 204(1-4), 150-167.

Sivapathasundaram, M. & Mahendran, M. (2016). Development of fragility curves for localised pull-through failures of thin steel roof battens. *Engineering Structures*, 124, 64-84.

Smith D, Henderson D, Ginger J, Wehner M, Ryu H & Edwards M (2016). *Improving the resilience of existing housing to severe wind events: Annual project report* 2015-2016. Bushfire and Natural Hazards CRC.

Smith, D., & Henderson, D. (2015). *Suncorp group limited: Cyclone resilience research – Phase II*. Report TS1018, Cyclone Testing Station, James Cook University, Australia.

Stratco (2019). *Roof batten design guide*. Stratco Pty Limited, Australia.

Stewart, M. G. (1992). Modelling human error rates for human reliability analysis of a structural design task. *Reliability Engineering & System Safety*, 36(2), 171-180.

Stewart, M. G. (1993). Structural reliability and error control in reinforced concrete design and construction. *Structural safety*, 12(4), 277-292.

Stewart, M. G. (2003). Cyclone damage and temporal changes to building vulnerability and economic risks for residential construction. *Journal of Wind Engineering and Industrial Aerodynamics*, 91(5), 671-691.

Stewart, M. G. (2015). Risk and economic viability of housing climate adaptation strategies for wind hazards in southeast Australia. *Mitigation and Adaptation Strategies for Global Change*, 20(4), 601-622.

Stewart, M. G. (2016). Climate change impact assessment of metal-clad buildings subject to extreme wind loading in non-cyclonic regions. *Sustainable and Resilient Infrastructure*, 1(1-2), 32-45.

Stewart, M. G., Bastidas-Arteaga, E. (2019). Introduction to Climate Adaptation Engineering. In: E. Bastidas-Arteaga and M.G. Stewart (ed) *Climate Adaptation Engineering: Risks and Economics for Infrastructure Decision-Making*.

Stewart, M. G., & Deng, X. (2014). Climate impact risks and climate adaptation engineering for built infrastructure. *ASCE-ASME Journal of Risk and Uncertainty in Engineering Systems, Part A: Civil Engineering*, 1(1), 04014001.

Stewart, M. G., & Melchers, R. E. (1988). Simulation of human error in a design loading task. *Structural Safety*, 5(4), 285-297.

Stewart, M. G., Ellingwood, B. R., & Mueller, J. (2011). Homeland security: A case study in risk aversion for public decision-making. International *Journal of Risk Assessment and Management*, 15(5-6), 367-386.

Stewart, M. G., Ginger, J. D., Henderson, D. J. & Ryan, P. C. (2018). Fragility and climate impact assessment of contemporary housing roof sheeting failure due to extreme wind. *Engineering Structures*, 171, 464-475.

Stewart, M. G., Wang, X., & Willgoose, G. R. (2014). Direct and indirect cost-and-benefit assessment of climate adaptation strategies for housing for extreme wind events in Queensland. *Natural Hazards Review*, 15(4), 04014008.

Straube, J. F., & Burnett, E. F. P. (2000). Simplified prediction of driving rain on buildings. *Proceedings of the international building physics conference*. Eindhoven, Netherlands.

Suncorp (2013). *Calculated Risk: A look into Suncorp's pricing calculations*. Suncorp, Brisbane, Australia.

Tieleman, H. W., Elsayed, M. A., Ge, Z. & Hajj, M. R. (2008). Extreme value distributions for peak pressure and load coefficients. *Journal of Wind Engineering and Industrial Aerodynamics*, 96(6), 1111-1123.

Torkian, Boback & Pinelli, Jean-Paul & Gurley, Kurtis & Hamid, Shahid. (2014). Cost-and-Benefit Evaluation of Windstorm Damage Mitigation Techniques in Florida. *Natural Hazards Review*. 15. 150-157.

Tuleya, R. E., DeMaria, M., & Kuligowski, R. J. (2007). Evaluation of GFDL and simple statistical model rainfall forecasts for US landfalling tropical storms. *Weather and forecasting*, 22(1), 56-70.

Tversky, A., & Kahneman, D. (1992). Advances in prospect theory: Cumulative representation of uncertainty. *Journal of Risk and uncertainty*, 5(4), 297-323.

Tzeng, L. Y., Huang, R. J., & Shih, P. T. (2013). Revisiting almost second-degree stochastic dominance. *Management Science*, 59(5), 1250-1254.

Unnikrishnan, V. U., & Barbato, M. (2016). Performance-based comparison of different storm mitigation techniques for residential buildings. *Journal of Structural Engineering*, 142(6), 04016011.

Unnikrishnan, V. U., & Barbato, M. (2017). Multihazard interaction effects on the performance of low-rise wood-frame housing in hurricane-prone regions. *Journal of Structural Engineering*, 143(8), 04017076.

van de Lindt, J. W., & Dao, T. N. (2009). Performance-based wind engineering for wood-frame buildings. *Journal of Structural Engineering*, 135(2), 169-177.

van de Lindt, J. W., & Dao, T. N. (2012). Loss analysis for wood frame buildings during hurricanes. II: Loss estimation. *Journal of Performance of Constructed Facilities*, 26(6), 739-747.

van de Lindt, J. W., & Nguyen Dao, T. (2010). Construction quality issues in performance-based wind engineering: effect of missing fasteners. *Wind and Structures*, 13(3), 221.

van de Lindt, J. W., & Rosowsky, D. V. (2005). Strength-based reliability of wood shearwalls subject to wind load. *Journal of structural engineering*, 131(2), 359-363.

Vickery, P. J., Lin, J., Skerlj, P. F., Twisdale Jr, L. A., & Huang, K. (2006a). HAZUS-MH hurricane model methodology. I: Hurricane hazard, terrain, and wind load modeling. *Natural Hazards Review*, 7(2), 82-93.

Vickery, P. J., Skerlj, P. F., Lin, J., Twisdale Jr, L. A., Young, M. A. & Lavelle, F. M. (2006b). HAZUS-MH hurricane model methodology. II: Damage and loss estimation. *Natural Hazards Review*, 7(2), 94-103.

Vickery, P. J., Skerlj, P. F., Steckley, A. C., & Twisdale, L. A. (2000). Hurricane wind field model for use in hurricane simulations. *Journal of Structural Engineering*, 126(10), 1203-1221.

Vickery, P. J., Wadhera, D., Powell, M. D., & Chen, Y. (2009). A hurricane boundary layer and wind field model for use in engineering applications. *Journal of Applied Meteorology and Climatology*, 48(2), 381-405.

von Neumann, J., & O. Morgenstern. (1944). *Theory of games and economic behavior*. Princeton, NJ: Princeton University Press.

Walker, G. R. (1975). *Report on Cyclone Tracy–Effect on buildings–Dec1974*. Australian Dept. of Housing and Construction, Hawthorn, Australia.

Walker, G. R. (2011). Modelling the vulnerability of buildings to wind - a review. *Canadian Journal of Civil Engineering*, 38(9), 1031-1039.

Walker, G. R., Mason, M. S., Crompton, R. P., & Musulin, R. T. (2016). Application of insurance modelling tools to climate change adaptation decision-making relating to the built environment. *Structure and Infrastructure Engineering*, 12(4), 450-462.

Wang, C. H., Wang, X., & Khoo, Y. B. (2013). Extreme wind gust hazard in Australia and its sensitivity to climate change. *Natural hazards*, 67(2), 549-567.

Wang, C., & Zhang, H. (2018). Probability-based estimate of tropical cyclone damage: An explicit approach and application to Hong Kong, China. *Engineering Structures*, 167, 471-480.

Wang, Y., & Rosowsky, D. V. (2018). Hazard-based regional loss estimation considering hurricane intensity, size and sea surface temperature change. *Sustainable and Resilient Infrastructure*, 3(4), 151-164.

Wolfe RW. & McCarthy M. (1989). *Structural performance of light-frame roof assemblies*: I. *Truss assemblies with high truss stiffness variability*. FPL-RP-492. Madison (WI): Forest Products Laboratory, USA.

Woods, A. R. & Blackmore, P. A. (1995). The effect of dominant openings and porosity on internal pressures. *Journal of Wind Engineering and Industrial Aerodynamics*, 57(2-3), 167-177.

Xu, Y. L. & Reardon, G.F. (1992). *Behaviour of different profiled roofing sheets subject to wind uplift*. Technical Report No.37. Cyclone Testing Station, James Cook University.

Yang, Z. L., Bonsall, S., Wall, A., Wang, J., & Usman, M. (2013). A modified CREAM to human reliability quantification in marine engineering. *Ocean Engineering*, 58, 293-303.

Yazdani, N., Dowgul, R. W., & Manzur, T. (2010). Deficiency analysis of coastal buildings toward storm damage reduction. *Journal of Performance of Constructed Facilities*, 24(2), 128-137.

Zhang, S., Nishijima, K., & Maruyama, T. (2014). Reliability-based modeling of typhoon induced wind vulnerability for residential buildings in Japan. *Journal of Wind Engineering and Industrial Aerodynamics*, 124, 68-81.

Zhou, W., & Nessim, M. A. (2011). Optimal design of onshore natural gas pipelines. *Journal of Pressure Vessel Technology*, 133(3), 031702.

Zscheischler, J., Westra, S., Hurk, B. J., Seneviratne, S. I., Ward, P. J., Pitman, A., ... & Zhang, X. (2018). Future climate risk from compound events. *Nature Climate Change*, 8, 469–477.

APPENDIX

Structural Safety 79 (2019) 80–93

Contents lists available at ScienceDirect

Structural Safety

journal homepage: www.elsevier.com/locate/strusafe

System fragility analysis of roof cladding and trusses for Australian contemporary housing subjected to wind uplift

Hao Qin*, Mark G. Stewart

Centre for Infrastructure Performance and Reliability, The University of Newcastle, New South Wales 2308, Australia

ARTICLE INFO

Keywords:
Fragility
Wind uplift pressure
Housing
Non-cyclonic regions
Roof connections
Structural reliability

ABSTRACT

This paper describes a reliability-based fragility method to evaluate the wind damage to roof cladding and trusses for contemporary houses in non-cyclonic regions of Australia. The fragility assessment considers roof sheeting loss and roof truss failure due to overloading of cladding-to-batten, batten-to-rafter/truss and rafter/truss-to-wall connectors that are typically the 'weakest links' of a roof system under wind uplift pressure. The wind fragility herein is expressed by the mean extent of roof sheeting loss and roof truss failures as a function of gust wind speed. Monte Carlo Simulation in conjunction with a finite element approach are employed to carry out the wind fragility assessment, which enables the probabilistic characterization of spatially varying wind uplift pressure, connection resistances, structural response, failure progression of roof connections and internal pressure evolution with increasing roof sheeting loss. The proposed fragility method was illustrated on representative contemporary housing built in Brisbane and Melbourne with complex hip-roof geometries and corrugated metal roof sheeting. It was found that, for the gust wind speed corresponding to a 500-year return period, the mean proportion of roof sheeting loss and roof truss failures is negligible for the representative contemporary house built in Melbourne, whereas considerable roof damage is predicted for those built in Brisbane when windward dominant openings exist.

1. Introduction

Severe windstorms (excluding tropical cyclones) account for nearly 25% of annual economic losses caused by natural hazards in Australia [5] with most damage occurring to housing (e.g. [16,24]). The prediction of housing damage caused by extreme winds plays an important role in the development of optimal risk mitigation strategies and climate adaptation measures (e.g. [47,45,46]). A wind fragility function typically expresses the damage state as a function of wind speed, which offers a convenient and effective metric to forecast the extent of wind damage (e.g. [23,25,13,46]), and therefore facilitates the risk assessment and mitigation for housing under extreme wind loading.

Roof cladding and trusses are among the most vulnerable components of timber-framed houses under wind uplift pressure, the failure of which may incur significant economic losses for housing and impose safety threats on building occupants. Post-damage surveys (e.g. [50,24]) have indicated that roof damage typically initiates at and propagates through failure of roof connections that mainly include cladding-to-batten (CTB), batten-to-rafter/truss (BTR) and rafter/truss-to-wall (RTW) connectors. Although the reliability/fragility analysis of individual roof components is relatively straightforward, a comprehensive fragility modelling for the roof system is more challenging, and requires stochastic characterizations of spatially varying wind uplift pressure, component resistances, structural response and load redistribution after the failure of one or more roof connections.

There has been much research focusing on the reliability/fragility assessment for timber roof sheathing and toe-nail RTW connectors typically used on houses in hurricane-prone regions of North America (e.g. [38,35,7,23,49,25,33,34,37,9,8]). However, only limited reliability-based fragility models are available for Australian timber-framed houses that are commonly installed with metal roof sheeting, steel battens and framing anchors (e.g. triple grip) for RTW connectors (e.g. [13,18,43,46]). In most of these studies, the first connection failure was set as the system limit state [13,43] or only individual roof components at critical locations [18] were considered in the fragility analysis. Therefore, the progressive failure after the initiation of local damage has been neglected, and the resiliency of roof system may not have been well addressed. Recently, Stewart et al. [46] developed a fragility model to evaluate the metal roof sheeting loss for Australian contemporary houses, which takes into account the progressive failure of cladding fasteners by using a simplified load redistribution rule based on engineering judgement that 90% of wind load originally undertaken

* Corresponding author.
E-mail addresses: hao.qin@uon.edu.au (H. Qin), mark.stewart@newcastle.edu.au (M.G. Stewart).

https://doi.org/10.1016/j.strusafe.2019.03.005
Received 15 October 2018; Received in revised form 21 January 2019; Accepted 8 March 2019

by one failed fastener would be redistributed to adjacent fasteners on the same crest of the corrugated metal roof sheet. However, this redistribution rule may fail to fully capture various load redistribution scenarios involved in the failure progression of connections. The failure of roof trusses was also not assessed by Stewart et al. [46].

To improve the prediction for system fragility of roof cladding and trusses, this paper aims to develop a reliability-based fragility method to evaluate the extent of roof damage for contemporary housing in non-cyclonic regions of Australia. The roof of the representative contemporary house presented in this study mainly consists of corrugated metal roof sheets, metal top-hat battens, timber trusses and roof connections. The overloading of CTB, BTR and RTW connectors was deemed to cause the failure of these roof components. The spatially varying wind uplift pressure was probabilistically modelled based on wind loading standards and wind tunnel testing. Connection capacities were obtained from full-scale tests conducted by James Cook University (JCU) in Australia [40,41]. A Monte Carlo Simulation (MCS) analysis, in conjunction with a finite element (FE) approach for the roof system were proposed to evaluate the structural response, load redistribution and failure progression of roof connections under the spatially varying wind uplift pressures. The evolution of internal pressure with increasing roof sheeting loss was also taken into account in the fragility analysis. The fragility curves were developed to relate the extent of damage to roof cladding and trusses with gust wind speed. To illustrate the proposed fragility method, fragility analyses were carried out for the representative contemporary house that are built in Brisbane and Melbourne (non-cyclonic regions as classified in Australian wind loading standard), and installed with corrugated metal roof sheeting, top-hat battens and triple grip RTW connectors.

2. Reliability-based fragility method

The fragility of a structural component or system is typically defined as the probability of damage state DS conditional on a given hazard H. The damage state herein is measured by the proportion of the roof sheeting loss and the roof truss failures, and the hazard is corresponding to gust wind speed. The wind fragility is therefore the extent of damage to roof cladding and trusses, R_{loss}, at a given gust wind speed v, expressed as

$$\Pr(DS|H) = \Pr[DS = R_{loss}|H = v] \tag{1}$$

This study considers the failure of roof sheeting and trusses caused by overloading of CTB, BTR and RTW connectors as these connections are deemed as the 'weakest links' of the roof system under wind uplift pressure [36,13]. Note that fatigue-induced connection failure is neglected in this study as metal roofs in non-cyclonic regions are less sensitive to fatigue, in contrast to cyclonic regions where strong fluctuating winds dominate. The loss of a single roof sheet is assumed to occur when a critical number of cladding fasteners fail as inadequate fixings may lead to a loss of functionality, stability and integrity of the roof sheet. The failure of BTR connectors is also a contributor to the roof sheeting loss. A roof truss is considered to fail if at least one of its RTW connectors is overloaded. The failure of a single CTB, BTR or RTW connector is governed by the following limit state function.

$$g = R - (W - D_L) \tag{2}$$

where R represents the resistance of the considered connection, and W is the wind uplift load acting on this connection. The connection resistance and wind loading are both modelled probabilistically which are described in Section 4.1. The dead load arising from the weight of roof components is D_L. A connection fails if $g \leq 0$. In this study, the uplift loads acting on roof connections are obtained by using a FE approach. The dead load is considered in the FE modelling by specifying the density of roof components. The failure of a single roof sheet occurs when the number of failed fasteners on the roof sheet N_f exceeds a threshold value N_{cr}. A BTR connection failure is modelled as if all roof fasteners connected to the batten have failed. The sheet failure threshold value (N_{cr}) is equivalent to the sheet failure criterion (SFC) defined in Stewart et al. [46]. A reasonable lower bound for SFC assumes two fasteners cause roof sheet failure in line with Henderson et al. [12] which represents SFC = 10%. The upper bound assumes that 80% of fasteners must fail to cause roof sheet failure [11]. The evidence suggests that failure of a few fasteners will result in sheet failure rather than failure of many fasteners [20]. Hence, a triangular probability distribution proposed in Stewart et al. [46] is used to model N_{cr} (expressed as the percentage of the total number of fasteners on a single sheet), see Fig. 1. The lower and upper bounds of the triangular probability distribution are 10% and 80%, respectively. A sensitivity analysis indicates that the fragility results are not sensitive to N_{cr} assumptions [46]. For more details about the triangular distribution model of N_{cr}, see Stewart et al. [46].

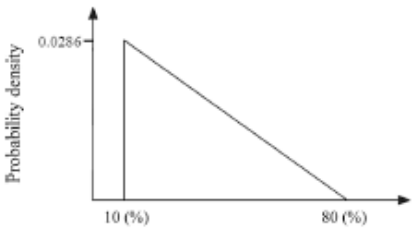

Fig. 1. Triangular probability distribution of N_{cr} [46].

To assess the number of failed CTB, BTR and RTW connectors requires the fragility model to account for the load sharing and redistribution among these roof connections. The wind uplift load acting on a single connection, W, is conventionally evaluated using the tributary area approach (e.g. [13,46]) or influence coefficients (e.g. [19]). However, the former approach may not accurately capture the wind loading effects by assuming no load sharing between connections [21], and it is a very complex task to use the latter approach to model the failure progression of roof connections by continuously providing updated influence coefficients for numerous load redistribution scenarios [44]. Instead, in this study, the uplift forces for roof connections are obtained by using a FE approach, which takes into account the load sharing and redistribution among roof connections under the spatially varying wind uplift pressure. The FE approach models the roof system including metal roof sheets, top-hat battens, timber roof trusses, wall top plates, and CTB, BTR and RTW connections. The details of the FE modelling are described in Section 5.

A Monte Carlo Simulation (MCS) analysis in conjunction with the FE approach are employed in this study to evaluate the wind fragility for roof cladding and trusses, which enables the stochastic characterization of spatially varying wind uplift pressure, uplift forces in roof connections, failure progression and load redistribution, and evolution of internal pressure with increasing sheeting loss. In each run of the MCS, the spatially distributed wind pressures and structural resistances of roof connections are randomly generated as the input to the FE model of the roof system. The wind uplift loads acting on the roof connections are then obtained from the FE analysis, and the failure of a single connection is checked by the limit state function given by Eq. (2). Any overloaded (failed) CTB, BTR and RTW connections are then deactivated in the FE model, and the FE analysis is further conducted to evaluate the load redistribution and failure progression of other connections. It should be noted that, given a short gust duration, the FE analysis of load redistribution and failure progression is only conducted once after the initial failure of connections. The MCS and FE approach

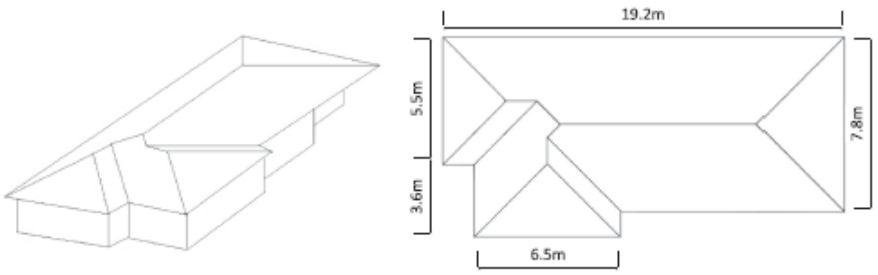

(a) 3D view (b) Plan view

Fig. 2. One-story representative contemporary house.

proposed in the present study enables the development of two fragility curves: (I) the extent of roof sheeting loss, and (II) proportion of roof truss failures.

3. Representative contemporary house

A representative contemporary house built in the suburbs of Melbourne and Brisbane, Australia is used to illustrate the fragility method proposed in the present study. The dimension, shape and construction type of the house were determined by field surveys completed by the Cyclone Testing Station (CTS) at James Cook University (JCU) [31]. The median values of house plans and features from the survey such as footprint dimensions, roof pitch and wall heights were selected to determine the configuration of the representative contemporary house. Fig. 2 shows the 3D and plan view of the representative one-story house. It is a timber-framed construction with 21.5° timber roof trusses at 600 mm spacings on a complex hip-end roof. Trusses are arranged with standard trusses in the middle part of the roof and jack trusses connected to truncated girder trusses at the hip ends. The housing survey reveals that both metal and tile roof are popular for contemporary houses in Melbourne and Brisbane. In this study, the metal roof is considered for the representative house as the 'unzipping' of the whole or a large proportion of metal roof is more likely to occur, which results in more severe roof damage. Metal roof cladding for the representative house is 762 mm wide corrugated metal sheeting. Metal top-hat battens are attached to timber roof trusses at 900 mm spacings. More details of the representative contemporary house can be found in Parackal et al. [31].

4. Probabilistic modelling of wind loading and connection resistance

4.1. Wind uplift load

The wind uplift load (W) is modelled probabilistically as (e.g. [15,46]).

$$W = \lambda \cdot M \cdot A \cdot (C \cdot T \cdot E^2 \cdot D^2 \cdot G \cdot \frac{\rho}{2}) \cdot v^2 \quad (3)$$

where v is the maximum 0.2 s gust velocity at 10 m height in Terrain Category 2 (i.e. open terrain defined in Australian wind loading standard AS/NZS 1170.2 2011); λ is a factor accounting for wind loading modelling inaccuracies and uncertainties; M accounts for wind tunnel modelling inaccuracies such as incorrect Reynolds number, building details, and site modelling; A is the loaded area uncertainty arising from geometric uncertainties of the cladding fastener, batten and truss spacing; C is the quasi-steady pressure coefficient, which is a combination of external (C_{Pe}) and internal pressure coefficient (C_{Pi}); T is the shielding factor; E is a terrain height multiplier that accounts for the exposure and height of the building considered; D is a factor accounting for wind directionality effects; G is a factor related to area reduction, and ρ is the density of air. These parameters, except for C, are assumed to follow a lognormal distribution[13] with estimated means and coefficient of variations (COV) listed in Table 1 that are derived from the statistics given in Holmes [15] and Stewart et al. [46]. Note that the subscript 'N' in Table 1 denotes the nominal value, which can be obtained from AS/NZS 1170.2 [4]. Random variables, λ, M, E, T, D, G, A and ρ are statistically independent for each simulated house, but then fully correlated for each roof connection in the simulated house. Sensitivity analyses indicate that, if one or two of the random variables given in Table 1 are assumed as deterministic, then fragilities reduce by less than 2%. Note that the spatially variable nature of wind uplift pressure is mainly attributed to the spatially distributed external pressure coefficients, which are measured from a wind tunnel test in this study.

Table 1
Statistical parameters for wind load modelling.

Parameter	Mean	COV
λ/λ_N	1.0	0.10
M/M_N	1.0	0.10
A/A_N	1.0	0.05
E/E_N	0.95	0.10
T/T_N	1.0	0.10
D/D_N	1.0	0.00
G/G_N	1.0	0.05
ρ/ρ_N	1.0	0.02

4.1.1. External pressure coefficients

External pressure coefficients provided in wind loading standards are typically based on wind tunnel tests conducted on rectangular hip and gable roofs. As the representative contemporary house has complex hip-roof geometries, wind tunnel testing was carried out to obtain the external pressure coefficients for the entire roof surface. The wind tunnel test was conducted for a scaled model of the representative contemporary house in the Boundary Layer Wind Tunnel at JCU [31]. Three hundred and twenty pressure taps were installed on the external roof surface to measure the spatial and temporal variation in external pressure. The fluctuating external pressures on these taps were measured for approach wind directions of 0–350° at intervals of 10°. More details about the wind tunnel test are described in Parackal et al. [31].

A Gumbel distribution is used to model the spatially varying peak suction pressure coefficients (e.g. [14,48]) with the location and scale parameters estimated from the wind tunnel observations for each tap location and each wind direction using the maximum likelihood

method (e.g. [32]). The use of a Gumbel distribution with no upper limit results in conservative predictions for peak external pressure coefficients, which to some extent compensates for statistical uncertainties given finite wind tunnel data, and uncertainties in applying wind tunnel data to full scale [17]. Hence, it is reasonable to model the extreme pressure coefficients using a Gumbel distribution. More details about the interpolation of wind tunnel observations and the modelling of external pressure coefficients can be found in Parackal et al. [31] and Stewart et al. [46]. Note that the non-simultaneous occurrence of peak suctions across large roof surface is accounted for by the factor G given in Eq. (3). As wind tunnel testing has shown a very high correlation of peak pressure values between taps in edge zones [10], the present fragility analysis assumes a correlation coefficient of 0.9 for the pressure tap data in roof edge. It is noted that the calculated fragilities are not sensitive to assumptions about the pressure tap correlation coefficients (see also [46]).

4.1.2. Internal pressure coefficients

Internal pressure is an important factor for the assessment of roof uplift, which combining with external pressure may produce the most adverse effect on the roof system. Internal pressure is highly dependent on locations and sizes of openings as well as the external pressures around the openings. The progressive failure of windows, doors and roof sheets during an extreme wind event creates multiple openings, which may significantly change the internal pressure and therefore affect the roof damage assessment. Although the evaluation of internal pressure under multiple wall openings has been reported in the literature (e.g. [22,30]), few studies attempt to investigate the evolution of internal pressure with increasing roof sheeting loss for houses and the consequent effect on roofing fragility.

As internal pressure coefficients were not measured in the wind tunnel test described in Section 4.1.1, two typical scenarios are assumed for internal pressure, i.e. (i) dominant openings existing on windward wall and (ii) effectively sealed building without any wall openings. A general equation used to obtain the quasi-steady internal pressure coefficient considering multiple openings is derived from Holmes [16] by applying mass conservation, which is given by

$$\sum_{j=1}^{N} A_j \sqrt{|C_{Pe,j} - C_{Pi}|} = 0 \tag{4}$$

where N is the number of openings in the building envelope; A_j is the size of opening j; $C_{Pe,j}$ is the quasi-steady external pressure coefficient at opening j, and C_{Pi} is the quasi-steady internal pressure coefficient. It should be noted that Eq. (4) neglects inertial effects.

To avoid the computational burden involved in solving Eq. (4) by numerical methods considering multiple openings, we combine the area for several openings on the windward wall and roof as A_W and A_R, respectively. Then based on Eq. (4), the internal pressure coefficient for the windward wall dominant opening scenario is calculated as

$$C_{Pi} = \frac{C_{PW}}{1 + \left(\frac{A_R}{A_W}\right)^2} + \frac{C_{PR}}{1 + \left(\frac{A_W}{A_R}\right)^2} \tag{5}$$

where C_{PW} is the average of external pressure coefficients at multiple windward wall openings, C_{PR} is the average of external pressure coefficients at multiple roof openings, A_W is the total size of wall openings, and A_R is the total size of roof openings. It should be noted that Eq. (5) neglects any openings on leeward and side walls.

Windward wall openings may include windows and doors that are damaged and/or left open during a windstorm. Only roof openings due to the damage progression of metal sheets are considered in this study (i.e. ignoring possible effect of flashings, vents, etc). With windward wall dominant openings, if $C_{PW} = +0.7$ and $C_{PR} = -0.3$ (nominal values in AS/NZS 1170.2), the change of C_{Pi} with increasing loss of roof sheeting (i.e. increasing A_R/A_W), is depicted in Fig. 3(a). As shown in Fig. 3(a), internal pressure coefficients decrease with increasing A_R/A_W, which suggests that the adverse effect of internal pressure subjected to windward wall dominant openings is relieved with increasing roof sheeting loss. If $A_w = 8\,m^2$ (e.g. two 2 m × 2 m windows), the internal pressure evolution with increasing number of failed roof sheets (the size of a typical corrugated sheets used in the representative contemporary house is $3.4\,m^2$) is depicted in Fig. 3(b). Note that Fig. 3 is only used to illustrate the approximate trend of internal pressure evolution with increasing roof sheeting loss. In each run of the MCS for fragility assessment, instead of AS/NZS 1170.2 values, C_{PW} and C_{PR} will take values of the average of external pressure coefficients at windward wall openings and roof breaches, respectively. Various sizes of windward wall dominant openings, A_w, that are possible to occur during a windstorm are considered in a sensitivity analysis later in Section 6.2.2 to examine the corresponding effects on the fragility assessment.

The internal pressure coefficient is assumed to follow a normal distribution with a COV of 0.33 (e.g. [23,43]) as loss of roof sheeting will result in high variability of internal pressures. A lower COV value is considered later in Section 6.2.2 to show the sensitivity of fragility to internal pressure variability. The corresponding mean value of C_{Pi} is calculated by Eq. (5) with a 10% reduction when combined with the external pressure coefficient to account for the non-simultaneous occurrence of peak internal and external pressures. For the scenario without any wall openings, the mean value of C_{Pi} would simply be equal

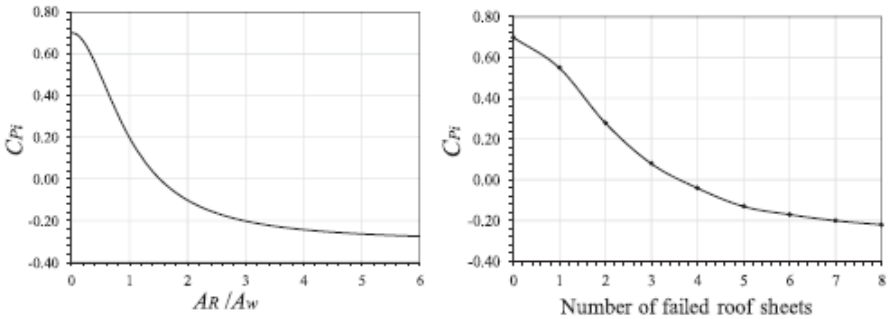

(a) Internal pressure evolution with increasing A_R/A_W ($A_W > 0$)

(b) Internal pressure evolution with increasing number of failed roof sheets ($A_w = 8\,m^2$)

Fig. 3. Internal pressure evolution with increasing roof sheeting loss with windward wall dominant openings.

Table 2
Statistical parameters for resistances of CTB and BTR connectors.

Connection type	Connection failure mode	Mean	COV	Distribution type	Source
Cladding-to-batten (CTB)	Roof sheeting pulling over fastener	1.2 kN	0.30	Lognormal	Stewart et al. [46]
	Roof fastener pulling out of roof batten	1.2 kN	0.20		
Batten-to-rafter/truss (BTR)	Roof batten pulling over batten fastener	4.5 kN	0.15	Lognormal	Stewart et al. [46]
	Batten fastener pulling out of rafter/truss	5.5 kN	0.20		

to the mean value of C_{pi} and the same COV value is used. Note that the effect of porosity on internal pressure is deemed to be negligible when large openings occur [52], and therefore is not taken into account in this study.

4.2. Connection resistance

The representative contemporary house is installed with corrugated metal sheeting secured by screw fasteners at every 2nd corrugation of the roof edge and every 3rd or 4th corrugation for other regions of the roof. Metal top-hat 40 battens are used as roof battens and secured to every truss at 900 mm spacings [31]. The resistances of the CTB and BTR connectors are modelled as random variables and the failure modes considered are (i) pull-over and (ii) pull-out failures. Both the pull-over and pull-out capacities of CTB and BTR connectors are assumed to follow a lognormal distribution [13]. The statistical parameters for the resistances of CTB and BTR connectors are listed in Table 2, which were derived from laboratory tests and summarized in Stewart et al. [46]. The connection resistances are assumed to be statistically independent and taken as the lower of randomly generated pull-out and pull-over strengths in the fragility assessment.

Triple grip connections (see Fig. 4) are typically used for the rafter/truss-to-wall (RTW) connectors for Australian contemporary houses. The timber species for the truss is typically Australian radiata pine, and two types of fasteners, i.e. hand nails and gun nails, are used for the triple grip connections. The triple grip connection behaviour under uplift loads is captured by a piecewise-linear force-displacement relationship with its model parameters probabilistically characterized based on Australian housing test data in Satheeskumar [39]. Fig. 5 depicts the piecewise-linear model for the behaviour of triple grip RTW connectors in the vertical direction (i.e. y shown in Fig. 4). In Fig. 5, F_y is the yield load and the connection has a linear-elastic response when its force $F \le F_y$, k_0 is the initial secant stiffness, and δ_y is the displacement at yielding. When $F_y < F \le F_u$, where F_u is the peak load (considered as the uplift capacity for the connection), permanent deformation and load redistribution start to occur. If the displacement of the connection, δ, is greater than the displacement at peak load, δ_u, the separation of triple grip from the top plate is likely to occur, and δ_{max} is the displacement of triple grip connection at complete separation.

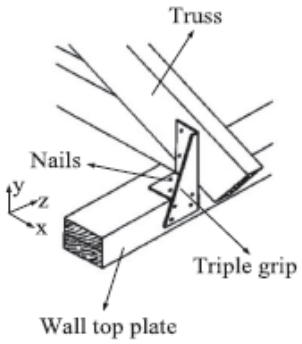

Fig. 4. Triple grip RTW connector.

The overloading of roof connections ($F \ge F_u$) is considered as the limit state for the current reliability-based fragility method. Thus, the connection behaviour after peak load is neglected in the FE analysis and it is assumed that the overloaded RTW connector tends to lose its load carrying capacity very quickly. Clearly, this is a slightly conservative assumption. Another consideration for ignoring the so-called 'negative stiffness' after the peak load is that it can cause non-convergence issues for the FE analysis. A much higher compression stiffness (i.e. 20 kN/mm) is assumed for the RTW connector in the vertical (y) direction. Three major parameters, i.e. k_0, F_u and δ_u, are used to define the piecewise-linear model in Fig. 5. All these parameters are assumed to follow lognormal distributions with the mean and COV values obtained from 10 individual static tests [39]. The statistical parameters of k_0, F_u and δ_u for triple grip connections fastened using hand nails and gun nails are listed in Table 3. The yield force (F_y) is defined as two-thirds of F_u based on the averaged ratio of F_y to F_u in the test data. The correlation coefficients between these three model parameters are also obtained from the test data as shown in Table 4, and when conducting the fragility analysis, the lognormally correlated parameters are sampled in the MCS using Nataf transformation [26] for the calculation of the covariance matrix.

Fig. 6 depicts the force-displacement curves of the test data and the mean piecewise-linear approximation for triple grip fastened using hand nails and gun nails. Note that the descending part in the piecewise-linear curve is arbitrarily assumed for illustration and it is not included in the fragility analysis as explained above. As shown in Fig. 6, the piecewise-linear model provides a reasonable approximation for the connection response under uplift loads. Note that the statistical accuracy can be further improved if more test data is available.

5. FE modelling of roof system

A FE approach using commercial FE software ANSYS [1] was used in this study to evaluate the wind uplift loads acting on roof

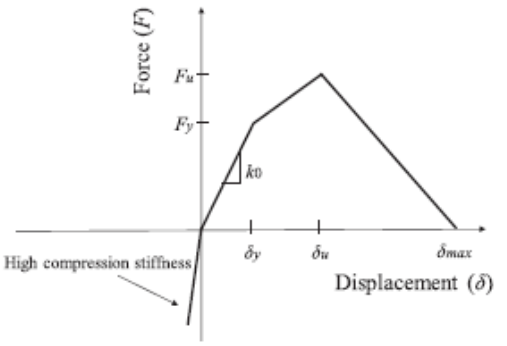

Fig. 5. Piecewise-linear force-displacement relationship for triple grip RTW connectors.

Table 3
Statistical parameters of the piecewise-linear model for RTW connectors.

RTW parameters	Mean	COV	Distribution type
(a) Hand nail triple grip			
Initial secant stiffness k_0 (kN/mm)	0.44	0.17	Lognormal
Peak load F_u (kN)	4.85	0.11	
Displacement at peak load δ_u (mm)	19.49	0.12	
RTW parameters	Mean	COV	Distribution type
(b) Gun nail triple grip			
Initial secant stiffness k_0 (kN/mm)	0.34	0.15	Lognormal
Peak load F_u (kN)	3.80	0.11	
Displacement at peak load δ_u (mm)	19.95	0.18	

Table 4
Correlation coefficients between three piecewise-linear model parameters for RTW connectors.

Parameters	Correlation coefficient	
	Hand nail triple grip	Gun nail triple grip
k_0 and F_u	0.63	0.45
k_0 and δ_u	−0.27	−0.16
F_u and δ_u	0.12	0.14

connections and load redistribution after the failure of one or more connections. The FE approach in conjunction with MCS enables an assessment of wind fragility considering the progressive failure of roof connections.

As shown in Fig. 2, the representative contemporary house has a complex hip-roof geometry that requires excessive cost in both FE modelling and computation (e.g. CPU hours) for the reliability-based fragility assessment. For example, a comprehensive FE model for the roof trusses requires the modelling of several types of trusses (e.g. standard truss, truncated standard truss, truncated girder truss, valley truss, hip truss, jack truss, etc.) with various dimensions as well as many truss-to-truss connections (e.g. hip truss to truncated truss connections, jack truss to truncated girder truss connections, etc.). To reduce the cost in FE modelling and computation, the FE approach used in this study models the roof cladding and trusses separately, and only critical roof trusses are modelled.

The roof cladding FE model consists of corrugated metal roof sheets, metal top-hat battens, CTB and BTR connectors, which is employed in the MCS analysis to evaluate roof sheeting loss under the spatially varying wind uplift pressure. The details of the roof cladding FE model are described in Section 5.1.

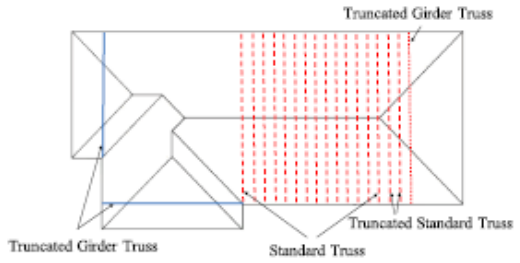

Fig. 7. The selected trusses modelled in the FE analysis.

The roof truss FE model mainly comprises a critical proportion of the timber trusses in the representative contemporary house, which includes 14 standard trusses, 2 truncated standard trusses and 1 truncated girder truss as shown in Fig. 7. These modelled trusses cover most of the critical trusses (i.e. trusses that are more likely to fail under wind uplift) in the roof system. Two additional truncated girder trusses depicted in solid line as shown in Fig. 7, though not included in the FE modelling, are also considered in the fragility assessment using a simple tributary area approach as they are among the most vulnerable trusses in the roof system. In a single MCS run, the wind uplift loads acting on the BTR connectors obtained from the roof cladding FE model were subsequently applied to the roof truss FE model for truss failure assessment. Satheeskumar et al. [41] and JCU have conducted a full-scale test for a subassembly of roof trusses containing five standard trusses

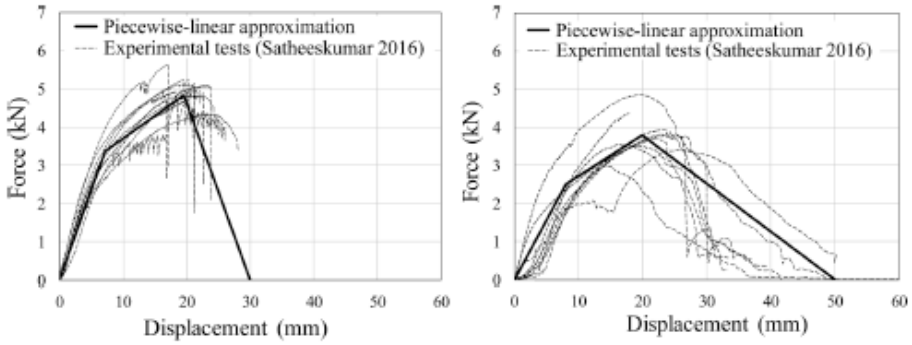

(a) Triple grip fastened using hand nails (b) Triple grip fastened using gun nails

Fig. 6. Force-displacement curves of the test data and piecewise-linear approximation.

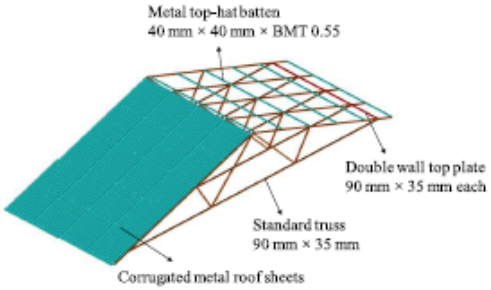

Fig. 8. Schematic diagram of the roof structure in the full-scale test [41].

from the same representative contemporary house. Material properties and dimensions of the trusses used in the FE models were obtained from this full-scale test. The schematic diagram of this roof structure in the full-scale test is depicted in Fig. 8. The details of the roof truss FE model are described in Section 5.2.

5.1. FE modelling of roof cladding

The FE model of the roof cladding layout containing 75 corrugated metal roof sheets is shown in Fig. 9(a). Four-node quadrilateral shell elements including both bending and membrane stiffness are used to model the corrugated metal sheet with six degrees of freedom at each node. The FE model of a typical corrugated metal roof sheet installed on the representative house is depicted in Fig. 9(b). A total of 22,792 shell elements are included in a typical metal roof sheet. The corrugated metal sheet has a width of 762 mm, base metal thickness (BMT) of 0.42 mm and crest height of 22 mm. Roof sheets with other shapes are configured by trimming the typical sheets at ridgelines and hips as shown in Fig. 9(a).

As metal roof sheeting loss is primarily due to overloading of CTB and BTR connectors [36,13], and for computational efficiency as well, the proposed FE approach does not assess detailed mechanical behaviour of the corrugated metal roof sheets. Instead, the FE approach is mainly aimed at evaluating the wind uplift forces in the roof connections, which in conjunction with the sampled connection resistances are used to assess the roof sheeting loss. To this end, localized dimpling, buckling and fracture of the metal roof sheet are not considered in the proposed FE approach. In addition, according to Xu & Reardon [53] and Mahendran [29], the majority of the corrugated metal sheeting are still in the elastic range when the fasteners fail. Thus, the material properties for the corrugated metal sheets are assumed to be isotropic and linear-elastic with a Young's modulus of 220,000 MPa and a Poisson's ratio of 0.3 [27]. Note that the variation in sheet material properties only has a slight effect on the overall cladding response [27], and therefore deterministic material properties are used.

Two-node beam elements are used to model the metal top-hat roof battens with material and section properties obtained from manufacture's specifications [28]. It is assumed that the CTB and BTR connectors no longer carry any loads when corresponding uplift forces exceed their pull-out and/or pull-over resistances, and the overloaded connections are then deactivated in the roof cladding FE model for further analysis of load redistribution and failure progression. The CTB and BTR connectors are approximately modelled by linear spring elements. The stiffness of the linear spring elements is also assumed to follow a lognormal distribution with a mean value of 300 N/mm and 1800 N/mm [42] for CTB and BTR connectors, respectively. A COV value of 0.20 is assumed for the stiffness variability due to a lack of relevant data. Although the linear spring is not able to capture the actual pull-through and withdrawn behaviour of screw fasteners, it is considered adequate to obtain the connection forces due to wind uplift and evaluate the overloading of roof connections in the context of the current reliability-based fragility method. The roof trusses are not modelled in the roof cladding FE model and flexible supports are assumed to represent the attachment points of batten fasteners to rafters. Using the proposed roof cladding FE model, the failure progression of CTB and BTR connectors can be evaluated. For example, if the corner fastener as shown in Fig. 9(b) is the first failed fastener for a typical corrugated metal roof sheet, about 80% of the load originally taken by this fastener is redistributed to neighbouring fasteners in the same corrugation and the remaining 20% redistributes to neighbouring fasteners in adjacent corrugations. Similarly, if the failure initiates at the interior fastener as shown in Fig. 9(b), 90% is the proportion of load redistribution along the corrugation. If more fasteners have failed, different scenarios of load redistribution would occur.

5.2. FE modelling of roof trusses

A total of 17 timber roof trusses are modelled in the roof truss FE model, which contains most of the critical trusses in the roof system. The truncated girder truss has a large tributary area (i.e. 10.4 m^2), the failure of which may impact other trusses (e.g. jack trusses) connected to it. The hip trusses and jack trusses typically have the same RTW connector as for a standard truss, while with relatively small tributary areas, they are less vulnerable under wind uplift and therefore are not modelled in the FE approach. This simplification has largely reduced the cost in FE modelling and computation time.

Two-node beam elements with a rectangular section of 90 mm × 35 mm are used to assemble the timber trusses, and the

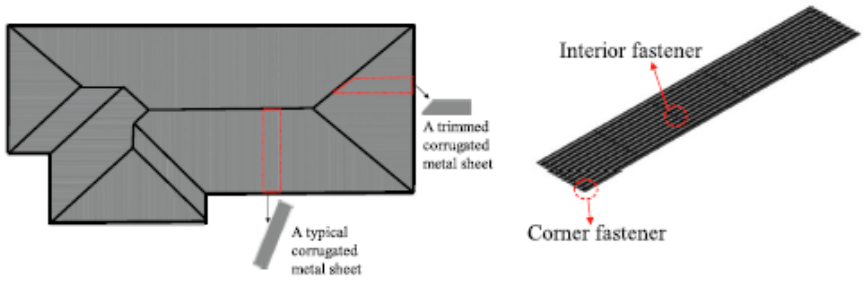

Fig. 9. Roof cladding FE model.

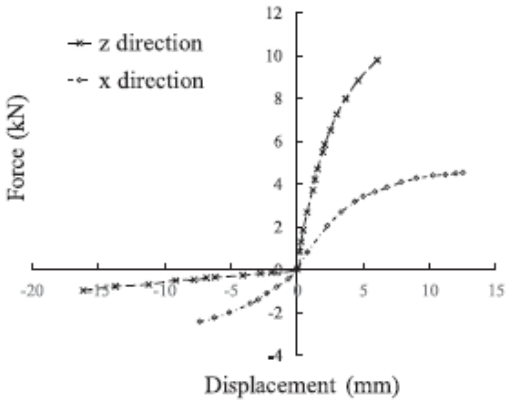

Fig. 10. Force-displacement relationship for spring elements in x and z directions for RTW connectors [42].

material properties of the truss members are assumed to be isotropic and linear-elastic with a Young's modulus of 10,000 MPa and a Poisson's ratio of 0.37 [42]. The same beam elements are used to model the double ribbon wall top plates at each side of the trusses but with a section of 70 mm × 90 mm (twice of each top plate). The wall frame below the top plates are not modelled and flexible supports are assumed to represent the attachment points of top plates to wall studs.

The triple grip connections as shown in Fig. 4 are used for the RTW connectors, which are modelled by three non-linear spring elements to characterize the connection behaviour in uplift and shear. The force-displacement relationship for the spring elements in the vertical direction (y direction in Fig. 4) is probabilistically characterized by the piecewise-linear model as described in Section 4.2. This can account for the variability in connection stiffness and strength as well as the effect of relative stiffness of RTW connectors on the load sharing and redistribution in vertical load paths. The load-deflection behaviour for the spring elements in x (i.e. along the truss) and z (i.e. normal to the truss plane) directions as shown in Fig. 4 are assumed to be deterministic as wind uplift is the focus of this study. The mean force-displacement curves depicted in Fig. 10 are used for these two spring elements [42]. These force-displacement relationships are derived from laboratory tests of triple grip RTW connectors [39] identical to those used for trusses in the representative contemporary house.

The progressive failure of CTB and BTR connectors affects the vertical load transfer for RTW connectors. For example, the loss of a roof sheet reduces the uplift loads on corresponding RTW connectors. In one MCS run, the uplift forces in BTR connectors obtained from the roof cladding FE model are applied to the roof truss FE model to evaluate the failure of RTW connectors, which accounts for the effect of failure progression of CTB and BTR connectors on the vertical load transfer to RTW connectors. Besides the uplift loads from BTR connectors, additional point loads obtained from the roof cladding FE model in the same MCS run are applied to the bottom chord of the truncated girder truss. These additional loads are derived from the sampled wind uplift loads acting on the hip and jack trusses supported by the truncated girder truss.

The top-hat battens play a major role in load sharing and redistribution of the truss system, and hence the metal battens are assembled in the roof truss FE model as shown in Fig. 11. As a secondary roof component for load sharing and redistribution, the metal roof sheeting is also assembled in the roof truss FE model in a simplified manner as opposed to the detailed modelling in the roof cladding FE model. Plane shell elements are used to approximately model the metal roof sheeting, which have the same flexural rigidity ($EI = 3.3 \times 10^3$ N·m^2 per metre

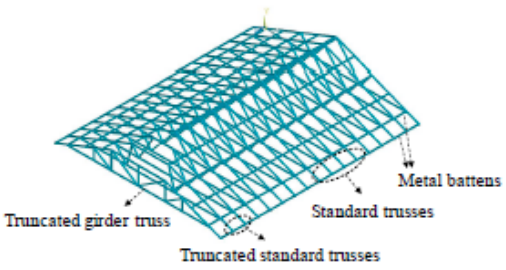

Fig. 11. Timber trusses and metal battens in the roof truss FE model.

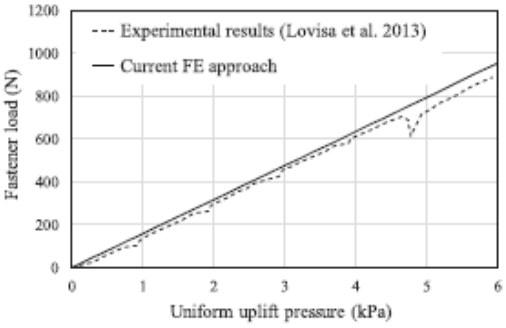

Fig. 12. Fastener load with increasing uniform uplift pressure.

width) with the corrugated metal sheets in the direction along trusses and a much smaller EI value (i.e. 1/10 of the EI value in the direction along trusses) is assumed in the direction along battens (i.e. normal to truss plane).

5.3. Model validation

5.3.1. Validation of roof cladding FE model

The roof cladding FE model is validated by the test results of a two-span corrugated metal roof sheet [27] that has the same material properties, width and fastener spacings as those used for the representative contemporary house. The same metal sheet has been modelled using the current FE approach. At the central support of the double-span metal sheet, the fastener load (largest fastener reaction) with increasing uniformly distributed uplift pressure yielded by the FE approach is compared with the experimental results as shown Fig. 12. In general, the FE analysis results agree well with the experiments in evaluating the wind uplift loads acting on cladding fasteners. The sudden drop of fastener load around 4.8 kPa in the experimental results is due to local dimpling around the fastener, which, as mentioned before, is not considered in the current FE approach for computational efficiency. In addition, the corrugated metal sheeting in non-cyclonic regions are unlikely to experience a wind pressure in excess of 4.8 kPa.

5.3.2. Validation of roof truss FE model

To demonstrate the capability of the roof truss FE model in capturing the complex load sharing mechanism and assessing the wind uplift loads acting on RTW connectors, the roof structure in the full-scale test by Satheeskumar et al. [41] (see Fig. 8) is modelled using the current FE approach, and the vertical reaction coefficients (VRCs) of RTW connectors under a static point load obtained from the FE analysis are compared with the full-scale test data. The plan view of the roof trusses and battens is shown in Fig. 13. The five trusses are labelled as

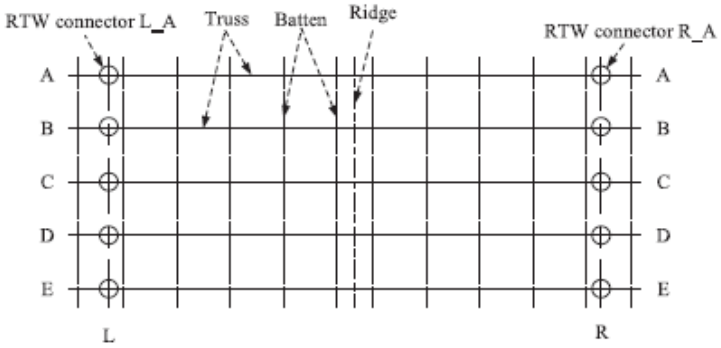

Fig. 13. Schematic diagram of the roof truss layout.

A, B, C, D and E. The RTW connectors in the left and right side of Truss A are labelled as L_A and R_A, respectively. Similar notations for RTW connectors in the other trusses (L_B, R_B, L_C, R_C, L_D, R_D, L_E, R_E). In the full-scale test, a point load of 1 kN was applied normal to the roof surface at the location of BTR connections, and the VRC of a RTW connector is defined as the ratio of the vertical connection reaction to the applied point load. The VRCs of the RTW connectors when the unit point load is applied at six locations are available in Satheeskumar et al. [41].

In the FE analysis, the model parameters of the piecewise-linear force-displacement relationship for RTW connectors are randomly sampled using statistics in Tables 3 and 4, and a total of 1000 simulation runs are carried out. The simulated VRCs of ten RTW connectors are obtained from the probabilistic FE analysis when the point load is applied at six different locations, and the results are then compared with the full-scale test data as shown in Fig. 14. As shown in Fig. 14, most of the VRCs of RTW connectors, obtained from the full-scale test, are within the 5% and 95% percentile values of the simulated VRCs. In general, the FE approach used well reproduces the load sharing of the roof system and accurately evaluates the wind uplift loads acting on RTW connectors. Discrepancies between the simulated VRCs by FE analysis and the full-scale test data tend to appear in those RTW connectors sharing a relatively small portion of applied load (i.e. VRCs within ± 0.2). These discrepancies are likely due to the difference in the stiffness of RTW connectors between the FE model and full-scale test structure. The stiffness of RTW connectors in the FE analysis is modelled based on force-displacement relationships obtained from laboratory tests for individual RTW connectors (Section 4.2), which may differ from the actual stiffness of a connection serving in a roof system (e.g. having interactions with other roof components).

6. Fragility results

6.1. Design considerations and Simulation procedure

In this section, fragility analyses for the representative contemporary house using the proposed MCS and FE approach are described. The fragilities up to gust wind speed of 80 m/s are calculated for roof cladding and trusses considering two wall opening scenarios: (i) presence of windward wall dominant openings and (ii) effectively sealed building without any wall openings. It is assumed that potential openings such as windows and/or doors are located at all four external walls, and only large openings on the windward wall exist for the dominant opening scenario. This is because windows and/or doors on windward wall are most likely to be damaged by wind pressure and/or windborne debris during a windstorm. In a baseline case, a typical size of windward wall openings (i.e. A_w) is assumed to be 8 m^2 (e.g. two 2 m × 2 m windows).

The wind direction was assumed to be uniformly distributed in 10° increments from 0° to 350° to allow for the variability of building orientation – this allows for fragilities to be assessed for a house for a specific wind speed. The fragility is expressed by the mean extent of roof sheeting loss and roof truss failures as a function of gust wind speed. A total of 1800 MCS runs are conducted for the fragility assessment (50 runs for each 10° increment of wind attack angle), which, according to a convergence check, is deemed to be acceptable. To conduct the MCS, a total of 50 sets of connection resistances were randomly generated to represent 50 house samples. For each house sample, a wind speed (starting at 30 m/s) and a building orientation (or wind angle relative to building axis, starting at 0°) were selected. The wind loading parameters in Eq. (3) were then randomly generated as inputs to the FE model for damage assessment. For every house sample, this procedure was repeated for each wind speed (30–80 m/s with 1 m/s interval). The MCS process was then repeated for each building orientation (0–350° with 10° interval). The mean extent of roof damage at a given wind speed was then obtained from aggregated results over all building orientations and house samples. The MCS and the FE approach for the representative contemporary house includes 1646 cladding-to-batten (CTB), 532 batten-to-rafter/truss (BTR) and 38 rafter/truss-to-wall (RTW) connectors.

According to AS4055 [3], most suburban houses in Brisbane have a design wind classification of N2 or N3 excluding those built on the top-third zone of a hill, ridge or escarpment, whereas a design wind classification of N1 or N2 is appropriate for most suburban houses in Melbourne. The design and construction considerations for RTW connectors of the representative contemporary house in Brisbane and Melbourne are given in Table 5, which conforms to AS 1684.2 [2]. Note that the CTB and BTR connections are generally identical for houses in Brisbane and Melbourne. The design and construction considerations for RTW connections in Table 5 is only one option that satisfies housing standards. Other construction practices are not taken into account.

6.2. Simulation results

6.2.1. Baseline scenarios

The fragility curves for the representative contemporary house built in the suburbs of Brisbane and Melbourne considering two wall opening scenarios are shown in Fig. 15. As indicated in Fig. 15, both the roof cladding and truss fragilities corresponding to the windward wall dominant opening scenario are much higher than those without any wall openings. This is expected because the house suffers much higher internal pressures when large openings appear in the windward wall.

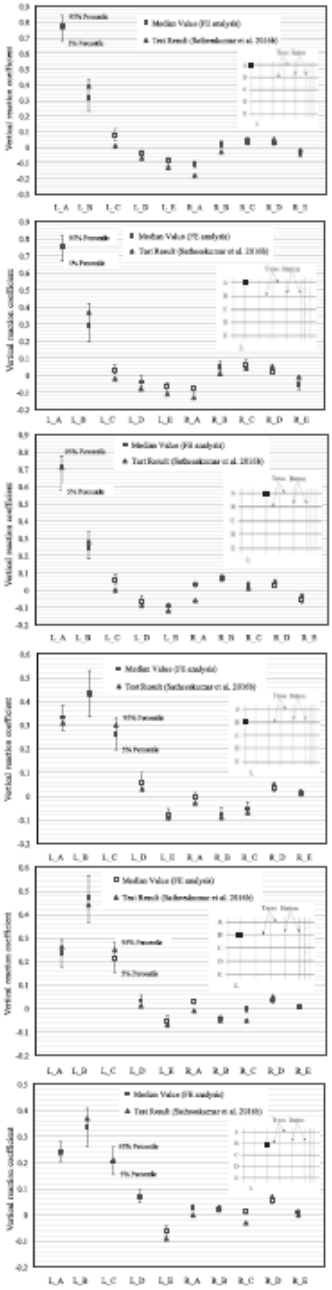

Fig. 14. Comparison of simulated VRCs with full-scale test data at six point load locations (solid square represents the location where the point load acts on).

The design wind speed corresponding to a 500-year return period for Brisbane is 57 m/s (AS/NZS 1170.2 [4]). At this gust wind speed, the mean roof sheeting loss for the representative contemporary house is 4.5% with windward wall dominant openings and only 0.1% for the scenario without any wall openings. While the latter loss is insignificant, the former may result in a considerable economic loss. For example, a loss of roughly 15% of the total building and contents value can result from a 4.5% roof sheeting loss as inferred from Stewart et al. [46]. The mean proportion of roof sheeting loss at the 500-year gust wind speed of Melbourne, i.e. 45 m/s (AS/NZS 1170.2 [4]), is negligible for both wall opening scenarios. Note that the obtained fragility curves in Fig. 15 apply to houses located on a flat, level site and subjected to wind coming from the prevailing direction (i.e. the nominal values used for the topographic and directional factor in Eq. (3) are unity). However, these fragility curves have the flexibility to account for other wind directions and topographic conditions. Site-specific wind directional multipliers for eight cardinal directions given in AS/NZS 1170.2 [4] can be multiplied to the wind speed to account for non-prevailing wind directions, which is to be incorporated in a future study for housing vulnerability assessment and loss estimation. The mean roof damage for a different topographic condition can be obtained using the same fragility curves shown in Fig. 15. For example, at a wind speed of 55 m/s, the mean roof sheeting loss read from the fragility curve is about 3% (dominant opening scenario). For a house on a slope of a hill, assuming a topographic factor of 1.10 (the exact value can be calculated according to AS/NZS 1170.2 [4] for a specific site condition), then the mean roof sheeting loss is about 8% that is obtained from the fragility curve at the adjusted wind speed, i.e. $55 \times 1.10 = 60.5$ m/s.

The mean proportion of roof truss failures for the representative contemporary house built in Brisbane at the 500-year design wind speed (i.e. 57 m/s) with windward wall dominant openings is 3.3% and 0.6% for wind classifications N2 and N3, respectively. At the 500-year gust wind speed for Melbourne (i.e. 45 m/s), the mean proportion of roof truss failures for suburban house in Melbourne with windward wall dominant openings is 0.2% and 0.1% for wind classifications N1 and N2, respectively, which is deemed as negligible damage. In the scenarios that no wall openings exist, the mean proportions of roof truss failures for both Brisbane and Melbourne houses at the 500-year design gust wind speed are less than 1%.

Table 6 shows the mean number of failed CTB, BTR and RTW connectors for the dominant opening scenario at various gust wind speeds. This table suggests that more CTB connectors fail under wind uplift pressure than BTR connectors, which is expected as damage surveys (e.g. [24]) reveal that roof sheeting loss is mostly due to cladding fastener failures. As expected, the failure of RTW connectors initiates only at relatively higher wind speeds.

6.2.2. *Sensitivity analyses*

A lower COV value (50% of the value used in the baseline case as mentioned in Section 4.1.2) is considered to show the sensitivity of fragilities to internal pressure variability. As illustrated in Fig. 16, the mean proportion of roof sheeting loss and roof truss failures decreases slightly as the variability in the internal pressure coefficient reduces. The size of windward wall dominant openings can also affect the internal pressure modeling. Hence, $A_{uo} = 4$ and $12\ m^2$ are assumed in addition to the baseline case ($A_{uo} = 8\ m^2$). The effects of these dominant opening sizes on wind fragilities for the windward wall dominant opening scenario are shown in Fig. 17. It is indicated that a larger size of windward wall openings (A_{uo}) leads to higher wind damage, which is expected as the internal pressure increases with A_{uo}.

The relative stiffness due to variable stiffness of RTW connectors affect the load sharing in a roof truss assembly [51], and consequently influences the roof truss fragility for the representative contemporary

Table 5
Design and construction considerations for RTW connectors based on AS4055 [3] and AS 1684.2 [2].

Wind classification	Location	RTW connectors	
		Standard/truncated standard truss	Truncated girder truss
N1	Melbourne	One gun nail triple grip	One gun nail triple grip
N2	Melbourne/Brisbane	One gun nail triple grip	Two gun nail triple grips
N3	Brisbane	One hand nail triple grip	Two hand nail triple grips

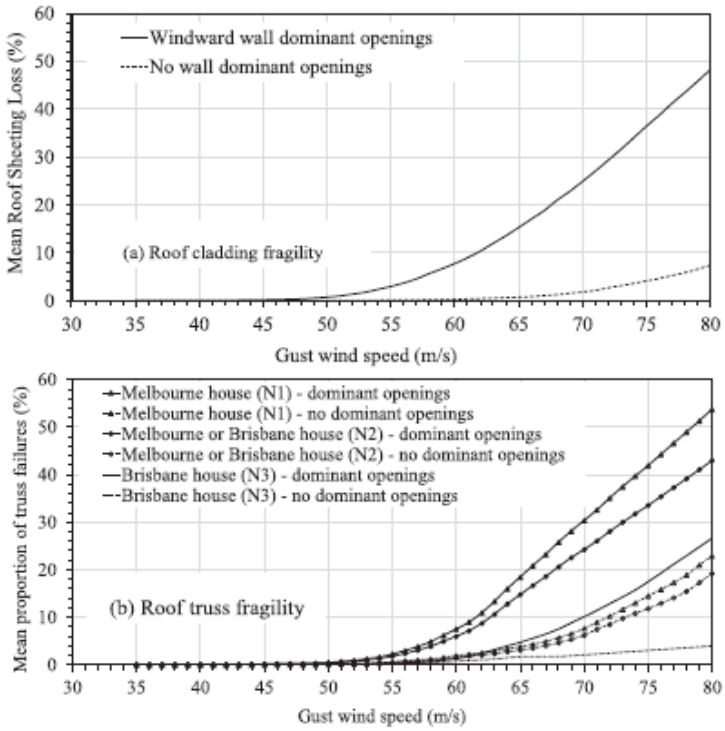

Fig. 15. Fragility curves for roof cladding and trusses for two wall opening scenarios.

house. Hence, the effect of strength variability and relative stiffness of RTW connectors on the mean proportion of roof truss failures is examined by assuming four scenarios for the connection behaviour. The baseline scenario adopts the probabilistic piecewise-linear model for RTW connectors as described in Section 4.2. The second scenario assumes a deterministic piecewise-linear force-displacement relationship as shown in Fig. 6 (the mean curve) for all the RTW connectors (i.e. COV = 0 for k_0, F_u and δ_u). The third scenario assumes that the initial secant stiffness (k_0) and the displacement at peak load (δ_u) for RTW connectors are random variables and the uplift capacity is deterministic (i.e. COV = 0 for F_u). In the fourth scenario, only the uplift capacities for RTW connectors are assumed to be probabilistic (i.e. COV = 0 for k_0 and δ_u).

The fragility curves for roof truss failure with windward wall dominant openings are depicted in Fig. 18 for these four scenarios. As expected, the fragilities corresponding to the fully deterministic scenario are the lowest, which indicates that ignoring the variability in stiffness and uplift capacity for RTW connectors leads to an

Table 6
Mean number of failed roof connections for the dominant opening scenario.

Wind speed (m/s)	Cladding-to-batten (CTB)	Batten-to-rafter/truss (BTR)	Rafter/truss-to-wall (RTW)		
			N1	N2	N3
40	0	0	0	0	0
50	8 (0.5%)	1 (0.2%)	1 (2.6%)	0	0
60	62 (3.8%)	4 (0.8%)	4 (10.5%)	3 (7.9%)	0
70	192 (11.7%)	11 (2.1%)	12 (31.6%)	10 (26.3%)	3 (7.9%)

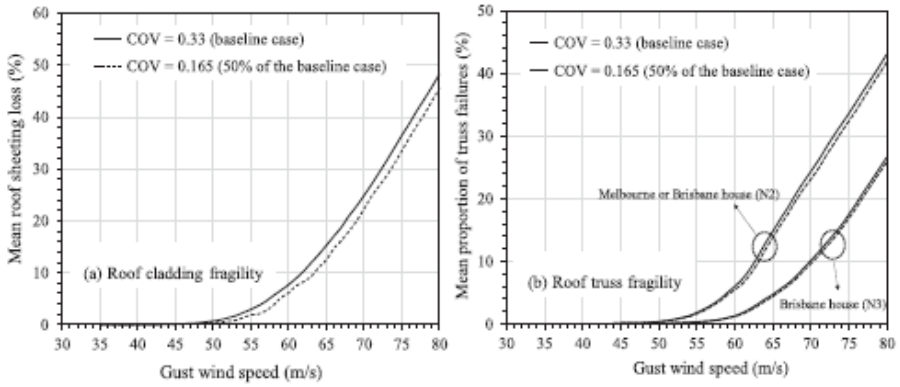

Fig. 16. Fragility curves considering different degrees of variability in the internal pressure coefficient for the windward wall dominant opening scenario.

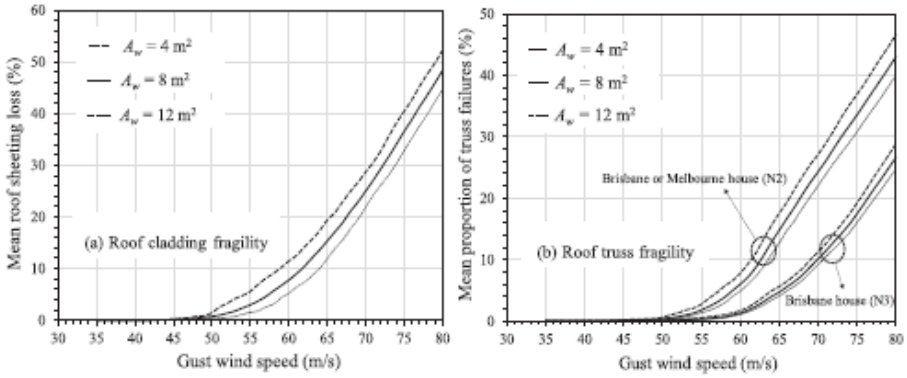

Fig. 17. Fragility curves considering different opening sizes for the windward wall dominant opening scenario.

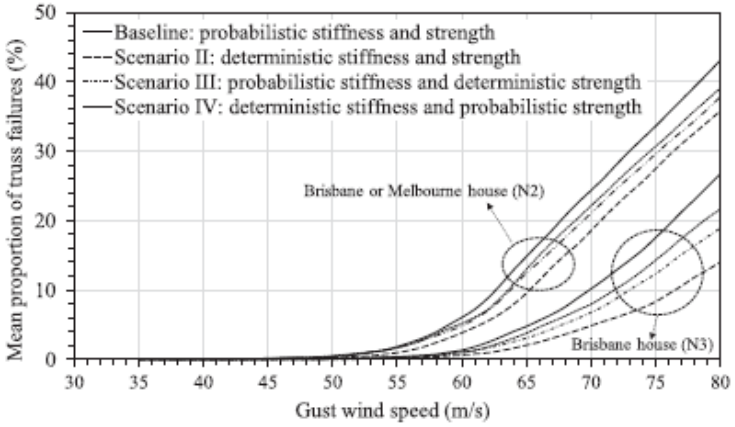

Fig. 18. Fragility curves for roof truss failure considering different scenarios for stiffness and strength variability of RTW connectors with windward wall dominant openings.

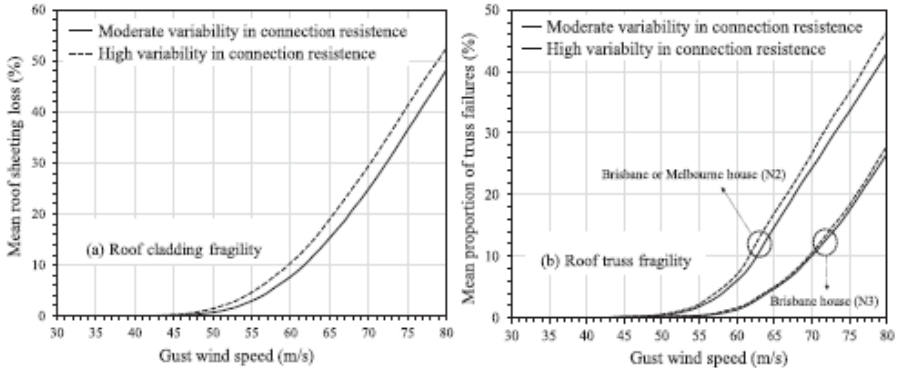

Fig. 19. Fragility curves considering different degrees of variability in connection resistances for the windward wall dominant opening scenario.

underestimation of roof truss failure. The fragility curves corresponding to the third and fourth scenarios suggest that both the variability in stiffness and uplift capacity of RTW connectors influence the roof truss fragilities. The variability in uplift capacity of RTW connectors has more impact on the mean proportion of roof truss failures than the stiffness variability of triple grip connections.

The COV values for connection capacities in Tables 2 and 3 are considered for a good construction quality in the installation of roof connections. Poor installation practice often results in a relatively high proportion of improperly installed CTB, BTR and RTW connectors. For example, Boughton et al. [6] found that over-driving batten fasteners to timber rafter/truss leads to lower withdrawn capacities and higher variability in both withdrawn and pull-through strength. For triple grip RTW connectors, missing nails and grouping nails are common construction defects [40] that reduces connection capacities. The effect of construction quality on fragility assessment is examined by considering a higher variability in connection resistances. The COV values in Tables 2 and 3 are increased by 25% to represent a higher variability in connection resistances considering a relatively poor quality in construction practice. The original COV values are considered as a moderate resistance variability for an average construction quality. Fig. 19 suggests that more roof damage is predicted by the fragility assessment as resistance variability increases. This is expected as higher variability results in a larger number of weak connections with relatively low resistances, and connection failures are more likely to initiate at these 'weakest links'. A preliminary defect model was developed by Stewart et al. [46], however, there is a need to develop a more detailed construction defect model in the fragility assessment that includes observed construction error rates, Bayesian updating, and how they affect the mean and COV of connection resistance.

7. Future work

A detailed model for the damage of windows and/or doors by high wind pressure and windborne debris needs to be incorporated in the current reliability-based fragility method. Further validations of the fragility results using post-damage observations and insurance data, if available, are needed. Damage accumulation during a windstorm with varying wind directions or from multiple windstorms need to be further incorporated in the wind damage assessment. Based on the proposed reliability-based fragility model, a risk assessment can be further conducted to assess the economic losses and risks due to wind damage to roof cladding and trusses. In the risk assessment, stochastic wind field model can be further integrated with the fragility curves that will allow different prevailing wind directions in Melbourne and Brisbane. The effect of climate change on wind damage risks can also be investigated based on the developed fragility method. A cost-benefit analysis is then needed to evaluate the cost-effectiveness of relevant risk reduction and climate adaptation measures for wind hazard mitigation.

8. Conclusions

This paper developed a reliability-based fragility method to evaluate the roof sheeting loss and roof truss failure for contemporary housing under wind uplift pressure in non-cyclonic regions of Australia. The fragility analysis considered the roof damage due to overloading of cladding-to-batten (CTB), batten-to-rafter/truss (BTR) and rafter/truss-to-wall (RTW) connectors. The spatially varying wind uplift pressure and connection resistances were probabilistically modelled, and a FE approach was proposed to evaluate the structural response, load redistribution and progressive failure of roof connections. A MCS analysis in conjunction with the FE approach were employed to carry out the fragility assessment. It was found that, if no wall dominant opening exists, the mean proportion of roof sheeting loss and roof truss failures is negligible under a 500-year return period wind speed. When subjected to windward wall dominant openings, considerable roof sheeting loss and roof truss failure are predicted at the 500-year gust wind speed for Brisbane. Increasing the COV values for connection resistances leads to higher wind fragilities, which indicates that the construction quality may have a significant influence on the fragility assessment.

Acknowledgements

The financial support from the Australian Government Research Training Program Scholarship is greatly acknowledged. We would like to thank Dr. Satheeskumar for providing the force-displacement curves from his triple grip tests at the Cyclone Testing Station (James Cook University) as well as the helpful discussions on this study. The support from Mr. Aaron Scott for high performance computing at The University of Newcastle is greatly appreciated. We would like to thank the two anonymous reviewers for their helpful suggestions and comments.

References

[1] ANSYS Inc. ANSYS mechanical APDL introductory tutorials. USA: Canonsburg, PA; 2013.
[2] AS 1684.2. Residential timber-framed construction. Sydney: Standards Australia; 2010.
[3] AS 4055. Wind loads for housing. Sydney: Standards Australia; 2012.
[4] AS/NZS 1170.2. Structural design actions, Part 2: wind actions. Sydney: Standards Australia; 2011.
[5] BITRE. About Australia's regions. Canberra, Australia: Bureau of Infrastructure,

Transport and Regional Economics; 2008.
[6] Boughton GN, Falck DK, Vinh Nghi Duong A, Pham S, Nguyen A. Static testing of batten connections at university of Western Australia Technical Report No62 Cyclone Testing Station, James Cook University; 2015.
[7] Ellingwood BR, Rosowsky DV, Li Y, Kim JH. Fragility assessment of light-frame wood construction subjected to wind and earthquake hazards. J Struct Eng 2004;130(12):1921–30.
[8] Gavanski E, Kopp GA. Fragility assessment of roof-to-wall connection failures for wood-frame houses in high winds. ASCE-ASME J Risk Uncertainty Eng Syst, Part A: Civil Eng 2017;3(4):04017013.
[9] Gavanski E, Kopp GA, Hong HP. Reliability analysis of roof sheathing panels on wood-frame houses under wind loads in Canadian cities. Can J Civ Eng 2014;41(8):717–27.
[10] Ginger JD, Letchford CW. Characteristics of large pressures in regions of flow separation. J Wind Eng Ind Aerodyn 1993;49(1):301–10.
[11] HAZUS. Multi-hazard loss estimation methodology - hurricane model, Hazus–MH 2.1 Technical Manual Washington, D.C: Federal Emergency Management Agency, Mitigation Division; 2014.
[12] Henderson D, Williams C, Gavanski E, Kopp GA. Failure mechanisms of roof sheathing under fluctuating wind loads. J Wind Eng Ind Aerodyn 2013;114:27–37.
[13] Henderson DJ, Ginger JD. Vulnerability model of an Australian high-set house subjected to cyclonic wind loading. Wind Struct 2007;10(3):269–85.
[14] Ho TCE, Surry D, Morrish D, Kopp GA. The UWO contribution to the NIST aerodynamic database for wind loads on low buildings: Part 1. Archiving format and basic aerodynamic data. J Wind Eng Ind Aerodyn 2005;93(1):1–30.
[15] Holmes JD. Wind loads and limit states design. Civil Eng Trans, Inst Eng Australia, CE 1985;27(1):21–6.
[16] Holmes JD. Wind loading of structures. 3rd Edition Florida, USA: CRC Press Boca Raton; 2015.
[17] Holmes JD, Cochran LS. Probability distributions of extreme pressure coefficients. J Wind Eng Ind Aerodyn 2003;91(7):893–901.
[18] Jayasinghe NC, Ginger JD. Vulnerability of roofing components to wind loads. Wind Struct 2011;14(4):321–35.
[19] Ji X, Huang G, Zhang X, Kopp GA. Vulnerability analysis of steel roofing cladding: Influence of wind directionality. Eng Struct 2018;156:587–97.
[20] Konthesingha KC, Stewart MG, Ryan P, Ginger J, Henderson D. Reliability based vulnerability modelling of metal-clad industrial buildings to extreme wind loading for cyclonic regions. J Wind Eng Ind Aerodyn 2015;147:176–85.
[21] Kopp GA, Morrison MJ, Henderson DJ. Full-scale testing of low-rise, residential buildings with realistic wind loads. J Wind Eng Ind Aerodyn 2012;104:25–39.
[22] Kopp GA, Oh JH, Inculet DR. Wind-induced internal pressures in houses. J Struct Eng 2008;134(7):1129–38.
[23] Lee KH, Rosowsky DV. Fragility assessment for roof sheathing failure in high wind regions. Eng Struct 2005;27(6):857–68.
[24] Leitch C, Ginger J, Harper B, Kim P, Jayasinghe N, Somerville L. Investigation of performance of housing in Brisbane following storms on 16 and 19 November 2008 Technical Report No 55 Cyclone Testing Station, James Cook University; 2009.
[25] Li Y, Ellingwood BR. Hurricane damage to residential construction in the US: Importance of uncertainty modeling in risk assessment. Eng Struct 2006;28(7):1009–18.
[26] Liu PL, Der Kiureghian A. Multivariate distribution models with prescribed marginals and covariances. Probab Eng Mech 1986;1(2):105–12.
[27] Lovisa AC, Wang VZ, Henderson DJ, Ginger JD. Development and validation of a numerical model for steel roof cladding subject to static uplift loads. Wind Structures 2013;17(5):495–513.
[28] Lysaght. TOPSPAN Design and Installation Guide for Building Professionals. Australia: Bluescope Lysaght; 2014. 23 July 2014.
[29] Mahendran M. Behaviour and design of crest-fixed profiled steel roof claddings under wind uplift. Eng Struct 1994;16(5):368–76.
[30] Pan F, Cai CS, Zhang W. Wind-induced internal pressures of buildings with multiple openings. J Eng Mech 2012;139(3):376–85.
[31] Parackal KI, Humphreys MT, Ginger JD, Henderson DJ. Wind loads on contemporary Australian housing. Aust J Struct Eng 2016;17(2):136–50.
[32] Peng X, Yang L, Gavanski E, Gurley K, Prevatt D. A comparison of methods to estimate peak wind loads on buildings. J Wind Eng Ind Aerodyn 2014;126:11–23.
[33] Pinelli JP, Gurley KR, Subramanian CS, Hamid SS, Pita GL. Validation of a probabilistic model for hurricane insurance loss projections in Florida. Reliab Eng Syst Saf 2008;93(12):1896–905.
[34] Pinelli JP, Pita G, Gurley K, Torkian B, Hamid S, Subramanian C. Damage characterization: application to Florida public hurricane loss model. Nat Hazard Rev 2011;12(4):190–5.
[35] Pinelli JP, Simiu E, Gurley K, Subramanian C, Zhang L, Cope A, et al. Hurricane damage prediction model for residential structures. J Struct Eng 2004;130(11):1685–91.
[36] Reardon GF. Simulated wind loading of full size houses. Proc. Int. Seminar: The Role of Large and Full Scale Testing. London, UK: Inst. of Struct. Eng. City University; 1996.
[37] Rocha D, Eamon CD, Murphy JF. Reliability analysis of roof sheathing panels exposed to a hurricane wind. Struct Saf 2011;33(1):74–81.
[38] Rosowsky DV, Cheng N. Reliability of light-frame roofs in high-wind regions. I: wind loads. J Struct Eng 1999;125(7):725–33.
[39] Satheeskumar Navaratnam. Wind load sharing and vertical load transfer from roof to wall in a timber-framed house PhD thesis Australia: James Cook University; 2016.
[40] Satheeskumar N, Henderson DJ, Ginger JD, Wang CH. Wind uplift strength capacity variation in roof-to-wall connections of timber-framed houses. J Archit Eng 2016;22(2):04016003.
[41] Satheeskumar N, Henderson DJ, Ginger JD, Humphreys MT, Wang CH. Load sharing and structural response of roof–wall system in a timber-framed house. Eng Struct 2016;122:310–22.
[42] Satheeskumar N, Henderson DJ, Ginger JD, Wang CH. Three-dimensional finite-element modeling and validation of a timber-framed house to wind loading. J Struct Eng 2017;143(9):04017112.
[43] Sivapathasundaram M, Mahendran M. Development of fragility curves for localised pull-through failures of thin steel roof battens. Eng Struct 2016;124:64–84.
[44] Smith D, Henderson D, Ginger J, Wehner M, Ryu H, Edwards M. Improving the resilience of existing housing to severe wind events: Annual project report 2015-2016. Bushfire and Natural Hazards CRC; 2016.
[45] Stewart MG. Climate change impact assessment of metal-clad buildings subject to extreme wind loading in non-cyclonic regions. Sust Resilient Infrastruct 2016;1(1–2):32–45.
[46] Stewart MG, Ginger JD, Henderson DJ, Ryan PC. Fragility and climate impact assessment of contemporary housing roof sheeting failure due to extreme wind. Eng Struct 2018;171:464–75.
[47] Torkian Boback, Pinelli Jean-Paul, Gurley Kurtis, Hamid Shahid. Cost-and-benefit evaluation of windstorm damage mitigation techniques in Florida. Nat Hazard Rev 2014;15:150–7.
[48] Tieleman HW, Elsayed MA, Ge Z, Hajj MR. Extreme value distributions for peak pressure and load coefficients. J Wind Eng Ind Aerodyn 2008;96(6):1111–23.
[49] Vickery PJ, Skerlj PF, Lin J, Twisdale Jr LA, Young MA, Lavelle FM. HAZUS-MH hurricane model methodology. II: Damage and loss estimation. Nat Hazard Rev 2006;7(2):94–103.
[50] Walker GR. Report on cyclone tracy-effect on buildings–dec1974. Hawthorn, Australia: Australian Dept. of Housing and Construction; 1975.
[51] Wolfe RW, McCarthy M. Structural performance of light-frame roof assemblies: I. Truss assemblies with high truss stiffness variability FPL-RP-492 Madison (WI): Forest Products Laboratory, USA; 1989.
[52] Woods AR, Blackmore PA. The effect of dominant openings and porosity on internal pressures. J Wind Eng Ind Aerodyn 1995;57(2–3):167–77.
[53] Xu YL, Reardon GF. Behaviour of different profiled roofing sheets subject to wind uplift Technical Report No37 Cyclone Testing Station, James Cook University; 1992.

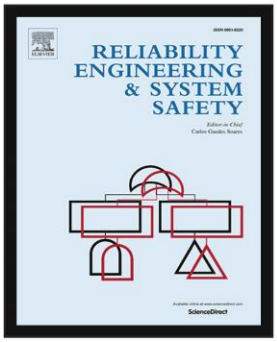

Construction Defects and Wind Fragility Assessment for Metal Roof Failure: a Bayesian Approach

Hao Qin , Mark G. Stewart

PII: S0951-8320(19)30461-2
DOI: https://doi.org/10.1016/j.ress.2019.106777
Reference: RESS 106777

To appear in: *Reliability Engineering and System Safety*

Received date: 4 April 2019
Revised date: 22 October 2019
Accepted date: 22 December 2019

Please cite this article as: Hao Qin , Mark G. Stewart , Construction Defects and Wind Fragility Assessment for Metal Roof Failure: a Bayesian Approach, *Reliability Engineering and System Safety* (2019), doi: https://doi.org/10.1016/j.ress.2019.106777

Highlights

- Probabilistic modelling of construction defects in housing.
- Bayesian approach combining expert opinion, HRA method and limited defect data.
- Integration of construction defect model into wind fragility assessment.
- Considerable effect of construction defects on roof cladding fragility is predicted.

Construction Defects and Wind Fragility Assessment for Metal Roof Failure: a Bayesian Approach

Hao Qin*
PhD Candidate, Centre for Infrastructure Performance and Reliability
The University of Newcastle, New South Wales, 2308, Australia
hao.qin@uon.edu.au

Mark G. Stewart
Professor and Director, Centre for Infrastructure Performance and Reliability
The University of Newcastle, New South Wales, 2308, Australia
mark.stewart@newcastle.edu.au

Revised 22 Oct 2019

Abstract

Post-damage observations reveal that construction error is one of the major contributors to roof damage for houses subjected to extreme winds. In this study, a Bayesian approach was developed to probabilistically quantify the construction defect rates in roof connections, which enables a systematic integration of expert judgement, human reliability analysis (HRA) techniques and limited construction defect data. The reductions of uplift capacities for defective roof connections were also probabilistically modelled based on experimental evidence and engineering judgement. The developed construction defect model was incorporated in a reliability-based fragility method to assess the wind damage to metal roof cladding and timber roof trusses for contemporary houses in non-cyclonic regions of Australia. It was found that, the effects of construction defects are significant for the predicted roof cladding fragility, whereas for roof truss fragility, such effects are lower.

Keywords: Construction defects; Contemporary houses; Roof connections; Fragility assessment; Bayesian method; Human reliability analysis

1. Introduction

It has been widely acknowledged that the occurrence of human error during design and construction may significantly reduce the reliability of structures (Ellingwood 1987; Stewart & Melchers 1988; Stewart 1992, 1993). In line with this statement, damage surveys have indicated that wind damage to housing in Australia often occurs at peak gust wind speeds below the corresponding design wind speed (e.g. Ginger et al. 2010; Smith et al. 2016). This is mainly due to the commonly observed defects in housing construction, and most defects occur in tie-down fixings/connections (Leitch et al. 2009; Ginger et al. 2010; Ginger et al. 2015), the effects of which have not been accounted for in most reliability/fragility assessments. Similar findings have been observed in North American houses (e.g. Yazdani et al. 2010) where damage during windstorms are largely due to construction defects. Wind damage is more likely to initiate on defective house components, which causes load redistribution to other components and may trigger a cascading failure. Clearly, ignoring construction defects in wind damage prediction leads to an underestimation of structural failure. Therefore, when conducting fragility/vulnerability assessment for houses subjected to extreme wind, it is essential to include the effects of construction defects (Stewart et al. 2018).

The modelling of construction defects in housing is a challenging task, which requires the quantification of defect rates and their consequent effects on structural performance. Human behaviour and performance are complex in nature, and the occurrence of human error depends on many psychological, physiological and sociological factors. Moreover, statistical data regarding defect rates in housing construction and their corresponding influence on structural resistance are scarce because housing damage is rarely (if at all) subject to a detailed forensic analysis that records individual defects, their location, and their frequency. Due to the complex error mechanism and a lack of data, it is not surprising that only a few

studies attempt to include construction defects in the reliability/fragility assessment for houses under extreme wind (van de Lindt & Dao 2010; Hong & He 2015; Stewart et al. 2018). van de Lindt & Dao (2010) examined the effect of missing nails on the wind fragility of timber roof sheathing panels that are commonly used in North American houses. Their study used a scenario-based approach by assuming various missing nail patterns. The quantitative estimation of error occurrence was not included in their work. Hong & He (2015) investigated the effect of missing and/or misaligned nails on the reliability of Canadian timber roof sheathing panels under wind uplift loading. This study adopted a constant defect rate which was obtained from the construction of a full-scale test house built by students in the laboratory. The uncertainty and variability involved in the occurrence of construction error may not have been well addressed given that there was only a single house specimen and it was constructed in a laboratory environment. Stewart et al. (2018) incorporated a preliminary probabilistic model of construction defects into the fragility assessment for metal roof sheeting failure due to extreme wind. This defect model was built on subjective information and defect data inferred from Hong & He (2015) that may not suit metal roof cladding fastened using screws instead of nails. In additional to wind fragility, Kim & Rosowsky (2005) examined the effects of missing fasteners in shear walls on the seismic fragility of wood-frame structures, and found significant influences of construction quality on shear wall behaviour.

To improve the modelling of construction defects, it is desirable to address the underlying mechanism of human error, uncertainties in error occurrences and consequences as well as the scarcity of construction error data. To this end, the present study proposes a Bayesian approach to probabilistically quantify the defect rates in housing construction. The Bayesian method is appealing for the modelling of construction defects as it enables a systematic integration of expert judgement, human reliability analysis (HRA) models and limited

construction defect data. A Cognitive Reliability and Error Analysis Method (CREAM) (Hollnagel 1998), is applied in conjunction with expert judgement to assign the prior distributions for defect rates in a Bayesian framework. CREAM is a HRA technique with the capability to model cognitive aspects in human error (Hollnagel 1998). It provides both qualitative and quantitative predictions of human reliability which can be practically fitted into a probabilistic risk assessment (PRA). In addition, most HRA methods are largely applied to hazardous industries such as nuclear power and aviation (e.g. THERP, SPAR-H). CREAM is a generic approach, and has detailed and appropriate task representation and decomposition based on human cognition. CREAM has been widely used to deal with human error in various engineering fields including operator performance in nuclear power plants (e.g. He et al. 2008; Lee et al. 2011), marine engineering (e.g. Yang et al. 2013; Akyuz & Celik 2015), civil infrastructure management (Nan & Sansavini 2016; Nan & Sansavini 2017) and structural design (De Haan et al. 2013). To be sure, other HRA methods may also be used, however, this paper presents a framework that can be readily adapted to other HRA methods. Bayesian updating is carried out using incomplete and imperfect defect data in housing construction collected from existing literature and field observations. The defect data include the observed occurrence rates of missing and/or improperly installed roof connections in Australian contemporary housing. Wind uplift capacities for defective roof connections are also obtained from experimental studies for housing in Australia.

A reliability-based fragility method was recently developed by Qin & Stewart (2019) to evaluate the metal roof failure due to overloading of roof connections for contemporary houses in non-cyclonic regions of Australia without considering construction defects. However, this fragility model can readily adapt to the change of structural response and the reduction of structural resistance given (i) the occurrence rate and (ii) the magnitude of capacity reduction for construction defects. To this end, the probabilistic defect rates obtained

from the Bayesian inference and the weakened roof components due to construction errors are subsequently incorporated into the reliability-based fragility assessment. This provides a rational and systematic method to probabilistically characterise the effects of construction defects on the wind fragility of roof systems for Australian contemporary housing. The combination of HRA methods and sparse human performance data through a Bayesian framework has been originally advocated in the PRA for nuclear power plants (e.g. Hallbert & Kolaczkowski 2007; Podofillini & Dang 2013; Groth et al. 2014), and in this study it is modified to the new application in construction defect modelling and wind fragility assessment for housing.

2. Construction Defects in a Metal Roof

The present study aims to incorporate the effects of construction defects into the fragility assessment for metal roof failure due to wind uplift in non-cyclonic regions of Australia. Roof connections are generally the 'weakest links' of the roof system (Henderson & Ginger 2007), and damage surveys (e.g. Leitch et al 2009) have revealed that most roof failures occurred to contemporary houses are caused by poor construction details of roof tie-down fixings. In light of this, the construction defects considered herein are missing and/or improperly installed roof connections, which are commonly observed in housing construction (e.g. Ginger et al. 2010).

A representative contemporary house (Parackal et al. 2016; Stewart et al. 2018; Qin & Stewart 2019) is used in this study to illustrate the application of the proposed construction defect model to a fragility analysis. The dimensions, shape and construction type of the house were determined by field surveys completed by the Cyclone Testing Station (CTS) at James Cook University (JCU) (Parackal et al. 2016). The median values of house plans and features from the survey such as footprint dimensions, roof pitch and wall heights were selected to determine the configuration of the representative contemporary house. Figure 1 shows the 3D

and plan view of the representative one-story house. It is a timber-framed construction with 21.5° timber roof trusses at 600 mm spacings on a complex hip-end roof. Trusses are arranged with standard trusses in the middle part of the roof and jack trusses connected to truncated girder trusses at the hip ends. Roof cladding is 762 mm wide corrugated metal sheeting. Metal top-hat battens are attached to timber roof trusses at 900 mm spacings. More details of the representative contemporary house can be found in Parackal et al. (2016).

2.1 Typical defect types for roof connections

This study considers the most common types of construction defects in cladding-to-batten (CTB), batten-to-rafter/truss (BTR) and rafter/truss-to-wall (RTW) connectors for the representative contemporary house. Schematic diagrams for the three types of roof connections are depicted in Fig. 2. The typical defect types for these roof connections are inferred from various research reports and post-damage surveys (e.g. Leitch et al. 2009; Ginger et al. 2010; Ginger et al. 2015; Boughton et al. 2015; Satheeskumar 2016), and are listed in Table 1. The representative contemporary house has a total number of $n_1 = 1646$ CTB, $n_2 = 532$ BTR and $n_3 = 92$ RTW connectors. For a single BTR connector, it is possible that one screw fastener is missing and the other is improperly installed. However, this situation is highly unlikely to occur (extremely small probability), and therefore the two defect types considered for BTR connectors are reasonably assumed to be mutually exclusive.

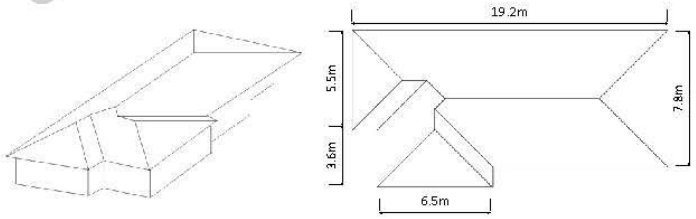

(a) 3D view (b) Plan view

Figure 1. One-story representative contemporary house.

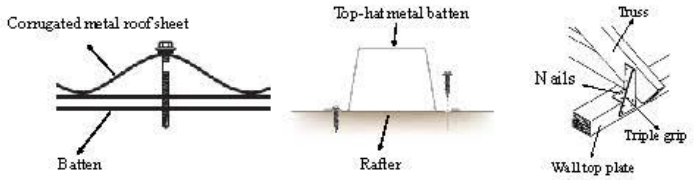

(a) CTB connector (b) BTR connector (c) RTW connector

Figure 2. Roof connections used for the representative contemporary house.

Table 1. Typical types of construction defects in roof connections.

Connection type	Description	Defect type
Cladding-to-batten (CTB)	Each CTB connector has one screw fastener, connecting corrugated metal roof sheets to top-hat metal battens	Missing (screw not installed) Improper installation (screw unattached to batten or over- and under-driven screws)
Batten-to-rafter/truss (BTR)	Each BTR connector has two screw fasteners, one at each bottom flange of the top-hat batten, connecting metal battens to timber roof trusses	Missing (one or both screws not installed) Improper installation (over- and under-driven screws)
Rafter/truss-to-wall (RTW)	Triple grip framing anchors, fastening timber roof trusses to wall top plates with nails	Missing one or two nails

2.2 Construction defect data

The construction error data of interest are the occurrence rates of defects and the reduction of uplift capacities for defective roof connections. However, only limited construction defect data for roof connections are available, which may base error quantification on insufficient objective information.

A 1.5% defect rate (per nail) for installing nails on timber roof sheathing panels was obtained in Hong & He (2015) by inspecting a full-scale North American house built by students in the laboratory. This data provides an indication for missing nails on roofing, however, it cannot be directly employed for missing and/or improperly installed CTB connectors (screw fasteners) on Australian contemporary houses because the construction methods are quite different. In this paper, the average occurrence rate of missing cladding

fasteners (i.e. CTB connectors) is obtained from field observations of as-built contemporary houses in the suburbs of Newcastle, Australia. It is not unreasonable to assume the average construction quality in Newcastle is similar to those in other Australian cities. A total of ten metal-clad contemporary houses were visually inspected by the first author. These houses are newly built with ages less than five years old. Due to the limited accessibility, for each house specimen, only the viewable parts of metal roof cladding were inspected from the street. Figure 3 shows sample photos of the inspected roof area with missing screw fasteners. The number of inspected fastener locations and the number of missing screws were recorded for each house. Fastener locations refer to the positions on metal roof sheeting where a screw fastener is required. Screw fasteners should be used to fix cladding at every 2nd corrugation of the roof edge and every 3rd or 4th corrugation for other regions of the roof. The missing fastener data obtained for the ten randomly selected contemporary houses are shown in Table 2. In total, 3,368 fastener locations were visually inspected, and 13 positions were found to have missing screw fasteners. This corresponds to an average defect rate of 0.39% per fastener. As no spatial patterns (e.g. missing screws are more likely to appear in roof edges than other roof areas) were found in the observed data for missing screw fasteners, it is assumed that defects are uniformly distributed across the roof, and the occurrence rate of missing fasteners in the inspected roof area (at least one side of roof) is comparable to the defect rate of the whole roof. An analysis of variance (ANOVA) test on the observed missing fastener data in Table 2 is also conducted, which yields a p-value of 0.35 corresponding to the F-test. This implies no significant difference between the means of defect rate for the ten house samples. The collected data are not perfect due to a small number of houses inspected and limited access to the entire roof. However, it provides a reasonable indication of the missing fastener rate for metal roof cladding on Australian contemporary houses. There is a clear need to collect more data with professional housing inspections.

The uplift capacities for BTR connectors with under- and over-driven screws are obtained from uplift tests by Boughton et al. (2015) conducted in Australia. It is indicated that over-driving screw fasteners lead to a 50% reduction of withdrawn capacity for BTR connectors, whereas the uplift capacities are similar for BTR connectors with correctly driven or under-driven screws.

Table 2. Visual inspection data for missing CTB connectors

House No.	Number of inspected fastener locations	Number of missing fasteners
1	256	0
2	525	2
3	362	1
4	408	3
5	344	0
6	378	3
7	372	0
8	324	3
9	213	1
10	186	0
Total	3368	13

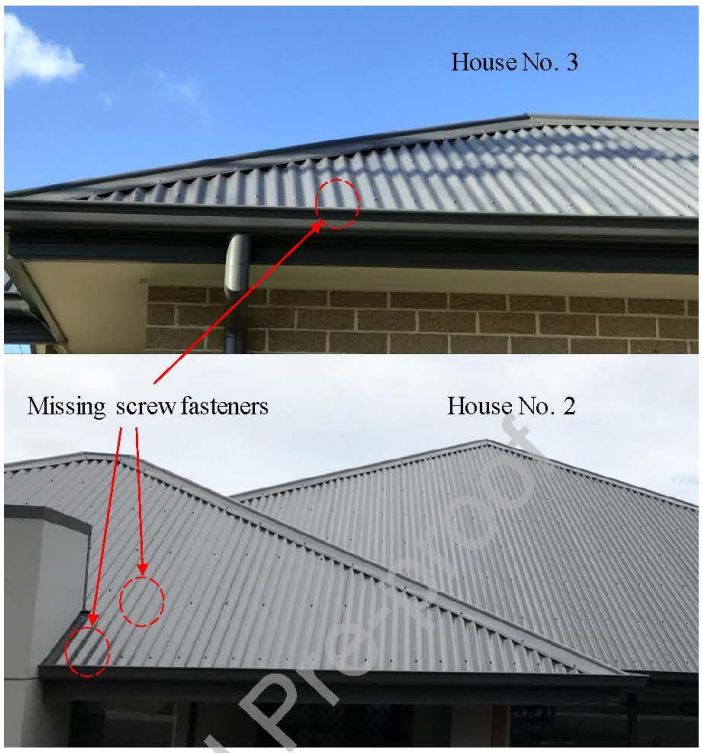

Figure 3. Missing cladding fasteners (CTB connectors) on as-built contemporary houses.

Another Australian study (Satheeskumar 2016) found that missing one or two nails in triple grip RTW connectors decreases uplift capacity by up to 40%. This is the most common type of construction defect for triple grip RTW connectors (Satheeskumar 2016), and the present study ignores another less observable type of faults, i.e. grouping nails in triple grip framing anchors. The housing surveys mentioned in Satheeskumar (2016) examined 87 suburban contemporary houses in non-cyclonic regions of Australia and indicated that about three RTW connectors are defective in most inspected houses but no detailed information are given for each inspected house in the housing surveys. The representative contemporary house considered in this study has 92 triple grip RTW connectors, then the average defect rate is 3/92 = 3.3% per RTW connector. This inferred data is adopted in the Bayesian

updating as anecdotal and indirect evidence with the intention to maximize the use of available information.

All the construction defect data mentioned above are summarized in Table 3. As shown in Table 3, defect data are incomplete and imperfect due to various limitations. A Bayesian approach is introduced in the next section, which provides a flexible and explicit framework for the quantification of defects in housing construction based on sparse objective information.

Table 3. Construction defect data collected from experimental and field observations.

Connection type	Defect type	Average defect rate per connection	Capacity reduction per defect
CTB (j = 1)	i = 1: Missing (screw not installed)	0.39%[a]	100%[b]
	i = 2: Improper installation (screw unattached to batten or over- and under-driven screw)	Not known	100%[b] (unattached to batten) Not known (over- or under-driven)
BTR (j = 2)	i = 1: Missing (one or both screws not installed)	Not known	100%[b] (missing both screws) Not known (missing one screw)
	i = 2: Improper installation (over- and under-driven screws)	Not known	50%[c] (over-driven) 0%[c] (under-driven)
RTW (j = 3)	i = 1: Missing one or two nails	3.3%[d]	Up to 40%[e]

[a] Based on field observations of as-built metal-clad contemporary houses
[b] A connection with all screws missing or screws unattached to batten has no capacity
[c] Based on test results in Boughton et al (2015), reducing withdrawn capacity only
[d] Inferred data from Satheeskumar (2016)
[e] Based on test results in Satheeskumar (2016)

3. Bayesian Method for Defect Rates

3.1 Probabilistic model

Suppose that in a house, there are k defect types for a given connection type. For the j^{th} type of roof connection, suppose that there are a total number of n_j connections of this type. To be specific for the representative contemporary house considered in this study, CTB, BTR and RTW connectors are deemed as the first (i.e. j = 1), second (i.e. j = 2) and third (i.e. j = 3) type of roof connection, respectively. As shown in Table 1, two typical defect types (i.e. k =

2) are considered for CTB connectors, whereas BTR and RTW connectors have two (i.e. k = 2) and one (i.e. k = 1) defect types, respectively.

For each connection type, the number of a certain type of defects occur in a total number of n_j roof connections of the j^{th} type is assumed to follow a multinomial distribution with a probability mass function (PMF) given as

$$f(x_{1j}, x_{2j}, \ldots, x_{kj}, x_{k+1,j}) = \frac{\Gamma(n_j+1)}{\prod_{i=1}^{k+1}\Gamma(x_{ij}+1)}\prod_{i=1}^{k+1}\theta_{ij}^{x_{ij}} = \frac{n_j!}{x_{1j}!\cdots x_{k+1,j}!}\prod_{i=1}^{k+1}\theta_{ij}^{x_{ij}} \quad (1)$$

where x_{ij} (i = 1, 2, … , k) and θ_{ij} (i = 1, 2, … , k) are the number and occurrence rate of the i^{th} type of construction defect in the j^{th} type of roof connection (see Table 3), respectively. $x_{k+1,j}$ and $\theta_{k+1,j}$ represent the number and occurrence rate of correctly installed roof connections of the j^{th} type, respectively, and $\Gamma(\cdot)$ is the gamma function. Note that $\sum_{i=1}^{k+1} x_{ij} = n_j$ (x_{ij} = 0, 1, 2, … , n_j) and $\sum_{i=1}^{k+1} \theta_{ij} = 1$ ($0 \le \theta_{ij} \le 1$). The multinomial distribution is a binomial distribution when k+1=2. Note that the dependence or correlation between defects, i.e. one error or defect is more likely to lead to other errors or defects, is neglected in the proposed defect model.

The defect rate θ_{ij} is inherently variable and uncertain, and in current practice, the defect rates are either assigned using subjective judgement (e.g. Stewart et al. 2018) or estimated from limited construction error data (e.g. Hong & He 2015). Therefore the associated uncertainties and variabilities may not have been well addressed. The Bayesian method provides an explicit structure to probabilistically infer the defect rates with a combination of expert judgement, HRA techniques and limited objective data, which reduces the degree of uncertainty arising from the complex human behaviour and sparse construction error data.

The subjective beliefs in defect rates $\boldsymbol{\theta_j}$ for the j^{th} type of roof connection are probabilistically expressed by the prior distribution. The data ($\boldsymbol{x_j}$) is used to update the prior information based on the Bayes' rule, and the obtained posterior distribution is then given by

$$f(\boldsymbol{\theta_j}|\boldsymbol{x_j}) = \frac{f(\boldsymbol{\theta_j}, \boldsymbol{x_j})}{f(\boldsymbol{x_j})} = \frac{f(\boldsymbol{x_j}|\boldsymbol{\theta_j})f(\boldsymbol{\theta_j})}{f(\boldsymbol{x_j})} \quad (2)$$

where $f(\boldsymbol{\theta}_j|\boldsymbol{x}_j)$ is the posterior distribution of $\boldsymbol{\theta}_j$ with $\boldsymbol{\theta}_j = (\theta_{1j}, \theta_{2j}, \ldots, \theta_{kj}, \theta_{k+1,j})$, $\boldsymbol{x}_j = (x_{1j}, x_{2j}, \ldots, x_{kj}, x_{k+1,j})$ is the observed data for defective and correctly installed roof connections of the j^{th} type, $f(\boldsymbol{x}_j|\boldsymbol{\theta}_j)$ is the likelihood function of $\boldsymbol{x}_j$, $f(\boldsymbol{\theta}_j)$ is the prior distribution of $\boldsymbol{\theta}_j$, and $f(\boldsymbol{x}_j)$ is an integral of the product $f(\boldsymbol{x}_j|\boldsymbol{\theta}_j)f(\boldsymbol{\theta}_j)$ over all possible values of $\boldsymbol{\theta}_j$, which can be regarded as a normalizing constant to ensure that $f(\boldsymbol{\theta}_j|\boldsymbol{x}_j)$ is a proper density.

3.2 Prior distributions

3.2.1 Dirichlet priors

To account for the uncertainty and variability involved in the defect rates, $\boldsymbol{\theta}_j$ are probabilistically modelled by the Dirichlet distribution, which is a conjugate prior distribution for the multinomial distribution. The Dirichlet distribution is a multivariate generalization of the beta distribution. The probability density function (PDF) of the Dirichlet prior for $\boldsymbol{\theta}_j = (\theta_{1j}, \theta_{2j}, \ldots, \theta_{kj}, \theta_{k+1,j})$ is given by

$$f(\boldsymbol{\theta}_j) = \text{Dirichlet}(\boldsymbol{\theta}_j \mid a_{1j}, a_{2j}, \ldots, a_{kj}, a_{k+1,j}) = \frac{\Gamma(\sum_{i=1}^{k+1} a_{ij})}{\prod_{i=1}^{k+1} \Gamma(a_{ij})} \prod_{i=1}^{k+1} \theta_{ij}^{a_{ij}-1} \tag{3}$$

where $\boldsymbol{\alpha}_j = (\alpha_{1j}, \alpha_{2j}, \ldots, \alpha_{kj}, \alpha_{k+1,j})$ are the positive-valued parameters for the Dirichlet distribution for the j^{th} type of roof connection. Let $\alpha_{0j} = \sum_{i=1}^{k+1} \alpha_{ij}$. The marginal mean and variance of θ_{ij} are then given by

$$\mathrm{E}(\theta_{ij}) = \frac{\alpha_{ij}}{\alpha_{0j}} \tag{4}$$

$$\mathrm{var}(\theta_{ij}) = \frac{\alpha_{ij}(\alpha_{0j}-\alpha_{ij})}{\alpha_{0j}^{2}(\alpha_{0j}+1)} \tag{5}$$

Generally, α_{0j} can be viewed as a measure of the prior informativity. The larger the value of α_{0j} is, the more informative the Dirichlet priors. Further, let $\boldsymbol{\alpha}_j = \alpha_{0j}\boldsymbol{v}_j$, where $\boldsymbol{v}_j$ is a vector of the marginal mean of $\boldsymbol{\theta}_j$ given by $\boldsymbol{v}_j = (v_{1j}, v_{2j}, \ldots, v_{kj}, v_{k+1,j}) = (\alpha_{1j}, \alpha_{2j}, \ldots, \alpha_{kj}, \alpha_{k+1,j})/\alpha_{0j}$, and it satisfies $\sum_{i=1}^{k+1} v_{ij} = 1$. The prior parameters for the defect rates $\boldsymbol{\theta}_j$ for the j^{th} type of roof

connection can then be determined by specifying $\boldsymbol{v_j}$ and α_{0j}. In the present Bayesian method, informative prior distributions are proposed to reflect expert's knowledge of the occurrence rates for distinct types of construction defects in CTB, BTR and RTW connectors as listed in Table 1. It might well be that expert judgements may select a different prior distribution, however, this is beyond the scope of the present paper.

CREAM (Hollnagel 1998), a widely used HRA technique, which offers a systematic modelling of human error occurrence based on cognitive engineering principles, is employed to give point estimates of $\boldsymbol{v_j}$. The application of CREAM to the determination of $\boldsymbol{v_j}$ is described in the next section. The parameter, α_{0j}, plays a role of weighing the expert judgement and the sparse data of construction defects. If α_{0j} is much smaller than the data size (e.g. n_1 = 3368 for CTB connectors as shown in Table 2), the evidence used in Bayesian updating overwhelms the prior beliefs. In other words, the prior distribution in this scenario can be viewed as a weakly informative prior with limited influence on the posterior distribution. Otherwise, if α_{0j} is much larger than the size of data, the prior dominants the Bayesian inference. Ideally, it is desirable to specify a relatively small value of α_{0j} (i.e. use non-informative or weakly informative priors) and conduct the Bayesian updating based on sufficient objective data. However, due to the scarcity of construction defect data, the selection of α_{0j} depends on the level of confidence towards the prior beliefs and the limited evidence. The analyst may set α_{0j} to be comparable with the data size to give similar weights to the expert opinion and the sparse data of construction defects.

3.2.2 Specifying prior parameters

Informative prior distributions are used for the defect rates to reveal experts' subjective knowledge and judgement. HRA techniques offer theoretical models to quantitatively predict human performance under given conditions and/or contexts, which can be used to express the prior beliefs about construction defect rates.

3.2.2.1 Point estimation using CREAM

All erroneous human actions are, to some extent cognitive, and cannot be properly modelled or understood without referring to the characteristics of human cognition (Hollnagel 1998). In this study, the HRA approach, CREAM, is employed to provide prior information for the defect rates. Based on cognitive engineering principles, CREAM can reasonably address the underlying mechanism of human error occurrence. The psychological, physiological and sociological factors involved in human error are captured by CREAM through the cognitive functions and common performance conditions. See Hollnagel (1998) for more details. A basic and an extended method are included in the quantitative analysis of CREAM. The purpose of the former is to produce a general assessment of human reliability for a given task, and the latter aims to provide point estimates for specific human error probabilities (i.e. HEP or what we call 'defect rates' in this study).

The task of installing a roof connection is considered to include two main subtasks based on the practical procedures adopted by construction workers: (i) install the roof connection at the right position, and (ii) visual check if any fastener is missing. The visual check can happen any time during the installation of roof connections, however, herein we consider only an overall check is conducted after the completion of the installation work. It is further assumed that any missing nails or screws that have been detected will be installed immediately, and only missing fasteners can be identified by a visual inspection. In other words, misaligned, over- and under-driven fasteners are deemed to be difficult to detect by a simple visual check. To complete these two subtasks, the builder needs to be equipped with many things such as the rules/procedures for connection installations, tips in fastening using an electric drill, and perceptions for detecting missing fasteners. Hence, the actual actions when conducting these subtasks are only the surface manifestations of the underlying human cognition.

In the basic method of CREAM, (i) common performance conditions (CPCs) and (ii) control modes are determined. CPCs are used to characterize the human interactions with contexts and/or circumstances. The control mode is determined by the CPCs, which provides an overall range of the defect rates. In this study, as the CPCs are not observed during the construction process, a set of neutral CPCs (i.e. no improvement or reduction for performance reliability) are considered as the expected or representative context for typical housing construction. Based on the neutral CPCs, the tactical control mode is then selected, where human performance is based on planning, and more or less follows a known procedure or rule (Hollnagel 1998). This control mode gives an overall evaluation that the defect rates are within 0.1% and 10% (Hollnagel 1998), which is compatible with the average defect rates shown in Table 3. The tactical control mode is also consistent with a qualitative view that the installation of roof connections is mostly a rule-based activity. In this study, the main purpose of using CREAM is to produce specific point estimates for construction defect rates. Hence, the basic method of CREAM is only briefly described in this section. More details about the determination of the CPCs and control modes can be found in Hollnagel (1998).

The extended method in CREAM is used to produce specific human action failure probabilities in this study. The basic method can be referred to Hollnagel (1998) and is not described herein. The cognitive demands associated with a task or subtask can be described by a single or combination of four basic cognitive functions, namely, observation, interpretation, planning, and execution (Hollnagel 1998). The possible failure modes for each cognitive function and corresponding nominal cognitive failure probabilities (i.e. error rates) in CREAM (Hollnagel 1998) are given in Table 4. The major cognitive activities and corresponding cognitive functions are assigned to each subtask for the roof connection installation which is shown in Table 5. Table 6 lists the main failure modes and nominal defect rates produced by CREAM for distinct types of construction defects in roof

connections. For example, the manifestation of a missing CTB connector is due to the situation that the screw fastener is simply not installed (failure type E5) and later this ignorance has not been detected by a simple visual check (failure type O3). Therefore, the defect rate for missing cladding fasteners in Table 6 is then calculated as 3% (i.e. nominal error rate for generic failure type E5) × 7% (i.e. nominal error rate for generic failure type O3) = 0.21%. As shown in Table 6, the nominal defect rates have comparable magnitudes with the available objective information (i.e. average defect rates) listed in Table 3, which indicates the compatibility of the elicited prior and defect data.

Table 4. Cognitive failure modes and nominal cognitive failure probabilities (Hollnagel 1998).

Cognitive function	Generic failure type	Nominal error rate
Observation	O1. Wrong object observed	0.10%
	O2. Wrong identification	7.0%
	O3. Observation not made	7.0%
Interpretation	I1. Faulty diagnosis	20%
	I2. Decision error	1.0%
	I3. Delayed interpretation	1.0%
Planning	P1. Priority error	1.0%
	P2. Inadequate plan	1.0%
Execution	E1. Action of wrong type	0.30%
	E2. Action at wrong time	0.30%
	E3. Action on wrong object	0.05%
	E4. Action out of sequence	0.30%
	E5. Missed action	3.0%

Table 5. Cognitive activities and functions for each subtask for roof connection installation.

Subtask	Description	Cognitive activity	Cognitive function
Install roof connections	Fasten nails or screws for CTB, BTR and RTW connectors	Execute	Execution
Visual check missing nails or screws	Overall visual inspection after installation work	Observe	Observation

Table 6. Cognitive failure modes and nominal defect rates produced by CREAM.

Connection type	Typical defect type	Generic failure type	Nominal defect rate	Average defect rate in Table 3
CTB (j = 1, k =2)	Missing (i = 1)	E5 and O3	θ_{11} = 0.21%	0.39%
	Improper installation (i = 2)	E1	θ_{21} = 0.30%	Not known
BTR (j = 2, k =2)	Missing (i = 1)	E5 and O3	θ_{12} = 0.42%	Not known
	Improper installation (i = 2)	E1	θ_{22} = 0.60%	Not known
RTW (j = 3, k = 1)	Missing one or two nails (10 nails in total, i = 1)	E5 and O3	θ_{13} = 2.12%	3.30%

The nominal defect rates can be further modified by applying the CPCs to quantify the improvement or reduction of human reliability due to the working contexts (Hollnagel 1998). For example, inadequate project time and/or unexperienced builders can reduce the human reliability and thus increase the defect rates. The CPCs are analogous to the performance shaping factors (PSFs) in many other HRA methods (e.g. Kirwan 1996; Blackman et al. 2008), and hereafter we use the term PSFs. As mentioned before that no observations and data are available, the PSFs are set to unity to represent the expected or representative context for typical housing construction. A sensitivity analysis is conducted in Section 5.2 to account for possible effect of PSFs other than unity. Therefore, the nominal defect rates are adopted as the point estimates produced by CREAM, which can be further used to assign the prior parameters. In a sensitivity analysis in Section 5.2, the potential effects of adverse working contexts (i.e. PSFs > 1.0) are further examined.

3.2.2.2 Dirichlet parameters

The point estimates produced by CREAM are employed to specify the Dirichlet prior parameters. As described in Section 3.2.1, the Dirichlet distribution for defect rates can be expressed as Dirichlet ($\boldsymbol{\theta}_j|\alpha_{0j}\boldsymbol{v}_j$). These point estimates for the defect rates of the j^{th} type roof connection are then used as the marginal mean values, $\boldsymbol{v}_j$, in the Dirichlet prior distributions.

A constrained non-informative prior is not widely used (Atwood et al. 2003), and it is not tractable for the pair of Dirichlet-multinomial distribution that has multiple parameters as needed for this paper (see Kelly & Atwood 2011 for details). Thus, the value of α_{0j} is determined by subjective judgement to reflect various levels of prior beliefs. The Dirichlet prior distributions assigned for the defect rates for CTB, BTR and RTW connectors are then given in Table 7. As only one typical defect type is considered for RTW connectors, the two-dimensional Dirichlet distribution is a beta distribution used as the prior for the defect rate. The prior distributions of construction defect rates for CTB, BTR and RTW connectors considering different $\boldsymbol{\alpha_0}$ values are plotted in Figs. 4, 5 and 6, respectively. Note that $\boldsymbol{\alpha_0}$ = (α_{01}, α_{02}, α_{03}) with j = 1, 2 and 3 are for CTB, BTR and RTW connectors, respectively. As expected, the larger the $\boldsymbol{\alpha_0}$ value, the smaller the variance and the higher degree of informativity for the prior distribution.

Table 7. Dirichlet prior distributions for defect rates

Connection type	Dirichlet prior distributions for $\boldsymbol{\theta_j}$	α_{0j} value
CTB (j = 1)	$\boldsymbol{\theta_1} = (\theta_{11}, \theta_{21}, \theta_{31}) \sim$ Dirichlet ($0.0021\alpha_{01}$, $0.0030\alpha_{01}$, $0.9949\alpha_{01}$)	Express the degree of prior beliefs about the defect rates for the j^{th} type of roof connection, determined by expert judgement
BTR (j = 2)	$\boldsymbol{\theta_2} = (\theta_{12}, \theta_{22}, \theta_{32}) \sim$ Dirichlet ($0.0042\alpha_{02}$, $0.0060\alpha_{02}$, $0.9898\alpha_{02}$)	
RTW (j = 3)	$\boldsymbol{\theta_3} = (\theta_{13}, \theta_{23}) \sim$ beta ($0.021\alpha_{03}$, $0.979\alpha_{03}$) or Dirichlet ($0.021\alpha_{03}$, $0.979\alpha_{03}$)	

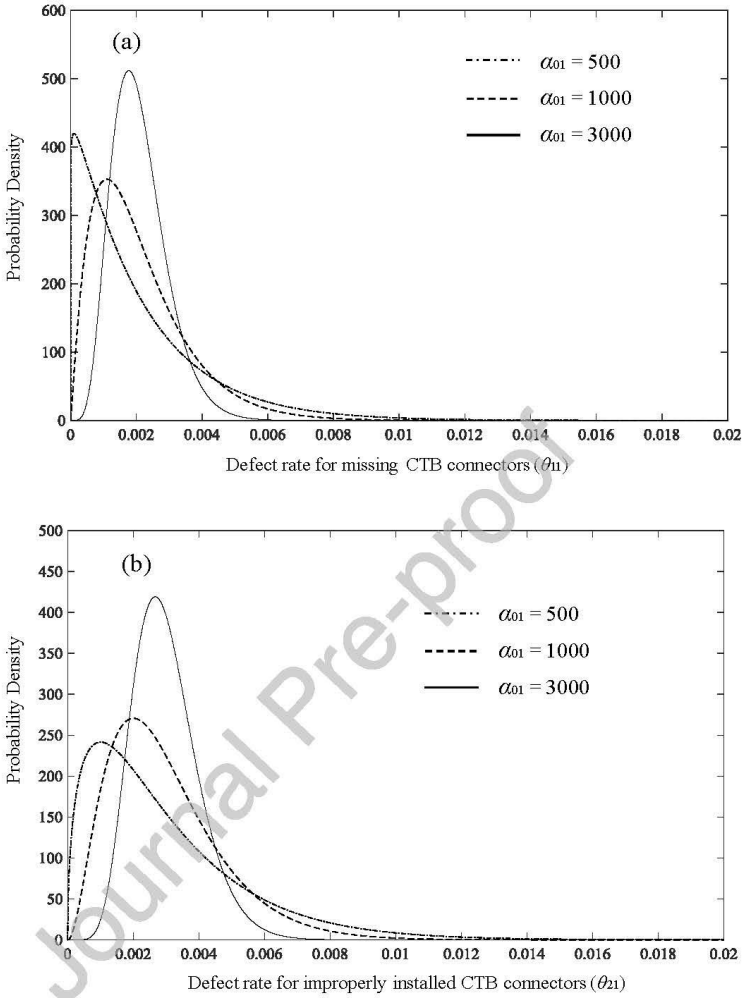

Figure 4. Marginal distributions of the Dirichlet prior for defect rates of CTB connectors with different α_{01} values.

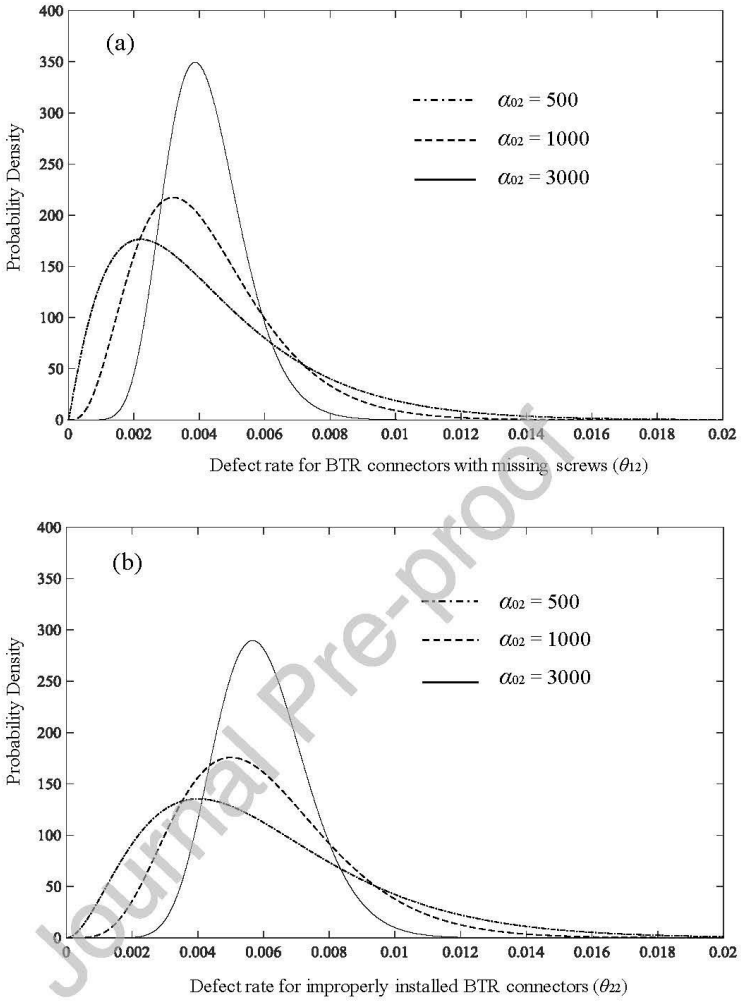

Figure 5. Marginal distributions of the Dirichlet prior for defect rates of BTR connectors with different α_{02} values.

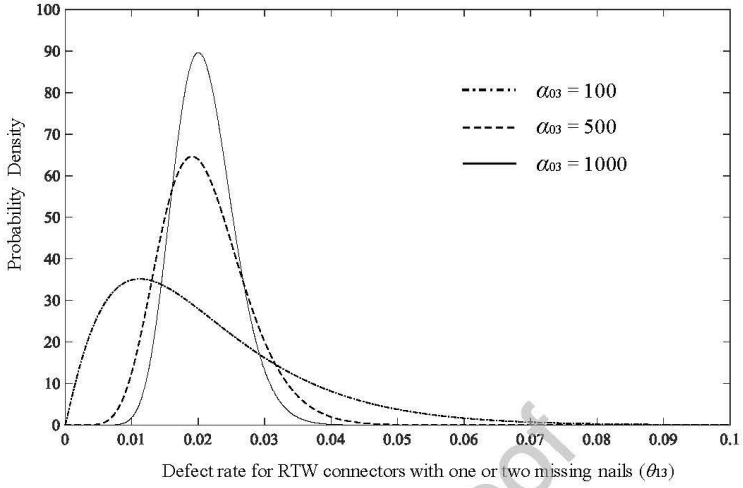

Figure 6. Prior distributions for the defect rate of RTW connectors with different α_{03} values.

3.3 Posterior distributions

The Dirichlet distribution is a conjugate prior to the multinomial distribution. Suppose a number of n_j roof connections of the j^{th} type have been inspected, and x_{ij} (i = 1, 2, … , k) defective connections are detected for the i^{th} type of construction defect. The posterior distribution for the defect rates θ_j of the j^{th} type roof connection is also a Dirichlet distribution given by

$$f(\boldsymbol{\theta}_j|n_j, \boldsymbol{x}_j) = \text{Dirichlet}(\boldsymbol{\alpha}_j + \boldsymbol{x}_j) \tag{6}$$

where $\boldsymbol{\alpha}_j = (\alpha_{1j}, \alpha_{2j}, \ldots, \alpha_{kj}, \alpha_{k+1,j}) = \alpha_{0j}\boldsymbol{v}_j$, $\boldsymbol{\theta}_j = (\theta_{1j}, \theta_{2j}, \ldots, \theta_{kj}, \theta_{k+1,j})$ and $\boldsymbol{x}_j = (x_{1j}, x_{2j}, \ldots, x_{kj}, x_{k+1,j})$. Note that $x_{k+1,j} = n_j - \sum_{i=1}^{k} x_{ij}$. The Bayesian updating is straightforward with conjugate prior distributions if complete data are given. However, as shown in Table 3, data are incomplete and imperfect for the construction defects in roof connections, and therefore more efforts are needed to make the Bayesian inference.

3.3.1 CTB connectors

For CTB connectors (the 1st type of roof connection, i.e. j = 1), there are two types of construction defects (i.e. k = 2) considered in this study as shown in Table 1. The model parameters of interest are $\boldsymbol{\theta}_1 = (\theta_{11}, \theta_{21}, \theta_{31})$, where θ_{11} and θ_{21} are the defect rates for missing and improperly installed CTB connectors, respectively, and $\theta_{31} = 1 - \theta_{11} - \theta_{21}$ is the occurrence rate for correctly installed CTB connectors. If a total of n_1 CTB connectors have been inspected, $\boldsymbol{x}_1 = (x_{11}, x_{21}, x_{31})$ then represent the number of missing, improperly installed and correctly installed CTB connectors, where $x_{11} + x_{21} + x_{31} = n_1$. According to Tables 2 and 3, n_1 = 3368, x_{11} = 13 and x_{21} is not known. The posterior distribution for defect rates of CTB connectors in Eq. (6) then transforms into $f(\boldsymbol{\theta}_1|n_1, x_{11})$, which is proportional to the multiplication of the Dirichlet prior and the observed data (incomplete) likelihood, expressed as

$$f(\boldsymbol{\theta}_1 \mid x_{11}, n_1) \propto (\prod_{t=1}^{3} \theta_{t1}^{\alpha_{t1}-1}) \theta_{11}^{x_{11}} (\theta_{21} + \theta_{31})^{n_1 - x_{11}} = \sum_{t=0}^{n_1 - x_{11}} \frac{(n_1 - x_{11})!}{t!(n_1 - x_{11} - t)!} [\theta_{11}^{x_{11} - \alpha_{11} - 1} \theta_{21}^{t + \alpha_{21} - 1} \theta_{31}^{n_1 - x_{11} - t + \alpha_{31} - 1}] \tag{7}$$

The posterior distribution for the defect rates of CTB connectors given by Eq. (7) can be numerically evaluated using the Markov Chain Monte Carlo (MCMC) methods (e.g. Gelman et al. 1995). Figure 7 depicts the marginal posterior distributions for the defect rates of CTB connectors considering different α_{01} values. The corresponding prior distributions are also plotted in the figure. As shown in Fig. 7, the posterior distribution is getting closer to the prior distribution as α_{01} increases. The smaller the α_{01} value, the more diffuse the posterior distribution. As no defect data is available for improperly installed CTB connectors, the obtained marginal posterior distribution for the defect rate θ_{21} from Bayesian updating is then more spread out to reflect a higher level of uncertainty involved.

3.3.2 BTR connectors

As shown in Table 3, no observed data are available for the two types of construction defects for BTR connectors (the 2nd type of roof connection, i.e. $j = 2$). Therefore, no Bayesian updating is carried out for BTR connectors, and the prior distribution, i.e. Dirichlet ($0.0042\alpha_{02}$, $0.0060\alpha_{02}$, $0.9898\alpha_{02}$) as shown in Table 7 is directly used for the defect rates for BTR connectors.

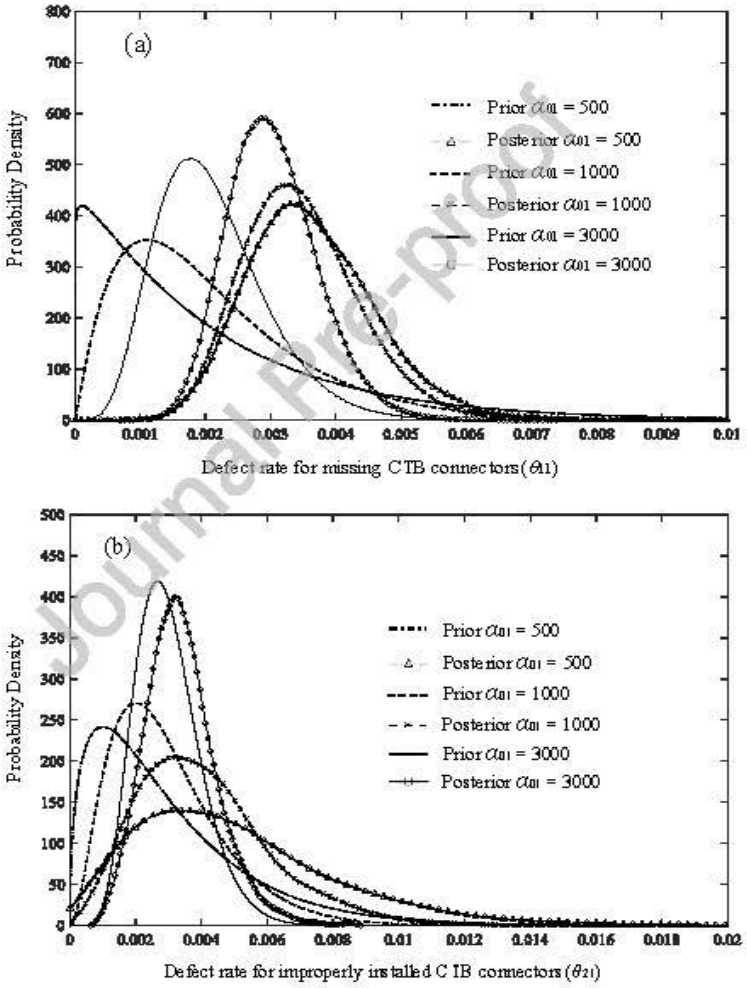

Figure 7. Marginal posterior distributions for defect rates of CTB connectors with different α_{01} values.

3.3.3 RTW connectors

For RTW connectors (the 3rd type of roof connection, i.e. j = 3), the defect data is inferred from Satheeskumar (2016) that states 87 Australian contemporary houses were inspected in housing surveys and most inspected houses have about three defective triple grip RTW connections with no more details given. This evidence about construction defects for RTW connectors is based on vague descriptions, which is somewhat anecdotal and uncertain. The inferred defect data are then deemed to have three defective triple grip connections in the representative contemporary house with 92 RTW connectors. In other words, only the most representative case for the number of observed defects in a typical contemporary house is considered as the evidence used for Bayesian updating, which may introduce relatively high uncertainties for the defect rate. Given the conjugate prior distribution, i.e. beta ($0.021\alpha_{03}$, $0.979\alpha_{03}$) as shown in Table 7, the posterior distribution for the defect rate of RTW connectors θ_{13} is straightforward to obtain through the Bayesian updating, which is given by beta ($0.021\alpha_{03}$ + 3, $0.979\alpha_{03}$ + 89). A relatively higher value of α_{03} (e.g. 500 and 1000) may be used to give more preference to the prior beliefs produced by the HRA method. Figure 8 shows the posterior distributions for the defect rate of RTW connectors considering different α_{03} values. The corresponding prior distributions are also plotted in the figure. Smaller α_{03} values lead to more dispersive posterior distributions for the defect rate θ_{13} of RTW connectors, which has similar trends with those shown in Fig. 7. Table 8 shows the mean defect rates yielded by the posterior distributions for CTB and RTW connections.

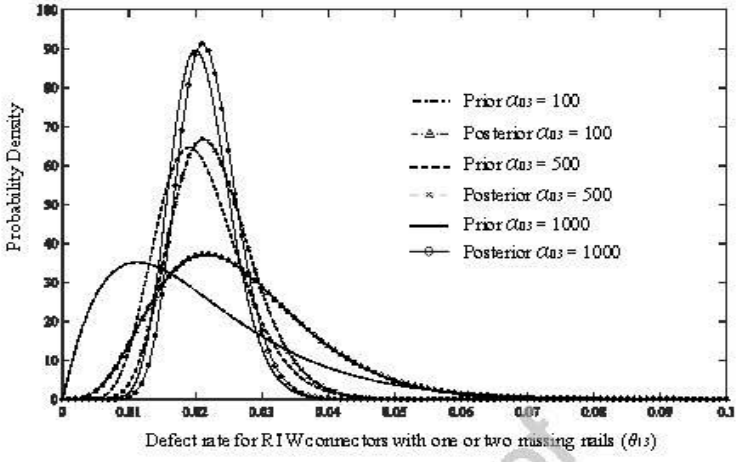

Figure 8. Posterior distributions for the defect rate of RTW connectors with different α_{03} values.

Table 8. Mean defect rates yielded by the posterior distributions for CTB and RTW connections

Connection type	Typical defect type	Mean defect rates			
		α_0 = 100	α_0 = 500	α_0 = 1000	α_0 = 3000
CTB (j = 1, k =2)	Missing (i = 1)	n/a	0.36%	0.35%	0.30%
	Improper installation (i = 2)	n/a	0.50%	0.41%	0.34%
RTW (j = 3, k = 1)	Missing one or two nails (i = 1)	2.66%	2.28%	2.20%	n/a

4. Uplift Capacities for Defective Roof Connections

The uplift capacities for correctly installed (i.e. defect free) roof connections are presented in Stewart et al. (2018) and Qin & Stewart (2019). The pull-over and pull-out capacities of CTB and BTR connectors are assumed to follow a lognormal distribution (Henderson & Ginger 2007) with the statistical parameters listed in Table 9. The connection capacities are assumed to be statistically independent and taken as the lower of the randomly generated pull-out and pull-over strengths when conducting a fragility analysis.

Table 9. Statistical parameters for resistances of CTB and BTR connectors.

Connection type	Connection failure mode	Mean	COV	Distribution type	Source
Cladding-to-batten (CTB)	Roof sheeting pulling over screw fastener	1.2kN	0.30	Lognormal	Stewart et al. (2018)
	Screw pulling out of roof batten	1.2kN	0.20		
Batten-to-rafter/truss (BTR)	Roof batten pulling over batten screw fastener	4.5kN	0.15	Lognormal	Stewart et al. (2018)
	Batten screw fastener pulling out of rafter/truss	5.5kN	0.20		

The timber species for the truss is typically Australian radiata pine, and two types of fasteners, i.e. hand nails and gun nails, are used to fasten the triple grip connections. A piecewise-linear model was developed by Qin & Stewart (2019) to model the behaviour of RTW connectors under wind uplift loads. The probabilistic modelling of three major parameters, i.e. initial secant stiffness k_0, peak load F_u (defined as uplift capacity) and displacement at peak load δ_u, and the correlation coefficients between these parameters for triple grip RTW connectors fastened using hand nails and gun nails, are given in Tables 10 and 11. The statistics in these two tables are derived using the force-displacement curves obtained from the static tests for Australian contemporary houses given in Satheeskumar (2016). More details about the piecewise-linear model for RTW connectors can be found in Qin & Stewart (2019).

The data regarding the capacity reduction for roof connections given the occurrence of various types of construction defects are discussed in Section 2.2 and summarized in Table 3. For missing CTB connectors, there is no uplift capacity at the missing fastener location. For improperly installed CTB connectors, if a screw fastener is not attached to the batten, the uplift capacity of the connection is also zero. If a cladding fastener is over- or under-driven, as no uplift capacity data is available, a triangular probability distribution used in Stewart et al. (2018) is employed to model the capacity reduction as shown in Table 12.

For BTR connectors, it is assumed that at least 50% capacity reduction with one missing batten screw and 100% capacity reduction if both screws are missing. As the latter has a much smaller occurrence rate than the former, a triangular probability distribution shown in Table 12 with a mode of 50% is used. Given the occurrence of an improperly installed BTR connector with over- or under-driven screws, it is considered that the over-driven scenario has a 50% probability of occurrence and reduces the pull-out capacity by about 50% (Boughton et al 2015). Note that there is no capacity reduction for the under-driven scenario. To account for the variability of capacity reduction, a triangular probability distribution given in Table 12 with a mode of 50%, a lower bound of 40% and an upper bound of 60% is assumed to model the reduction of pull-out capacity for BTR connectors with over-driven batten screws.

Table 10. Statistical parameters of the piecewise-linear model for RTW connectors.

(a) Hand nail triple grip

RTW parameters	Mean	COV	Distribution type	Source
k_0 (kN/mm)	0.44	0.17	Lognormal	Qin & Stewart (2019)
F_u (kN)	4.85	0.11		
δ_u (mm)	19.49	0.12		

(b) Gun nail triple grip

RTW parameters	Mean	COV	Distribution type	Source
k_0 (kN/mm)	0.34	0.15	Lognormal	Qin & Stewart (2019)
F_u (kN)	3.80	0.11		
δ_u (mm)	19.95	0.18		

Table 11. Correlation coefficients between piecewise-linear model parameters for RTW connectors.

RTW parameters	Correlation coefficient		Source
	Hand nail triple grip	Gun nail triple grip	
k_0 and F_u	0.63	0.45	Qin & Stewart (2019)
k_0 and δ_u	−0.27	−0.16	
F_u and δ_u	0.12	0.14	

Table 12. Capacity reduction for defective roof connections.

Connection type	Defect type	Capacity reduction
CTB	Missing (screw not installed)	100%
	Improper installation (screw unattached to batten or over- and under-driven screws)	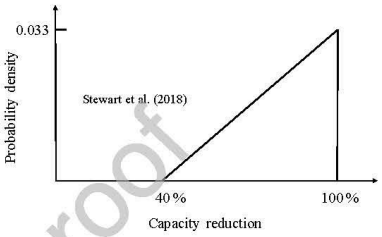
BTR	Missing (one or both screws not installed)	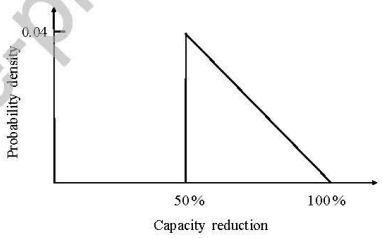
	Improper installation (over- and under-driven screws)	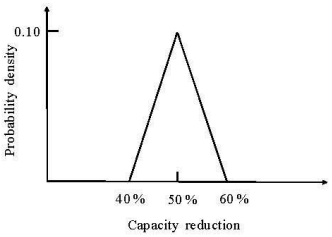 Reduction of pull-out capacity only for those with over-driven screws

RTW	Missing one or two nails	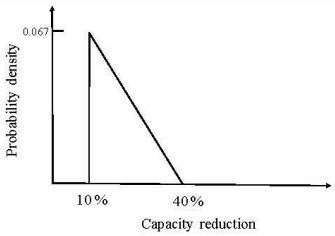

According to the test results in Satheeskumar (2016), approximately 10% capacity reduction was observed for triple grip RTW connectors with one missing nail and 40% reduction of the uplift capacity for those with two missing nails. A triangular probability distribution shown in Table 12 is then used to model the capacity reduction for triple grip RTW connectors with one or two missing nails. The piecewise-linear relationship is still used to model the load-deflection behaviour of defective RTW connectors. All three parameters (i.e. initial secant stiffness k_0, peak load F_u and displacement at peak load δ_u) in the piecewise-linear model are also assumed to decrease according to the triangular probability distribution.

The reduction of uplift capacities for defective roof connections are summarized in Table 12. Note that all the percentages of reduction mentioned above are compared to the uplift capacities of correctly installed roof connections given in Tables 9 and 10.

5. Roofing Fragility Analysis with Construction Defects

The probabilistic models for construction defect rates obtained from the Bayesian updating are further incorporated in a reliability-based fragility method developed by Qin & Stewart (2019). This fragility model is modified to account for the defect occurrence and the uplift capacities of defective roof connections in the fragility assessment. The fragility model and the incorporation of construction defects are described in this section.

5.1 Reliability-based fragility method

The reliability-based fragility method proposed by Qin & Stewart (2019) evaluates the metal roof sheeting loss and timber roof truss failure due to overloading of CTB, BTR and RTW connectors. A Monte Carlo Simulation (MCS) in conjunction with a finite element (FE) approach for the roof system were developed for the fragility assessment, which enables the probabilistic characterizations of spatially varying wind uplift pressures on roof surface, wind demands and uplift capacities for roof connections as well as the load redistribution and damage progression after the initial failure of connections. The representative contemporary house in non-cyclonic regions of Australia as described in Section 2 was employed to illustrate the proposed fragility model. This fragility method is briefly introduced in this section. Refer to Qin & Stewart (2019) for more details. The adaptation of the reliability-based fragility method to account for construction defects is also described in this section.

5.1.1 Fragility and limit state function

Herein, the fragility of the roof system is defined as the extent of the roof sheeting loss and the roof truss failures at a given gust wind speed, which is expressed as

$$\Pr(DS|V) = \Pr[DS = R_{loss}|V] \tag{8}$$

where DS denotes the damage state of the considered roof system, R_{loss} is the proportion of damage to metal roof cladding and timber roof trusses (per roof), and V is the gust wind speed.

The loss of a single roof sheet is assumed to occur when a critical number of CTB and/or BTR connectors are overloaded. A BTR connection failure is modelled as if all cladding fasteners connected to the batten have failed. A roof truss is considered to fail if at least one of its RTW connectors is overloaded. The failure of a single CTB, BTR or RTW connector is governed by the following limit state function

$$g = R - (W - D_L) \tag{9}$$

where R represents the capacity of the considered connection, W is the wind uplift force in this connection, and D_L is the dead load arising from the weight of roof components. A connection fails if $g \leq 0$.

5.1.2 Wind loads and connection capacities

The wind uplift load (W) is modelled probabilistically as (Holmes 1985; Stewart et al. 2018; Qin & Stewart 2019)

$$W = \lambda \cdot M \cdot A \cdot (C \cdot T \cdot E^2 \cdot D^2 \cdot G \cdot \frac{\rho}{2}) \cdot V^2 \quad (10)$$

where V is the maximum 0.2 second gust velocity at 10m height in open terrain; λ is a factor accounting for wind loading modelling inaccuracies and uncertainties; M accounts for wind tunnel modelling inaccuracies; A is the loaded area uncertainty arising from geometric uncertainties of the cladding fastener, batten and truss spacing; C is the quasi-steady pressure coefficient, which is a combination of external (C_{Pe}) and internal pressure coefficient (C_{Pi}); T is the shielding factor; E is a terrain height multiplier that accounts for the exposure and height of the building considered; D is a factor accounting for wind directionality effects; G is a factor related to area reduction, and ρ is the density of air. These parameters, except for C, are assumed to follow a lognormal distribution (Henderson & Ginger 2007). The nominal values of these parameters can be obtained from Australian wind loading standard AS/NZS 1170.2 (2011), and the mean-to-nominal ratios and coefficient of variation (COV) values for these parameters can be referred to Qin & Stewart (2019). Note that the wind uplift forces in roof connections are evaluated based on Eq. (10) and a FE approach (Qin & Stewart 2019). The FE model is described later in this section.

The Gumbel distribution is used to model the spatially varying external pressure coefficients based on data obtained from a wind tunnel test for the representative contemporary house. More details about the wind tunnel test can be found in Parackal et al. (2016) and Stewart et al. (2018). The internal pressure coefficient is assumed to follow a

normal distribution. Two typical scenarios are assumed for internal pressure, i.e. (i) dominant openings existing on windward wall and (ii) effectively sealed building without any wall openings. The evolution of internal pressure with increasing roof sheeting loss is also taken into account in the fragility assessment, see Qin & Stewart (2019) for more details.

The probabilistic modelling of the uplift capacities for correctly installed CTB, BTR and RTW connectors is described in Section 4 (Tables 9 and 10). The probabilistically modelled connection capacities are used in conjunction with the wind uplift loads in a MCS to evaluate the failure of a roof connection. The construction defects are further included in the fragility assessment by applying the capacity reduction for defective roof connections, which is discussed later in Section 5.1.5.

5.1.3 FE modelling

A FE approach is employed to evaluate the wind uplift forces in roof connections and the load distribution after connection failures. The representative contemporary house shown in Fig. 1 has large dimensions and complex hip-roof geometries, which requires excessive cost in the FE modelling and computation (e.g. CPU hours) for the MCS-based fragility analysis. A hybrid FE model was developed by Qin & Stewart (2019) to provide a reasonable compromise on the fidelity and computational cost of the FE modelling. In this FE model, a roof cladding FE model and a roof truss FE model are included. All the metal roof sheeting and metal top-hat battens are modelled in the roof cladding FE model. The spatially varying wind uplift pressures are randomly generated in each MCS run based on Eq. (10) and then applied to the roof cladding FE model to evaluate the wind uplift forces in CTB and BTR connectors. The load redistribution after roof connection failures are also taken into account, and the extent of roof sheeting loss at given gust wind speeds can then be evaluated. The roof cladding FE model is shown in Fig. 9. The roof truss FE model consists of most critical trusses in the representative contemporary house. The less vulnerable jack and hip trusses are

not modelled for simplification. The metal top-hat battens above the modelled trusses are also included to account for the load sharing effects. The roof truss FE model is shown in Fig. 10. In one MCS run, the uplift forces in BTR connectors obtained from the roof cladding FE model are subsequently applied to the roof truss FE model to evaluate the wind uplift forces in RTW connectors. The number of failed RTW connectors is then assessed considering the load redistribution and progressive failure. Refer to Qin & Stewart (2019) for more details about the FE approach.

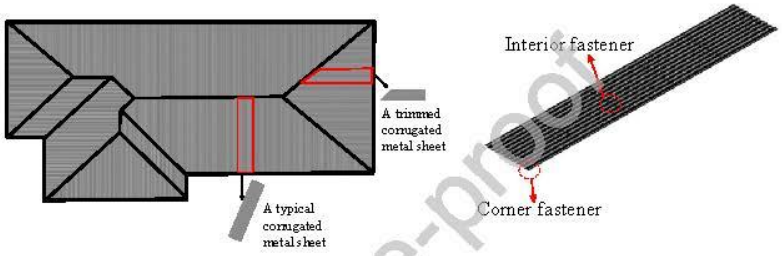

Figure 9. Roof cladding FE model (Qin & Stewart 2019).

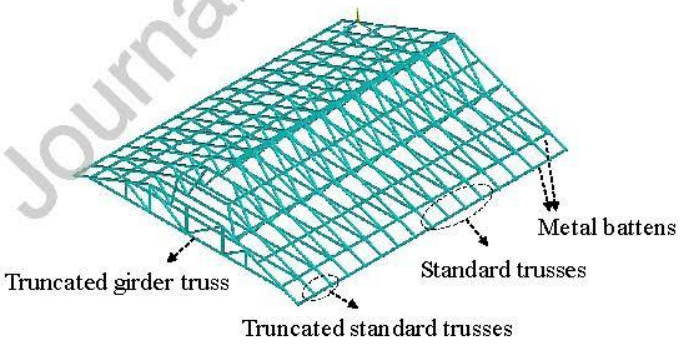

Figure 10. Roof truss FE model (Qin & Stewart 2019).

5.1.4 Monte Carlo Simulation

A MCS is employed to evaluate the wind fragility for roof cladding and trusses (Qin & Stewart 2019). The wind direction is assumed to be uniformly distributed in 10° increments

from 0° to 350° to allow for the variability of building orientation – this allows for fragilities to be assessed for a house for a specific wind speed. In each run of the MCS, a wind speed and a building orientation are selected, and then the spatially distributed wind pressures and uplift capacities of roof connections are randomly generated as the input to the FE model of the roof system. The wind uplift forces in the roof connections are then obtained from the FE analysis, and the failure of a single connection is checked by the limit state function given by Eq. (9). Any overloaded (failed) CTB, BTR and RTW connectors are then deactivated in the FE model, and the FE analysis is further conducted to evaluate the load redistribution and failure progression of other connections. The MCS is repeated for all the building orientations and wind speeds up to 80m/s. The MCS and FE approach enable the development of two fragility curves: (i) the extent of roof sheeting loss, and (ii) proportion of roof truss failures.

5.1.5 Incorporate construction defects

The construction defects are included in the reliability-based fragility method by adjusting the uplift capacities for defective roof connections according to the capacity reduction as described in Section 4. It is assumed that the construction defects in a given type of roof connection are uniformly distributed (i.e. the defect rate for all connections are statistically independent). In one MCS run, the occurrence rates for each type of defect in CTB, BTR and RTW connectors are randomly sampled from corresponding probability distributions obtained from the Bayesian inference as described in Section 3. Then according to the multinomial distribution given by Eq. (1), it can be determined whether a roof connection is correctly installed or has a certain type of construction defect. The capacity reductions are then randomly generated according to Table 12, and applied to the original capacities to obtain the decreased uplift capacities for the defective roof connections. The probabilistic defect model is thus integrated into the MCS, which allows the reliability-based fragility

assessment to account for the effects of weakened roof connections due to construction defects.

5.2 Effect of construction defects on wind fragility

The fragility assessment is conducted for the representative contemporary house with and without construction defects. As mentioned in Section 5.1.2, two typical opening scenarios are considered, i.e. (i) dominant openings on the windward wall and (ii) effectively sealed building without any wall openings.

Distinct degrees of prior beliefs about the defect rates are taken into account for the fragility analysis. The levels of confidence towards the prior are determined by the $\boldsymbol{\alpha_0}$ values as described in Section 3.2. The prior distributions are based on both the point estimates yielded by the HRA method (i.e. CREAM in this study) and the selection of $\boldsymbol{\alpha_0}$ values according to expert's opinion. The $\boldsymbol{\alpha_0}$ values selected in this paper for the defect rates in CTB, BTR and RTW connectors are listed in Table 13. The three sets of $\boldsymbol{\alpha_0}$ values in Table 13 reflect relatively strong, moderate and weak prior belief, respectively. The moderate prior is considered as a baseline case, and the strong and weak priors are employed to examine the sensitivity of fragility to the prior beliefs about construction defect rates.

Table 13. Degree of prior beliefs for each defect type

Connection type	Typical defect type	α_{0j} value reflecting the level of confidence towards prior beliefs		
		Strong	Moderate (baseline case)	Weak
CTB (j = 1)	Missing Improper installation	3000	1000	500
BTR (j = 2)	Missing Improper installation	3000	1000	500
RTW (j = 3)	Missing one or two nails	1000	500	100

The selection of α_{0j} value for the j^{th} type of roof connection is mainly based on subjective judgement. For CTB connectors, as a relatively large data size is available for the defect type

of missing cladding fasteners, more preferences are then given to the defect data (i.e. 'let data speak louder'). Thus, a relatively small α_{01} value of 1000 is selected in the baseline case, which is roughly one third of the data size (i.e. 3368) to give more weight to the defect data. The strong prior case has a α_{01} value comparable to the number of observations. In the weak prior case, a α_0 value of 500 is used to ensure that the posterior distribution for the defect rate for improper installed CTB connectors as shown in Fig. 7(b) is not too diffuse. For BTR connectors, as no defect data are available, the prior distributions for the defect rates are directly employed. The selected α_{02} values for the three cases produce reasonable probability distributions for the defect rates of BTR connectors as shown in Fig. 5. For RTW connectors, the defect data are inferred from vague descriptions in the literature, which is somewhat anecdotal. Hence, more preferences are given to the prior distribution that are derived from the HRA model (i.e. CREAM). In the weak prior case, the α_{03} value is comparable to the inferred data size (i.e. 92). The moderate and strong prior cases have α_{03} values that are about five and ten times the inferred data size, respectively. The average defect rates revealed by the defect data (see Table 3) mostly lies within the 5th and 95th percentile of the elicited prior distributions shown in Figs. 4-6, which conforms the consistency test suggested by Atwood et al. (2003). The α_{0i} values elicited in Table 13 also approximately capture the uncertainty bounds of error rate given by CREAM (see Hollnagel 1998 for details about the uncertainty bounds). The $\boldsymbol{\alpha}_0$ values can be further modified if more expert knowledge and/or objective observations from various sources (e.g. estimates from experienced construction workers) about the defect rates are available.

As mentioned in Section 3.2.2, an average construction quality is assumed in the baseline case, and the working contexts (usually characterized by PSFs) are not explicitly taken into account (i.e. neutral PSFs without improving or reducing human performance are assumed) as no observations for such contexts are available during the construction process. Some

adverse working contexts may result in poor construction quality with high defect rates. For example, builders with less experience/training, inadequate time and unclear procedures/plans all have negative effects on the human performance and reliability. Ideally, both the construction defect data and corresponding working contexts need to be collected, and the probability distribution of the defect rates conditional on PSFs can then be obtained through the Bayesian updating. However, unlike 'safety-first' industries such as nuclear power and aviation, such data are challenging to collect because there is no requirement (or incentive) for builders to reveal any information regarding construction errors, restrictive access to construction sites, privacy issues (e.g. people do not like to disclose their mistakes and/or to be monitored while working), etc. A single PSF value ranges from 0.5 to 5.0 in CREAM (Hollnagel 1998). Considering that most contemporary houses are constructed by qualified builders, a relatively low effect of PSFs on defect rates is assumed in a sensitivity analysis. Thus, the negative effects of adverse working contexts are implicitly included and examined by applying a factor of two (close to the average weighting factor of 1.9 to account for effects of PSFs suggested for the tactical control mode in CREAM) to the baseline defect rates obtained from the Bayesian inference. The subsequent effects on the proportion of roof sheeting loss and roof truss failures are then examined by conducting the fragility assessment with the adjusted defect rates.

The construction defects are often correlated or dependent, i.e. one error or defect is more likely to lead to other errors or defects, which is not included in the model formulation as described in Section 3. In a sensitivity analysis, the effect of correlation between defects on the wind fragility is simply examined by applying an empirical equation to the defect rates in the baseline case. The probability of a defect given a defect occurs in the previous task is obtained from the following equation (Swain & Guttmann 1983; Kirwan 1994)

$$\Pr(\text{defect} \mid \text{defect occurs in previous task}) = \left(\frac{1+A\cdot\text{defect rate}}{A+1}\right) \tag{11}$$

39

where A = 19, 6 and 1 for low, moderate and high dependence, respectively. A moderate correlation is assumed in the present analysis.

The fragility results, expressed as the mean proportion of roof sheeting loss and roof truss failures, are shown in Figs. 11 and 12, respectively, with the consideration of distinct degrees of prior beliefs, the effects of adverse working contexts and dependence between defects. The fragility analysis is carried out for a suburban house located on a flat, level site with no shielding and subjected to wind coming from the prevailing direction (i.e. the nominal values used for the terrain and height factor in Eq. (10) is 0.83, and the shielding and directional factors are unity). However, the obtained fragility curves have the flexibility to account for other wind directions and shielding conditions. Site-specific wind directional multipliers for eight cardinal directions given in AS/NZS 1170.2 (2011) can be multiplied to the wind speed to account for non-prevailing wind directions, which is to be incorporated in a future study for housing vulnerability assessment and loss estimation. A shielding factor less than unity can also be multiplied to the obtained fragility results to account for either a partial or full shielding condition. For example, at a wind speed of 55m/s, the mean proportion of roof sheeting loss obtained from the fragility curve without considering construction defects is about 3% for the dominant opening scenario – i.e. 3% of metal sheets on the roof are lost. For a house with partially shielding, assuming a shielding factor of 0.9 (the exact value can be calculated according to AS/NZS 1170.2 2011 for a specific site condition), then the mean roof sheeting loss is about 0.7% that is obtained from the fragility curve at the adjusted wind speed, i.e. $55 \times 0.9 = 49.5$ m/s.

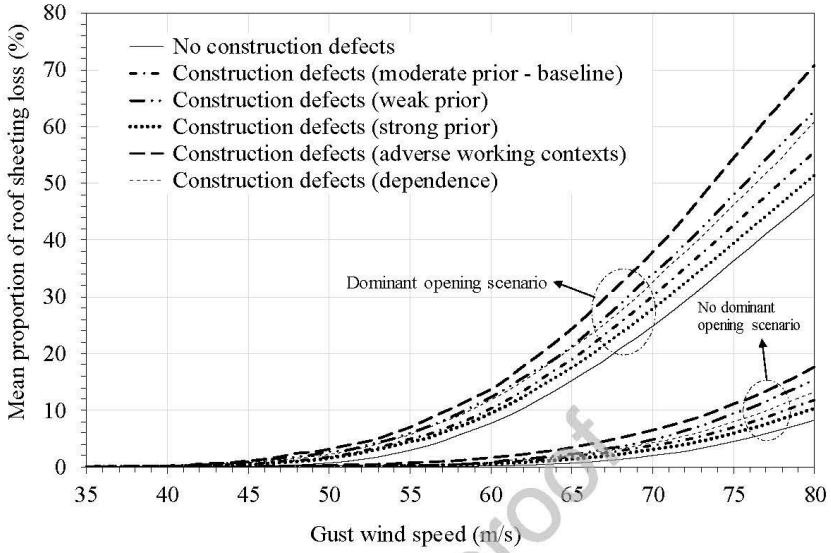

Fig. 11. Fragility curves for metal roof cladding considering construction defects.

As shown in Fig. 11, the effect of construction defects on the roof cladding fragility is significant. For example, compared to the fragility results ignoring construction defects, the predicted mean proportion of roof sheeting loss in the baseline case increases by up to eight times when gust wind speed is smaller than 55m/s, and up to 52% higher, when gust wind speed is larger than 55m/s with the presence of windward wall dominant openings. The mean proportions of roof sheeting loss at two design wind speeds with dominant openings are shown in Table 14. At the design wind speed for Brisbane (i.e. 57m/s) and for the dominant opening scenario, the mean proportion of roof sheeting loss increases from 4.5% to 6.5% when considering the construction defects in the baseline case. At the design wind speed for Melbourne (i.e. 45m/s) and for the dominant opening scenario, the mean proportion of roof sheeting loss increases five-fold from 0.1% to 0.5% when considering the construction defects in the baseline case. Accounting for the potential influence of adverse working contexts can increase the roof cladding fragility by approximately seven times on average (e.g. roughly two times at 57m/s and thirteen times at 45m/s). The consideration of

dependence between defects on average leads to approximately a fourfold increase in the predicted mean proportion of roof sheeting loss. The predicted mean proportion of roof sheeting loss increases with decreasing degrees of prior beliefs. This is expected as a weak prior distribution results in a relatively high variance for the posterior distributions of the defect rates as shown in Fig. 7.

Table 14. Mean proportions of roof sheeting loss at design wind speed with dominant openings.

Design wind speed	Mean proportion of roof sheeting loss					
	No defects	Baseline	Weak	Strong	Adverse working contexts	Defect dependence
45 m/s	0.1%	0.5%	0.8%	0.4%	1.3%	0.8%
57 m/s	4.5%	6.5%	8.0%	6.0%	10.8%	7.9%

Figures 12(a) and (b) indicate that the predicted mean proportion of roof truss failures increase only slightly when considering the effect of construction defects. This is not surprising, as surveys show more damage to roof sheeting and batten fixings than truss connections for non-cyclonic winds (e.g. Leitch et al. 2009; Ginger et al. 2010). This is also likely due to a relatively low reduction of the uplift capacities given the occurrence of a typical construction defect for RTW connectors. As shown in Table 12, the uplift capacity of a RTW connector decreases by only 10-40% and 20% on average, which is a much lower consequence compared to the effects of construction defects on CTB and BTR connectors (e.g. a missing CTB connector is equivalent to a 100% capacity reduction). In addition, the weakened RTW connector tends to receive less wind uplift load due to the load sharing of the roof truss system, which, to some extent, compensates the adverse effect of the defective RTW connectors. While the effect of defects on truss failure may not be as significant as that observed for roof cladding, the consequences of truss failure are much higher potentially leading to severe structural damage/collapse and home contents economic losses.

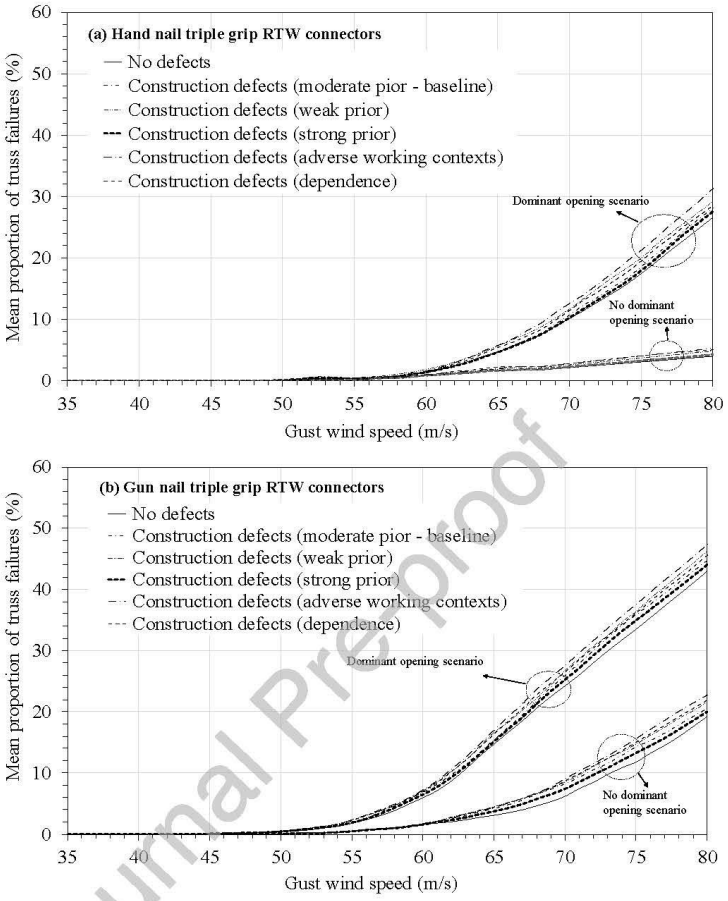

Fig. 12. Fragility curves for timber roof trusses considering construction defects.

6. Limitations and Future Research

Although the effect of correlation between defects is practically examined in a sensitivity analysis, further inclusion of the defect dependence in the theoretical model formulation is needed. In this paper, neutral PSFs (i.e. working contexts do not improve or reduce human performance) are assumed as a representative scenario for most qualified builders. Hence, the effect of working contexts is not explicitly accounted for by using PSFs due to a lack of information. There is also a need to consider the potential correlations between PSFs if they

are explicitly included. A challenging task is to collect more construction defect data and corresponding information regarding working contexts, which is essential for the improvement of the wind fragility assessment for housing with construction defects.

In current practice in Australia, home builders are self-regulated to perform inspections. It might be beneficial if authorized or permitted professional inspectors were introduced in some stages of the construction process to have detailed inspections on the construction quality and obtain the statistics for the occurrence rate of construction defects. Moreover, there is clear agreement that partial safety factors in building standards are not the appropriate means of dealing with the adverse effects of construction defects (e.g. Melchers & Beck 2018). A more appropriate strategy is improved quality control of the design and construction process. Further validations of the fragility results using wind damage data and/or insurance data, if available, are needed. Future research will assess economic risks arising from windstorms using these fragility results, stochastic wind fields and economic loss models, and these risks can be compared and validated with insurance loss data. The Bayesian approach developed in this study has the flexibility to incorporate other HRA methods such as THERP (Swain & Guttmann 1983) depending on the appropriateness for different engineering contexts. Finally, more development is still needed to model human cognition for the second generation HRA method such as CREAM (Kirwan 1998).

7. Conclusions

A Bayesian approach combining expert opinion, HRA method and limited construction defect data was developed in this study to probabilistically characterize the construction defect rates in roof connections. The capacity reductions of roof connections given the occurrence of distinct types of construction defects were also probabilistically modelled based on engineering judgement and available experimental evidence. The proposed construction defect model was then integrated into a reliability-based fragility method to

assess the wind damage to metal roof cladding and timber roof trusses for contemporary houses in Australia.

The fragility results were expressed as the mean proportion of roof sheeting loss and roof truss failures. It was found that the effect of construction defects on the roof cladding fragility is significant. Compared to the fragility results ignoring construction defects, the predicted mean proportion of roof sheeting loss in the baseline case increases by up to eight times when gust wind speed is lower than 55m/s, and up to 52% when gust wind speed is higher than 55m/s with the presence of windward wall dominant openings. The influence of construction defects can further increase if adverse working contexts and dependence between defects are taken into account. The roof truss fragility is only marginally affected by construction defects.

Conflict of interest: None

Acknowledgement

The first author is supported by the Australian Government Research Training Program Scholarship. We would like to thank Dr. Satheeskumar from The University of Melbourne (formerly at James Cook University) for the helpful discussions on this study. The support from Mr. Aaron Scott for high performance computing at The University of Newcastle is greatly appreciated. We also thank Dr. Phil Clausen for providing access to multiple software licenses for the finite element analysis.

References

Akyuz, E., & Celik, M. (2015). Application of CREAM human reliability model to cargo loading process of LPG tankers. *Journal of Loss Prevention in the Process Industries*, 34, 39-48.

AS/NZS 1170.2 (2011). *Structural Design Actions, Part 2: Wind Actions*. Standards Australia, Sydney, Australia.

Atwood, C. L., LaChance, J. L., Martz, H. F., Anderson, D. J., Englehardt, M., Whitehead, D., & Wheeler, T. (2003). *Handbook of parameter estimation for probabilistic risk assessment*. US Nuclear Regulatory Commission, Washington, DC, Report No. NUREG/CR-6823.

Blackman, H. S., Gertman, D. I., & Boring, R. L. (2008). Human error quantification using performance shaping factors in the SPAR-H method. *Proceedings of the human factors and ergonomics society annual meeting*, Los Angeles, CA, USA.

Boughton, G.N., Falck, D.K., Vinh Nghi Duong, A., Pham, S. and Nguyen, A. (2015). *Static Testing of Batten Connections at University of Western Australia*. Technical Report No.62. Cyclone Testing Station, James Cook University.

De Haan, J., Terwel, K. C., & Al-Jibouri, S. H. S. (2013). Design of a Human Reliability Assessment model for structural engineering. *Proceedings of the 22nd European Safety and Reliability Conference*, Amsterdam, The Netherlands.

Ellingwood, B. (1987). Design and construction error effects on structural reliability. *Journal of structural engineering*, 113(2), 409-422.

Gelman, A., Carlin, J. B., Stern, H. S., & Rubin, D. B. (1995). *Bayesian data analysis*. London: Chapman and Hall/CRC.

Ginger, J., Henderson, D., Edwards, M. and Holmes, J. (2010). Housing damage in windstorms and mitigation for Australia. *Proceedings of 2010 APEC-WW and IG-WRDRR Joint Workshop: Wind-Related Disaster Risk Reduction Activities in Asia-Pacific Region and Cooperative Actions*, 1-18.

Ginger J., Henderson D., Humphreys, M., and Parackal, K. (2015). *Climate Adaptation Engineering for Extreme Events (CAEX), Project* 1.1 *Progress report* 4. Cyclone Testing Station, James Cook University, Australia.

Groth, K. M., Smith, C. L., & Swiler, L. P. (2014). A Bayesian method for using simulator data to enhance human error probabilities assigned by existing HRA methods. *Reliability Engineering & System Safety*, 128, 32-40.

Hallbert B, Kolaczkowski A. (2007). *The employment of empirical data and Bayesian methods in human reliability analysis: a feasibility study*. US Nuclear Regulatory Commission, Washington DC.

He, X., Wang, Y., Shen, Z., & Huang, X. (2008). A simplified CREAM prospective quantification process and its application. *Reliability Engineering & System Safety*, 93(2), 298-306.

Henderson, D. J., & Ginger, J. D. (2007). Vulnerability model of an Australian high-set house subjected to cyclonic wind loading. *Wind and Structures*, 10(3), 269-285.

Hollnagel, E. (1998). *Cognitive reliability and error analysis method (CREAM)*. Oxford: Elsevier.

Holmes, J. D. (1985). Wind loads and limit states design. *Civil Engineering Transactions*, Institution of Engineers Australia, CE27(1): 21-26.

Hong, H. P., & He, W. X. (2015). Effect of human error on the reliability of roof panel under uplift wind pressure. *Structural Safety*, 52, 54-65.

Kelly, D., & Atwood, C. (2011). Finding a minimally informative Dirichlet prior distribution using least squares. *Reliability Engineering & System Safety*, 96(3), 398-402.

Kim, J. H., & Rosowsky, D. V. (2005). Incorporating nonstructural finish effects and construction quality in a performance-based framework for wood shearwall design. *Structural Engineering and Mechanics*, 21(1), 83-100.

Kirwan, B. (1994). A guide to practical human reliability assessment. London: Taylor & Francis.

Kirwan, B. (1996). The validation of three Human Reliability Quantification techniques - THERP, HEART and JHEDI: Part 1 - technique descriptions and validation issues. *Applied ergonomics*, 27(6), 359-373.

Kirwan, B. (1998). Human error identification techniques for risk assessment of high risk systems - Part 1: review and evaluation of techniques. *Applied ergonomics*, 29(3), 157-177.

Lee, S. M., Ha, J. S., & Seong, P. H. (2011). CREAM-based communication error analysis method (CEAM) for nuclear power plant operators' communication. *Journal of Loss Prevention in the Process Industries*, 24(1), 90-97.

Leitch C, Ginger J, Harper B, Kim P, Jayasinghe N, Somerville L (2009). *Investigation of performance of housing in Brisbane following storms on* 16 *and* 19 *November* 2008, Technical Report No. 55. Cyclone Testing Station, James Cook University.

Melchers, R. E., & Beck, A. T. (2018). *Structural reliability analysis and prediction*. John Wiley & Sons, UK.

Nan, C., & Sansavini, G. (2016). Developing an agent-based hierarchical modeling approach to assess human performance of infrastructure systems. *International Journal of Industrial Ergonomics*, 53, 340-354.

Nan, C., & Sansavini, G. (2017). A quantitative method for assessing resilience of interdependent infrastructures. *Reliability Engineering & System Safety*, 157, 35-53.

Parackal, K. I., Humphreys, M. T., Ginger, J. D., & Henderson, D. J. (2016). Wind Loads on Contemporary Australian Housing. *Australian Journal of Structural Engineering*, 17(2), 136-150.

Podofillini, L., & Dang, V. N. (2013). A Bayesian approach to treat expert-elicited probabilities in human reliability analysis model construction. *Reliability Engineering & System Safety*, 117, 52-64.

Qin, H., & Stewart, M. G. (2019). System fragility analysis of roof cladding and trusses for Australian contemporary housing subjected to wind uplift. *Structural Safety*, 79, 80-93.

Satheeskumar, Navaratnam (2016) *Wind load sharing and vertical load transfer from roof to wall in a timber-framed house*. PhD thesis, James Cook University, Australia.

Smith D, Henderson D, Ginger J, Wehner M, Ryu H, Edwards M (2016). *Improving the resilience of existing housing to severe wind events: Annual project report* 2015-2016. Bushfire and Natural Hazards CRC.

Stewart, M. G. (1992). Modelling human error rates for human reliability analysis of a structural design task. *Reliability Engineering & System Safety*, 36(2), 171-180.

Stewart, M. G. (1993). Structural reliability and error control in reinforced concrete design and construction. *Structural safety*, 12(4), 277-292.

Stewart, M. G., Ginger, J. D., Henderson, D. J., & Ryan, P. C. (2018). Fragility and climate impact assessment of contemporary housing roof sheeting failure due to extreme wind. *Engineering Structures*, 171, 464-475.

Stewart, M. G., & Melchers, R. E. (1988). Simulation of human error in a design loading task. *Structural Safety*, 5(4), 285-297.

Swain, A. D., & Guttmann, H. E. (1983). *Handbook of human reliability analysis with emphasis on nuclear power plant applications*. Final report. NUREG/CR-1278. SAND80-200, Sandia National Laboratories Statistics Computing and Human Factors Division, Albuquerque, US.

van de Lindt, J. W., & Nguyen Dao, T. (2010). Construction quality issues in performance-based wind engineering: effect of missing fasteners. *Wind and Structures*, 13(3), 221.

Yang, Z. L., Bonsall, S., Wall, A., Wang, J., & Usman, M. (2013). A modified CREAM to human reliability quantification in marine engineering. *Ocean Engineering*, 58, 293-303.

Yazdani, N., Dowgul, R. W., & Manzur, T. (2010). Deficiency analysis of coastal buildings toward storm damage reduction. *Journal of Performance of Constructed Facilities*, 24(2), 128-137.